School of Civil and Mechanical Engineering

Dynamic Response and Life-Cycle Analysis of Floating Production Storage and Offloading Systems

Rini Nishanth

This thesis is presented for the Degree of
Doctor of Philosophy
of
Curtin University

October 2018

DECLARATION OF THESIS

To the best of my knowledge and belief this thesis contains no material previously published by any other person except where due acknowledgment has been made.

This thesis contains no material which has been accepted for the award of any other degree or diploma in any university.

Signature: 

Date: 11 Oct 2018

DEDICATION

To my husband and Son

To my mother and sister

To my grand parents

To my family members

To my friends

ACKNOWLEDGEMENTS

First and Foremost, I thank the GOD Almighty for directing me towards this research opportunity, giving me the knowledge and ability to complete this research and for giving strength and patience to face the trials and challenges in life, I faced over this period. Without his provisions and blessings, this achievement would not have been possible.

I am immensely grateful to Dr. Andrew Whyte, Associate Professor and Head of the Department, Civil Engineering, at Curtin University, for supervising me and encouraging me to find my way through the life-cycle aspects of FPSO. I am indebted to him for the confidence he placed in me and for all the provisions he made possible at Curtin University. Apart from keeping a constant check on my research progress, I am immensely grateful for the time and effort he spent on helping me complete this thesis, without his help, the timely submission of this thesis would not have been possible. I am grateful for the moral support provided by him while completing the thesis corrections and I can surely say this thesis wouldn't have been possible without his guidance and support.

I would like to express my deep and sincere gratitude to my research supervisors, Prof Ir Dr. Mohd Shahir Liew and Dr. Kurian Velluruzhathil John, Universiti Teknologi PETRONAS, for supporting me immensely through this journey, giving valuable suggestions, encouragement and support to pursue this joint PhD programme. I am deeply grateful for choosing me as the candidate for this Collaborative PhD programme and for giving me support and answers to my relentless queries consistently, while I was at Universiti Teknologi Petronas and at Curtin University.

I am thankful to my supervisor Prof Ir Dr. Mohd Shahir Liew for his kind help and support in the final submission of this thesis and for the moral support while completing

the thesis corrections. I am extremely grateful for his guidance while completing the thesis corrections and the confidence he placed in me.

I am thankful to my previous supervisor Dr Kurian Velluruzhathil John for not only being a good teacher and mentor, but also for being an inspiration. He made sure I develop not only as a researcher, but also as a professional Engineer in my work. He gave me all the freedom, while silently ensuring that I stay on course and complete work on time. Without his guidance, this thesis would not have been possible and I am forever grateful for his assistance.

I am grateful to Curtin University and Universiti Teknologi PETRONAS staff, particularly School of Civil and Mechanical Engineering Staff, offshore laboratory technicians and the Centre of Graduate Studies staff, this smooth voyage would not have been possible without them. Their time and effort is gratefully acknowledged. I am deeply grateful to the Det Norske Veritas team for supplying me with the SESAM license throughout this research period and immensely grateful to their software support team for clearing my doubts and answering to my queries. The financial support for this study was provided by Universiti Teknologi PETRONAS, Malaysia and Curtin University, Perth. I thank my family members and friends, particularly my mother for giving me constant strength and moral support to complete this thesis. I am eternally grateful to everyone who has contributed to make this journey a success.

Last, but not the least, I am forever grateful to my husband and son for all the sacrifices they made during this PhD journey, for being understanding and supporting in all the ways possible and for placing their confidence in me during the hardest times.

ABSTRACT

Floating Production Storage and Offloading (FPSO) systems are efficient means of natural resource management in the deep-water fields of South East Asia and Western Australia. For short-term projects of 10 years, most energy-companies use FPSOs with refurbished hulls, stabilised by mooring-line connections subjected to unpredictability of waves and non-linearities from mooring lines along with risk associated from fluctuating market rates. The suitability of both converted tankers and newly built floating platforms for projects under site specific metocean conditions can be assessed by the computation of respective motion responses and operational downtime, with life cycle cost analyses providing a means to compare alternative vessel specifications. In this study, uncoupled and coupled software simulation models for both spread moored and turret moored FPSOs are developed using SESAM software. The uncoupled simulation model is validated using the model testing results performed at Universiti Teknologi PETRONAS (UTP) Offshore Laboratory in the presence of unidirectional random waves and coupled simulation model using published results from tests performed at Offshore Technology Research Center wave basin at Texas A&M university, by investigating the six degree of freedom responses of FPSOs under the action of wind, waves and current. The results correspond well for wave period ranges of 5 s – 25 s. Life-cycle cost analysis methodology is developed and used to compute the whole life cost of the FPSO system, identifying economic FPSO options for 10-year and 25-year design periods. Riser turret moored FPSOs are found to be the costliest. The parametric study results covering the influence of metocean conditions, water depth, hull loading conditions, hull length to beam ratio, mooring line azimuth angle, mooring line length, and position of mooring line fairleads can be used along with the life-cycle costs and net present values when choosing the economic and efficient option in the initial design phase as well as relocation of FPSO. The response amplitude operators, relative motions as well as sensitivity analysis chart reflecting the varying market rates are also developed for the Malaysian and Australian waters.

TABLE OF CONTENT

LIST OF FIGURES

LIST OF TABLES

LIST OF ABBREVIATIONS

2D	Two Dimensional
3D	Three Dimensional
CALM	Catenary Anchor Leg Mooring
CAPEX	Capital Expenditure
CF	Compact Flash
CG	Center of Gravity
DOF	Degree of Freedom
DWT	Dead weight tonnage
ET	External Turret
FB	Freeboard
FEED	Front End Engineering Design
FP	Forward Perpendicular
FPSO	Floating Production Storage and Offloading
FSO	Floating Storage and Offloading
IT	Internal Turret
LBP	Length between Perpendicular
LCCA	Life-cycle Cost Analysis
LCG	Longitudinal Center of Gravity
LCR	Long-crested Random
LF	Low Frequency
LNG	Liquefied Natural Gas
LOA	Overall Length
LPG	Liquefied Petroleum Gas
LWT	Light Ship Weight
MBOPD	Thousand Barrels Oil Per Day
MWL	Mean Water Level
MPM	Most Probable Maximum
NPV	Net Present Value
NWA	North Western Australia

OPEX	Operating Expenditure
OTRC	Offshore Technology Research center
PTF	Paddle Transfer Function
RAO	Response Amplitude Operator
RCIS	Royal Institution of Chartered Surveyors
RTM	Riser Turret Mooring
SCR	Short-crested Random
SLR	Single-Lens Reflex
SPM	Single Point Mooring
STP	Submerged Turret Production
UTP	Universiti Teknologi PETRONAS
USD	US Dollars
VCG	Vertical Center of Gravity
WF	Wave Frequency

LIST OF SYMBOLS

B	Beam of vessel
B8	Revenue generated
B9	Salvage value/Scrap value
C_A, C_d, C_m	Added mass, drag force and inertia force coefficients respectively
C1	Capital costs
C2	Installation costs
C3	Operation costs
C4	Maintenance costs
C5	Refurbishment/Replacement costs
C6	Downtime costs
C7	Decommissioning/Disposal cost
D	Diameter of cylinder
F_D	Drag Force
F_I	Inertia Force
FB	Freeboard
H	Wave height
H_s	Significant wave height
L	Wave Length
N	life expectancy of FPSO
P_E	Short term probability of exceedance
PV_n	Discounted present value
R_m	Relative motion of FPSO
R_n	Real costs incurred per year
$S_R(\omega)$	Response Spectrum
$S(\omega)$	Wave Spectrum
T	Wave Period
T_p	Peak Period
U_{rel}	Relative velocity between structure and wave

$\ddot{X}$	Structural acceleration
d	Water depth
g	Acceleration due to gravity
k	Wave number
m	Mass of the vessel
m_{0R}	Zeroth order moment of area under the relative motion spectrum
t	Instantaneous time
u, v	Fluid particle velocity in x, y direction respectively
$\dot{u}, \dot{v}$	The fluid particle acceleration in x, y direction respectively
(x, y, z)	Cartesian co-ordinate system used for the definition of wave kinematics
γ	Spectrum peak enhancement factor
Δ	Weight displacement of FPSO
Δt	Time interval
∇	Displaced volume of vessel
η, η_a	Wave amplitude
η_t	Wave Profile
θ_1	Roll motion
θ_2	Pitch motion
θ_3	Yaw motion
λ	Linear scale factor
ρ	Density of water
τ	Spectral shape parameter
ϕ	Potential Function
ϕ_0	Incident wave potential
ϕ_s	Scattered wave potential
ω	Circular frequency of the incident wave
ω_o	Peak circular wave frequency

CHAPTER 1

INTRODUCTION

1.1 Chapter Overview

In this chapter, the history and advantages of Floating Production Storage and Offloading (FPSO) systems are explained together with the need for conducting the dynamic analysis of FPSO, how cost and motion are interrelated while choosing FPSO configurations and the relevance of conducting Life Cycle Cost Analysis (LCCA) for the same. Further, the objectives of the present study are stated and, the scope of the study is furnished. Finally, the significance of the project is addressed.

1.2 Background of FPSO

The history, advantages and structure of FPSO are detailed in the below sections.

1.2.1 History of FPSO

Over the past 40 years, ship – shaped offshore units have proven to be reasonably reliable solutions for deep water offshore fields. These include FPSOs and FSOs operating in harsh environmental conditions and waters of more than 1500 m depth. Even though oil storage and shuttle tanker – mooring facilities using converted trading tankers existed in late 1960s, the entry of ship – shaped units to the offshore industry is not known accurately. The first such vessels were connected by hawsers to catenary anchor leg mooring (CALM) systems. These then evolved into the familiar systems employing single – point mooring. The first FPSO was Arco in the Ardjuna field in the Java Sea offshore Indonesia in 1976. This was a concrete barge with steel tanks, used

to store refrigerated liquefied petroleum gas (LPG) moored to a buoy using a rigid arm system in 42.7 m water depth. The first tanker-based single-point moored FPSO facility for oil is said to be the Castellon for Shell offshore Spain in 1976. This facility was meant to produce oil from a subsea completed well, some 65 km offshore Tarragona. It began operations in 1977, and was designed for a 10-year field life. Compared to these early days, floating production systems have now evolved to a mature technology that potentially opens the development of offshore oil and gas resources that would be otherwise impossible or uneconomical to tap. The technology now enables production far beyond the water-depth constraints of fixed-type offshore platforms and provides a flexible solution for developing short-lived fields with marginal reserves and fields in remote locations where installation of a fixed facility would be difficult [1]. Many FPSOs have been installed and operated worldwide and many new FPSOs will be installed in the coming years. Out of a total of 178 FPSOs operating now globally, 9 are in Western Australia offshore, 8 are in Malaysia offshore, 2 are in Thailand offshore and 9 are in Indonesia offshore regions. Another 5 FPSOs are ready for redeployment in Australia and 2 in Malaysia. Figure 1.1 shows the distribution of FPSO worldwide [2].

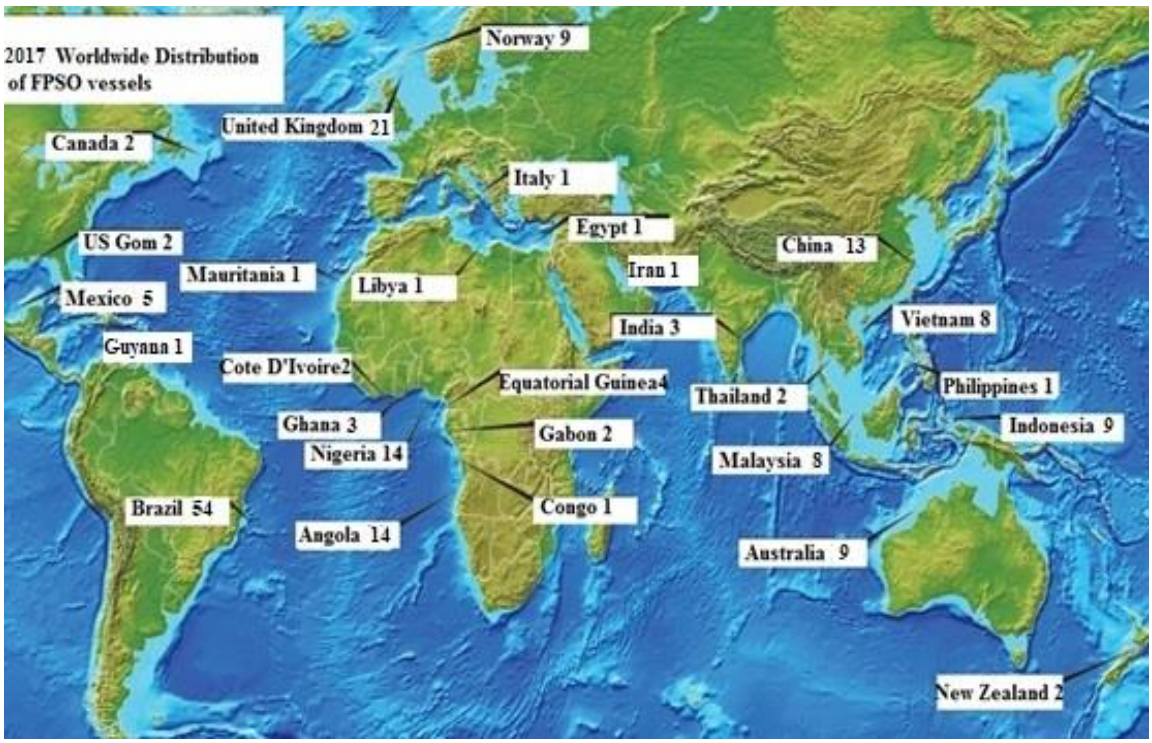

Figure 1.1: Worldwide Distribution of FPSO 2017

(source: Offshore Magazine, 2017)

1.2.2 Structure of FPSO

FPSOs are usually ship shaped floating structures, even though other variety shapes of FPSOs are coming into industry like the cylindrical FPSO. An FPSO is equipped with provisions for production, storage and offloading hydrocarbons. A typical FPSO consists of mooring area, process area, storage and offloading systems, hull structure, utilities and marine systems, dynamic positioning system or station keeping system and means of escape and evacuation. Mooring systems can be spread mooring or turret mooring. There are different types of turret moored FPSOs, they can be external turret moored, internal turret moored, riser turret moored or with submerged turret production systems. For spread moored FPSOs, riser hang-off points are attached at the side of the vessel. For turret moored FPSOs, turrets should be located at or near the bow so that the FPSO can weathervane passively without thruster assistance. Table 1.1 summarises typical differences between spread moored and turret moored FPSO.

Table 1.1: Typical Differences Between Spread Moored and Turret Moored FPSO

Description	**Spread Moored**	**Turret Moored**
Environment	Can be used in mild to moderate environment	Can be used in mild to extreme environment
Vessel Orientation	Fixed orientation	360° weathervaning
Riser Systems	Adapts to various riser systems	Location of turret requires robust design
Station keeping Performance	Variable offsets (due to low frequency wave)	Minimized offsets
Vessel Motions	Dependent on relative vessel-environment directionality	Weathervaning capability reduces motion
Offloading Performance	Dependent on vessel-environment orientation	Aligned with mean environment

FPSOs can have double skin hull or single skin hull. While most of the newly built hulls have double hulls, the old converted tankers have only single hulls [2]. The process area consists of the gas separation and compression systems and metering systems. Storage is provided in the center tanks, with water ballast in the double bottom

(if fitted) and side tanks. A common way of exporting crude oil from a FPSO is by shuttle tanker transport to a shore terminal. The export may take place by direct transfer from the FPSO to a shuttle tanker by a hose, or by transfer from FPSO via separate offloading system (hose-riser pipeline- riser). The former method is mainly used when the production/storage unit is a ship or barge shaped floating production, storage and offloading unit (FPSO). Both alongside transfer and tandem transfer methods can be used, depending on operational criteria [3]. Figure 1.2 shows the various parts of an FPSO.

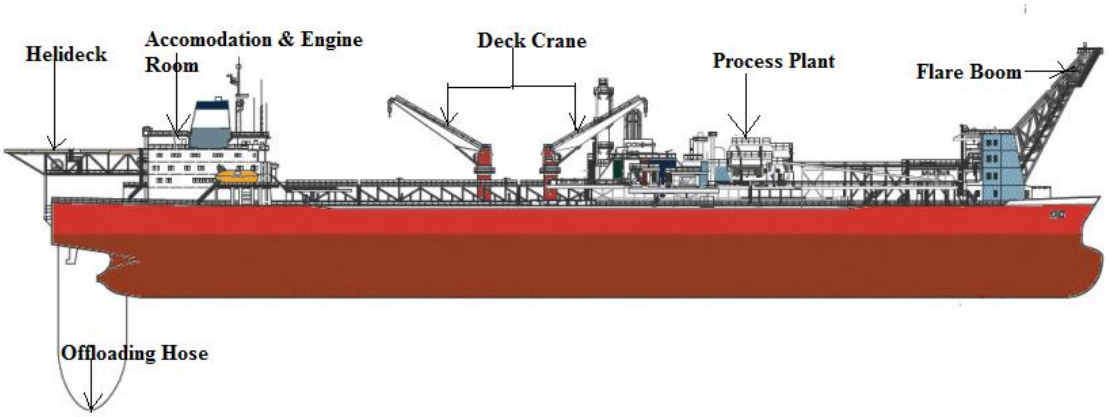

Figure 1.2: Various Parts of FPSO

(source: Marine Insight, 2011)

1.2.3 Advantages of FPSOs

Advantages of FPSOs are

- Early Production and huge storage capacity.
- Easy to remove and reuse.
- Reduced upfront investment.
- Can be used in any water depth.
- Abandonment costs are less than for fixed platforms.

- Retained values; because they can be relocated to other fields.
- Earlier cash flows because they are faster to develop than fixed platforms.
- Ample deck space reducing risk of oil spilling.

1.3 Relevance of Cost and Motion Analysis of FPSO

Extreme FPSO motion can lead to significant operational downtime, disrupting processing and production of oil on board FPSO and offloading to tankers. Excessive heave and pitch motion of FPSO can result in green water on board FPSO damaging production equipment and fatalities in some case. Roll motion of FPSOs should be within ±5° to enable crew habitability. Excessive roll motion of FPSO can also lead to green water impacts on deck. Extreme surge and yaw motion of FPSO can disrupt offloading operation during tandem and side-by side offloading configuration by driving off the oil tanker or by imposing risk of collision with them. In turret moored FPSOs, excessive sway and yaw motion can result in fishtailing phenomenon, again disrupting offloading operations [4]. Hence all six FPSO motions need to be minimised to ensure safe, profitable and efficient oil production using FPSOs. Hence an extensive parametric study covering hull, mooring and metocean parameters are conducted in this research and the results are presented, identifying the range of parameters over which FPSO motions are minimum.

Spread moored and turret moored FPSOs are two main types of FPSO configuration. While spread moored FPSOs have a fixed orientation, turret moored FPSOs can weathervane reducing the loads on mooring lines. The FPSO motion behaviour in varying wave heights are studied with and without wind and current in the presence of wave to understand the range of FPSO motion amplitudes in the six degrees of freedom, trend in FPSO motion variation with wave height and to study the influence of current and wind in FPSO motions. Especially, excessive heave and pitch motion in extreme wave heights can result in green water on FPSO deck. If the relative motion of FPSO (heave) and wave is higher than 3m, medium to high risk level green water impacts can occur, resulting in operational downtime. This in turn can influence the

life-cycle cost of the system. Hence a downtime analysis is done to compare the loss in production when spread moored and turret moored FPSOs are used. Relative motions are found by performing dynamic analysis and probability distribution for freeboard exceedance are generated. If the free board exceedance is above 3 m, this can result in downtime cost. Downtime cost computed by measuring motion responses in the event of green water is one of the cost factors affecting the total life-cycle cost of the FPSO and associated mooring line system.

FPSO hull and mooring system should be designed such that the six motions of FPSO are minimum as well as its cost. Cost of FPSO hull is only 10-15% of the cost of mooring system. Hence proper care should be taken while using converted hulls in FPSO, as it is not specifically designed for the metocean conditions it is installed and can sometimes lead to frequent mooring line damages. Hence cost and motion are two important aspects while choosing an FPSO configuration to maximize operational time and profit. The study was done to compare the different FPSO configuration in terms of motion performance and cost and can significantly aid in the decision-making process in the FFED phase of FPSO projects. This research is a unique attempt to identify the factors affecting the choice of FPSO in terms of its motion performance and cost.

1.4 Relevance of Dynamic Analysis of FPSO

Floating Production Storage and Offloading System (FPSO) has proven to be one of the most effective means to carry out oil drilling and processing especially in deep waters. Malaysian and West-Australian waters are prominent regions in supplying the energy resource for the global needs with over 15 FPSOs operating in this region from water depth ranging from 50 m to 3000 m. Even though Malaysian and West-Australian waters are calm when compared to the North Sea, proper consideration should be given to the various criteria like water depth and metocean data. FPSO motions are minimised by employing proper mooring and hull configurations which has sufficient storage facilities, deck space, required natural period and designed to project specific metocean criteria. Often, this is done through an iterative procedure,

where FPSO hull sizing is determined through a reverse iteration to achieve target natural periods and minimum FPSO motions. A sensitivity study covering the metocean, hull and mooring line parameters can aid in minimising the FPSO motion by identifying the critical parameters, their range of effectiveness and trend of FPSO motion to those varying parameters. Hence model tests and extensive simulations have been performed using SESAM suit of programs – SESAM HydroD and SESAM DeepC under first order wave loads, current and wind to study FPSO motion responses in wave frequency ranges through uncoupled and coupled analysis approach to identify the parameters and their range of application to ensure minimum FPSO motion.

Since FPSOs under study have ship- like forms with one plane of symmetry and with the longitudinal dimension much larger than the transverse one with large aspect ratio (L/B ratio) in the range of 5 to 6, it makes them particularly sensitive to the direction of incoming waves. Sometimes the waves, winds and current can be quite non- parallel, and subject the vessel to quartering or beam seas that can significantly influence the response of a ship – shaped vessel. To determine the stress distribution on such a structure the motions of the structure should be known in addition to the wave forces on it.

Spread mooring system helps to maintain a fixed orientation of FPSO in global coordinates [5] under calm weather conditions while turret mooring system helps in timely deployment of the mooring system under hostile weather conditions, preventing further damage to the mooring lines. If the mooring system is not specifically designed for the location, the repair and maintenance of the same prove costly. It is thus necessary to have the knowledge of the FPSO motion responses in the preliminary design phase, where appropriate choice of the mooring system can be made. Also, for short projects of 10 years, most companies use converted tankers. The suitability of these converted tankers or even newly built tankers in these projects under site specific metocean condition can be assessed by the computation of motion responses by conducting a dynamic analysis of the floater. An accurate prediction of hydrodynamic response involves the use of model testing and numerical simulations in a balanced way. Hence dynamic analysis of FPSOs to compute vessel response and wave loads acting on it are extremely important in the initial design phase of any FPSO project.

1.5 Relevance of Life-cycle Cost Analysis for FPSO

Every offshore structure has a 'life', starting with the planning, design or development of the structure, followed by resource extraction, production, use or consumption and finally end of life activities including decommissioning or conversion of structure while the oil field is nearly exploited. The life cycle costing method is an economic evaluation technique which is well suited to compare alternative designs with different cost expenditures over the project life. Generally, life cycle cost is defined as sum of all costs over the full life span of a system, which includes purchase price, installation cost, operating costs, maintenance and upgrade costs, and remaining value at the end of ownership or its useful life. The changes made in one phase of life cycle of an offshore structure can have a drastic effect in the succeeding phases. For example: reduction in initial cost of the hull by using converted old tankers may result in higher maintenance cost or vice versa; production costs of FPSOs can be higher when compared to the cost of oil available from the field; and, choosing turret mooring instead of spread mooring in calm waters. Hence LCCA should be performed early in the design process while there is still a chance to refine the design to ensure a reduction in life cycle costs. Designing of each phase needs to be done carefully and well planned as the safety of structure is very important in this case. If decisions are taken based on effects in only one part of the life cycle, it may do more harm than good. LCCA assists in choosing the conceptual design which is best in both performance and safety. Hence a thorough life cycle cost analysis of the FPSO is required to have practicably profitable, safe and successful oil production and consumption.

1.6 Problem Statement

The number of floaters operating in Malaysian and West-Australian waters is mounting and FPSOs are prominent structures contributing to the exploitation of oil and gas resources in these regions. From a detailed review of the existing FPSOs off Australia and Malaysia, it was found that most of the operating FPSOs are converted tankers. In 2016, out of the 10 FPSOs operating in Australia, 7 of them are converted tankers modified to serve the purpose and all the operating FPSOs in Malaysia (5 FPSOs) are

converted tankers [2]. The conversion of the FPSO includes replacing certain parts or sometimes all of them except the hull [6]. Also, converted FPSOs are frequently removed to replace the mooring system and usually supplied with turret mooring to be more resistant to environmental loads. Sometimes this process will be costlier when compared to building new purpose-built vessels if the mooring system must be replaced more often than planned replacements. Since the CAPEX of the mooring system is very high when compared to that of the hull, care should be taken while designing a newly built hull or choosing a converted one.

Hull motions should be minimised to achieve increased operational time and maximum productivity. Extreme surge, sway and yaw motion can disrupt offloading operations while excessive roll motions could disable crew habitability [4]. Excessive heave, roll and pitch motions can cause green water on deck and can cause downtime [7]. The relative motion due to combined heave, roll and pitch should not exceed 3 m as it can damage equipments on the deck [8]. Hence all the six FPSO motions should be minimum to ensure longer operational time. FPSO motions can be controlled by choosing hull and mooring system with minimum motions when subjected to site specific metocean conditions. Often, the hull sizing is done through a reverse iteration to achieve target natural periods and minimum motion responses. These iterative processes can be time consuming and cost incurring due to the use of special softwares and personnel with specific skills. Hence parametric studies covering hull dimensions, loading conditions and mooring line parameters are conducted to find an effective initial solution to be used in this iterative procedure to reduce this design process time. Along with that the motion response of turret moored and spread moored FPSO in varying wave heights are studied to compare their motion behaviour in increased wave heights. This is important as the West Australian region is often prone to extreme cyclonic conditions [4] and can result in high wave heights which can result in damage to FPSO deck due to green water impacts.

Often, industries choose turret mooring in hostile weather conditions and spread mooring in calm weather conditions to avoid these iterative procedures. These decisions should be backed up by proper research data, cost calculations and motion response study and that is achieved through this research. The cost of the FPSO configuration

should also be minimum when compared to its motion, for that to be an effective solution. Life-cycle cost study for the existing FPSOs in Malaysia and Australia are never reported and a cost study would be ideal to assess the long-term worth of these assets. Since FPSOs are rarely demolished during decommissioning and has high resale values and its reusable in other locations, an initial construction cost can mask its long-term asset value. A life-cycle cost analysis reporting the initial cost, down time cost due to green water, net present value for short-term and long-term use would be ideal as this will strengthen the decision made during FEED phase and can avoid huge expenses later in the life of FPSO.

The research addresses the issues mentioned above through dynamic analysis of FPSOs using state of the art hydrodynamic analysis software SESAM and life-cycle costing from first principles.

1.7 Objectives of the Study

To solve the issues mentioned above, the objectives of this research are as follows:

1. Validation of software simulation model and simulation procedures by comparing with model test results to assess the capability of simulation model and analysis procedures adopted to predict wave frequency motion responses.

2. To compare spread moored and turret moored FPSO behaviour in varying wave heights to assess the suitability of these options in extreme weather conditions.

3. To investigate the effect of mooring line azimuth angle, mooring line length, spread mooring fairlead location, hull length to beam ratio and hull loading condition and water depth on FPSO motions and identify range of parameters over which FPSO motion will be minimum and to produce parametric charts.

4. To calculate the down time cost due to green water by computing the relative motion and freeboard exceedance for the FPSOs operating in Malaysia and Australia when subjected to wind generated sea conditions and in turn assess

the operability under site specific metocean condition where the FPSOs are installed.

5. To identify cost effective FPSO configurations for 10-year and 25-year use by comparing life-cycle cost, downtime cost and Net Present value of chosen FPSOs in Malaysia and Australia through data collection and life-cycle cost analysis.

1.8 Scope of the Study

The scope of the study is as follows:

- The FPSO is considered free to move in all six degrees of freedom, i.e. surge, sway, heave, roll, pitch and yaw as shown in figure 1.3 and is subjected to regular, unidirectional and multidirectional random waves under the action of wind and current.

- The FPSO is anchored to sea bed using horizontal spread mooring system modelled using soft springs with negligible mass and damping in model tests and only horizontal excursion of the mooring line is considered for the experimental study.

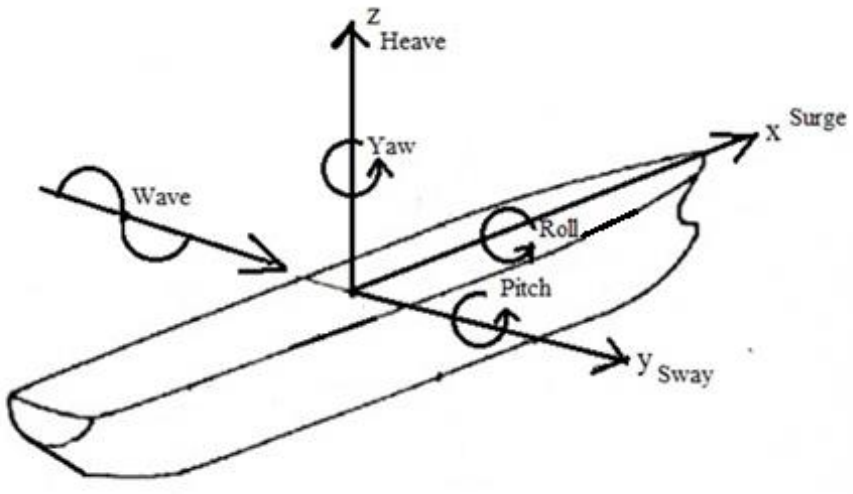

Figure 1.3: Six Degrees of Freedom of FPSO

- First order 3D Diffraction potential theory is used to calculate the wave load on FPSO and Modified Morison equation is used to calculate the mooring load in coupled analysis[9] using commercial software. Second order forces and responses are not included in the study [10]. Uncoupled analysis using commercial software calculates motion by distributing free surface source potentials across the hull surface as the Green's functions and using Green's theorem in frequency domain [11].

- The research parameters are metocean conditions, water depth, hull loading conditions, hull length to beam ratio, mooring line length, mooring line azimuth angle, and position of spread mooring fairleads.

- The metocean and market conditions are limited to Malaysian and Australian waters to generate the FPSO motion response and life cycle cost data of FPSOs in this region.

- Market fluctuations in capital, operation and maintenance, lease rate and income from oil are not considered while calculating life-cycle cost in section 4.8 – 4.10 and section 4.12 for the ease of comparison of different FPSO configurations. Hence a sensitivity analysis has been performed to incorporate the market fluctuations in section 4.11 and the variation in NPV and life-cycle cost in a good and bad market condition is studied.

- Operability analysis is conducted only for green water incidents and downtime cost is calculated only if downtime is reported for chosen FPSOs under the action of wind generated waves. Site specific annual wave scatter table based analysis was performed.

- FPSO is assumed to be producing oil to its maximum capacity and life-cycle cost is calculated based on capital cost, operation and maintenance cost, revenue from oil production and downtime cost due to green water events when subjected to wind generated sea condition only.

- Accidents, shut downs due to factors other than green water, mooring line breakages and profit from oil production are not considered in LCCA.

1.9 Significance of the Project

FPSO and the associated mooring system is chosen for a project mainly based on its performance and the profit from the project. An initial cost calculation of the project can help in choosing the best possible FPSO system and the mooring type based on its life-cycle cost. But the cost alone is not sufficient to determine the mooring system to be used. FPSO motions are greatly dependent on the site specific metocean conditions and water depth, apart from the hull condition and mooring system data. Hence the results generated by conducting the parametric study can be used in obtaining an idea of the motion performance of similar configured FPSOs during conversion, based on the dimension of FPSO hull and mooring line length and configurations, in addition to the metocean data and water depth details, which covers the major environmental conditions and structural details for the FPSOs in Malaysia and Australia and thus can be used as a reference while planning for a converted tanker or newly built hull. If any of the converted tankers are not suitable for the designated oil field, the RAOs generated for the location can be used to generate a new purpose-built vessel, while relative motions generated for FPSOs in Malaysia and Australia gives the trend and magnitude of subsequent freeboard exceedance to be expected. Hence precaution can be taken while choosing the FPSO dimension to avoid green water phenomenon and further downtime cost. Also, the life cycle cost data generated for the FPSOs in Malaysia and Australia gives information about their net asset value and cost details during their construction, which can be used as a reference for upcoming projects in this region. In short, this project brings the technical and cost aspects of FPSOs under one umbrella, enabling the design of FPSOs with maximized productivity and field life, leading to maximum financial benefits from the project.

1.10 Overview of the Thesis

Chapter 1 introduces the study conducted. Chapter 2 reviews the literature pertaining to the subject of this thesis. The reported researches are classified in eight categories and a general description of each category is given. After reporting the past researches in this area, a critical discussion is presented along with a table of gaps in the studies.

Chapter 3 details the methodology adopted to conduct the dynamic analysis of FPSOs using software simulation, model tests and numerical code. The modelling of FPSO using SESAM Genie V5.3-10 is detailed along with the analysis procedures used for frequency domain analysis in SESAM HydroD V4.5-08 to generate RAOs, relative motions and motion response time series in SESAM DeepC V5.0-06. The physical model testing setup, facilities, model specification and laboratory tests conducted are also detailed. The life-cycle costing methodology used to compute the life-cycle cost of FPSOs are detailed towards the last sections of this chapter. Methodology to evaluate the significant cost for different FPSO options, adding the expenditures and subtracting the revenues and choosing the final design with the minimum life cycle cost is detailed including data collection, sensitivity analysis and calculation of Net Present Value (NPV).

Chapter 4 presents the results of the study. The validation of the numerical models, graphs generated by conducting the parametric study, RAOs, relative motions, downtime cost and cost data for FPSOs in Malaysia and Australia are presented. All results are accompanied by critically detailed discussions.

Chapter 5 concludes the study conducted. An overview of the research work carried out is given based on the problem discussed throughout the thesis, addressing each objective of the study. Finally, recommendations for further improvements and future works related to the research work carried out are proposed.

CHAPTER 2

LITERATURE REVIEW

2.1 Chapter Overview

In this chapter, the research studies on the dynamic response and the life cycle cost analysis of the FPSO are reviewed. Major focus is given to the theoretical background for the FPSO responses, experimental and numerical works conducted in the past decades and the life cycle cost analysis procedures adopted. The reported studies are classified into eight major sections and are presented here. Finally, a critical review of the conducted literature survey is furnished along with the gap study.

2.2 Reported Studies

In this literature survey, the reported researches are grouped into eight categories based on the research direction. The studies related to the dynamic analysis of single point mooring systems and ships using model testing and numerical investigations, dynamic analysis of FPSO using model testing and numerical investigations, coupled and uncoupled analysis of FPSO, hydrodynamics of FPSO, operability studies on FPSO including parametric studies and green water impacts and finally, life-cycle cost analysis studies and LCCA for FPSO are reviewed in detail in the following sections. A significant amount of studies were done to investigate the dynamic behavior of ship shaped vessels and single point mooring systems as done by Pinkster et al [10] by conducting model tests on single point mooring attached to a tanker. Also, it should be noted that considerable research work has been reported on numerical and experimental investigation of dynamic response of FPSO in the presence of wind, wave and current. For example, Wichers [11] initiated a comprehensive study for numerical simulations of a turret moored FPSO in irregular waves with winds and Garett [12] developed a

numerical model to allow accurate and efficient fully coupled global analysis of Floating Production systems including the vessel, mooring system and the riser system. However, very few studies have reported the comparison of motion behaviour of spread moored and turret moored FPSOs under varying environmental loads and their susceptibility to green water and subsequent downtime in their life-cycle. Also, it is noted that very few studies are conducted on life-cycle costing methodology for FPSO, while no studies have reported cost comparison for ET, IT, RTM and SM FPSOs and impact of choosing converted hulls on their life-cycle cost, albeit that life cycle costing analysis for ships have been reported as investigated by Gratsos et al [13]. Detailed knowledge gaps from previous studies are discussed later in the chapter in section 2.3.

2.2.1 Dynamic Analysis of SPM and Ships

The preceding developments in the field of dynamic analysis of ship shaped vessels have given ample insight on the dynamic behavior of FPSOs. Researches were conducted to study the dynamic response of SPM and ships using model testing and numerical investigations.

2.2.1.1 Model testing on SPM and ships

Pinkster et al [10] studied the role of model tests in the design of single point mooring (SPM) terminals attached to a tanker. They gave necessary information regarding how to set up test programs, the scope of tests, the characteristics simulated, and measurements carried out, possible sources of error and analysis of results. They concluded that the results from the model tests should be used without applying any correction to rectify error due to scale effect because of uncertainties exist concerning the drag coefficient of prototypes. Since Froude scale of models are used, viscous force will be overestimated, but the significance of inertia and wave effect on the structure

can be effectively presented. Mansard et al [14] conducted physical model tests to show the effect of wave grouping on moored vessel response. It was shown that the wave grouping present in irregular waves is an important parameter in assessing vessel response and a correct reproduction of bounded long wave component is required in model studies to get a realistic response of vessels. Chakrabarti [15] gave emphasis on the sea keeping and towing tests of an offshore structure on station or in transit and gave an insight in to the difficulties in conducting tests and the remedial measures used in the setup. Fournier et al [16] conducted a physical model test to study the ship response to establish critical wave conditions that cause excessive vessel motions for safe/ efficient cargo transfer.

2.2.1.2 Numerical investigation of SPM and ship motions

The preliminary step in the calculation of vessel responses are the computation of added mass, damping and exciting force which is then incorporated to the equation of motion along with mass and restoring matrix. Korvin-Kroukovsky [17] developed the first motion theory in this field which was used for computation of vessel responses. It was later found that, there were inconsistencies in this theory in the mathematics and Salvesen et al [18] modified it. Newman [19] developed unified slender body theory, which was later extended to a diffraction problem by Sclavounos [20].

Unlike Strip theory and unified slender body theory, 3D methods like Green function method and Rankine Panel method can give detailed force distribution over hull surface of large structures. Chang et al [21] and Inglis et al [22][23] proposed the Green function method which is later extended by Wu et al [24] and Chen et al [25]. While Green function method uses a time harmonic function with forward speed on the free surface, Rankine Panel Method which was initiated by Dawson [26] uses Rankine sources on body surface as well as free surface, allowing more general free surface conditions to be used. These 3D methods have proved to give better agreement with

the experimental data [27], at the same time, strip theory requires only less computational effort and gives reliable reasonable results for engineering applications. Also, the 3D method requires the user to input the full 3D vessel co-ordinates while Strip theory requires only the cross-sectional water line breadths, draft and area, if the conformal mapping technique is used.

Vugts [28] conducted experimental and theoretical investigations to determine the hydrodynamic coefficients and exciting forces in swaying, heaving and rolling for 2D cylinders with various cross-sections in beam sea condition. The results can be used to predict the hydrodynamic coefficients and exciting forces of matching Lewis forms or actual section fits. The sway and heave results showed good agreement. The simpler force calculation derived by Newman [29] fits the experimental results for exciting forces by Vugts [28], but it does not predict the phase angles. His studies also prove that the force and moment calculation using Froude-Krylov hypothesis underestimates the actual wave force and moment. Salvesen et al [18] presented the equations of motion for ships which consists of two sets of independent linear coupled differential equations. Since the floating structure under consideration has lateral symmetry, the surge, heave and pitch are not hydrodynamically coupled with sway, roll and yaw. He also derived the equation for the calculation of exciting forces in these degrees of freedom.

Journee [30] used two parameter Lewis conformal mapping method to develop a quick strip theory calculation. His approach helps in avoiding the major human error in giving inputs of ship offsets. For this method, only the cross-sectional water line breadths, draft and area is needed. Das et al [31] investigated the coupled sway, roll and yaw responses of a floating body with hydrodynamic coefficients derived from Frank's close-fit curve. His results showed that yaw motions exist for a floating body under the action of regular waves in beam sea condition if the center of gravity of the floating body does not coincide with assumed position of co-ordinate origin and that the magnitude of yaw rotation decreases as the wave period decreases. Hem Lata et al

[32] compared the hydrodynamic coefficients obtained using conformal mapping and state of the art analysis software AQUA and SESAM. The recurrent form of Bieberbach Method was used for conformal mapping and the results were agreeing with a maximum error less than 10%. Fan et al [27] computed ship motions based on methods provided by Salvesen et al [18] in time domain and seconds in applying a correction factor to the roll damping coefficients to achieve accurate results. Momoki et al [33] gives calculation methods for the pressure acting on the hull for analyzing the ship structural response in waves. Ship motion was calculated using a nonlinear strip method. Using this as input to the CFD program, pressures acting on the hull were found. This pressure distribution was used to analyze the ship's structural response using Finite Element Method (FEM).

2.2.2 Dynamic Analysis of FPSO

The foregoing developments in the field of FPSOs have given generous insight on the dynamic behavior of ship shaped FPSO in unidirectional random waves and irregular waves. Researches were conducted to study the dynamic response of FPSO using both model testing and numerical experiments utilising coupled and uncoupled approach. Wichers [11] initiated a comprehensive study for numerical simulations of a turret moored FPSO in irregular waves with winds and currents, neglecting the inertia and damping effect of mooring lines. A procedure to obtain practical values of added mass and damping to calculate the nature of the stability and natural frequencies of the system was also given by him. The uncoupled analysis technique was later found to give smaller values for the motion response after verification through a multitude of experiments and analysis techniques by several scholars.

Low frequency and wave frequency motions of FPSOs due to environmental loads were studied by Jiang et al [34], putting forward the possibility of large amplitude slow drift oscillations in the horizontal degree of freedom due to low frequency wave

components. However, heave, roll and pitch motions are significantly affected by the presence of first order wave excitations [35]. Heurtier et al [36] compared the coupled and uncoupled analysis for a moored FPSO in harsh environments and suggested that the uncoupled analysis results are efficient to be used in the early design phase of the mooring system. There was relatively good agreement between the uncoupled and coupled analysis values even though the maximum values were different; while Wichers et al [37], [38] established the need for including coupling effects between FPSO hull and mooring lines and the effect of viscous damping. These studies showed that, uncoupled analysis will give large errors in the case of FPSOs due to the mooring line interactions; fully coupled time domain analysis is required in obtaining accurate results, was their final respective conclusion.

Lou et al [39] studied the FPSO motions using both coupled and uncoupled time domain analysis methods and suggested coupled analysis should be the preferred method for investigating FPSO responses; Lou also concludes that model testing should be combined with numerical analysis for accurate prediction of system responses as model testing alone is not sufficient. Low et al [40] developed a computer program to calculate the coupled motion response of floating structures. The program used both frequency domain and time domain approaches to estimate the response. The results obtained after the simulation of a spread moored FPSO in 2000 m water depth under the action of wave with 100 m significant wave height, matched very well for the two approaches. The frequency domain method gave good results where the geometric non-linearity is not prevalent.

Tahar et al [41] developed a hull/mooring/riser coupled analysis program for a turret moored FPSO in the presence of wind, wave and current to understand the motion characteristics, coupling effects and the role of various hydrodynamic contributions. The results obtained were compared with MARINS wave tank test results. The numerical time domain program developed by Kim et al [42] to calculate vessel and line dynamics were validated using OTRC wave basin model testing results, and are

matching very well except for roll motions. This discrepancy can be attributed to the use of truncated mooring system which underestimates the dynamic mooring tension.

Some of the reported studies on FPSO were carried out by providing additional attachments on FPSO and by varying the usual ship shape of FPSO. Priyanto et al [43] examined the wave exciting surge forces on FPSO when provided with a submerged plate on lee side of FPSO using numerical method based on diffraction theory and the results were verified by conducting experimental tests. He concluded that, at low frequencies, the surge forces are effectively reduced due to the presence of submerged plate. Siow et al [44] provided preparatory procedures for round shaped FPSO model testing and details on mooring design and model set up. The vertical motion of FPSO experienced only wave frequency motions. Siow et al [45] also conducted model tests to study the effect of different mooring system on FPSO motions. He concluded that the mooring system do not have significant effect on FPSO motions in wave frequency range. He also showed that in wave frequency ranges, absence of mooring lines does not produce any difference in results and is matching with the experimental results.

Long term FPSO responses are found to be critical when compared to other sea states by Vázquez-Hernández et al [46] while Rho et al [47] has studied the FPSO motion responses in most conservative environmental condition with 100-year return period. Fontaine et al [48] reassessed the reliability of mooring system of an existing FPSO in West Africa using field metocean conditions and compared the different design approaches for FPSO. The effectiveness of response based design is emphasized, noting the main drawback as computing time. Ma et al [49] conducted numerical experiments using fully nonlinear potential theory and experimental investigation to study the interactions between a simplified FPSO and focusing waves. The incoming waves produced during experimental tests were reproduced in numerical wave tank by in cooperating a self-correction time domain technique which produced agreeable results with experimental outcome. Feng et al [35] and Chen et al [50] have

demonstrated the efficacy of commercial softwares like ANSYS and SESAM in the modelling and meshing of the FPSO vessel.

Recently, Ji et al [51] has studied the influence of middle water arch in FPSO motion response and its capability of suppressing FPSO motions except heave. Kang et al [52] conducted fatigue analysis on mooring lines of a spread moored FPSO and observed that it is highly impacted by the wave frequency motions of FPSO. Lopez et al [53] conducted experimental investigations using hybrid passive truncated FPSO and mooring model to assess hydrodynamic performance of a proposed FPSO in Gulf of Mexico at a water depth of 1000 to 2000 m. The surge motion of FPSO was found to be twice in non-collinear environmental loads when compared to be under the influence of collinear loads and the mooring lines are more sensitive to dynamic response in non-collinear condition. Hong et al [54] investigated the effect of impact load by steep waves on FPSO bow using model tests. The impact loads were found to be increasing with wave steepness and so a recommendation was given to include steep waves in addition to the representative wave condition of significant wave height and pitch forcing period while applying structural load during design of FPSOs in North Sea.

2.2.3 FPSO Motion Response Using Uncoupled and Coupled Analysis

In the traditional methods of vessel response calculation, an uncoupled approach to calculate the same was utilized by considering the load effects from moorings modelled as linear restoring forces applied at nodes of the finite element model of the FPSO. Once the vessel response is calculated, these motions were applied as terminal excitation at the top end of the mooring to calculate the line dynamics. But this approach has many drawbacks such as:

- The current induced mean loads on mooring lines are not considered;
- The damping from mooring lines on LF vessel motion must be simplified;

- Mooring line dynamics is not considered while calculating vessel response.

As the water depth increases, the effect of these drawbacks will increase the inaccuracy of the results [55]. In shallow waters, floater motions are triggered to a large extent by the fluid forces on the floater itself. As the water depth increases, the length of the mooring line increases as does the coupling effects between mooring and FPSO [56], [57]. Where the non-linearities are not prevalent, uncoupled frequency domain analysis gives good results [40], [58]. So, to study the floater responses due to the change in hull dimensions, hull loading conditions and for water depth parametric studies below 100 m, uncoupled analysis seems to be a good choice and can be time saving. First order motion responses could be studied using an uncoupled approach where non-linearities from mooring lines are not the primary concern of the study, although mooring lines affects the mean position of FPSO in low frequency regime [59], [39]. However, change in these mean offsets are not the primary concern of this research. Wave frequency regimes fall between wave frequencies 0.2 rad/s – 2 rad/s with low frequency regimes for wave frequency around 0.02 rad/s [40]. The first harmonic wave energy is contained in the wave period range of 5 s – 25 s [56]. The effect of spread mooring system on the linear wave induced motion is generally quite small. In special cases, like in higher wave periods (greater than 25 s is a rare occurrence), the mooring system will have an influence [60]. This allows the usage of uncoupled frequency domain analysis tools like wadam wizard in SESAM HydroD to be used for finding motion RAOs.

However, in deep waters, the effect of geometric non- linearities and cable dimensions affect the system response in two ways. Firstly, the restoring forces of the vessel due to the mooring lines are affected. Secondly, large changes to the line configuration affect the dynamic response characteristics and damping levels provided to the vessel [58]. The presence of mooring and risers introduces sources of damping that are not included in the classical roll damping problem used in uncoupled analysis [61]. Coupling effects are contributed by static restoring forces, current loading,

mooring line damping effect, hull/mooring contact and additional inertia forces other than that of a hull [55]. These effects are considered in a fully time domain coupled analysis. Hence when the effect of mooring line dimensions and metocean conditions on FPSO motions are studied, coupled analysis is a must to obtain accurate results in deep waters. SESAM DeepC is a fully coupled time domain program that can be used for dynamic analysis of deep water floating bodies [58], [55]. It utilises an implicit time stepping scheme and the dynamic equation of motion is solved by equilibrium iterations at every time step. Material non-linearity, geometric non-linearity, explicit loads and hydrodynamic loads can be effectively treated using DeepC [55].

2.2.4 FPSO Motion Response using Model Testing

Literatures pertaining to the modelling of FPSO hull and mooring system are reported below.

2.2.4.1 Modelling of FPSO

The choice of FPSO model scale depends on water depth of the basin, accuracy of results (the smaller the model, less accurate results) and capability of generating required wave height and period at a particular scale in the basin. There are mainly two ways to relate the prototype and model. One is by matching the non-dimensional terms developed by inspection analysis of the mathematical description of the physical system under investigation. In this method, the equality of the corresponding non-dimensional parameters in model and prototype govern the scaling laws. The non-dimensional form of differential equations derived from the physical system dynamics is ensured to be duplicated by the simulated physical system. The non-dimensional quantities in the differential equations must be equal for both model and the prototype; albeit that this method can be adopted only when the governing equation of the prototype and the

model is explicitly known. The second method is based on Buckingham Pi theorem by relating the model properties to the prototype properties. In this method, the important variables influencing the dynamics of the system are identified first along with their dimension. Then, from these variables, an independent and convenient set of non-dimensional parameters is constructed. The similitude requirements are yielded from the equality of the pi terms for the model and the prototype. The model and the prototype structural systems are similar if the corresponding pi terms are equal [62].

Table 2.1: Scale Factors as per Froude's Law of Similitude [62]

Variable	**Quantity**	**Scale factor**
Length	L	λ
Area	L^2	λ^2
Angle	none	1
Mass	M	λ^3
Time	T	$\lambda^{1/2}$
Acceleration	LT^{-2}	1
Velocity	LT^{-1}	$\lambda^{1/2}$
Variable	**Quantity**	**Scale factor**
Spring constant	MT^{-2}	λ^2
Force	MLT^{-2}	λ^3
Wave height	L	λ
Wave period	T	$\lambda^{1/2}$
Wave length	L	λ
Density	ML^{-3}	1

Where the action of waves and the inertia of the body is predominant, the law of similitude between prototype and model is formulated using Froude's law [10]. If λ is the linear scale factor, application of Froude's law of similitude results in the scaling shown in Table 2.1 to be adopted for model testing [62]. Using these scale factors, adjustments for water depth, centre of gravity of model and calibrations for wind,

current and wave can be done prior to the actual model tests [62]. These adjustments and calibrations are done before keeping the model in the basin [10]. The spectral energies of the generated wave are compared with the numerical one and adjusted through an iterative procedure until the required accuracy is obtained [62].

Wood is used to construct the models of FPSO hulls. The principle of physical pendulum is used to adjust the longitudinal weight distribution and the transverse stability is adjusted by means of inclining tests [10]. While ballasting the model to adjust the CG, Moment of Inertia and draft, it is better to use weight than to use water to avoid sloshing and alteration of loads acting on it. Once the mooring lines are attached, the natural periods of the system can be found by conducting free decay tests [62].

2.2.4.2 Modelling of mooring lines

Horizontal mooring lines are reported to be used to restraint FPSO during model tests under the action of unidirectional waves, regular waves and current [63] [64]. Horizontal soft moorings are mostly used due to the limitation in maximum water depth in the wave basins. To model the mooring lines and the associated viscous effects, Reynold's scaling should be adopted and the model should be comparatively big [62]. This is not possible in wave tanks with depths of 1 m. Also soft mooring lines are preferred over stiffer ones in model testing, so that the wave induced vessel motion will not be affected while enough restoring forces and moments sufficient to prevent large drift motions are given [59]. In such circumstances, truncated mooring systems can be used along with a numerical tool to extrapolate them to full depth (Hybrid verification method) [55]. But, it underestimates the dynamic mooring load and the dynamic similitude is very hard to achieve even if clumps/buoys and springs are used to match the surge stiffness in model testing by Kim et al [42]. Also, the effect of mooring lines on FPSO motions are quite small in shallow waters at WF [59], [60]. Hence soft

horizontal mooring with negligible mass and damping will be ideal to be used under such circumstances.

2.2.5 Hydrodynamics of FPSO

2.2.5.1 Representation of wave

Theoretical simulation of water waves and sea motion, in general involves rigorous mathematical analysis. The basic hydrodynamic equations that govern the wave kinematics are the equation of continuity (Laplace's equation) and the equation of the conservation of the momentum (Bernoulli's equation). The form and solution of these equations vary depending on the intended application of the wave kinematics. However, in general, all solutions assume incompressible, inviscid and irrotational fluid particles. The solution of the boundary value problem can be solved in different ways using the existing wave theories [65]. The simplest solution of the hydrodynamic equations involves further assumption, that the waves are of small amplitude compared to the water depth and the wave length. This solution was introduced by Airy (1845) and became known as the linear Airy wave theory or sinusoidal wave theory [66], [65]. This assumption allows the free surface boundary condition to be linearized dropping the wave height terms beyond first order. It was shown to provide a good solution in deep water when water depth to wave length ratio is greater than 0.5 [67]. For the range of water depths, wave periods and wave heights used for the first order analysis using regular waves, the linear wave theory was used since it is simple and reliable over a large segment of whole wave regime and sufficient to obtain the kinematics of waves to be used in the analysis of FPSO in deep water [65]. A schematic diagram of an elementary, sinusoidal progressive wave is presented in Figure 2.1.

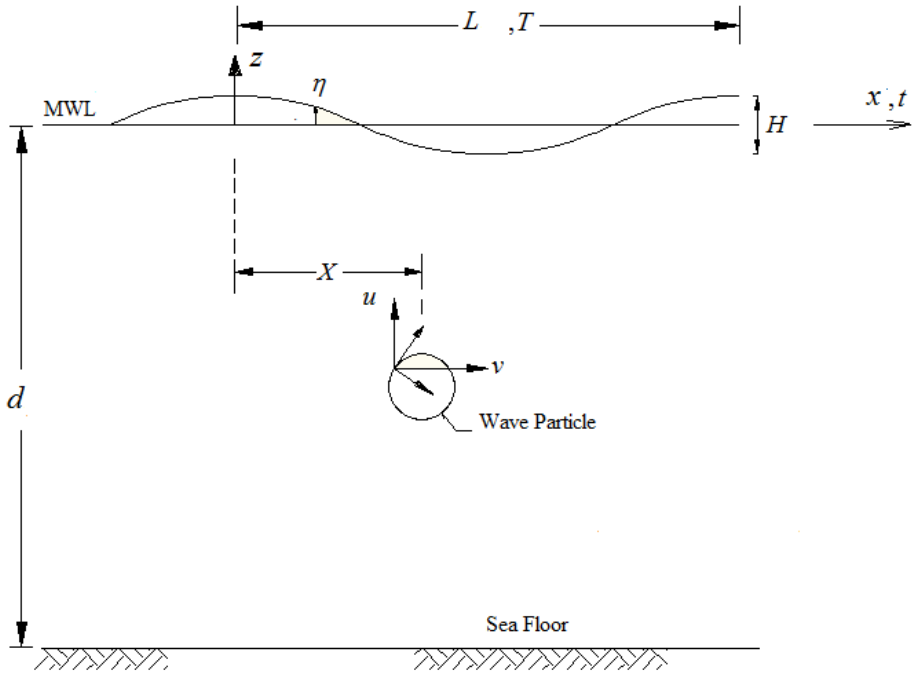

Figure 2.1: Schematic Diagram for a Progressive wave in x direction

In representing the random sea state, mathematical spectrums are widely used, which are based on significant wave height, wave period or shape factors [65], [67], [42]. Two of the most commonly used spectrums are Pierson-Moskowitz (P-M) spectrum with single parameter (based on either significant wave height or wind speed) and JONSWAP five parameter spectrum; usually three parameters held constant, which describes fully developed and fetch limited seas respectively [68], [65].

The JONSWAP spectrum, which was derived from fetch-limited measurements made in the North Sea has a mean shape represented with a peak enhancement factor, γ, equal to 3.3, which in engineering application is often adopted on the assumption that this spectral shape is valid for all locations with the North Sea known for the most hostile weather conditions [68]. The JONSWAP spectrum model is given by Eq. 2.1 [65].

$$S(\omega) = \frac{0.0081g^2}{2\pi^4}\omega^{-5}\exp\left[-1.25\left(\frac{\omega}{\omega_o}\right)^{-4}\right]\gamma^{exp\left[-\frac{(\omega-\omega_O)^2}{(2\tau^2\omega_o{}^2)}\right]} \quad (2.1)$$

where

$$\omega_o = \frac{0.161g}{H_s} \tag{2.2}$$

Also P-M spectrum was widely used by the engineers as it is one of the most representative spectrum for many areas over the world [67]. The P-M spectrum model is mathematically represented as shown in Eq. 2.3 [65].

$$S(\omega) = \frac{0.0081g^2}{2\pi^4}\omega^{-5}\exp\left[-1.25\left(\frac{\omega}{\omega_o}\right)^{-4}\right] \tag{2.3}$$

2.2.5.2 Wave force on FPSO

Since FPSO is a very large structure compared to the wave length of the incident wave, the incident wave reaching the structure experiences scattering from the surface of the structure in the form of reflected wave that is of the order of the magnitude of the incident wave. In this case the diffraction of the waves from the surface of the structure should be considered in the wave-force calculations [27] . Under diffraction theory, the basic flow is assumed to be oscillatory, incompressible and irrotational so that the fluid velocity may be represented as the gradient of a scalar potential, ϕ. In diffraction potential theory, the total velocity potential representing the flow around the hull is obtained as a sum of the incident (ϕ_0) and scattered potential (ϕ_s) [65].

$$\phi = \phi_0 + \phi_s \tag{2.4}$$

It satisfies the Laplace equation given in a rectangular Cartesian coordinate system OXYZ as shown in Eq. 2.5 within the fluid region where $\phi = \phi(x, y, z)$ and (x, y, z) are the coordinates of a point in the fluid at which the potential ϕ is calculated at time t [65]. The definition of the boundary conditions for the linear diffraction problem is given in Figure 2.2.

$$\nabla^2\phi = \frac{\partial^2\phi}{\partial x^2} + \frac{\partial^2\phi}{\partial y^2} + \frac{\partial^2\phi}{\partial z^2} = 0 \tag{2.5}$$

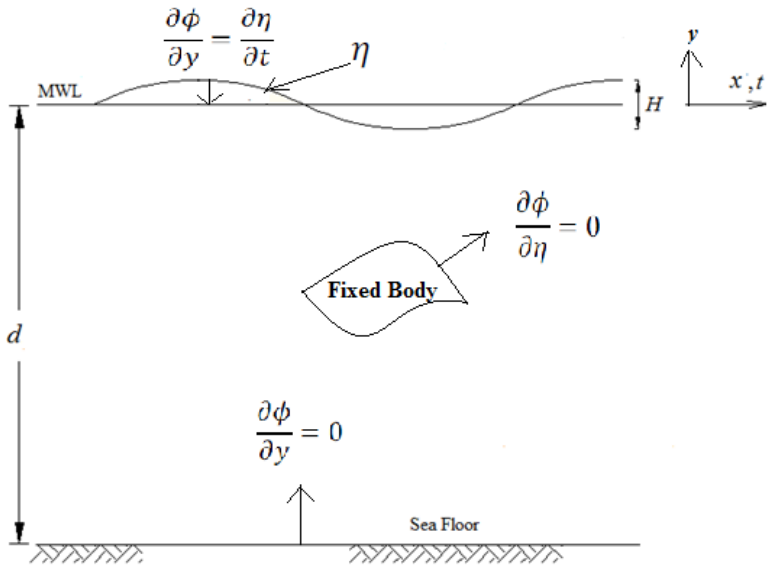

Figure 2.2: Definition of Boundary Conditions for the Linear Diffraction Problem

The free surface boundary conditions are [65]:

1. Dynamic Boundary Condition

$$\frac{\partial\phi}{\partial t} = g\eta + \frac{1}{2}\left[\left(\frac{\partial\phi}{\partial x}\right)^2 + \left(\frac{\partial\phi}{\partial y}\right)^2 + \left(\frac{\partial\phi}{\partial z}\right)^2\right] = 0 \text{ on } y = \eta \tag{2.6}$$

2. Kinematic Boundary Condition

$$\frac{\partial\eta}{\partial t} + \frac{\partial\phi}{\partial x}\frac{\partial\eta}{\partial x} + \frac{\partial\phi}{\partial z}\frac{\partial\eta}{\partial z} - \frac{\partial\phi}{\partial y} = 0 \text{ on } y = \eta \tag{2.7}$$

3. Bottom Boundary Condition

$$\frac{\partial\phi}{\partial y} = 0 \text{ on } y = -d \tag{2.8}$$

4. Body surface Boundary Condition

$$\frac{\partial \phi}{\partial \eta} = 0 \text{ on } -d \leq y \leq \eta \tag{2.9}$$

The problem is to solve for the velocity potentialϕ, where ϕ is the sum of incident potential, ϕ_0 and scattered potential, ϕ_s. The incident potential satisfies the boundary value problem mentioned above in the absence of the structure with a change in body surface condition as shown in Eq. 2.10 [65].

$$\frac{\partial \phi_0}{\partial \eta} = \frac{\partial \phi_s}{\partial \eta} \text{ on } -d \leq y \leq \eta \tag{2.10}$$

The additional boundary condition for the scattered potential is the Sommerfeld radiation condition which is stated as below where φ is Eigen values [65].

$$\lim_{R \to \propto} \sqrt{R} \left(\frac{\partial}{\partial R} \pm i\varphi \right) \phi_s = 0 \tag{2.11}$$

The complete boundary value problem is highly nonlinear, especially because of the free surface boundary conditions. Once ϕ is solved for boundary value problem, the pressure on the surface, p of the body and water particle velocities can be calculated as [65]

$$u = \frac{\partial \phi}{\partial x} \tag{2.12}$$

$$v = \frac{\partial \phi}{\partial y} \tag{2.13}$$

$$w = \frac{\partial \phi}{\partial z} \tag{2.14}$$

$$p = \rho \frac{\partial \phi}{\partial t} + \frac{1}{2} \rho (\nabla \phi)^2 \tag{2.15}$$

Once pressure is known, the force in specific direction is obtained from the integration of the component of the pressure in that direction over the submerged surface [65]. This

method is used in the 3D diffraction analysis of floating structures [55]. Instead of solving the total velocity potential function ϕ ,the diffraction problem can be solved using other methods like strip theory as well using approximations to calculate the hydrodynamic coefficients [29], [18] and subsequently the responses.

2.2.5.3 Wave force on mooring lines

Since mooring lines are slender members compared to the wave length, Modified Morison equation is used to calculate the wave load acting on them. The original version of was proposed by Morison [69] for the evaluation of the exciting wave force on vertical pile, which composed of two inertia and drag components. This equation is considered semi-empirical equation and was proved reliable for evaluating forces on slender rigid cylinders. Later, for compliant structures the original force equation can be modified to account for relative velocity and acceleration between the structure and the fluid particles. The drag F_D and inertia F_I forces on an element of a unit length of the cylinder are given by Eq. 2.16 and Eq. 2.17 respectively. This formula of the force equation was used for evaluation of wave frequency forces.

$$F_D = \rho C_d \frac{D}{2} U_{rel}|U_{rel}| \tag{2.16}$$

$$F_I = \frac{\rho\pi D^2}{4}\left(C_m\dot{U} - C_A\ddot{X}\right) \tag{2.17}$$

Where U_{rel} is relative velocity between structure and wave [65], [55], [70].

2.2.6 Operability Conditions for FPSO and Downtime Cost

FPSO operability is determined based on ability of FPSO to perform under extreme weather conditions without interrupting the offloading operation and processing on deck. Factors affecting the operability of FPSO are identified as follows:

1. Offloading operability: FPSO should avoid fishtailing motion (i.e. large sway and yaw motion) mainly applicable to turret moored FPSOs while high amplitude low frequency horizontal FPSO motions (Surge, sway and yaw) should be avoided as well for both turret moored and spread moored FPSOs [4].

2. Green water impacts: When relative motion of waves and FPSO heave motion (deck clearance against green water) exceeds freeboard, impact loads are placed on deck due to green water. These events can even result in fatalities if accommodation modules are affected by the impact. In the event of impact to processing plants, loss of containment may occur. These events can cause operational downtime and subsequent loss in oil production [7]. Green water height on FPSO deck should be less than 3 m to have low level of risk associated with it.

3. Excessive vertical motion of FPSO: Excessive heave, roll and pitch motion can affect processing on board FPSO and crew habitability. Extreme motions in heave, roll and pitch occurs in WF ranges [71]. Roll motion of FPSOs should be within ±5° to enable crew habitability [61].

Green water on FPSO deck should be minimised to achieve safe operation period and avoid damage to equipments on board FPSO. Related to FPSO station keeping capabilities, accepted risk level for loss of production by Whitman [72] is exceeded if the probability of occurrence of green water exceeds 0.01 and if FPSO motions exceeds acceptable limit with a probability of occurrence higher than 0.001. Studies should be aimed at reducing such risks so that both loss of life and loss in production could be avoided.

FPSO parameters conductive to occurrence of phenomena disrupting operational time are large vertical motions of ship because of length of ship, continuously changing FPSO draft and heavy weather conditions [73]. In actual, all the six FPSO motions should be minimised to ensure safe processing and offloading operation. The following section details the previous efforts taken to conduct parametric studies to optimise

FPSO motions, influence of environmental loads on FPSO motions, green water effects due to vertical motions of FPSO and operability analysis undertaken to calculate FPSO downtime due to these vertical motions and green water impacts.

2.2.6.1 Parametric studies for environmental loads and water depth on FPSO motions

Li et al [74] investigated the motion performance of a fully loaded single point moored FPSO in heave, roll and pitch in water depth varying from 21 m to 26 m for 100-year environment condition. He used water depth to draft ratio ranging from 1.3 to 1.1 and the results shows that as the water depth decreases, the WF motions of the FPSO decreases in shallow water. Wang et al [75] studied the surge, heave and pitch motions of a FPSO with soft yoke mooring system using ANSYS AQUA, comparing Newman's approximation and Pinksters method for water depth varying from 20 m to 33 m. Result using Newman's approximation differed from the results from later and concluded that it is due to the inclusion of second order forces in Newman's approximation. Hence a model test to study the variation of FPSO surge, heave and pitch motion in water depth up to 100 m is of interest to arrive at conclusion regarding the motion behaviour of FPSO since the shallowest oil field in Malaysia is at 55 m in Berantai oil field and in Australia is at 78 m in Cossack-Wanaea-Lambert-Hermes.

Soares et al [76] concluded in his study that surge, heave and pitch motions of a turret moored FPSO varied linearly with significant wave height and reported that the surge motion for turret moored FPSO decreases while heave and pitch increases. The motions are reported to be varying linear with wave height [77], however a detailed investigation comparing all the 6 motions of FPSO for spread mooring and turret mooring configuration has not reported before and the trend in variation of vertical and horizontal motions of FPSO while different mooring are used. This is very much in need as the vertical motions of FPSO highly determines the mooring system employed and there by associated costs in the life-cycle of FPSO.

Caire et al [57] studied the effect of wave directionality on FPSO riser top tension responses and concluded that the responses in heave and roll decreases as spreading parameter decreases. Munipalli et al [77] studied the effect of wave steepness on yaw motions of a weathervaning FPSO and observed large yaw rotations for low wave steepness and large wave lengths.

2.2.6.2 Parametric studies for mooring line and hull parameters on FPSO motions

Kannah et al [78] did experimental study on an externally turret moored FPSO of 1:100 scale. The study was conducted for different loading conditions and hawser lengths while the water depth was limited to 1m. Their study reported that the surge RAO increases with an increase in DWT and an increase in hawser length to ship length ratio. They have identified the limitations of their results that, it cannot be applied to FPSOs in deep water. Due to the limitation in water depth modelling in wave tank, a numerical modelling to investigate the effect of mooring line length to ship length ratio is of interest and will aid in filling the knowledge gap.

Kannah et al [79] also studied the effect of turret position on FPSO motions and found that keeping turret in forward position reduces surge, heave and pitch motion when compared to keeping it in midship. Yadav et al [80] conducted parametric study on a weathervaning FPSO studying the effect of turret position and hull length on FPSO yaw motion. It was observed that yaw motion is more influenced by ship length to wave length ratio than natural roll period and the horizontal offset increased as turret moved close to mid-ship. However, the effect of spread mooring fairlead on FPSO motion has not been reported before.

Baghernezhad et al [81] compared the effect of FPSO shape in the overall performance. He studied both ship shaped and cylindrical shaped FPSO in full loading condition at a water depth of 100 m. They concluded that cylindrical FPSO

performance is better in terms of stability, sea keeping, mooring and riser tension as it absorbs less energy from waves due to its geometry.

Montasir et al [82] studied the effect of mooring line azimuth angle on a turret moored FPSO's heave, pitch and surge motions. The heave motion was observed to be highly sensitive to increase in azimuth angle from 30º to 60°.

2.2.6.3 Metocean conditions and FPSO motions

The presence of current and wind can significantly influence the wave viscosity. Viscous damping was found to be increasing linearly with the tanker surge velocity [62], also mentioning that when current is introduced, the amount of viscous damping in wave increases. As per Ewans et al [83] wind has a greater part in determining the heading of the turret moored FPSO. Hassan et al [84] studied the effect of current in the damping ratio of the system for a catenary and horizontal mooring system. For both the systems, the damping ratio of the system increased after introducing current. The damping of the catenary mooring system was higher when compared to that of the horizontal mooring system due to the interaction of mooring lines with wave and current.

The current loading on the mooring system may dominate the total steady force while slowly varying wind loads may give rise to LF motions in horizontal directions. Also, wind and current can sometimes induce fishtailing effects in the FPSO motions by inducing unstable coupled sway and yaw motions [56]. Stansberg et al [85] deduced that the wave-current interaction effect on FPSO and semisubmersible motions can be much larger when compared to the effects from current and wind alone. Teles et al [86] conducted model testing and sensitivity study to investigate the wave current interaction effects and found that the mean horizontal velocities near the free surface are significantly affected by the introduction of current in the presence of waves.

The presence of wave-current –wind interaction is shown to affect the FPSO motions significantly from the previous studies. The choice of the mooring system is based mainly on the floater motions [9]. Hence a thorough study is required to determine the variation of floater motion in the presence of wind, wave and current.

2.2.6.4 FPSO motions and green water effects

Green water is defined as unbroken waves overtopping FPSO deck [87]. Buchner [88] studied the impact of green water on FPSOs using model tests. He considered the relative motion of FPSO with respect to wave height, water flowing on to the deck and water hitting FPSO. He concluded that green water effects are sensitive to wave height, wave period and current velocity. He [8] also studied the impact of green water through the sides of a weathervaning FPSO and linear diffraction theory may be used to assess the green water effects in the preliminary design phase [71] [89]. Nielson studied green water loads on ships having forward velocity using numerical methods [90]. Buchner et al suggests the use of 3D diffraction theory to predict green water incidents [91].

Kleefsman et al performed green water simulation for FPSO using a domain decomposition method. The method of decomposing far field and near filed of FPSO gave good results when linear diffraction theory was used to represent far field. Local flow around deck was simulated using Navier-Stokes solver [92]. Lu et al [93] studied the green water effect on moored FPSO, freely floating FPSO and a side-by-side moored FPSO/LNG in extreme waves and he was successfully able to model the highly non- linear interactions and mooring effects. Tao et al [94] detailed the simulation of green water using numerical and experimental methods. Akandu et al [95] developed a numerical program called ProGreen to optimise the principal dimensions of FPSO based on freeboard exceedance analysis. Veer et al [96] emphasized the importance of model testing in green water flow analysis and gave detailed description of three typical

flooding events by experimentally studying the phenomenon using deck mounted wave probes and on-board video.

Recently, Werter [97] investigated the short term and long-term probability of green water on FPSO and used ANSYS Aqwa to generate vessel motion RAOs. It was seen that ANSYS Aqua generated motion RAOs higher than DNV software. Zhang et al [98] investigated overtopping through a CFD tool and proposed to use relative overtopping duration to combine the coupled effects of overtopping duration and freeboard exceedance to estimate damage on deck.

Green water on FPSO is now recognized as an important aspect during the design of FPSO [71] and deck and topside design should be considered as an ultimate limit state rather than accidental limit state criteria [7]. Green water impacts can have dangerous effects on processing facilities on FPSO deck [71]. This event is likely to occur in low wave height and period and in conditions lower than design criteria where the wave height and period could be close to 1-year return period conditions than the design 100-year period. The largest relative wave elevation occurs when wave length is equal to ship length [99]. Also, freeboards may be insufficient to prevent this from happening at high loading condition of FPSO [87]. Freeboard exceedance is categorised into low, medium and high levels. Low level of freeboard exceedance is when the water height is less than 3 m, medium level when it is between 3 m and 6 m and high level of susceptibility if it is above 6 m of water height. Buchner assumed freeboard exceedance limit of 2.8 m to be acceptable [99].

2.2.6.5 Operability analysis

Workability or the operability of an offshore structure is whether it is capable to operate in wind, wave and current where it is installed in a safe and reliable functioning condition. Wal et al outlines the scatter diagram and scenario based method to calculate

workability of offshore structures. He developed a tool called Dredsim 2000 to calculate the workability of dredging tools used in oil and gas industry [100].

Djatmiko et al studied the operability of FPSO based on green water and slamming effects and observed that most persistent green water loads are at the fore upper deck at 15% LBP from FP and downtime is increased when FPSO draft was changed to 9.92 m from 8.05 m [101]. Ewans et al studied the heave, roll and pitch motions of a FPSO to determine operability conditions for locations at offshore Namibia and at west coast of New Zealand where the swells act perpendicular to wind sea [83]. Correa et al investigated offloading downtime of a spread moored FPSO in tandem with a dynamically positioned shuttle tanker. He observed that by incrementing angle that defines the area where the shuttle tanker is allowed to weathervane, offloading downtime was reduced [102].

Downtime due to green water in location under consideration is of great interest as no reported studies have previously assessed the same. Also, the results generated will aid in the choice of mooring system in these locations based on both cost and motion criteria.

2.2.7 Life-cycle Cost Analysis

2.2.7.1 Definition of LCCA

LCCA is defined as the process of economic analysis to assess the total cost of acquisition and ownership of a product over its life-cycle or a portion thereof [103]. The main objective of LCCA is to quantify the total cost of ownership of a product or a project throughout its full life-cycle, which includes research and development, construction, operation and maintenance, and disposal or reuse. Life-cycle costing is a concept used for making decisions between alternative options, optimizing design,

scheduling maintenance and revamping project planning. The option identified with the highest net present value is the most economical or least cost option/ approach [104]. The two major factors that influence such options are scalability and customizability and thus such new concepts need powerful life-cycle cost models that can cope with the influence of scale and customer requirements on the whole life cycle [105].

2.2.7.2 Benefits of LCCA

The benefits of doing LCCA are as follows [106], [107]:

- It results in earlier actions to generate revenue or to lower costs than otherwise might be considered.
- It ensures better decision from a more accurate and realistic assessment of revenues and costs, at-least within a particular life-cycle stage.
- It promotes long-term rewarding.
- It provides an overall framework for considering total incremental costs over the life span of the product.

2.2.7.3 Previous studies using LCCA

One of the earliest recognizable LCCA application in civil engineering is the World Bank Highway Cost model in 1969. Life-cycle costing application in offshore structures is a relatively new research area and some of the previous studies using LCCA for offshore structures are reported below.

Nam et al [108] developed a new life-cycle cost methodology with the risk expenditure taken in to account for comparative evaluation of offshore process options at their conceptual design stage. The risk expenditure consisted of the failure risk expenditure and the accident risk expenditure. The former accounted for the production loss and the maintenance expense due to equipment failures while the latter reflected the asset damage and the fatality worth caused by disastrous accidents such as fire and explosion. It was demonstrated that the adopted LCCA methodology can play the role of a process selection basis in choosing the best of the liquefaction process options including the power generation systems for a floating LNG (Liquefied natural gas) production facility.

Thalji et al [105] conducted a case study on innovative vertical axis wind turbine concept to generate a scalable and customer oriented life-cycle costing model for the same. The cost analysis of the wind turbine concept covers the whole life processes, manufacturing, installation, operating and maintenance. Santos et al [109] developed a theoretical methodology to study the life-cycle cost of floating offshore wind farms. Six life-cycle phases needed to install a floating offshore wind farm was defined: conception and definition, design and development, manufacturing, installation, exploitation and dismantling. They suggested that the proposed methodology could be used to calculate the real cost of constructing the floating offshore wind farms.

Gratsos et al [13] investigates through a cost/benefit analysis, how the average annual cost of ship transport varies with the corrosion additions elected at the design stage. The results of this study clearly indicated that ships built with corrosion allowances dictated by experience, adequate for the ship's design life, when all factors have been considered, have a lower life-cycle cost per annum for the maintenance of the integrity of their structure.

Howell et al [110] discusses the various factors affecting the CAPEX and OPEX of turret moored and spread moored FPSOs and the technical issues related to the design

of mooring system. He also computed the NPV for a spread moored FPSO and a turret moored FPSO in Brazil with 10.5% discount rate. However, the detailed cost estimate was not given. He affirmed that in addition to the CAPEX of both systems, they are different in terms of their motion performance and offloading performance as well.

Dina et al [111] performed LCCA to compare maintenance cost of an oil and gas production facility in the sensitive environment of Arctic, while implementing different technical solutions. Out of the whole life-cycle, only maintenance phase was considered in this study.

Recently, Kurniawati et al [112] evaluated the long-term charter rate in volatile or uncertain condition of FPSO by capital budgeting principal where NPV was one of the evaluation criteria. Miranda et al [113] derived a target reliability index for FPSO for ultimate limit state design of turret moored FPSO's mooring lines for hypothetical tanker dimensions. A life-cycle cost model was used to optimise the disconnection criteria by counting failure instances due to green water, hull and mooring and to obtain design criteria in reliability format. However, the results cannot be generalised as there will be cuts to life-cycle expenditures if the optimisation criteria are implemented. Other than this, there are very limited detailed studies reporting LCCA of FPSOs. Also, there are no previous studies reporting NPV variation when different types of turret mooring are used.

2.2.7.4 LCCA Procedure

The success of LCCA largely depends on the level of accuracy of the cost data in use, variable selection and ensuring that the correct economic criteria are followed [114]. It is a method to evaluate the significant cost for different design options, adding the expenditures and subtracting the revenues and resale values and before choosing the final design with the minimum life-cycle cost, non-economic considerations are given

to accommodate benefits of the project. The primary step in LCCA includes the identification of cost variables [103] [114]. The major steps in conducting an LCCA study are detailed below compiling and summarizing the technique followed by Ferry et al [115] and Kirk et al [116] and the same is given in Figure 2.3 [116].

Step1: Identification of design alternatives to be compared

Life-cycle costing assessment stems from the need to evaluate the true cost of a construction project/asset over its entire life-cycle period. Based on the need and after a brainstorming session, various design alternatives are identified. These alternatives are subjected to an initial screening based on design constraints, benefits measurable in monetary terms, ease of implementation, ability to perform the function and magnitude of savings in the initial design phase. The remaining alternatives are developed to obtain enough data for whole life cost computation [116].

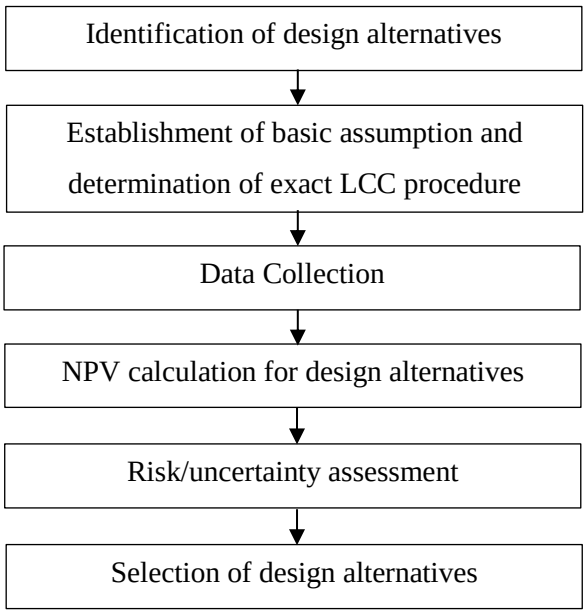

Figure 2.3: LCC Framework

Step2: Establishment of basic assumptions and determination of exact LCCA procedure to be adopted.

Assumptions on life expectancy of asset, period of study, cash flow timings, resale/residual values, inflation, discount rate, source and reliability of data, maintenance policies and comprehensiveness of life-cycle costing is identified as the next step of the procedure. A Discount-rate is required to assist with an understanding of the time value of money such that a dollar today is worth more than a dollar in the future. The discount rate can be calculated from the method specified by Royal Institution of Chartered Surveyors (RCIS) [103].

Step3: Data Collection

Data collection is the most difficult step in the entire phase of LCCA unless a design team can supply the data from their experience and brief the level of cost data accuracy. In its absence, data collection fundamentally depends on networking with expert practitioners related to the specific asset under analysis, literature reviews or modification of available data to suit the study. Because of this, LCCA is done for projects with potential benefits only. Most of the researchers start the data collection by 'estimates' of elemental costs, manufacturer's and supplier's quotations. Monetary costs include, Capital costs (C1), installation costs (C2), operating costs (C3), maintenance costs (C4), refurbishment/replacement costs (C5), downtime costs (C6) and decommissioning/disposal cost (C7). The monetary benefits such as revenue generated (B8) and salvage values (B9) should be subtracted while computing the Net Present Value (NPV) [103]. As per Al- Hajj's study, the absence of sufficient data is seen to be the major barrier in doing a life-cycle cost assessment (LCCA) [117]. Ferry et al [115] observes that the unreal variables can put the findings generated through LCCA in doubt category. Ashworth suggests proper care should be taken to reduce the uncertainty in results [118]. That being said, experienced practitioners' can/do provide suitable datasets.

Step 4. NPV calculation for design alternatives

Life-cycle cost for each life-cycle phase mentioned in step 3 are calculated by applying discount rate and finally summarized to achieve the system LCCA. Once the system LCCA is calculated as per Eq. 2.25, system NPV is calculated as shown in Eq. 2.26 [103].

$$System\ LCC = C1 + C2 + C3 + C4 + C5 + C6 + C7 - B8 - B9 \quad (2.18)$$

$$NPV\ system = \frac{System\ LCC}{(1+discout\ rate)\times period\ of\ study} \quad (2.19)$$

Step 5. Risk/uncertainty assessment

LCCA involves uncertainty in its very nature and the degree of uncertainty determines the degree of accuracy of results. LCCA results are credible only when the uncertainties are considered and sensitivity analysis is performed to do single variant/ multi-variant analysis to study the variation in one parameter by varying a second parameter on which it depends [116]. The output parameter in a sensitivity analysis is always the life-cycle cost of the least cost alternative and the input parameter is always the input cost element. The analysis helps in studying the variation of life-cycle cost for an economic design alternative under varying circumstances where its life-cycle cost can be high and help in finding the breakeven point where the alternative will no longer be cheaper when compared to the next lowest alternative design. Uncertainties can be classified into two: alternative-independent uncertainties (resulting from assumptions concerning all the alternatives to some degree) and alternative dependent uncertainties (due to specific alternatives) [116]. The simplest method in weighing the alternative-independent uncertainties is by using the discount rate in the analysis which is greater than the one in the absence of uncertainty as used by Whyte [103] in calculating NPV of best and worst systems. Alternative dependent uncertainties

are those related to differential escalation rates, obsolescence, cost-estimate accuracy, useful life and physical failure [116].

Step 6. Selection of design alternative

If ‘benefits’ are included in the LCCA study, then NPV or annualized equivalent value of the alternatives are compared while deciding the design alternative. The alternative with negative NPV means the project is going to yield a return lower than its capital cost. If NPV is positive, then the project will bring profit through the implementation of that design alternative. If life-cycle cost of two or more alternatives are found to be equal or within 10% difference, then the nonmonetary benefits like environmental sustainability, aesthetics, safety, expansion potential and obsolescence avoidance are considered. The technique of weighted evaluation is used when nonmonetary benefits are considered [116][103].

2.2.7.5 Limitations of LCCA

The limitations in LCCA study are normal restrictions in every engineering tool. Surpassing these limitations, LCCA has passed the test of time by engineers who combine proper judgement using their experience and knowledge in minimising these limitations. The limitations of LCCA study are [119]:

- LCCA is able to indicate reasonable or unreasonable specification comparisons
- LCCA expertise relies upon a range of subjective experiences of whole-cost.
- Accuracy of LCCA depends on the cost data inputs.
- Errors in LCCA accuracy are addressed chiefly through sensitivity analysis.
- Cost data can be limited, and given its longitudinal nature difficult to obtain.

- LCC models require volumes of data (such as the building specific BCIS) and often non-onshore-construction data is somewhat indicative in nature.

Notwithstanding the limitations above, LCCA is deemed a tried and tested means to better understand design options and minimise the life-cycle cost of projects [119].

2.2.8 Life-cycle costs for FPSO

Every FPSO has a "whole-life" , starting with the conception and definition of FPSO, design/development of the FPSO for serviceability, producibility and safety, followed by extracting the resources and delivering the FPSO by conducting fabrication, installation of FPSO to the offshore field, maintenance, inspection, repair, support and modification of the FPSO or equipment throughout its operational life and finally after the design period of usually 30 years, the FPSO is removed from the offshore field or decommissioned or converted for other purpose [110], [120]. Figure 2.4 shows the life-cycle of FPSO.

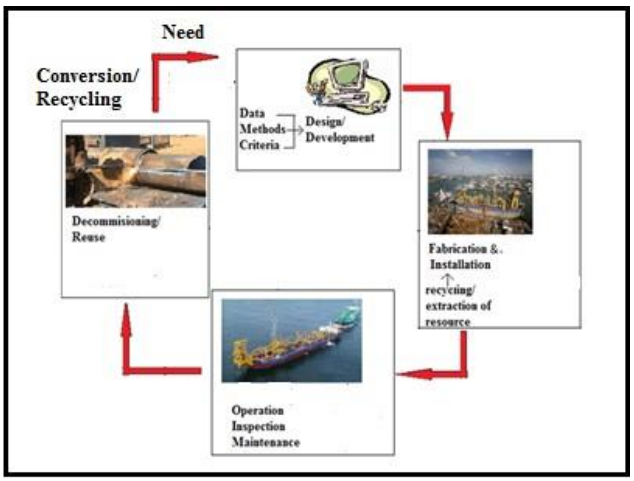

Figure 2.4: Life-cycle of FPSO

The cost variables considered for each life cycle phase of FPSO is summarized as follows:

a) Capital cost (C1): The capital expenditure for an FPSO includes cost of materials for a newly built hull or purchase fee for second hand hull and conversion cost for second hand hull. The conversion costs also include cost of fabrication to install mooring system as well, since it is not designed for oil drilling purposes, while a purpose-built tank is built with the facility to install mooring system based on the area it is going to be installed. Also, cost of materials for topside, cost for labour charges in design, development and construction of FPSO or cost of labour charges in planning and carrying out modification for converted tanker (professional design fee, construction supervision fee and labour charge for workers) should also be considered. The costs for equipment hired for construction should also be considered [110], [120].

b) Installation cost (C2): Installation cost for the FPSO includes the cost for transport of FPSO from dock to the oil field. Sometimes only the fuel charges and ship personnel charges needs to be considered if the FPSO sails to the field of location. If the FPSO is towed to the location, then the cost for towing arrangement, emergency anchor and bunkering arrangements should be considered in addition to the labour charges of riding crew and warranty surveyor. The other costs arise from installing the mooring and riser system. The related labour costs and equipments costs will also fall under installation costs [110], [120].

c) Operation cost (C3): The operation costs for the FPSO mainly consists of the cost of fuels and electricity in running the plant, labour charges for FPSO crew and technicians and cost of rented equipment. This may vary for old and new tankers based on efficiency. This is the phase were oil production revenue is addressed (B8) [120].

d) Maintenance cost (C4): Maintenance costs mainly consists of labour charges for inspection personnel, technicians and cleaners and the like. The cost of dry dock hiring for planned maintenance schedules should also be considered [110].

e) Refurbishment/ Replacement cost (C5): Cost of materials for planned replacements and cost of equipment for carrying out the same are calculated in this phase. Material, equipment and labour costs for covering irregularities in hull integrity and storage compartments should also be considered [110], [120].

f) Downtime cost (C6): Downtime costs arises from shutdown of oil drilling due to unfavorable weather or accidents, green water events and mooring line damages. The cost is calculated in terms of transporting the crew back to onshore facilities (costs of hiring helicopter) and loss in terms of time value of money (unable to drill and produce oil). Especially in the case of converted tankers, frequent mooring line damages are reported. The replacement costs for moorings are higher and to be calculated based on average number of damages reported. Labour charges for inspecting accidental damages and break downs should also be counted for [110], [120].

g) Decommissioning/Disposal cost (C7): Once an oil field is fully exploited, FPSOs are either transported back to onshore facility or to another oil field. FPSOs are seldom dismantled or discarded like fixed offshore structures. They are converted for other purposes or may be reused in another oil field. Hence it will always have a residual or salvage value or resale value (B9). The decommissioning cost of FPSOs includes the cost of fuel for riding back to another location/field or cost of towing arrangements. Dismantling cost of mooring/riser system and the labour charges for the crew should also be counted for [110].

2.3 Critical Literature Review

In this literature review the focus is mainly given to literatures about FPSO motion response, their life-cycle cost and operability conditions. The critical literature review conducted is presented in Table 2.2, where the crucial gaps in the literature has been

identified via key references. The following sections analyses these gaps in detail and other critical aspects which are found out in the literature.

2.3.1 FPSO Motion Performance and Cost

The cost and motion performance of a tanker are the two important factors while choosing the FPSO hull and the associated mooring system, especially when converted tankers are used for oil explorations. Malaysia and Australia own the maximum number of FPSOs in the Indian ocean region. Also, the number of FPSOs with converted hulls are more when compared to that of with newly-built ones in Malaysia and Australia [2]. No studies have reported the impact of choosing a converted hull on the capital and life time cost of the FPSO system and their life-cycle cost when ET, IT, RTM, STP and SM is used. An initial life-cycle cost calculation of the FPSO system is desirable since they are high investment projects and large structures with difficulty in its construction and installation. It is better to conduct LCCA in the planning stage to choose the best possible FPSO hull and mooring type based on cost. The preliminary step in conducting an LCCA is data collection; the major sources of data must come from industry practitioners, albeit that a reluctance exists to share cost data due to the competent nature of oil industry. In life-cycle analysis, cost data is often indicative in nature [117], but in this research care is taken to ensure the quality of cost data by collecting them from reliable industry practitioners and published cost reports. Conducting an LCCA for FPSOs in Malaysian and Australian waters remains important as no previous detailed studies have been carried out to address the whole-cost aspects of FPSOs /converted FPSOs with different mooring configurations.

As discussed above, cost alone is not sufficient to determine a FPSO system, rather respective motion performance must complement (specification) choice [110]. Whole cost data requires to reflect different metocean conditions, water depths and, different FPSO sizes and loading conditions. This calls for a detailed parametric study covering

the effect of wave, wind, current, hull dimensions and loading conditions, mooring line configurations and dimensions on FPSO motions.

If the FPSO system is not designed properly, it will result in frequent mooring line breakages, hull damages due to green water and result in shut down. To avoid operational downtime due to such circumstances, motion performance of FPSOs for various design parameters should be thoroughly studied before choosing them for an oil field [110]. Also, downtime cost due to green water phenomena is studied to assess the performance of FPSO in Malaysia and Australia under wind generated sea state using location specific wave scatter table approach.

A comprehensive study to assess the motion performance, life-cycle cost and downtime for spread moored and turret moored FPSO has never been reported before and is of great interest as the need for cost and design optimisation is becoming more and more prevalent in the FEED phase of project now- a- days. Results generated could be of great impact, especially for the FPSO operators in Malaysia and Australia while choosing FPSO configurations as there are many FPSO projects in the FEED phase by the start of 2018 and oil and gas market is showing remarkable recovery when compared to the last few years.

2.3.2 Dynamic Responses of FPSO

The size of the FPSO is comparable with the wave length and hence results in a disturbance of the wave field causing diffraction of incident waves. Hence diffraction theory is used to calculate the wave load acting on FPSO [65], whereas Modified Morison equation is used to calculate the wave load on mooring lines as they are slender members. Also, Linear Airy Wave theory is used to represent sinusoidal waves as the wave heights in deep waters of Malaysia are small compared to the water depth. Unidirectional wave spectrums are the conservative wave assumption used in

hydrodynamic studies [57]. P-M and JONSWAP spectrum are found to be more suitable to represent the long-crested waves in locations of study. Limited study thus far has examined motion performance of operating FPSOs in Malaysia and Australia.

Simplified analysis like using strip theory requires only less computational effort and gives reliable reasonable results on the conservative side for engineering applications, but the 3D diffraction methods agrees better with the experimental results [27]. Hence 3D diffraction analysis should be used to study the FPSO motion performance and hence used for the location under interest in this study.

Uncoupled frequency domain analysis is reported to have many drawbacks [55]. But, where the non-linearities are not dominant, uncoupled frequency domain analysis gives good results [40], [58]. So, to study the floater responses due to the change in hull dimensions, hull loading conditions and for water depth parametric studies below 100 m, uncoupled analysis seems to be a good choice and can be time saving. Also, the effect of mooring lines and risers may not be significant for determining RAOs in wave frequency regime, although it affects the mean position in low frequency regime [59], [39] and the change in these mean offsets are not the primary concern of a dynamic analysis. Since the mooring system has less effect on linear wave induced motions in wave period range of 5 s – 25 s [61], [56], the usage of uncoupled frequency domain analysis tools like wadam wizard in SESAM HydroD can be used for finding motion RAOs.

But in deep waters, the effect of geometric non- linearities and cable dimensions affect the system response considerably. When the effect of mooring line dimensions and metocean conditions [83], [85] on FPSO motions are studied, coupled analysis is a must to obtain accurate results in deep waters. SESAM DeepC is a fully coupled time domain program that can be used for dynamic analysis of deep water floating bodies [55], [58]. It utilises an implicit time stepping scheme and the dynamic equation of motion is solved by equilibrium iterations at every time step. Material non-linearity,

geometric non-linearity, explicit loads and hydrodynamic loads can be effectively treated using DeepC [55].

It is argued here that numerical experiments however can never fully replace wave tank experiments, because many physical uncertainties will still prevail in a numerical model and hence the numerical needs to be verified before further application of it [62]. An efficient structural design involves complementing numerical and physical experiments to properly guide the engineers [62]. Horizontal mooring using soft linear springs is reported to be used for representing mooring lines of the distorted physical model due to water depth limitation in wave tank [59], [60], [63]. Also, the effect of mooring lines on FPSO motions are quite small in shallow waters at WF [59], [61]. Hence soft horizontal mooring with negligible mass and damping is ideally used under such circumstances. Since multi-directional waves represent the real sea state more closely, a comparison of FPSO motion response in long-crested and short-crested waves is best studied using model testing.

2.3.3 FPSO Operability

As mentioned in section 2.2.6, all the six FPSO motions should be minimised to ensure safe operating conditions for FPSO. Hence a parametric study covering metocean parameters, mooring line parameters and hull parameters are carried out to identify optimum configurations were FPSO motions will be minimum.

Parametric studies including water depth in shallow water so far has been conducted only for a maximum of 33 m water depth [74] [75]. In this study, model test is conducted to study the variation of FPSO motion in water depth up to 100 m since the shallowest oil field in Malaysia is at 55 m in Berantai oil field and in Australia is at 78 m in Cossack-Wanaea-Lambert-Hermes. The motions are reported to be varying linear with wave height [77], however a detailed investigation comparing all the 6 motions of

FPSO for spread mooring and turret mooring configuration has not reported before and the trend in variation of vertical and horizontal motions of FPSO while different mooring are used. Hence influence of wave height on FPSO motions is studied with and without the presence of wind and current for spread and turret moored FPSOs.

Effect of FPSO loading condition and mooring length was studied previously for a water depth of 1 m and they have identified the limitations of their results that it cannot be applied for deep waters [78]. Hence parametric studies are conducted for loading condition and mooring line length in the present study for deep waters, so that the results are applicable for deep waters in Malaysia and Australia. Studies have reported the influence of turret position on FPSO motion [79] [80], however no studies have reported the influence of spread mooring fairleads on FPSO motion. Hence the influence of spread mooring fairleads is investigated in the present study. Also, mooring line azimuth angle was varied from 30° to 60° for turret moored FPSO to study its influence on motions. However, effect of mooring line azimuth angle on spread moored FPSO motion is yet to be studied and experimental study could lead to realistic results in optimizing the mooring configurations of spread moored FPSOs. Hence model tests are conducted to study for mooring line azimuth angles 15°, 30°, 45° and 55° for spread moored FPSO. In addition to these, influence of hull length to beam on FPSO motions is also studied.

For efficient design of FPSO and associated mooring system, the numerical model should be able to consider six degrees of freedom motion and depends on factors including FPSO size, water depth, environmental condition and mooring line parameters [81]. Hence parametric studies to investigate the six motions of FPSO varying hull parameters and mooring line parameters are conducted in the present study to identify factors reducing FPSO motions and thereby enabling increased operational time.

Motion response from parametric studies for varying wave height in the presence of wind and current, FPSO loading condition and hull length to beam ratio in the heave, pitch and roll can also be used in minimising green water impacts. Also, downtime analysis is carried out to calculate downtime cost of FPSOs for long-term and short-term wave statistics for Malaysia and Australia.

2.3.4 Life-cycle cost of FPSO

As reported in the section 2.2.7.4 the parts of the technique followed by Ferry et al [115] and Kirk et al [116] are combined to conduct this (new unique) LCCA study of FPSOs. The associated risks and independent uncertainties are addressed by applying calculated discount rates and sensitivity analysis as used by Whyte [103] in calculating NPV of best practicable options from a range of available systems. Other than Howell [110], no other studies have previously reported the life cycle cost of FPSO mooring options. Also, no studies have been previously carried out to determine the life-cycle cost of FPSOs operating in Malaysia and Australia comparing the options of mooring types and hull condition (newly-built/converted).

The following table summarises research thus far and the gaps being addressed by this work.

Table 2.2: Critical Literature Review

Topic of Interest	**Important References and Points addressed**	**Identified Gap in the Literature**
Main research aspect- Cost and motion of FPSO	Howell et al [110] emphasized importance of studying motion performance along with cost of FPSO. However no previous studies are conducted in this aspect.	The current study computes the motion performance under various parameters as well as cost of FPSOs comparing mooring options and hull conditions.
Cost and Motion response of Operating FPSOs in Malaysia and Australia	No study has previously reported the operating FPSOs cost and Motion performance.	Cost and Motion performance of operating FPSOs in Malaysia and Australia is studied here.
FPSO motion response	Physical model testing should be combined with numerical modelling to achieve accurate model [62].	Numerical and physical experiments are conducted here to find FPSO motion responses.
Full 3D diffraction analysis of FPSO	Limitation of strip theory was given by Fan et al and the need for conducting 3D diffraction analysis was emphasized [27].	Diffraction analysis has been carried out here using frequency domain and time domain approach.
Coupled and uncoupled dynamic analysis	Coupled analysis gives accurate results where non-linearities are predominant [55]. Uncoupled analysis gives good results where non-linearities are not predominant [40] [58]	Coupled analysis is performed for parametric studies involving metocean parameters and mooring line parameters. Uncoupled analysis is used for hull parametric studies involving loading condition and dimensions.

Topic of Interest	Important References and Points addressed	Identified Gap in the Literature
Parametric studies on FPSO – Water depth	Water depth parametric studies are performed in shallow waters of up to 33 m [74] [75].	Parametric study is conducted for water depth up to 100 m as shallowest oil field in Malaysia and Australia starts from 55 m using model tests.
Parametric studies on FPSO – Wave height	No studies have compared the FPSO motion behaviour in varying wave heights when spread mooring and turret mooring is used	Present study compared FPSO motion for different mooring configuration for wave height 4 m to 8 m with and without the presence of wind and current.
Parametric Studies – Hull parameters	Influence of loading condition and hull length to beam ratio is not reported to be studied for deep water locations and the results generated for different loading conditions by Kannah et al points out that to be a limitation [78] .	Influence of loading condition and hull length to beam ratio is studied for deep water locations.
Parametric studies - Mooring line parameters	Influence of spread mooring fairlead location on FPSO motion is not studied previously and effect of mooring line length is studied only for shallow waters, again Kannah et al pointing it out to be a limitation of results generated [78]. Effect of mooring line azimuth angle is studied only for turret moored FPSOs.	Influence of spread mooring fairleads and mooring line length is studied using fully coupled analysis for deep water locations. Effect of mooring line azimuth angle is studied for spread moored FPSOs.

Topic of Interest	Important References and Points addressed	Identified Gap in the Literature
Downtime cost analysis	Downtime cost due to green water incidents in Malaysian and Australian seas have not previously been reported.	Downtime cost is calculated based on vertical relative motions of FPSO in heave, roll and pitch contributing to green water on FPSOs using Malaysian and Australian long term and short term metocean statistics.
LCCA of FPSO	Howell et al [110] computed life-cycle cost for FPSO in Brazil.	This study is carried out for FPSOs in Malaysia and Australia.
LCCA comparing mooring type	Howell et al [110] compared spread moored and internal turret moored FPSOs.	Comparison is made here between spread moored, ET, IT, RTM and STP.
LCCA comparing newly built hull and converted hull	No studies are reported.	Life-cycle cost for newly built hull and converted hull has been compared in this work.

2.4 Chapter Summary

The research studies handling the FPSO motion responses, operability analysis and life cycle costing approaches in the past decade were reviewed above and categorised into eight general research motivations. The previous studies and developments in each category were reported. Finally, a critical review of researches pertaining to the study has been carried out to identify the theories and methodologies to be adopted; the gaps in literature have been identified and tabulated above with the extent to which this work shall fill knowledge gaps has been made explicit.

CHAPTER 3

METHODOLOGY

3.1 Chapter Overview

This chapter discusses the methodology adopted to obtain the research objectives mentioned in Chapter 1. The method of investigating the FPSO motion responses are detailed using the model testing procedures followed and software simulation procedures carried out. The frequency domain and time domain approaches are discussed in detail using the theories and assumptions used during the analysis. Followed by that, the calculation of freeboard exceedance to identify green water event is detailed. Finally, the life-cycle costing procedure adopted for FPSO is detailed in Malaysia and Australian context. The adopted methodology presented here is in the same order as they were performed in the study; the scientific basis and the critical review of the methods adopted here having been already delineated in the previous chapter.

3.2 Overall Research Methodology

The previous chapter emphasized the role of both performance and cost in an efficient cost-effective design of FPSO and associated mooring system. Two main points were highlighted in the study, namely the dynamic motion response of FPSO and the life-cycle cost of the FPSO. Firstly, the FPSO motion responses were computed using numerical simulations and model testing, as both are equally significant in obtaining accurate results [62]. Operability analysis was then performed to identify downtime due to green water events which can lead to downtime cost in the life-cycle of FPSO. Then, the life-cycle cost analysis of FPSO was carried out to calculate the NPV and life-cycle costs of chosen FPSOs in Malaysia and Australia.

A complete 3D diffraction analysis was performed using SESAM HydroD in frequency domain analysis to obtain the 6 DOF Response Amplitude Operators and the results were compared with the physical model testing results conducted at the UTP Offshore Laboratory. Later, a fully coupled analysis of FPSO was carried out using SESAM DeepC and the analysis procedure and the results were verified against the published experimental results from the FPSO tests conducted at the OTRC Wave basin, Texas A&M. The calibrated models were then used for the further parametric studies and operability analysis based on green water using the verified procedure in SESAM HydroD, where SESAM DeepC was used while mooring lines plays a significant role in motion response.

Finally, the LCCA study of FPSO was carried out using the techniques mentioned in the previous chapter. The FPSO cost data was collected from PETRONAS Carigali Sdn Bhd, Chevron Australia, Wood Mackenzie Asset Reports and related sources. The different FPSO systems are compared in terms of their whole life-cycle cost to identify the economic option of mooring system and whether to build a newly built hull or use a converted tanker for oil drilling and processing purposes in the Malaysian and Australian waters. Since the cost data are for FPSOs from different metocean conditions, water depths and of different FPSO sizes and loading condition, appropriate parametric studies have been carried out to evaluate the motion performance and cost of these FPSOs.

The following figure 3.1 represents the overview of the research methodology performed:

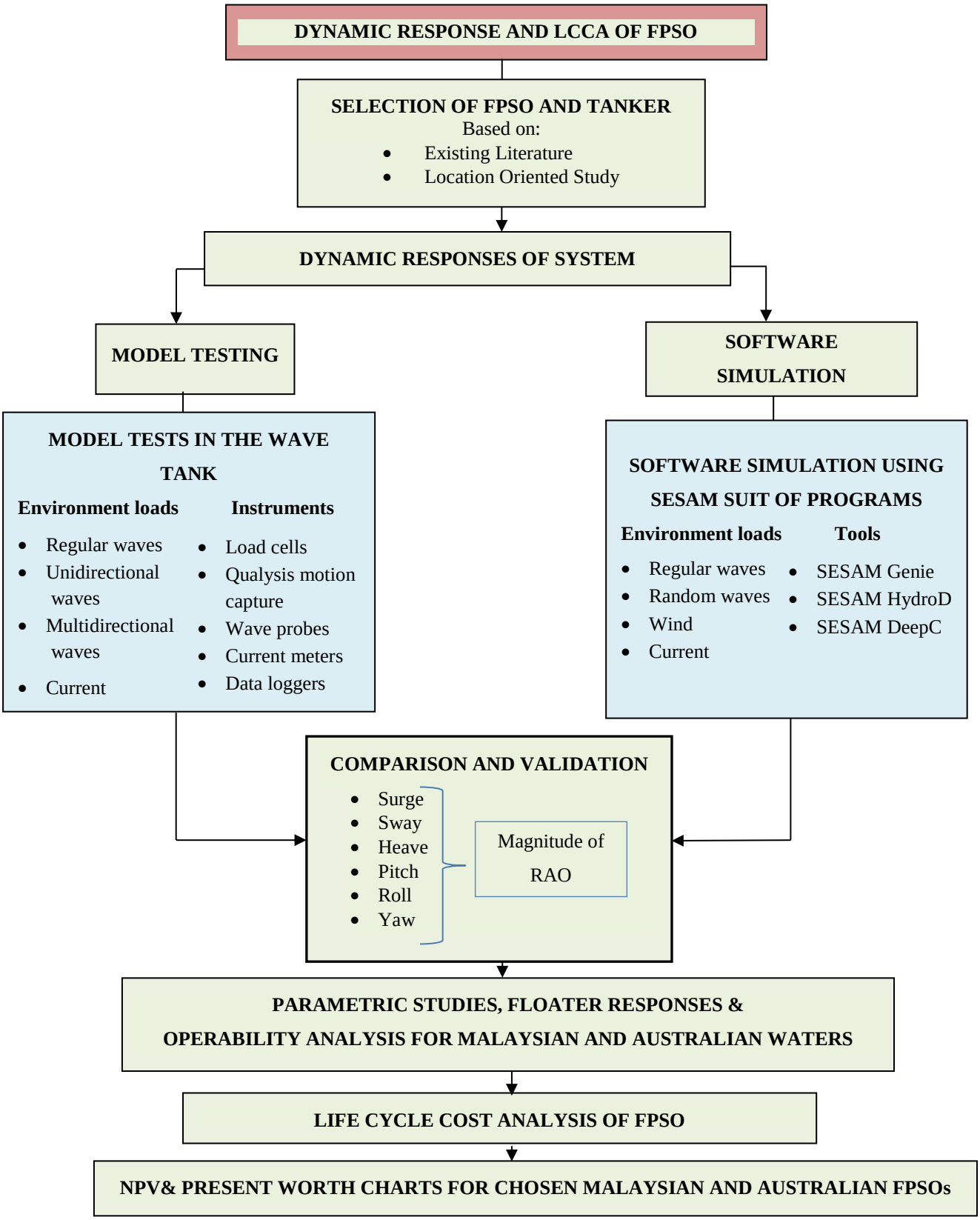

Figure 3.1: Overview of Research Methodology

3.3 Experimental Tests

As mentioned earlier in this chapter, the uncoupled frequency domain numerical model with mooring modelled as linear spring is validated by conducting an experimental study at the UTP offshore laboratory in the presence of long-crested waves and current. Apart from that, parametric study was carried out through several test runs at different water depths and different mooring line azimuth angles. So, the first phase of model test was aimed at providing data for the validation of the numerical model and the second phase included parametric studies. In this section, the physical model of the FPSO, mooring system used and the environmental conditions are described along with the laboratory tests conducted. Moreover, the instrumentations and the data acquisition systems for the tests are described.

3.3.1 Test Facility and Instrumentation

The experimental investigation was carried out in a 22 m long, 10 m wide, and 1.5m deep wave tank in the offshore laboratory, Universiti Teknologi PETRONAS, Malaysia which is shown in Figure 3.2. The detailed drawing of the wave tank is shown in Figure 3.3 with the basin plan and the east-west section. The wave tank is fitted with multi-element HR Wallingford wave maker containing 16 paddles and wave dissipator. The wave absorber at the other end of the wave tank consist of foam filled plate fixed to a rigid framework. The lab is equipped with a current generator capable of generating a maximum current of 0.2 m/s for a water depth of 1m. Qualysis Oqus 500+p 4 high speed motion capture system with SLR optics is mounted on the walls with the coordinates calibrated by choosing the centre of wave tank as origin. The wave elevations were measured by twin wire wave probes. The detailed description of the facilities and equipment is as follows:

Figure 3.2: UTP Offshore Lab

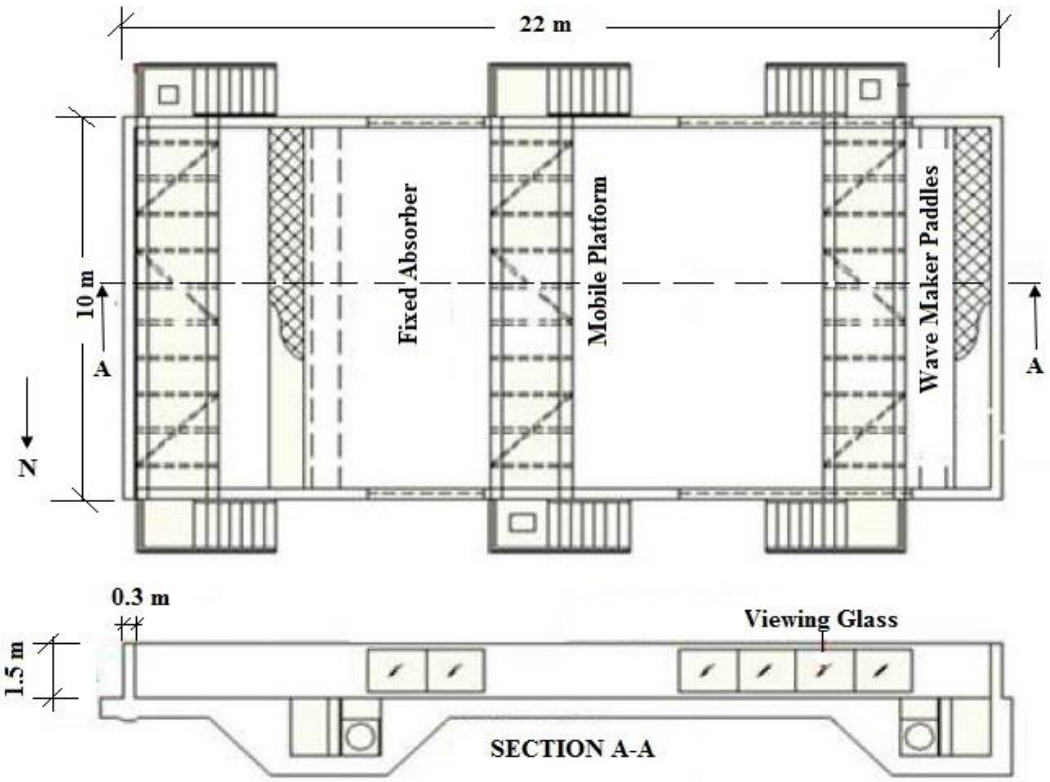

Figure 3.3: Wave Basin at UTP Offshore Laboratory

3.3.1.1 Wave maker system

The wave maker system at UTP offshore laboratory consists of wave maker, signal generation computer, remote control unit and dynamic wave absorption beach. The wave generator shown in Figure 3.4 has two modules with each having 8 individual paddles that can move independently to one another. The paddles can move back and forth to create waves in the wave basin.

Figure 3.4: H R Wallingford Wave Maker

The wave maker can generate waves of up to 0.3 m wave height and wave period as short as 0.5 s (model scale) as per the performance graph plotted in Figure 3.5 in water depth of 0.8 m and 1 m. The specifications of the wave maker system are given in Table 3.1. The progressive mesh beach system at the other side of the wave tank helps in minimising the interference from reflected waves during test runs. It is designed to absorb the waves which are reflected from the model. It consists of foam filled plate which is fixed to a rigid framework. The efficiency of the beach was found to decrease slightly with bigger waves, dropping from 98.1 % to 97.4 % as the wave height was increased from 0.05 m to 0.3 m [121]. Hence the wave height used for model tests were limited to 0.05 m.

Table 3.1: Specifications of Wave Maker System

Description	**Value**
Wave Maker Specification	
Paddle Width (m)	0.62
Paddle Height (m)	1.3
Paddle Stroke (m)	1.08
Paddle Velocity (m/s)	0.87
Paddle Force (kN)	1.5
No. of Modules	2
Module Width (m)	4.98
Maximum Water Depth (m)	1
Spectra Available	
JONSWAP	
Bretschneider	
P-M	
ISSC	
ITTC	
BTTP	
Derbyshire Coastal	
Derbyshire Ocean	
Neumann	
Top hat	
Sea State can be defined by	
Wave height	
Wave frequency	
Fetch	
Wind speed	
Spectral density	

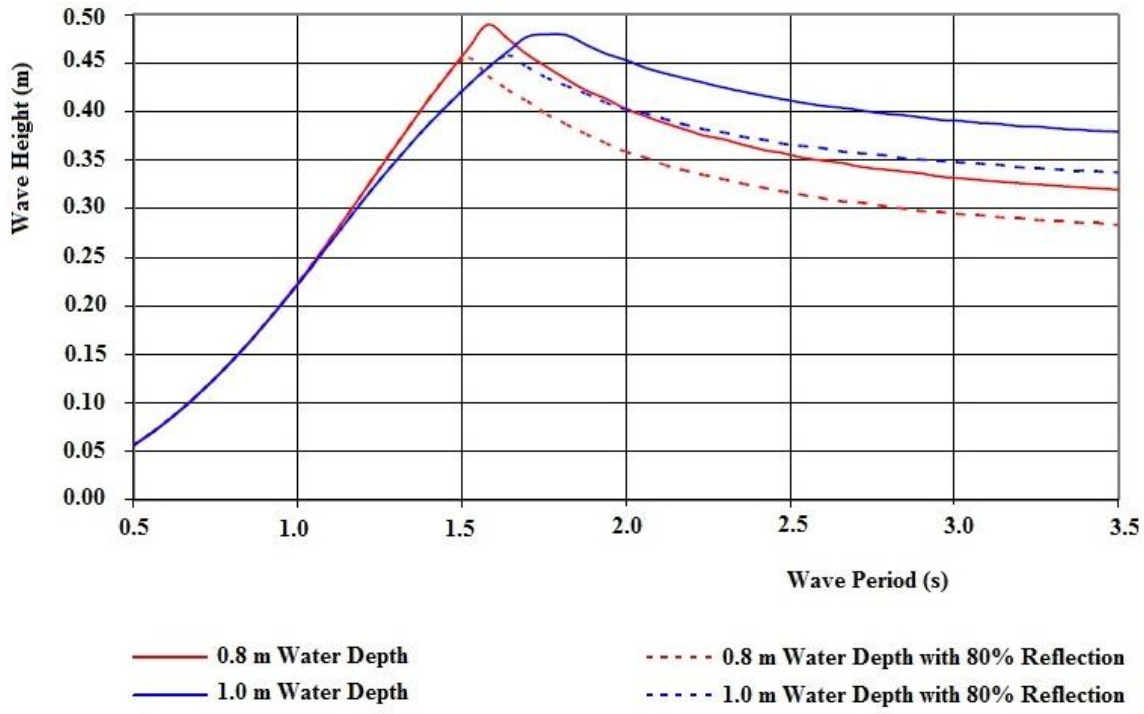

Figure 3.5: Performance of the Wave Generator at 1 m and 0.8 m water Depth [85]

3.3.1.2 Qualysis motion tracking system

Qualysis Oqus 500+p 4 high speed motion capture system with SLR optics is used to measure the motion response of the FPSO model. Principle of triangulation is the basis for the measurement technique. Four infrared sensitive camera are set to view the area where the model moves. Five infrared passive reflecting markers are fitted on the top of the model, such that their positions relative to each other remains constant and care should be taken to avoid the overlapping of marker reflections when the model is moving [121]. Hence it is better to keep the markers at a minimum distance of 10 cm – 15 cm and it is important to keep them in patterns which helps in identifying all the 5 markers at all the time.

The Qualysis tracking system was set to measure with 100 Hz real time frequency while capturing and made sure that the wave elevation and load cell data is also being recorded with the same frequency of data inputs. The 6DOF motion output from the Qualysis motion tracking system is in the TSV file formats which comprises the number of frames, number of markers, number of cameras, frequency of measurement, time and motion data [122].

3.3.1.3 Wave probes

Twin wire wave probes were used to measure the instantaneous wave elevations. Wave elevations were measured mainly for 1) calibration purposes, and 2) as a means of measuring the wave – platform interaction effects by measuring the instantaneous wave elevations during test runs. It consists of a head which is fixed to the calibration stem and a mounting block, that allows the calibration stem to be fixed to any vertical surface. The wave probes were attached to the tripod with the probe diameter 6.0 mm and length 900 mm. Wave probes were connected to computer system to monitor and record the change of water level during each test. Each probe was calibrated regularly to ensure the accuracy of recording by measuring the change in output voltage when the probe is raised or lowered by a known amount in still water. This operation is enabled by means of a calibration stem which is attached to the wave probe and which has a succession of precisely spaced holes drilled along the length of the stem.

3.3.1.4 Load Cells and Data Loggers

TML's submersible tension/compression load cells with low capacity (250 N) are cylindrical shaped (80 mm diameter and 42 mm height) and light weight (0.45 kg). They can be used to measure the mooring load with high precision as these load cell's internal structure has both ends fixation beam for the strain sensing element. These

sensors are equipped with 4-core shielded chloroprene cable which is 60m long and 6 mm diameter in size, and can produce an output rate of 3000×10^{-6} strain and it can be operated in the temperature ranging from -20 ^{o}C to +70 ^{o}C.

The TML's smart dynamic strain recorder is a compact, flash recording type 4-channel, of dimension 15.7 cm x 8.4 cm x 4.2 cm and weight 0.5 kg. It can be used to measures strain, DC voltage and thermocouples. Measured data is automatically stored on a compact flash card up to 2GB. The 4-channel unit can be connected in parallel up to 8 units (total 32 channels). It consists of a built-in un-interrupted power supply (UPS) to function when power supply is suddenly interrupted. The highest sampling speed is 5 μs with one channel and the measured data are recorded on a specified CF memory card at the same speed.

3.3.2 Choice of the Scale and Physical Modelling Law

As mentioned in Chapter 2, Froude's law of scaling is found to be the most suitable scaling law to represent the action of waves and the inertia of the body due to the limitation in the size of the wave tank and the size of the model it can occupy. The scaling factors shown previously in Table 2.1 was used to follow the law of similitude. The FPSO model was chosen such that it is easy to handle as well as it is economic to construct. To obtain reliable results, the common scales used are [122]:

1. for coastal structures – 1:150 to 1:20 in towing tank

2. in 3D wave tank – 1: 150 to 1: 80 and

3. for free and moored floating platforms – 1: 100 to 1: 10.

In this study, the FPSO model is constructed using wood and the scale used is 1: 100, so that it is easy to handle.

3.3.3 FPSO Model

3.3.3.1 Model description

Berantai FPSO dimensions were used to construct the FPSO model using wood and 1:100 scale factor was used. Choosing the 1:100 scale allows easy handling of the models as FPSO's are normally having length in the range of 200 m – 300 m. The fabrication was done at the Marine Teknology Lab of UTM Skudai, as they have much experience in fabricating ship and platform models. Figure 3.6 shows the Berantai FPSO model and the Figure 3.7 gives the detailed drawing of the FPSO model. Table 3.2 gives the FPSO model dimensions and structural data.

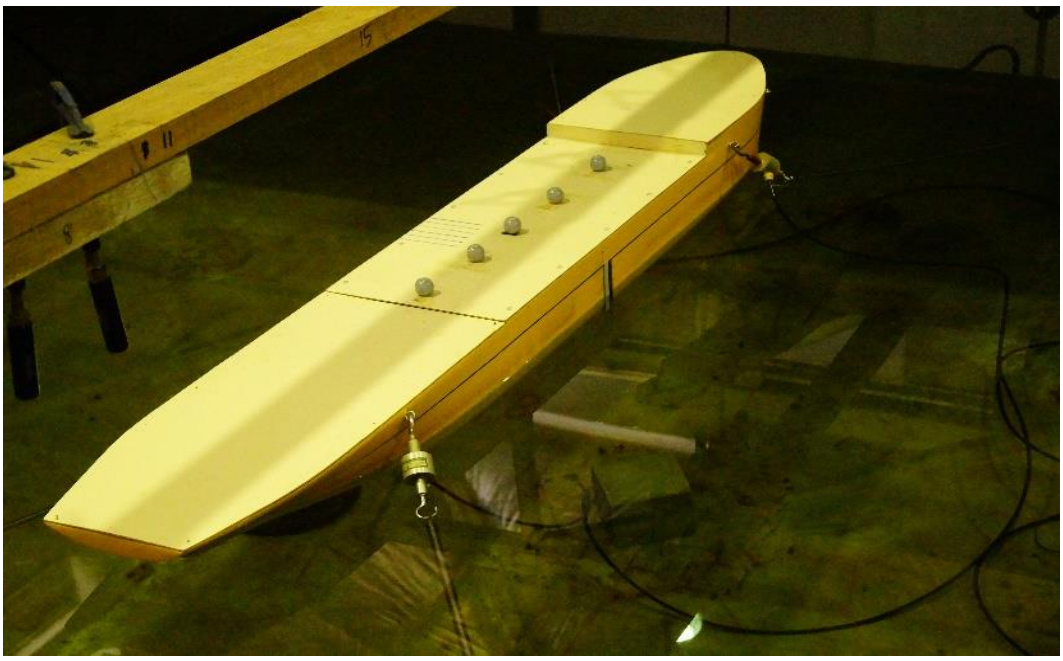

Figure 3.6: Berantai FPSO Model

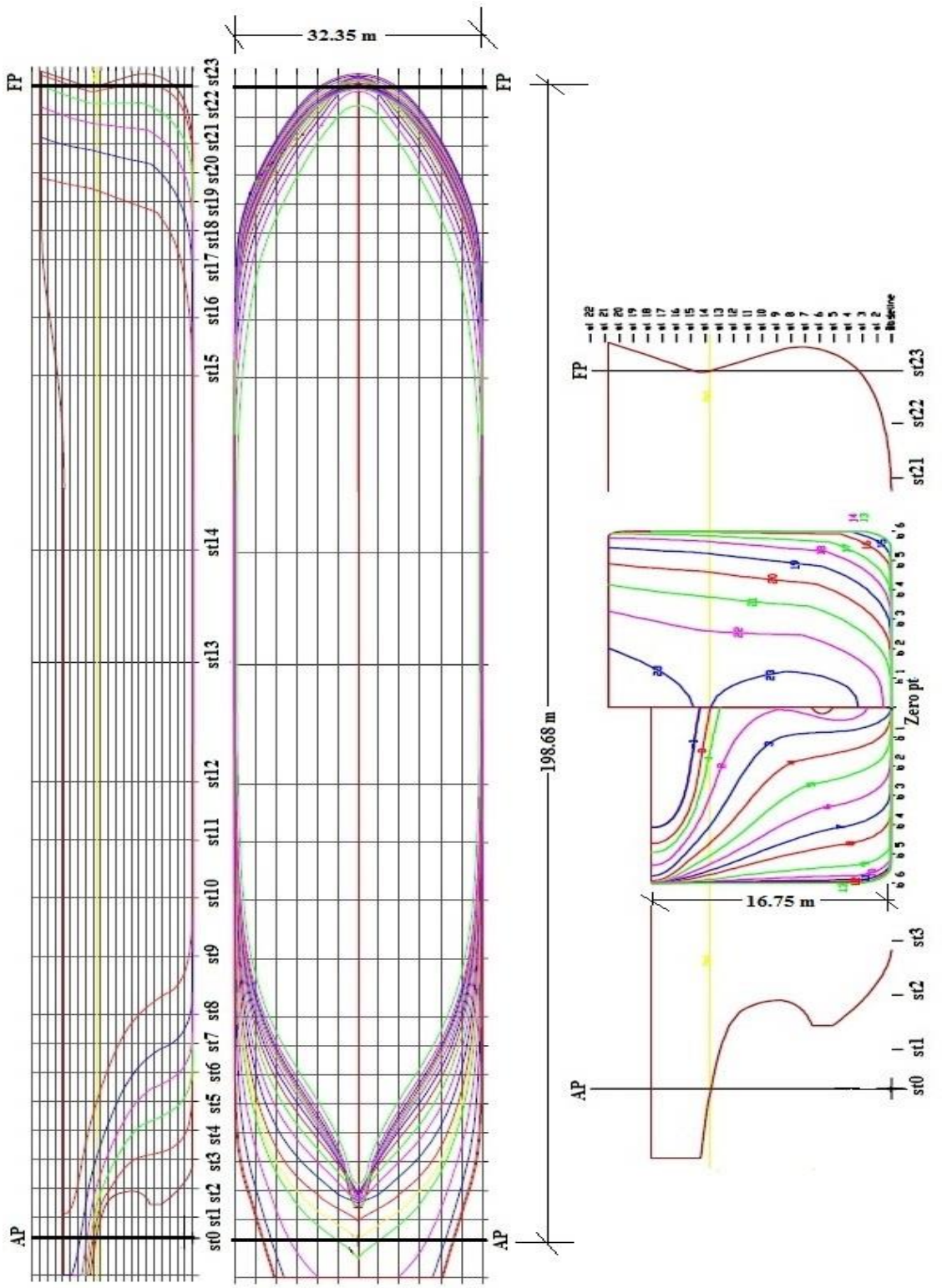

Figure 3.7: Drawing of FPSO Model

Table 3.2: FPSO Model Details

Measurement		**Model (1:100)**	**Unit**
LOA		2.074	m
LBP		1.987	m
Beam		0.322	m
Depth of hull		0.17	m
Max cross sect area		0.04	m^2
Waterplane area		0.575	m^2
Empty Hull Weight (without top cover)		15.8	kg
Mass of model at 50% loading condition		30.9	kg
Draft at 50% loading condition		0.063	m
L.C.G (from aft)		1.09	m
V.C.G (from keel)		0.075	m
Radius of Gyration	k_{xx}	14.5	cm
	k_{yy}	51.75	cm
	k_{zz}	51.75	cm

3.3.3.2 Mooring system

Modeling of FPSO system involves modeling both the floating structure and the mooring system. Due to the limitations of the wave basin mentioned earlier in this chapter, it is common to model the mooring lines as linear springs [123]. Soft springs were used to minimise their influence on FPSO motions and to prevent the FPSO from drifting away. Soft linear springs with 9 N/m stiffness, 0.8 mm wire thickness, 14.5 mm outer diameter and 300 mm long (model scale) were used to represent the horizontal spread mooring system as shown in Figure 3.8. Load cells were connected between the model and the spring for measuring the mooring line tension at the fairlead. It should be noted that the restraining system was pre-tensioned and clamped in a way to ensure that no slacking of the wire occurred during the tests.

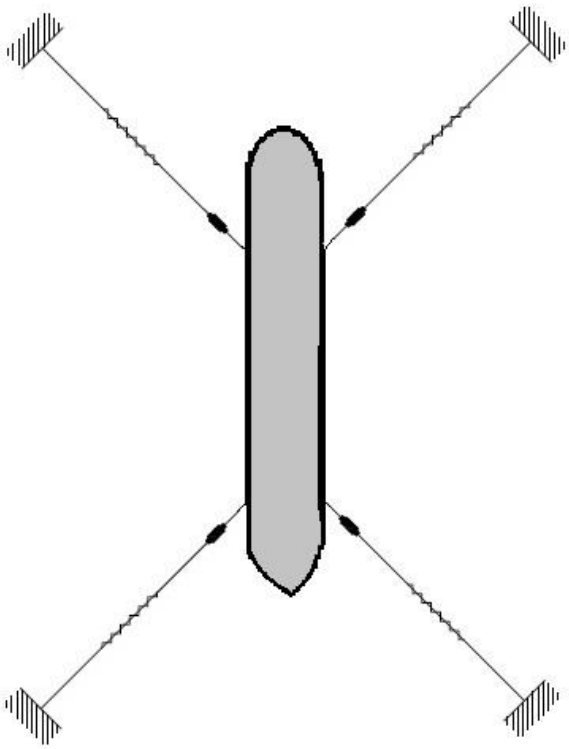

Figure 3.8: Mooring Line Arrangement for Model Tests

3.3.4 Laboratory Tests

3.3.4.1 General

The initial lab tests were conducted to calibrate all the waves used and to calibrate the FPSO model to achieve sufficient draft and mass distribution. Then, after arranging the experimental setup, free decay and static offset tests were conducted prior to the seakeeping tests. Utmost care was taken during each phase to ensure the accuracy of measurement and minimization of errors.

3.3.4.2 Wave calibration

Before starting the model tests, all the waves which are intended to be used in the tests were calibrated at the model position in the absence of the model. The instantaneous wave elevation was measured using the twin wire wave probes and each time the water depth was changed, the wave probes were calibrated and the required water depth was set with free surface set to zero position. During wave calibration, five wave probes were mounted at least 2 m (model scale) apart, with one wave probe being at the centre of the tank. Figure 3.9 shows the wave probe arrangement for wave calibration and Figure 3.10 shows the wave calibration setup in the absence of FPSO model.

To enable the generation of wave conditions, it is necessary to know the dimensionless Paddle Transfer Function (PTF) which relates the desired wave height up on the model and the associated paddle movement. This relationship is dependent on both water depth and frequency [124]. Hence it is mandatory to calibrate waves with same wave height and period if they are used at different water depths. For regular waves, the theoretical wave height and wave period is matched with the measured wave height and wave period from the wave probe in the place of model, by adjusting the gain factor in the HR wave maker software.

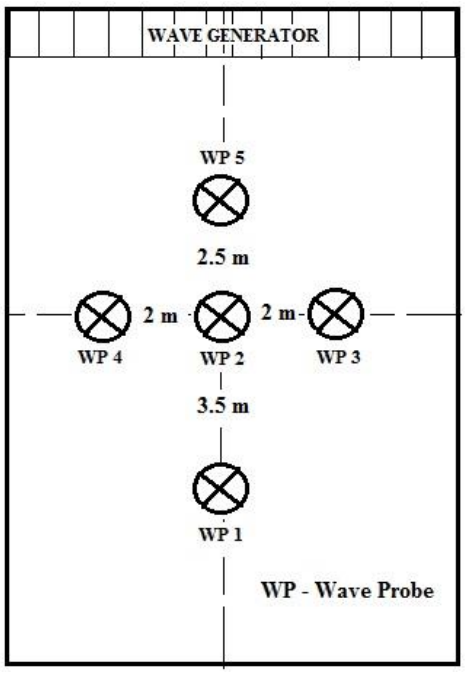

Figure 3.9: Wave Probe Arrangement for Wave Calibration

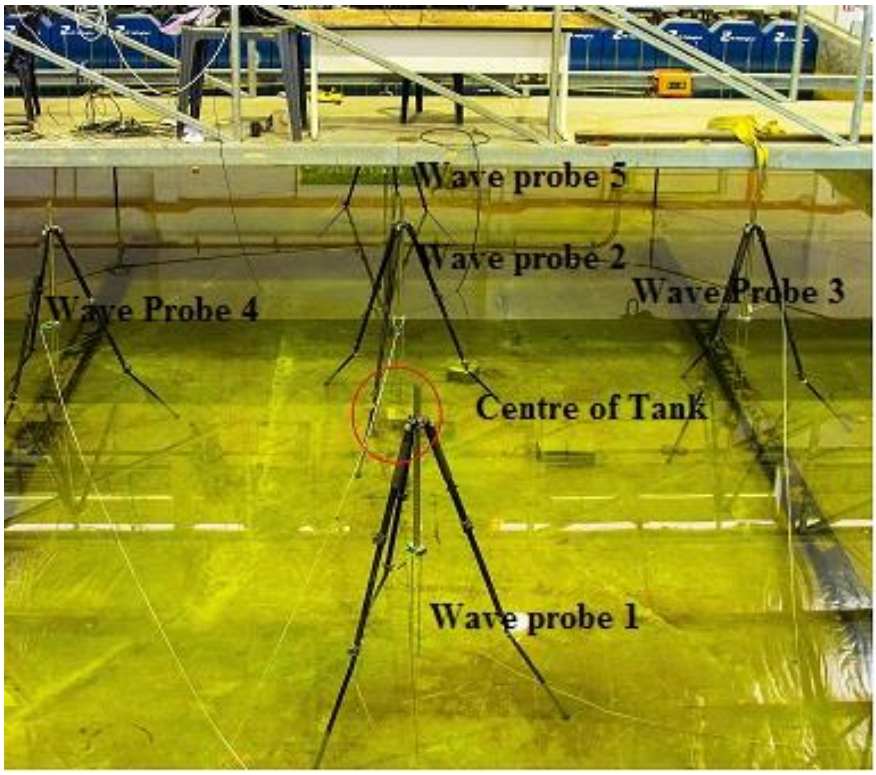

Figure 3.10: Wave probes in tank during wave calibration

For long-crested random waves, JONSWAP spectrum is used to represent the sea state. Spectra is generated from the digital time history signal of the instantaneous wave elevation output from the wave probe placed at the model position. Then keeping the gain factor constant, PTF is adjusted until the energy density of measured and targeted spectrums match [125]. Once the required PTF is found, it is saved for later use. This will assure repeatability of the wave spectrum from one run to the next.

A thorough calibration of the current generation is also performed before the model was placed in the basin. The current speed was measured with current meter covering the model neighborhood. Several measurements were made over this grid to ensure that the current speed is reasonably simulated and the current is reasonably steady and uniform. In this study, the maximum current velocity used is 1 m/s for the water depth of 1 m.

3.3.4.3 Calibration of model

Initially, the measurement of the model is taken to ensure that the model is constructed with the specified dimensions. Then, the air weight of the model is taken in the absence of any extra loads. The air weight of present FPSO hull model with cover is 17.1 kg. Then the model was placed in the wave basin to check the draft in the absence of any external loads. Once the initial draft was measured, additional weights are equally distributed inside the hull model. The preferred ballasting technique is sand bags of known weights. Small sand bags each weighing 1 kg was used to ballast the model to get 50 % loading condition with a draft of 0.063015 m (model scale) and hull model weight 30.9 kg (model scale).

The longitudinal centre of gravity of vessel can be found by using the 3-point mass system [126]. The weight of a vessel is distributed along its length, acting downwards over the entire structure. However, we consider all the weight to be acting vertically

downwards through one point which is the centre of gravity (CG). The vessel is placed on two known weights P_1 and P_2 as shown in Figure 3.14, mostly P_1 is measured by keeping that end on weighing machine. Moving the vessel back and forth we find the point where the vessel is balanced; this point is the centre of gravity. If the vessel is perfectly even through its length, the centre of gravity will be exactly in the middle, if it is not even, CG will be in such a position that the weight on one side will balance the other. Once the distances l_1 and l_2 as shown in Figure 3.11 is measured, then longitudinal CG at a distance X_{CG} from the aft end can be found by computing moment about CG as following.

$$X_{CG} = \frac{P_1}{P_1+P_2}(LOA - l_2 - l_1) + l_2 \tag{3.1}$$

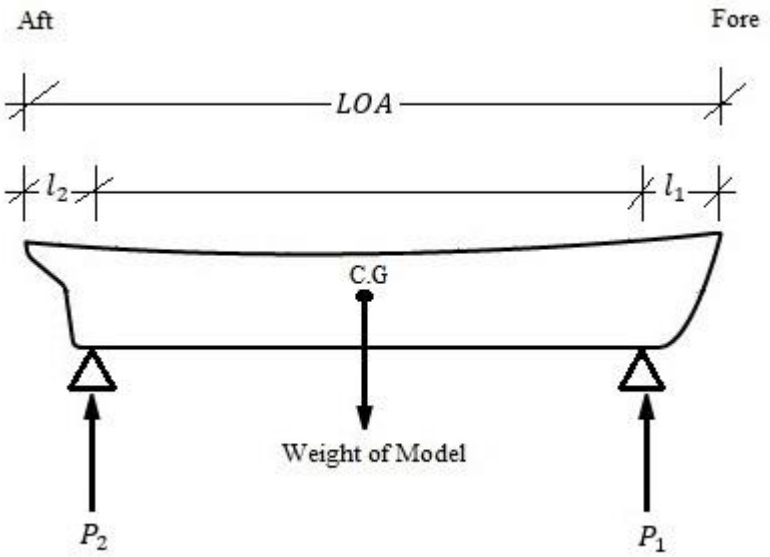

Figure 3.11: Three Point Mass System

To measure the vertical CG of the model, the model was hanged at a universal joint that is free to swing to perform an inclination test. By lifting the bow of the model, the lifting load (F_{lift}) and the inclination angle ($\theta_{inclination}$) were recorded along with the distance from lifting point to rotational point (d_1). Then distance from CG to

rotational point, d_{cg} is obtained by substituting the data recorded to the following formula,

$$d_{cg} = \frac{F_{lift} \times d_1}{Weight\ of\ model \times \sin\theta_{inclination}} \tag{3.2}$$

3.3.4.4 Experimental setup

In the present study, the FPSO model with the horizontal mooring system was kept at the centre of the wave tank. Four wave probes were used to measure the instantaneous water surface elevation, each kept at the four sides of FPSO without obstructing the view of the motion capture system. The maximum current which can be generated for 1m water depth was measured using Vectrino velocimeter. Five trackables were kept on top of the FPSO to measure the displacement of the FPSO by reflecting the invisible infrared light emitted by the Qualysis Oqus cameras. The suitably ballasted FPSO model with 50% DWT loading condition was held on position using the horizontal mooring system which consists of four soft springs of stiffness 9N/m connected with a cable is used to hold the FPSO on position. Load cell was connected between the FPSO and mooring line to measure the tension in the mooring line. In-place calibration of the load cells over the expected measurement range was performed. A pretension of 2.804 N (model scale) was given on each mooring line while the FPSO was clamped to the centre of the tank, to make sure that the FPSO is floating with its equilibrium position as the centre of the tank, and to minimize the error in measuring the displacement of FPSO. The spread moored FPSO was thus oriented along the centre line of the wave tank with its bow facing the wave maker to simulate the head sea condition. The layout of the experimental setup is as shown in Figure 3.12 and Figure 3.13 shows the FPSO model in the wave tank.

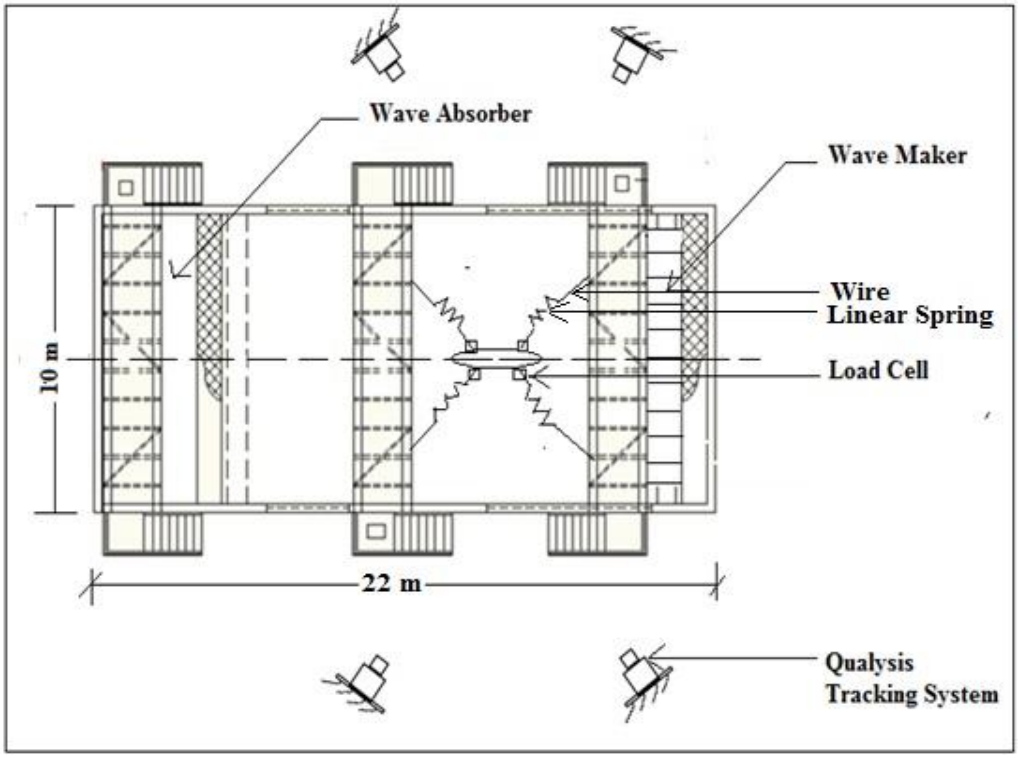

Figure 3.12: Experimental Setup

Figure 3.13: FPSO Model in Wave Tank

3.3.4.5 Static offset test

The static offset test was conducted to obtain the mooring system stiffness. The mooring line tensions were measured using the attached load cell-data logger system. The mooring line tensions were recorded for every 2 cm (model scale) incremental displacement of the model. Stiffness was obtained from the slope of the restoring force and displacement plot.

3.3.4.6 Free decay test

The system natural period and damping ratio was found by conducting a free decay test. An initial displacement was given to the restrained model in the desired DOF and released to move freely. The free decay time series were recorded using the Qualysis motion tracking system and the natural period in each DOF was obtained from the respective time series plot.

3.3.4.7 Seakeeping tests

To investigate the dynamic motion responses of the model in the seakeeping condition, regular as well as random waves, both long-crested and short-crested were generated. The 6 DOF motion responses were captured using the Qualysis motion capture system. To obtain the 6 DOF response amplitude operators for the model, the wave elevations were generated and measured prior to the installation of the models as shown in section 3.3.4.2 by the wave probe placed at the same location where the models are now installed. Long-crested regular and random waves were recorded for the duration of 3 minutes and 6 minutes respectively. Short-crested waves were generated and recorded for 3 minutes [19]. JONSWAP spectrum with peak enhancement factor, 3.3 was used to represent the random sea state.

Seakeeping tests were done for two purposes. One, for validating the numerical model and the other, is to conduct parametric studies. Validation of the software simulation model was done using the long crested white noise random wave generated, as the water surface time series signal is infinitely unique, the statistical properties of the waves are regarded as more similar to those found in nature. This should mean the behaviour of the model under test should resemble the full-scale system more accurately, especially in the extremes [127], [128]. Then the frequency dependent motion RAOs for first order systems (linear) are obtained as [65]

$$RAO\ (\omega) = \sqrt{\frac{S_R(\omega)}{S(\omega)}} \tag{3.3}$$

The effect of water depth was studied under the action of regular waves and long-crested waves were used to study the effect of mooring line azimuth angles on FPSO motions. Also, a comparison study was done to identify the effect of short-crested waves with directional spreading $cos^2\theta$ in different mooring line azimuth angles.

The effect of water depth was studied by conducting sea keeping tests at 0.62 m, 0.70 m, 0.75 m, 0.85 m and 1 m. Table 3.3 shows the regular waves used for this study and their calibrated values at each water depths. The wave module defined the regular wave as the sine function. The motion RAOs when subjected to regular waves are obtained as [65]

$$RAO = \frac{Response\ (t)}{\eta(t)} \tag{3.4}$$

The effect of mooring line azimuth angle was studied by varying mooring line azimuth angle from 15^o to 55^o at the maximum water depth possible in the wave tank, i.e. 1m. Both long-crested random waves and short-crested random waves were used in the study. Table 3.4 shows the long-crested random waves used and Table 3.5 shows the short-crested random waves used for this study.

Table 3.3: Regular Wave Series

Wave Series	Wave Frequency (Hz)	Wave Period (s)	Targeted Wave Height (m)	Measured Wave Height (m)
For Water Depth 1 m				
Wave 1	1.25	0.8	0.04	0.0398
Wave 2	1.1	0.91	0.04	0.0399
Wave 3	0.9	1.11	0.04	0.0396
Wave 4	0.8	1.25	0.04	0.0392
Wave 5	0.6	1.66	0.04	0.0409
Wave series	**Wave Frequency (Hz)**	**Wave Period (s)**	**Targeted Wave Height (m)**	**Measured Wave Height (m)**
For Water Depth 0.85 m				
Wave 6	1.25	0.8	0.04	0.0405
Wave 7	1.1	0.91	0.04	0.0401
Wave 8	0.9	1.11	0.04	0.0395
Wave 9	0.8	1.25	0.04	0.0386
Wave 10	0.6	1.66	0.04	0.0388
Wave series	**Wave Frequency (Hz)**	**Wave Period (s)**	**Targeted Wave Height (m)**	**Measured Wave Height (m)**
For Water Depth 0.75 m				
Wave 11	1.25	0.8	0.04	0.0381
Wave 12	1.1	0.91	0.04	0.0379
Wave 13	0.9	1.11	0.04	0.0398
Wave 14	0.8	1.25	0.04	0.0385
Wave 15	0.6	1.66	0.04	0.0381
Wave series	**Wave Frequency (Hz)**	**Wave Period (s)**	**Targeted Wave Height (m)**	**Measured Wave Height (m)**
For Water Depth 0.7 m				
Wave 16	1.25	0.8	0.04	0.0401
Wave 17	1.1	0.91	0.04	0.0377
Wave 18	0.9	1.11	0.04	0.0398
Wave 19	0.8	1.25	0.04	0.0409
Wave 20	0.6	1.66	0.04	0.0393

Wave series	Wave Frequency (Hz)	Wave Period (s)	Targeted Wave Height (m)	Measured Wave Height (m)
For Water Depth 0.62 m				
Wave 21	1.25	0.8	0.04	0.0402
Wave 22	1.1	0.91	0.04	0.0385
Wave 23	0.9	1.11	0.04	0.0427
Wave 24	0.8	1.25	0.04	0.0410
Wave 25	0.6	1.66	0.04	0.0383

Table 3.4: Long-crested Random Wave Series

Wave series	Wave Period (s)	Targeted Significant Wave Height (m)	Measured Significant Wave Height (m)
LCR1	0.7	0.05	0.0471
LCR2	0.8	0.05	0.0483
LCR3	0.9	0.05	0.0488
LCR4	1	0.05	0.0472
LCR5	1.2	0.05	0.0498
LCR6	1.5	0.05	0.0523
LCR7	1.7	0.05	0.0487
LCR8	2	0.05	0.0495
LCR9	2.3	0.05	0.0482
LCR10	2.5	0.05	0.0490

Table 3.5: Short-crested Random Wave Series

Wave series	Wave Period (s)	Targeted Significant Wave Height (m)	Measured Significant Wave Height (m)
SCR1	0.7	0.05	0.0528
SCR2	0.8	0.05	0.0480
SCR3	0.9	0.05	0.0478
SCR4	1	0.05	0.0522
SCR5	1.2	0.05	0.0512
SCR6	1.5	0.05	0.0526
SCR7	1.7	0.05	0.0481
SCR8	2	0.05	0.0479
SCR9	2.3	0.05	0.0525
SCR10	2.5	0.05	0.0491

3.4 Dynamic Analysis of FPSO

The numerical investigation of FPSO motion responses were performed using SESAM suit of programs. Initially, the ship lines were generated using Rhinoceros 5 3D software and then imported to SESAM Genie V5.3-10 for further modifications and finite element mesh generation. The finite element mesh from SESAM Genie V5.3-10 (Tn.FEM) is given as input to the SESAM HydroD V4.5-08. RAOs were obtained by performing a hydrodynamic analysis in SESAM HydroD V4.5-08. The RAOs generated are stored in the Hydrodynamic results interface file (G1. SI) which is then used for the time domain analysis in SESAM DeepC V5.0-06 along with the mesh generated in Genie. The fully coupled dynamic analysis program SESAM Deep C V5. 0-06 gives the time series plot for 6 DOF FPSO motions. Figure 3.14 shows the communication between the programs.

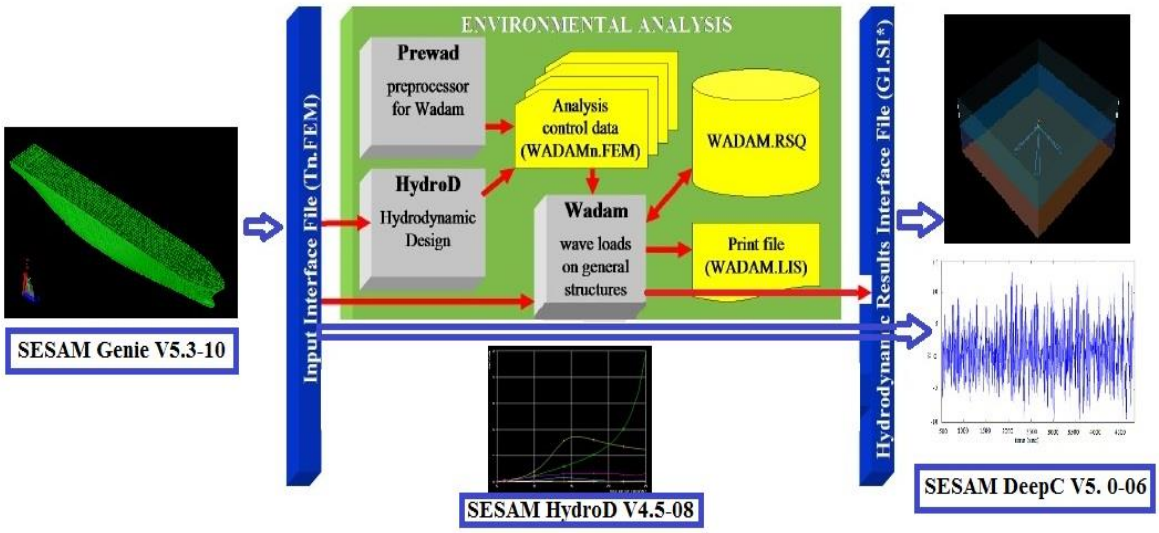

Figure 3.14: SESAM Communication

SESAM simulations were performed to conduct parametric studies on calibrated and validated Berantai FPSO model (Spread Moored) and OTRC FPSO model (Turret Moored). Using the verified modelling and simulation procedure, motion responses of other FPSOs in Malaysia and Australia were also investigated. Validation curves and parametric study results are given in Chapter 4. The modelling and analysis procedures and the assumptions and theories used in the program are detailed in the following sections.

3.4.1 FPSO Modelling

The vessel hull was lofted in Rhinoceros 5 3D with the corresponding hull dimensions and imported to SESAM Genie V5.3-10 were the FPSO hull was modified and prepared for further use in analysis. Some portion of the hull form was generated using the guiding tool followed by a plate skinning operation. Genie allows creating a concept model, from which the final finite element model will be created with refined meshing. The concept model of Berantai FPSO developed in Genie V5.3-10 is shown in Figure

3.15. It was made sure that the mass distribution, C G, radius of gyration and draft of the numerical model is same as the model used for physical model testing.

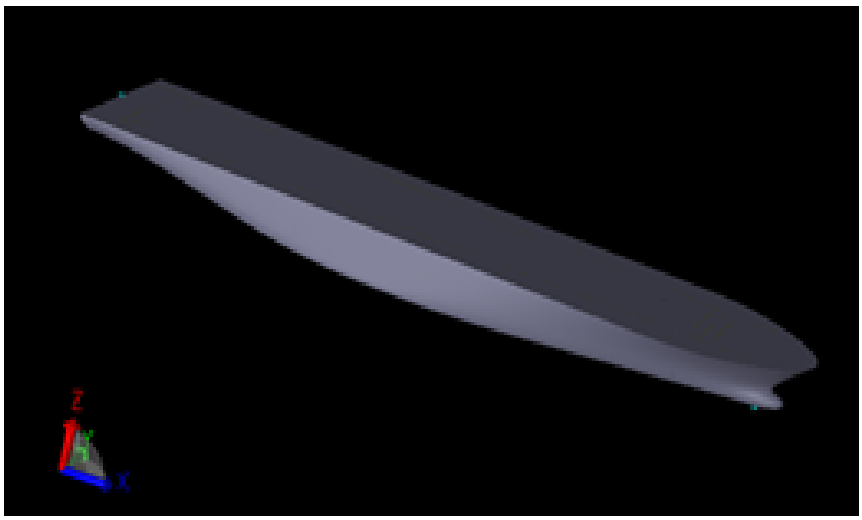

Figure 3.15: FPSO Concept Model

From the concept model, a panel model was generated with only one half of the FPSO, located in the positive global coordinates. The model was initially combined to be a single panel and then were divided at draft, fore and aft lines. Then the panels were then divided at equal intervals 5 m in the three co-ordinates. This ensures high quality panel model as per [129] . The wet surfaces were assigned and a load case was assigned were the hydro pressure was acting throughout the wet surface of the hull pointing towards the front side of the hull plates. The super element number was assigned as 2 and a finite element mesh was generated and exported. The panel model assigned with the wet surface is shown in Figure 3.16.

In HydroD, to connect the mooring elements, a 2D Morison element should be present in the structure. So, a Morison model was created by providing beams for the connection of mooring lines from the FPSO to the seabed. A mesh activity was defined with super element number 1 and the Morison model was exported. The structural model with super element number 3 was developed by generating the symmetrical side of hull and scaling the mass density to match the required mass distribution.

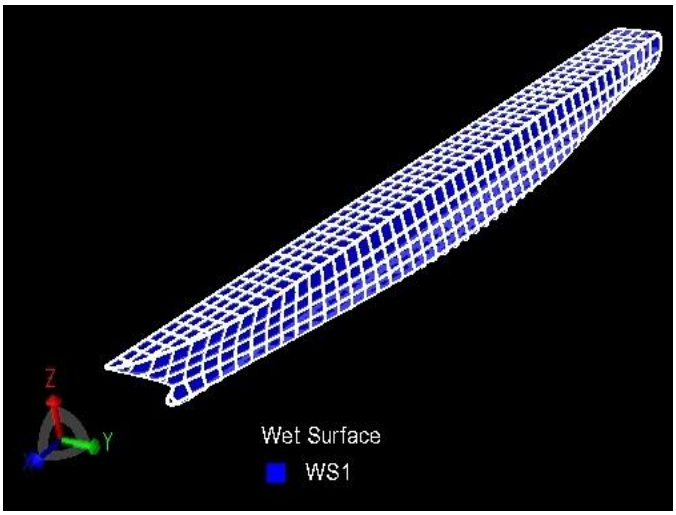

Figure 3.16: Panel Model Assigned with Wet Surface

Support conditions were provided so that the FPSO will act as a rigid body. The plates were then divided at the maximum draft, aft and fore to create a balanced mesh. The Morison and structural model were connected in a super element hierarchy and the finite element mesh was generated for the FPSO structural model to be used for further analysis in Hydro D V4.5-08. Figure 3.17 shows the finite element mesh generated for Berantai hull.

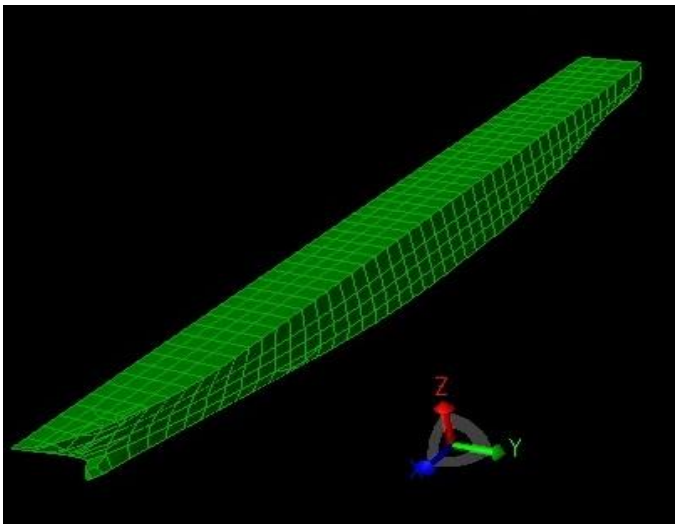

Figure 3.17: Finite Element Mesh Generated

3.4.2 Frequency Domain Analysis

The hydrodynamic analysis was performed using SESAM HydroD V4.5-08 with wadam wizard V8.2-02 in frequency domain to obtain the motion response amplitude operators.

3.4.2.1 Assumptions and theories

The flow is assumed to be ideal and the free surface condition is linearised for the first order potential theory. Only first order wave forces are considered in this study. The global coordinate system is right handed with the origin in the still water level. The Z-axis is normal to the still water level and the positive Z-axis is pointing upwards.

A combination of panel and Morison model (composite model) is used since potential theory and Morison's equation are applied to different parts of the hydro model. The panel model is used to calculate the hydrodynamic loads and responses from potential theory. A Morison model is used for calculation of hydrodynamic loads from Morison's equation. Mooring element is used to include external restoring forces from weightless mooring lines with linear stiffness characteristics. Since Morison element will contribute hydrostatic and Froude-Krylov force, as it has a certain volume, very small diameter is used for the mooring lines to avoid this.

The radiation and diffraction velocity potentials on the wet part of the body surface are determined from the solution of an integral equation obtained by using Green's theorem with the free surface source potentials as the Green's functions. The source strengths are evaluated based on the source distribution method using the same source potentials. The integral equation is discretized into a set of algebraic equations by approximating the body surface with several plane quadrilateral panels. The source strengths are assumed to be constant over each panel. Two, one or no planes of symmetry of the body geometry may be present. The solution of the algebraic equation

system provides the strength of the sources on the panels. The equation system, which is complex and indefinite is then solved by an iterative method [70].

3.4.2.2 Analysis Procedure

The uncoupled hydrodynamic analysis was performed using HydroD V4.5-08 in wadam wizard V8.2-02. Finite element models generated in SESAM Genie V5.3-10 is used as input to HydroD V4.5-08. In the wadam wizard settings, composite model is chosen to represent the structural model which is composed of both panel model and Morison model. The wave directions taken for computing the response was given with wave period ranging from 5 s to 25 s. Mooring lines were given by linear springs with matching stiffness and pretension as the mooring system of physical model for validation purpose. The wadam wizard generates the other half of the panel model to form the FPSO hull and strip model is defined to be used in iterative roll damping. The frequency domain analysis results were presented using Postresp V6.3-01. The Figure. 3.18 shows one of the spread moored FPSO model in HydroD V4.5-08 interface.

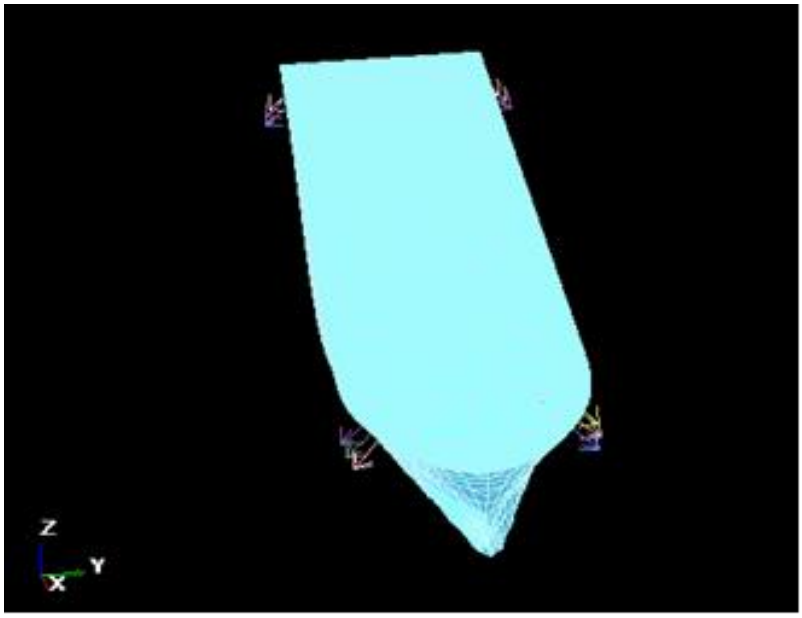

Figure 3.18: Spread Moored Model in HydroD V4.5-08

3.4.3 Time Domain Analysis

Fully coupled time domain analysis was performed using SESAM DeepC V5.0-06 in time domain to obtain the time series of motion response in 6 DOF. DeepC is a package of software programs, consisting of also the MARINTEK's program RIFLEX and SIMO [9].

3.4.3.1 Assumptions and theories

The mooring lines are discretised in to several beam elements in the finite element modelling. The FPSO vessel is considered as rigid body and treated as a nodal element. Linear wave potential theory is used all throughout in the present study. Modified Morison equation incorporating relative velocity term is used to find the wave load on mooring lines while diffraction theory is used to calculate the wave load on FPSO hull [9]. The wind velocity is simulated in the time domain by use of a state space model using NPD spectrum. The wind is directed only in the main direction and no transverse gust is allowed while this assumption is used. The current is described by a profile with specified direction and speed at different elevations. Linear interpolation is used to explicitly define the current profile. The current is taken to be constant from the lowest level specified to the bottom [130].

3.4.3.2 Analysis Procedure

The finite element mesh is imported to SESAM DeepC V5.0-06 along with the hydrodynamic results interface file from HydroD V4.5-08. The interaction between the wave and FPSO are described by a set of frequency dependent coefficients for inertia, damping and excitation forces. These coefficients are obtained from the diffraction/radiation analysis program Wadam in HydroD V4.5-08 which is converted to a retardation function, and the frequency dependent force is included as a convolution

integral, introducing a memory effect in the time domain analysis. To convert from the frequency to the time domain, the Kramers - Krönig relations are used (convolution integrals).

Both spread mooring and turret mooring FPSO were used for the study. The mooring lines were modelled by inputting material, sectional and structural properties. Both free decay and sea keeping tests were performed using SESAM DeepC V5.0-06.

Free decay test was conducted to verify if the numerical model and the physical model has the same mass distribution and hydrodynamic performance. This also helps to check if the mooring system is reasonable. The simulation model was calibrated to achieve the natural periods and damping ratios as later shown in the validation. Currently SIMO assumes that the buoyancy of a vessel equals the vessel mass. This is usually not correct because typically, lines also pull the vessel down (in addition to the gravity force on the vessel). To correct this erroneous buoyancy force, a force should be applied on the vessel centre of buoyancy. The force magnitude should equal the difference between the vessel buoyancy and mass, and its direction should be the global z-axis [93]. For translational degrees of freedom, a single force was applied in the particular direction, whereas for rotational degrees of freedom, a force pair was given. The best way to initiate a free decay analysis in DeepC, is to apply a horizontal force to give the wanted offset. The force is applied for 20 s – 30 s, and then released. The time and magnitude of the force will depend on the wanted offset and the stiffness of the system. The offset will be nearly linearly dependent of time and magnitude; but, from the trial and errors performed to achieve the required offset, the hydrodynamic performance of the system remains the same and the natural period and damping ratios are the same for different specified force and time set.

Once the model was calibrated, the same was used for conducting several parametric studies and the motion responses were generated as time series. Figure 3.19 shows the FPSO model in SESAM DeepC interface.

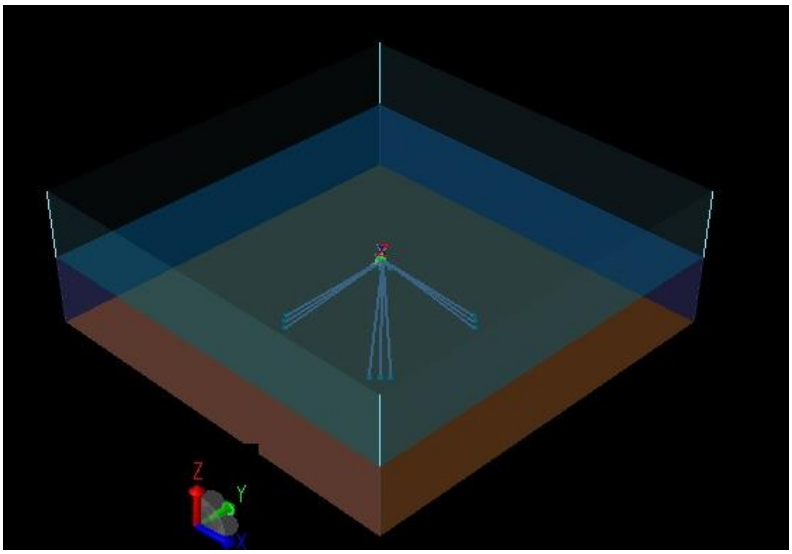

Figure 3.19: FPSO Model in SESAM DeepC Interface

3.5 Operability Analysis

Operability analysis is conducted to identify downtime due to green water on FPSO deck. The study uses motion responses calculated using dynamic analysis of FPSOs and use that as an input to identify green water on FPSO. If the FPSO is prone to green water occurrence, this will result in a downtime cost to be used in the LCCA. The below sections detail the analysis technique and the chosen FPSOs for operability analysis and site specific metocean conditions used.

3.5.1 Green water on FPSO and Downtime cost

Operability analysis based on green water phenomenon is conducted by calculating freeboard exceedance of FPSO by conducting a linear diffraction analysis using SESAM HydroD V4.5-08 by subjecting the FPSOs to site specific annual wave scatter data. Results are also found by subjecting the FPSO to extreme metocean conditions with 100-year return periods. Linear diffraction analysis is found to give good estimate

of probability of green water on FPSO [97]. The prerequisites for this analysis are the FEM model of the vessel and site specific metocean data. The modelling and meshing of the FPSO is as mentioned in section 3.4.1 using SESAM Genie V5.3-10. The finite element mesh of the vessel is then used in SESAM HydroD V4.5-08 to generate vessel motion RAOs and wave elevation RAOs. The procedure for hydrodynamic analysis in SESAM HydroD V4.5-08 is detailed in section 3.4.2. Vessel headings taken for the analysis are 180°, 165° and 150° based on the design basis for wave load analysis [131]. In the crossing sea conditions, green water can come from side as wells as on bow. So, wave elevation RAOs are calculated at nodes at 5m interval along the side of vessel from fore to aft at draft as shown in Figure 3.20. Only one half of the FPSO is considered as the vessel is symmetrical in transverse direction and analysis is done at maximum operating draft for each FPSO. The rest of the calculations are done using SESAM Postresp V6.3-01, which is the post processing tool for SESAM HydroD V4.5-08. The procedure to obtain freeboard exceedance is as following:

Step 1: Using SESAM Genie V5.3-10

Finite element mesh is created in SESAM Genie V5.3-10 and co-ordinates of points at which wave elevation RAO must be calculated is recorded.

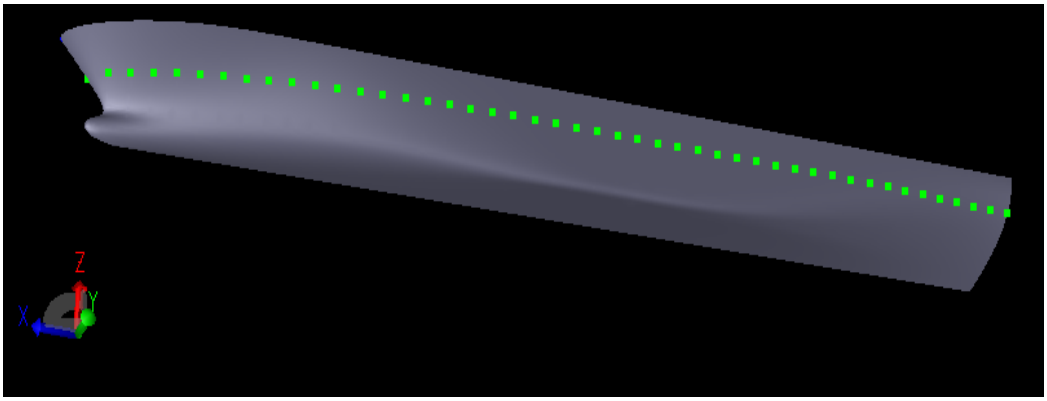

Figure 3.20: Points along the vessel hull at which wave elevation RAOs are calculated in SESAM HydroD V4.5-08

Step 2: Using SESAM HydroD V4.5-08

Hydrodynamic analysis is performed in SESAM HydroD V4.5-08 with offbody points as the co-ordinates of the points where wave elevation RAO should be calculated. The results from SESAM HydroD V4.5-08 is viewed in SESAM Postresp V6.3-01 where all outputs are based on the global co-ordinates where z axis is at the MWL.

Step 3: Using SESAM Postresp V6.3-01

Specific points at which wave elevation RAOs are obtained is automatically created in SESAM Postresp V6.3-01, since offbody points are given in hydrodynamic analysis in SESAM HydroD V4.5-08 mentioned in Step 2. A motion response amplitude variable is created in this location to calculate absolute vertical motion of vessel with combined effect of heave, roll and pitch as per Eq. 3.5. Global RAOs are calculated at the CG of FPSO and x and y are the distance from CG to the specific point in x and y direction respectively.

$$Combined\ vertical\ motion\ RAO\ of\ FPSO\ at\ a\ point\ = Global\ Heave\ RAO + (y \times Global\ Roll\ RAO) - (x\ \times Global\ Pitch\ RAO) \quad (3.5)$$

Then the relative motion RAO is computed by taking the difference in wave elevation RAO and combined vertical motion RAO at each specific point. A relative motion spectrum is then created based on sea state from wave scatter diagram using JONSWAP spectrum as shown previously in chapter 2, section 2.2.5.1 with γ as 3.3 which represents the most hostile weather condition [131] for the results to be on conservative side. From the created relative motion spectrum, Rayleigh distribution as shown in Eq. 3.6 is used to obtain the annual probability maximum and most probable maximum relative motion response of FPSO as it is tested and validated by experiments [97].

$$P_E\{R_m > FB\} = exp\left\{\frac{-FB^2}{2m_{0R}}\right\} \quad (3.6)$$

To understand short term green water effects, exceedance was computed for a probability of 0.01 in the case of extreme wave, wind and current conditions with 10-year return period and most probable maximum relative motion was found for annual wave scatter data corresponding to a probability of 0.63 [131].

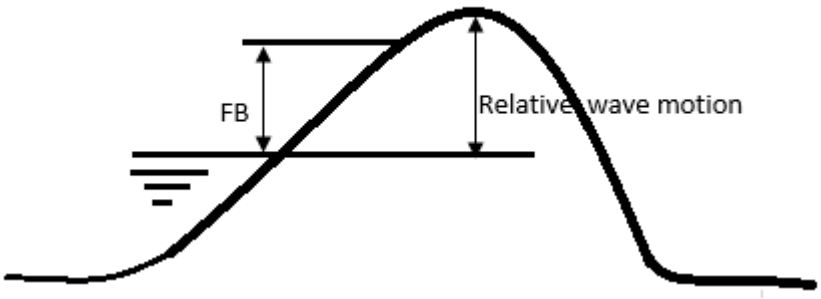

Figure 3.21: Representation of Relative Wave Motion

From the obtained maximum relative motion, freeboard of the vessel at maximum operating draft was subtracted to calculate the freeboard exceedance as shown in Eq. 3.7 as represented in Figure 3.21.

$$Freeboard\ Exceedance = Maximum\ Relative\ motion - Freeboard \quad (3.7)$$

If the relative motion of FPSO exceeds the freeboard by less than 3 m, then the susceptibility to green water is low. If it is between 3 m – 6 m, then it is medium susceptibility and if it exceeds 6m, FPSO is highly susceptible to green water. Downtime will occur if the freeboard exceedance is higher than 3 m [88]. If the vessel is prone to risk from green water occurrence, then in the long term, downtime (days) can be calculated by multiplying the probability of occurrence of green water with corresponding annual joint probability of that particular wave height and time period responsible for green water to the number of days in a year. Downtime cost per year can then be calculated by multiplying number of days of downtime with price of oil per barrel per day in USD.

3.5.2 FPSOs for operability analysis and site specific metocean data

The FPSOs in Australia and Malaysia chosen for the operability analysis based on green water and subsequent Life-cycle cost study are shown in Table 3.6, along with their structural, mooring and hull details. To account for the annual life-cycle cost in LCCA, annual downtime cost needs to be calculated, that is if any exists. Hence approximate downtime cost is calculated by using FPSO models generated with same dimension as mentioned in Table 3.6 in the absence of original ship lines. Getting original ship lines from the operators are difficult as they are confidential. However, these models are analyzed for site specific wave conditions where they are operating.

For Malaysian oil fields, Omar et al [132] gives the joint annual probability distribution of H_s and T_p in parts per thousand for selected zones in Malaysia. The chosen FPSOs in Malaysian seas for operability analysis and LCCA are operating in these selected zones. Operation location for these FPSOs are identified in these zones and are marked on Malaysian oil fields map obtained from [2] as shown in Figure 3.22. Zones are marked using the same name as in Omar et al for ease of identification of metocean data used. The annual wave scatter data in terms of joint annual probability in percentage is given in Table 3.7 – 3.9 for Malaysian locations. Percentage probability is calculated as no. of occurrence of each wave divided by 1000 and multiplied by 100 (For example, 78 waves in 1000 occurrence means 7.8% or in fraction 0.078).

Generally, Malaysian seas have low wave heights with peak period in the range of 6 s to 7 s [132], whereas Australian seas have higher peak periods [133]. Annual wave scatter data for Australian locations, where chosen FPSOs are operating are obtained from Metocean View [133] in terms of annual joint probability distribution of H_s and T_p in parts per hundred thousand and the locations are as marked in Figure 3.23 on map obtained from [134] .

Table 3.6: FPSOs for operability analysis and LCCA Study [2]

FPSO/FSO NAME	STATUS*	LOCATION	HULL LENGTH (m)	HULL WIDTH (m)	HULL DEPTH (m)	DRAFT (m)	FB (m)	DWT(MT)	WATER DEPTH (m)	LEASED (YES-Y OR NO-N)	CONVERTED (C) OR NEWLY BUILT (N)	MOORING TYPE
PERISAI KAMELIA	O	MALAYSIA	264	41	22	13	9	127540	60	Y	C	ET
KIKEH	O	MALAYSIA	337	55	27	21	6	273000	1350	Y	C	ET
CENDOR II(ONOZO)	O	MALAYSIA	245	41	21.6	14	7.6	100020	63	Y	C	SM
BERANTAI	O	MALAYSIA	207	32	17	12.6	4.4	55337	55	Y	C	SM
NINGALOO VISION	O	AUSTRALIA	238	42	24	15	9	101832	350	Y	C	SM
BUNGA KERTAS	O	MALAYSIA	233	43	19	12	7	87768	60	Y	C	STP
GLAS DOWR	O	AUSTRALIA	242	42	21	15	6	105000	344	Y	N	IT
MODEC VENTURE II	O	AUSTRALIA	258	46	24	16.86	7.14	149686	492	Y	C	IT
STYBARROW VENTURE	N	AUSTRALIA	265	48	24	11.7	12.3	140000	825	Y	N	IT
PYRENEES VENTURE	O	AUSTRALIA	274	48	23	15.8	7.2	143690	200	Y	C	IT
OKHA	O	AUSTRALIA	274	48	23	16.89	6.11	158000	78	N	C	RTM
NGANHURRA	O	AUSTRALIA	260	46	26	14	12	150000	400	N	N	RTM

* O-Operating, D- Decom, Not Operating- N

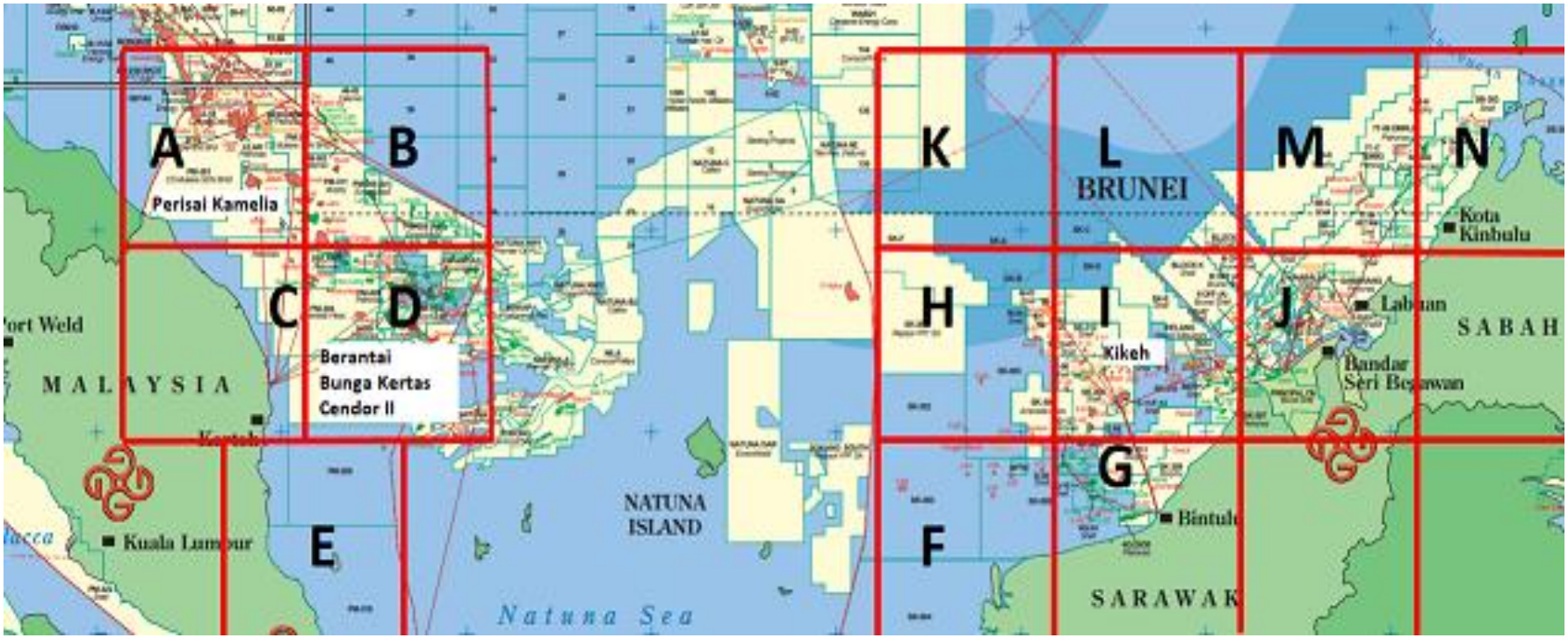

Figure 3.22: Operation location for selected Malaysian FPSOs for Operability analysis and LCCA

(source: Offshore Magazine, 2013 & Omar et al [132]*)*

Figure 3.23: Operation location for selected Australian FPSOs for Operability analysis and LCCA

(source: GEOATLAS, 2014)

Table 3.7: Annual wave scatter table for Zone A to be used for operability analysis of Perisai Kamelia FPSO

H_s(m)	0-1	1-2	2-3	3-4	4-5	5-6	6-7	7-8	8-9	9-10	>10
>3.0											
2.5-3.0											
2.0-2.5								0.10	0.10		
1.5-2.0					0.10		1.20	4.30	0.20		
1.0-1.5				0.20	0.04	7.50	15.60	1.70	0.10	0.10	0.02
0.5-1.0				0.80	26.40	31.30	3.60	0.40	0.10		
0-0.5				4.00	2.20	0.02					
T_p(s)											

Table 3.8: Annual wave scatter table for Zone D to be used for operability analysis of Berantai, Bunga Kertas and Cendor II FPSO

H_s(m)	0-1	1-2	2-3	3-4	4-5	5-6	6-7	7-8	8-9	9-10	>10
>3.0											
2.5-3.0									0.03		
2.0-2.5								1	2		
1.5-2.0							1.4	12.8	0.6		
1.0-1.5				0.1		4.9	12.9	3.4	0.03		
0.5-1.0				0.9	23.7	27.6	4.3	0.3	0.1		
0-0.5			0.1	3.2	0.6						
T_p(s)											

Table 3.9: Annual wave scatter table for Zone I to be used for operability analysis of Kikeh FPSO

H_s(m)	0-1	1-2	2-3	3-4	4-5	5-6	6-7	7-8	8-9	9-10	>10
>3.0											
2.5-3.0											
2.0-2.5								0.1	0.6		
1.5-2.0							1.3	6.7	2.2	0.03	
1.0-1.5						5.1	20.8	5	0.6	0.02	
0.5-1.0				0.02	12.7	31.7	9.6	0.8			
0-0.5				1.4	1.3						
T_p(s)											

Table 3.10: Annual wave scatter table at location 21°S 114°E to be used for operability analysis of Nganhurra, Pyrenees Venture, Stybarrow Venture and Ningaloo Vision FPSO

H_s(m)	T_p(s) <5	5-6	6-7	7-8	8-9	9-10	10-11	11-12	12-13	13-14	14-15	15-16	16-17	17-18	18-19	19-20
0-0.5																
0.5-1							0.19	0.18	0.16	0.12						
1-1.5						0.25	1.00	2.41	2.92	1.94	0.89	0.36	0.46		0.14	
1.5-2		0.21	0.11	0.12	0.15	0.31	1.11	4.10	8.28	6.74	3.14	1.18	1.37	0.28	0.34	0.16
2-2.5			0.42	0.25	0.14	0.31	0.68	2.07	6.77	9.55	5.70	1.93	1.67	0.46	0.35	0.19
2.5-3			0.12	0.36	0.15	0.14	0.23	0.55	2.17	5.34	4.97	2.06	1.44	0.43	0.20	0.12
3-3.5				0.14	0.12				0.31	1.45	2.36	1.63	1.09	0.26		
3.5-4										0.25	0.70	0.85	0.66	0.18		
4-4.5											0.13	0.23	0.39	0.11		
4.5-5													0.10			
5-5.5																

Table 3.11: Annual wave scatter table at location 19°S 116°E to be used for operability analysis of Okha and Modec Venture II

H_s(m)	T_p(s) <5	5-6	6-7	7-8	8-9	9-10	10-11	11-12	12-13	13-14	14-15	15-16	16-17	17-18	18-19	19-20
0-0.5																
0.5-1						0.21	0.72	1.62	1.66	1.17	0.51	0.23	0.26		0.10	
1-1.5	0.16	0.38	0.24	0.20	0.22	0.44	1.31	4.83	8.65	6.87	3.34	1.27	1.44	0.27	0.36	0.17
1.5-2		0.99	0.94	0.42	0.20	0.38	0.73	2.37	7.11	9.02	6.00	2.11	2.02	0.48	0.37	0.14
2-2.5		0.31	1.28	0.75	0.17	0.23	0.19	0.43	1.90	4.70	4.39	2.09	1.53	0.42	0.25	0.14
2.5-3			0.60	0.87	0.15				0.19	0.97	1.61	1.34	1.07	0.29		
3-3.5				0.54	0.16						0.30	0.38	0.48	0.14		
3.5-4				0.19	0.16											
4-4.5																
4.5-5																
5-5.5																

Table 3.12: Annual wave scatter table at location 10.5°S 125°E to be used for operability analysis of Glas Dowr FPSO

H_s(m)																	
0-0.5		0.13	0.17	0.11			0.14	0.58	1.64	1.93	1.47	0.58	0.25	0.30			
0.5-1	0.16	0.56	0.93	1.18	0.68	0.38	0.42	1.40	5.11	11.05	11.79	6.26	2.31	2.55	0.38	0.56	0.16
1-1.5		1.06	2.22	2.30	1.55	0.43	0.28	0.28	0.72	3.13	6.95	5.63	2.36	2.20	0.47	0.36	0.15
1.5-2			1.24	3.23	1.21	0.40	0.21	0.25	0.11	0.25	1.09	1.56	1.10	0.97	0.24	0.11	
2-2.5				0.93	1.18	0.18	0.11					0.14	0.15	0.19			
2.5-3					0.55												
3-3.5																	
3.5-4																	
4-4.5																	
4.5-5																	
5-5.5																	
T_p(s)	<4	4-5	5-6	6-7	7-8	8-9	9-10	10-11	11-12	12-13	13-14	14-15	15-16	16-17	17-18	18-19	19-20

Table 3.13: Representative Extreme cyclonic condition in NWA [61]

	Wave		**Wind**	**Current**
	H_s(m)	**T_p(s)**	**velocity (m/s)**	**velocity (m/s)**
100-year RP	14	14.5	44	1.9
1-year RP	3.2	8.5	14	0.6

The annual wave scatter data obtained from Metocean View is given in Table 3.10 – 3.12 in terms of their joint probability distribution in percentage. Percentage probability is calculated as no. of occurrence of each wave divided by 10000 and multiplied by 100 (For example, 78 waves in 100,000 occurrence means 0.078% or in fraction 0.00078). Downtime due to green water events using these wave scatter tables have been performed for Malaysia and Australia. However, these data are only for wind generated seas and does not consider the cyclonic conditions which North Western Australia is prone to as given in Table 3.13. Hence analysis has also been conducted on chosen Australian FPSOs to identify freeboard exceedance when subjected to 100-year extreme cyclonic conditions to be used by design engineers as per [131].

3.6 Life - Cycle Cost Analysis of FPSO

Life - cycle cost analysis of FPSO is conducted based on the following procedure. The cost data for FPSOs in Australia and Malaysia have been collected to compare the life cycle cost of FPSOs with different mooring configurations and hull conditions. The section below details the LCCA procedure adopted to calculate the LCCA for FPSOs as shown in Figure 3.24.

3.6.1 Identification of design alternatives to be compared

The two main design alternatives which are going to be compared are mooring system (spread/ ET/ IT/ RTM/ STP) and hull condition (newly-built/converted). The life-cycle phases of an FPSO can be discretised as shown in Section 2.2.8. Out of the life cycle phases identified, this study considers the capital cost for the whole project (C1), operation and maintenance (C3+C4), downtime cost due to production loss in the event of green water on FPSO deck (C6) and revenue from oil production (B9). The same is shown in Figure 3.24.

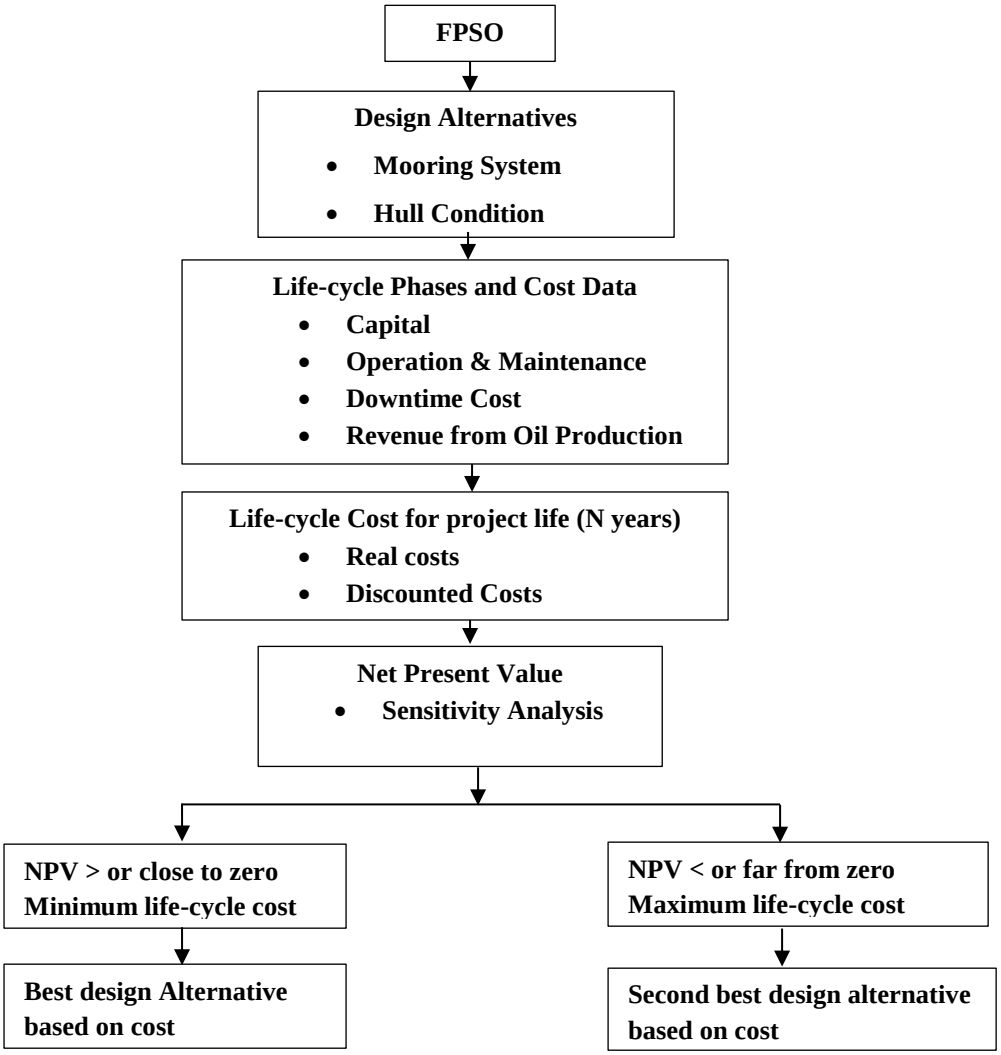

Figure 3.24: LCCA Procedure for FPSO

3.6.2 Establishment of basic assumptions and determination of exact LCC procedure to be adopted.

Assumptions on life expectancy of FPSO (N), cash flow timings, resale/residual values, inflation, discount rate, source and reliability of data and comprehensiveness of life cycle costing is the next step of the procedure.

3.6.2.1 Life expectancy of FPSO

Newly-built FPSOs are generally designed for 20-30-year fatigue life. But the converted ones are usually designed for a short period of 10 years; hence two life- cycle periods are chosen for this study, 10 years and 25 years.

3.6.2.2 Cash flow timings

Capital cost is included in the initial (zeroth)year, while annual operation and maintenance cost, annual revenue from oil production and annual downtime cost (that is if any exists as per the motion response of FPSO under wind generated sea condition which can result in green water as shown in section 3.5.1) is included from the 1st year through-to Nth year.

3.6.2.3 Discount rate

Inflation rate for Australian economy in 2017 can be taken as 1.9% from the Reserve Bank of Australia [135]. Treasury bond rate of return of 2.8% based on a reasonable 10-year yield from Investing [136] and an average equity return rate of 7.003% taken from Market Risk Premia [137]. Then the discount rate for Australian economy is 2.96% as per the method specified by Royal Institution of Chartered Surveyors (RCIS) as shown in Eq. 3.66. The discount rate has been decreasing since 2011, from 5.56% to 2.96% in 2017 [138]. Inflation rate for Malaysian economy in 2017 can be taken as 3.7% from the Bank Negara Malaysia [139]. Treasury bond rate of return of 4.1% based on a reasonable 10-year yield from Investing [136] and an average equity return rate of 7.001% taken from Investing [136]. Then the discount rate for Malaysian economy is 1.87% as per the method specified by RCIS as shown in Eq. 3.66. A Discount-rate is required to assist with an understanding of the time value of money such that a dollar today is worth more than a dollar in the future. The empirical formula

gives the discount rate based on the relevant input data as shown in Eq. 3.8, Eq. 3.9 and Eq. 3.10 shows how to calculate: no risk return and average risk premium discount rate from inflation rate, treasury bond rate of return and average equity return.

$$Discount\ rate = No\ risk\ return + 0.5 \times\ Average\ risk\ premium\ discount\ rate \quad (3.8)$$

$$No\ risk\ return = Treasury\ bond\ rate\ of\ return -\ Inflation \quad (3.9)$$

$$Average\ risk\ premium\ discount\ rate =$$

$$Average\ equity\ return - Treasury\ bond \quad (3.10)$$

3.6.2.4 Source and reliability of data

Data collection is a key step in the phases of LCCA application and utmost care has been taken in obtaining them. The data collection in this study is described in the next section.

3.6.3 Data Collection

The data collection for LCCA was done as per the method specified in Life-cycle costing standard DS/EN ISO 15663-1 [140]. A data collection sheet was prepared and sent to the potential data givers who are industry practitioners and experienced in different phases of FPSO project. Cost data elements were kept simple as the detailed cost breakdown for an FPSO project is confidential and unavailable. The data givers were asked to provide the total capital cost of FPSO, operation cost, maintenance cost and lease rate for leased FPSOs. From the various FPSOs for which cost data were obtained, only the FPSOs in Australia and Malaysia were chosen for the life-cycle cost study. Cost data were obtained from practitioners in PETRONAS, Malaysia, CHEVRON, Australia, WOOD MACKENZIE Asset reports, published articles and news letters on FPSO and other industry websites [141]–[152]. The maximum oil

production data are obtained from Offshore Magazine [2] [153] while downtime cost is calculated from the motion response generated through dynamic analysis.

3.6.4 Cost Data for FPSOs

The FPSOs under study are noted as alternatively: spread mooring, internal turret mooring, external turret mooring, submerged turret mooring and finally riser turret mooring. Most of the new FPSOs have riser turret mooring while the older systems are either spread moored or internal or external turret moored.

The capital cost includes the total cost of development of the project, i.e. the cost of mooring, risers, wells, subsea and floater, cost of hull construction and EPC (Engineering, Procurement and Construction) related expenditure which includes the equipment cost for topside. The daily bare boat charter (BBC) rate and daily operation and maintenance data were converted to annual data by multiplying with 2200 working hours per year as the average billable working hours per year is 2200 [154]. The capital cost, operation cost, maintenance cost and lease rate of FPSO are obtained from [141]–[152].

Downtime cost due to green water events can be calculated by knowing FPSO motion response responsible for the event by conducting a dynamic motion response analysis as shown in section 3.4.2 and 3.5.1. Downtime cost per year can then be calculated by multiplying number of days of downtime with price of oil per barrel per day in USD and oil produced in barrels per day. It is assumed here that the FPSO produces oil to its maximum capacity and then the revenue generated per year from oil production can be obtained by multiplying maximum oil production capacity in barrel of oil per day with 2200 working hours per year and cost of oil per barrel in USD. The maximum oil production capacity of FPSOs can be obtained from Offshore Magazine [2][153].

3.6.5 Life-cycle Cost Calculation for FPSO

The detailed cost data as per Eq. 2.18 has been adapted such that the life cycle cost for FPSO is calculated based on capital cost (O_1-outgoing 1), Operation and Maintenance cost (O_2- outgoing 2) over the life cycle period, Lease rate for FPSO (if the hull is leased) (O_3- outgoing 3) over the life cycle period, downtime cost calculated for green water events (O_4- outgoing 4) over the life cycle period and income from producing oil (I_1- Incoming 1) over the life cycle period. O_2 over the life cycle period is calculated as the sum of operation and maintenance cost from 1st year to Nth year, O_3 is calculated as the sum of lease rate of FPSO from 1st year to Nth year and O_4 is calculated as the sum of downtime cost of FPSO from 1st year to Nth year. O_4 can be zero if there is no downtime. I_1 is calculated as the sum of income generated from oil production from 1st year to Nth year which is taken as negative while calculating LCC_{FPSO}. All outgoing cash flow as positive value and incoming cash flow as negative value. Therefore, life cycle cost of FPSO is given by,

$$LCC_{FPSO} = O_1 + O_2 + O_3 + O_4 - I_1 \tag{3.11}$$

3.6.6 NPV Calculation for FPSO

Once capital costs, annual operation and maintenance cost, downtime cost and revenue generated from oil production are calculated, real costs incurred per year (R_n) is calculated, mainly consisting of annual operation and maintenance cost and downtime cost as negative value and income from oil as positive value from 1st year to Nth year; in the zero th year incorporating capital costs as negative value. Then discount factor as shown in Eq. 3.12 is multiplied with every years' real costs. If the discount factor for year n is calculated, then

$$Discount\ Factor_n = \frac{1}{(1+discount\ rate)^n} \tag{3.12}$$

Hence for the zero [th] year, the discount factor will be 1 and gradually reduces as the life of the FPSO expires. This takes into account the time value of the money. Then the discounted present value (PVn) of the FPSO for each year is calculated as the product of real costs incurred in that year (Rn) and Discount Factor for that year (Discount $Factor_n$) as shown in Eq. 3.13.

$$PV_n = R_n \times Discount\ Factor_n \tag{3.13}$$

Finally, NPV is calculated as the sum of discounted present values from year zero to year N as shown in Eq. 3.14.

$$NPV = \sum_{n=0}^{N} PV_n \tag{3.14}$$

A detailed spreadsheet was developed to compute the life-cycle costs and NPV for various FPSOs.

3.6.7 Risk/Uncertainty Assessment

Sensitivity analysis has been carried out as per Whyte's [103] method to calculate NPV of best and worst systems by using discount rates higher and lower than the actual one; in other words, to incorporate risks, a sensitivity analysis has been performed by varying the discount rate from 2% to 10% and the procedure described in the above section is applied to calculate NPV of the design alternatives. This study is highly relevant as the market condition has seen some of its worst years recently. The usual discount rate used for evaluating infrastructures were 7% in Australia previously, but that's when the treasury bond rate of return was 6.8%. But now the treasury bond return is only 2.8% [155] [136]. Hence a sensitivity analysis by taking discount rate from 2% to 10% would cover the worst and best market conditions while reflecting the effect of the same on NPVs of FPSOs.

3.6.8 Selection of Design Alternative

The design with the NPV close to zero and minimum life-cycle cost is identified as the cost effective FPSO alternative.

3.7 Chapter Summary

The numerical and physical model testing procedures adopted to evaluate the dynamic responses of FPSO are explained along with the model details. The modelling procedure, frequency domain simulations and time domain simulations carried out are discussed in detail using the theories and assumptions used during the analysis. Operability analysis to determine downtime cost due to green water events are then discussed and finally, the life-cycle costing procedure adopted for FPSO is detailed along with the chosen FPSOs in Malaysia and Australia for study. The results and discussions of this study are detailed in the next chapter.

CHAPTER 4

RESULTS AND DISCUSSION

4.1 Chapter Overview

In this chapter, the motion responses of FPSO obtained using model testing and software simulation methods are comprehensively presented in the prototype scale. At first, the model testing results are discussed, then, the uncoupled and coupled analysis performed using SESAM HydroD V4.5-08 and SESAM DeepC V5.0-06 is compared with the model testing results conducted in UTP Offshore laboratory and published results of experiments conducted at OTRC laboratory, Texas A&M. The calibrated simulation model was used to perform parametric studies for metocean data, water depth, hull parameters and mooring system details and the results are presented here. Then, the motion RAOs, relative motions and subsequent downtime cost generated for the FPSOs operating in Australia and Malaysia are presented. Also, the life cycle costs and NPVs of the FPSOs in Australian and Malaysian waters with different mooring systems and hull conditions are discussed along with the cost proportions due to each life cycle phase. Finally, a discussion has been made of the factors affecting the selection of an economic and efficient FPSO with good motion performance increasing the operational time.

4.2 Experimental Results

The results of static offset test and free decay test is given in the below sections.

4.2.1 Static Offset Test

From the static offset test, the system spring constant was found to be 168 kN/m. The force- excursion relationship of the system is shown in Figure 4.1. The linear regression of the collected data is plotted along with the test results.

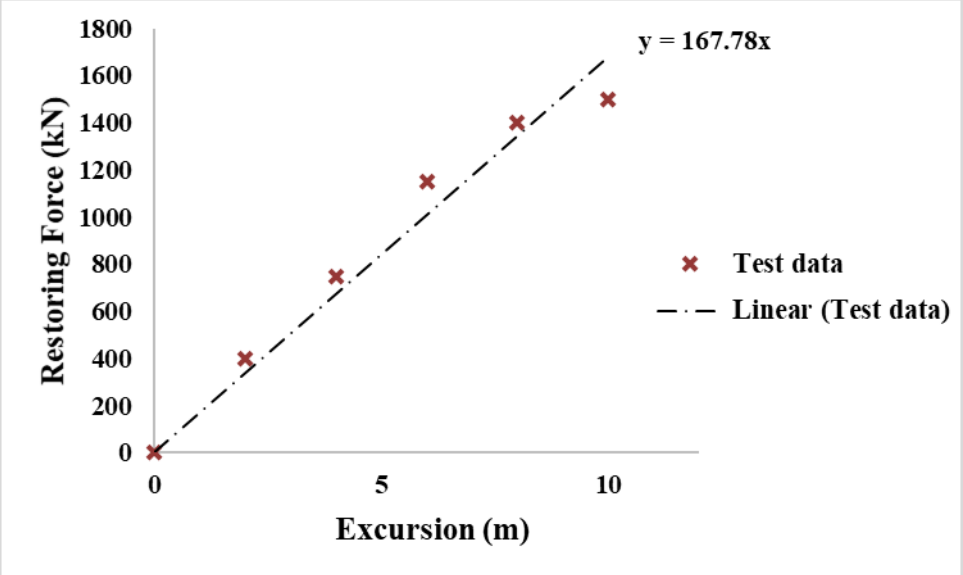

Figure 4.1: Force- excursion relationship of FPSO with horizontal mooring system (test result in prototype Scale)

4.2.2 Free Decay Test

The natural period of the system was found by conducting free decay test. The results shown in Table 4.1 are calculated by taking the average of time periods for the first few sinusoidal excitations of the free decay series. Savitzky-Golay filtering method was used in MATLAB to eliminate noise from the time series. The free decay graphs for the horizontal motions are given in Figure 4.2 ~ Figure 4.7. Coupling effect from horizontal mooring line restoring, damping and inertia forces [48][156] are observed during the free decay tests. Especially in heave, it was observed that the heave motion amplified after 111 s and then again decayed.

Table 4.1: Measured Natural Periods for FPSO [56]

Motion	Natural Period (s)	Typical natural Period (s)
Surge	103.5	>100
Sway	152	>100
Yaw	74.5	>100
Heave	9.25	5 - 12
Roll	25	5 - 30
Pitch	8.7	5 - 12

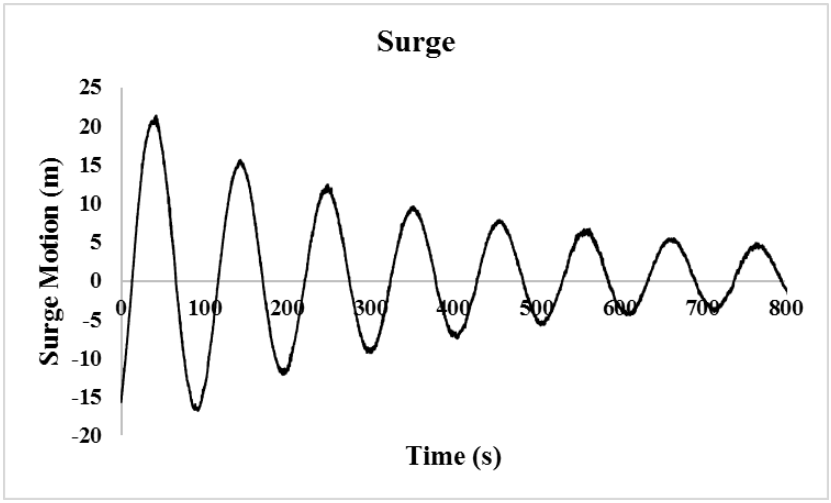

Figure 4.2: Free decay time series – Surge (test result in prototype scale)

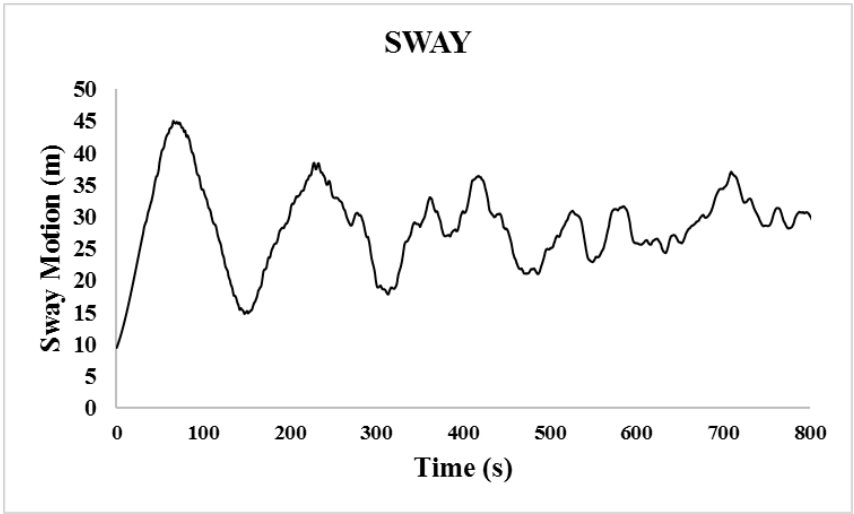

Figure 4.3: Free decay time series – Sway (test result in prototype scale)

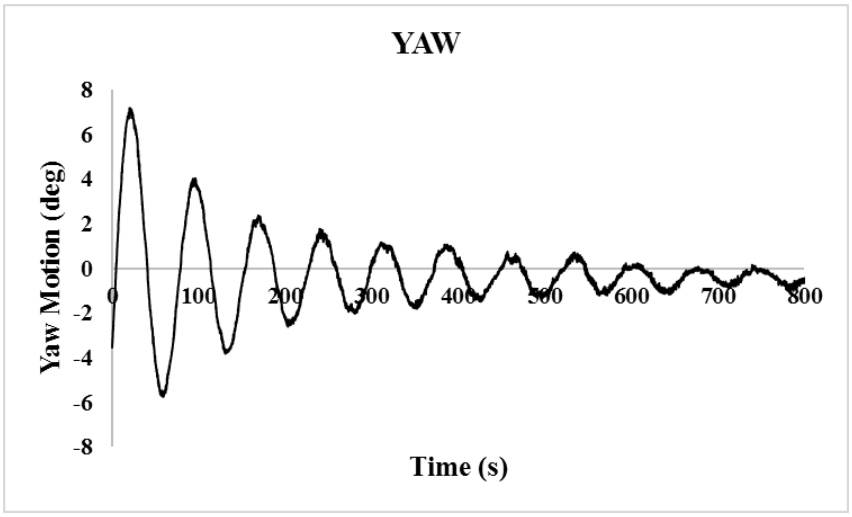

Figure 4.4: Free decay time series – Yaw (test result in prototype scale)

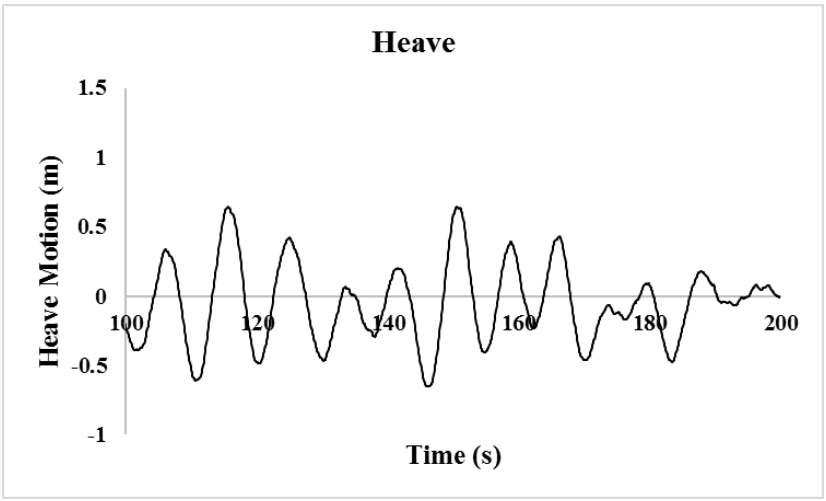

Figure 4.5: Free decay time series – Heave (test result in prototype scale)

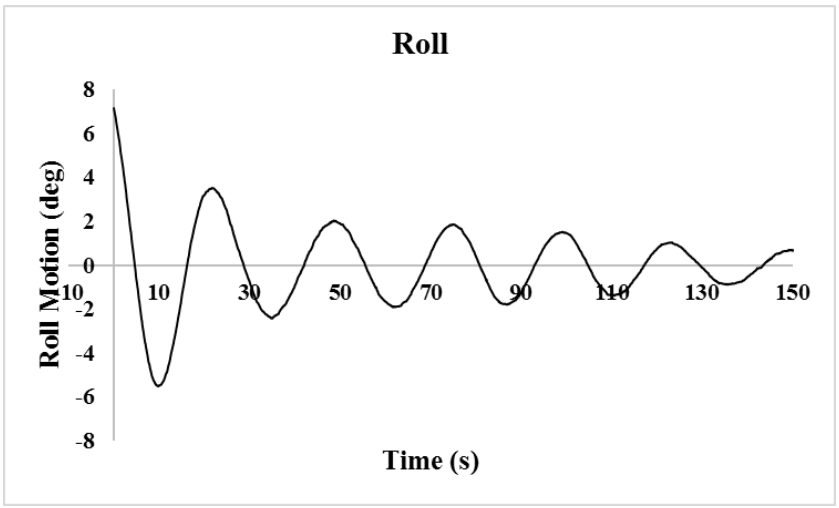

Figure 4.6: Free decay time series – Roll (test result in prototype scale)

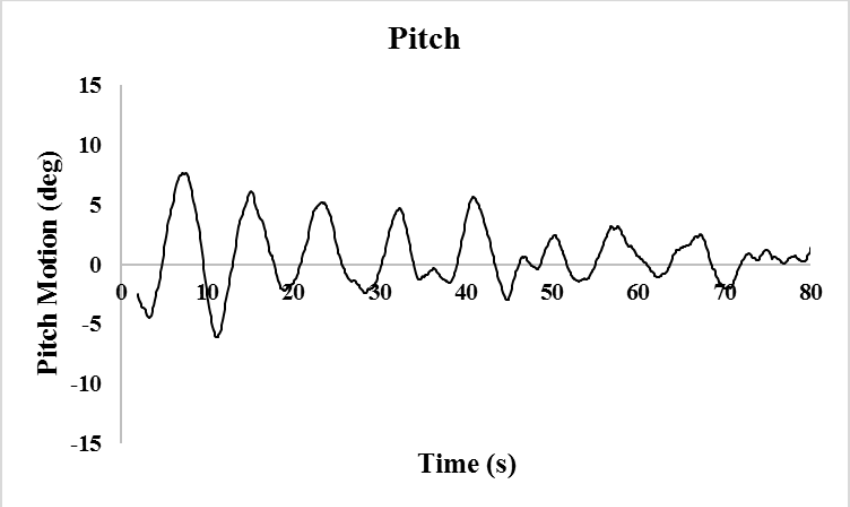

Figure 4.7: Free decay time series – Pitch (test result in prototype scale)

4.3 Validation of Uncoupled Frequency Domain Analysis

The frequency domain simulation performed using SESAM HydroD V4.5-08 for 50% loading condition of the Berantai FPSO at a water depth of 100 m was compared with the results from model tests performed at the UTP Offshore Laboratory. The vessel details are given in Table 3.2. The vessel was subjected to head sea (wave direction – 180°) and crossing sea (wave direction – 150°) condition. The vessel was anchored to position using four soft mooring lines which has limited influence on the vessel motion. The properties of the spring are same as the one used for model testing. The vessel responses are compared with the physical model testing results for the long crested white noise wave condition with significant wave height 5 m and peak period 15 s. White noise wave generated are more analogous to the real ocean surface and does not have the constraint of periodicity [127], [128]. In reality, ocean waves are never regular and each wave will be unique. This method of creating a water surface elevation time history is not constrained by the requirement that the wave components are harmonics of the primary wave. The motion RAOs are compared in Figure 4.8 ~ Figure 4.13. The surge, heave and pitch motions of the vessel are studied since they are the prominent degrees of freedom in head sea condition and the sway, roll and yaw motions are investigated in crossing sea condition.

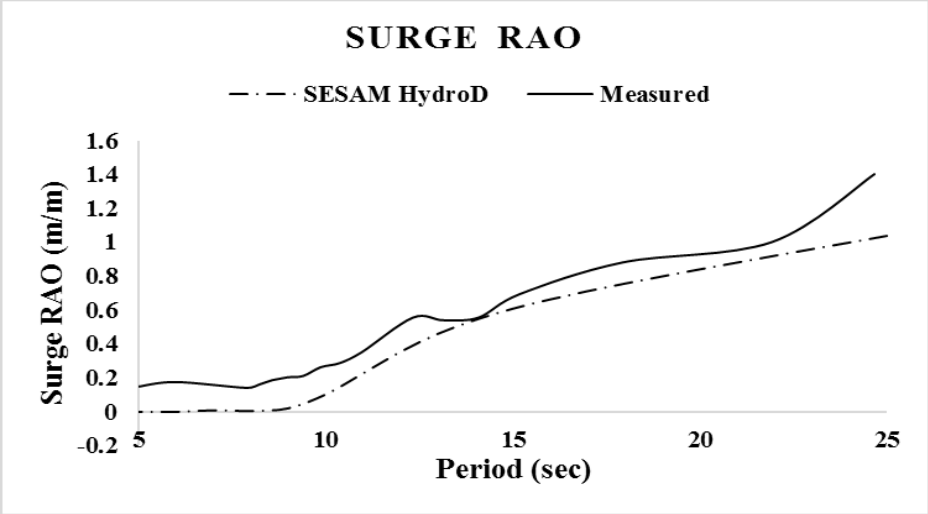

Figure 4.8: Surge RAO (Comparison of HydroD and experiment results)

Figure 4.8 illustrates the surge response of Berantai FPSO subjected to long crested waves by experimental study and SESAM HydroD V4.5-08. From the comparison, fairly good agreement could be observed with RMSD 0.16 with the experimental and software simulation results. The comparison of heave responses is show in Figure 4.9 with RMSD 0.14 with the experimental and software simulation results. The pitch motion RAO shown in Figure 4.10 has an RMSD value of 0.16 with the experimental and software simulation results.

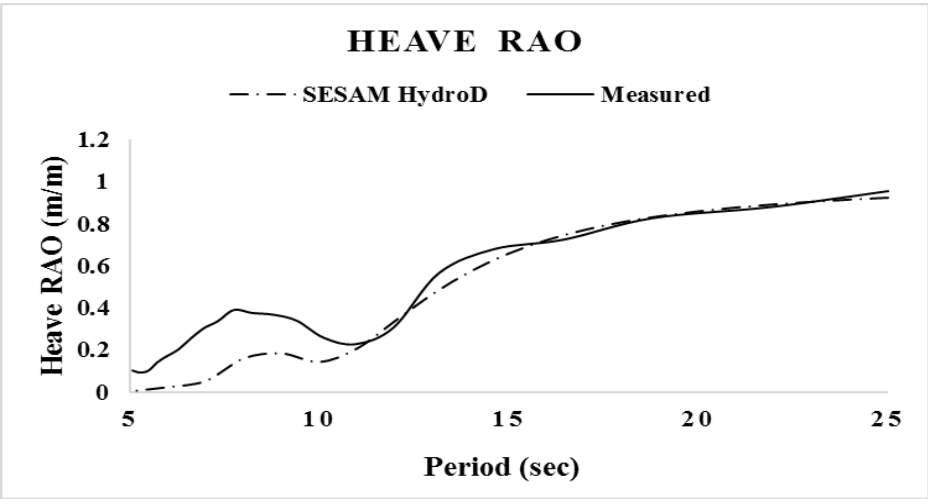

Figure 4.9: Heave RAO (Comparison of HydroD and experiment results)

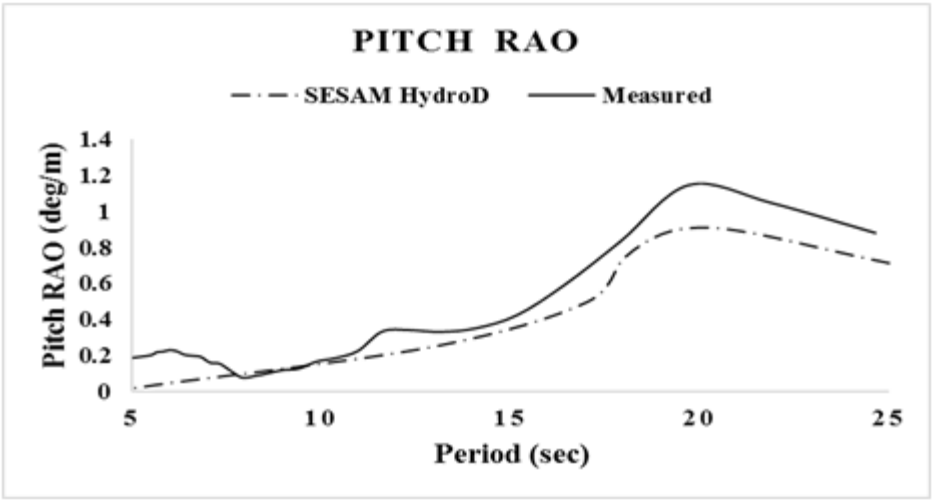

Figure 4.10: Pitch RAO (Comparison of HydroD and experiment results)

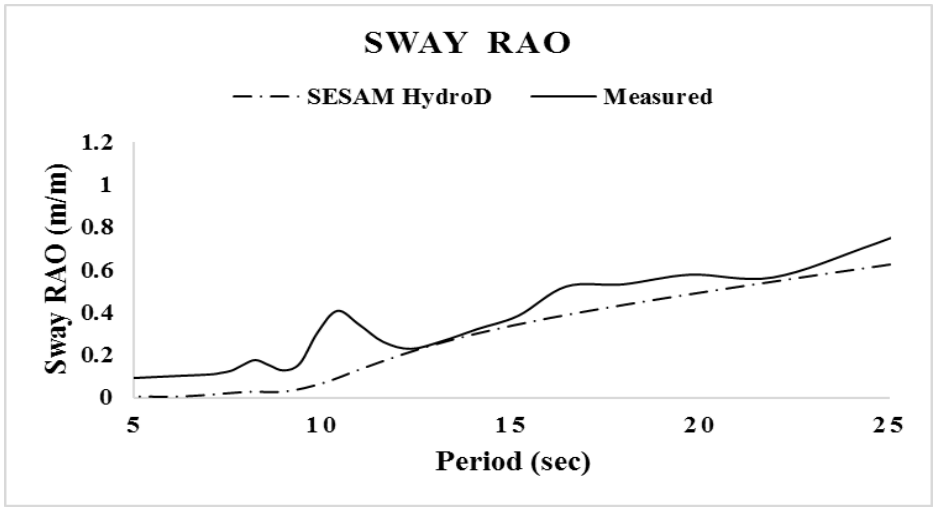

Figure 4.11: Sway RAO (Comparison of HydroD and experiment results)

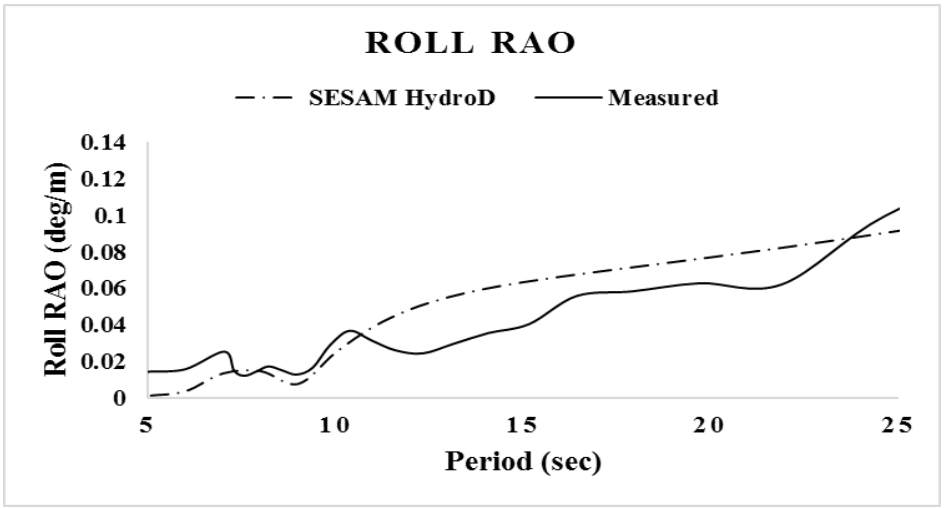

Figure 4.12: Roll RAO (Comparison of HydroD and experiment results)

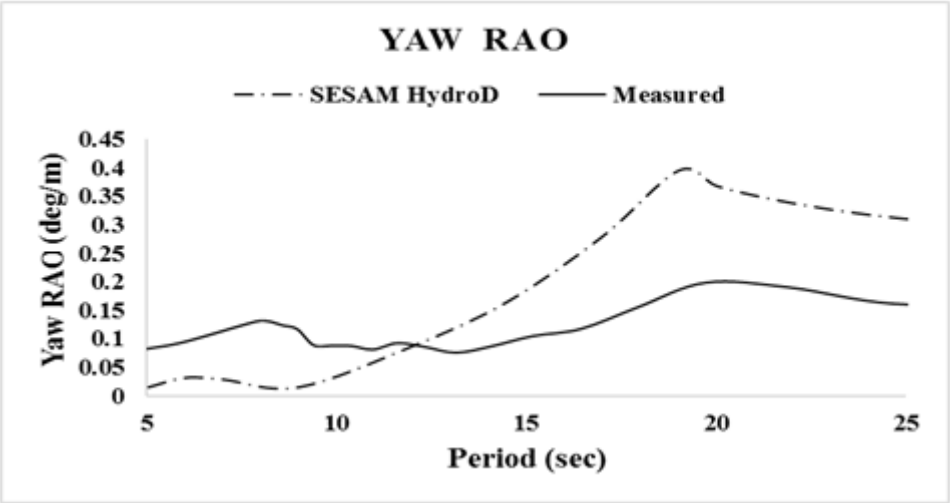

Figure 4.13: Yaw RAO (Comparison of HydroD and experiment results)

It can be seen in Figure 4.12 that the Roll RAO is not reducing at large wave periods (25 s). This is due to the resonance created when the vessel natural period equals the wave period. The natural period of vessel in roll is also 25 s as seen in Table 4.1. Also the roll damping is low as the FPSO model used for wave tank experiments do not have bilge keel, which is usually present in real scenario [97]. Also, the damping produced from horizontal mooring is also less when compared to catenary mooring [84].

The sway and roll RAOs shown in Figure 4.11 and Figure 4.12 has RMSD values 0.01 and 0.016 respectively with the experimental and software simulation results. The Yaw motion RAO has RMSD value of 0.11 with the experimental and software simulation results. The yaw motion RAO given in Figure 4.13 for software simulation result shows a peak around 20 s. This is because the yaw and roll motions are undermined in the experimental investigation. This is due to the use of horizontal spread mooring system preventing large rotation. A similar study by Xie et al using horizontal spread moored vessel [157] also reports the same for yaw and roll rotations obtained using experimental study.

In the comparison, it is noticeable that the numerical results agreed fairly with the experimental results. RMSD values found for the results comparing the model test and commercial software program results are very low with a maximum of only 0.16 for surge. It was seen that the commercial software results are smaller compared to the experimental results. This is due to the assumptions used in the software simulation

that it does not consider the higher order forces that cause smaller responses occurring especially at higher wave periods (low frequency region) [71]. Also, model testing results are observed to be higher than software simulation in the lower wave periods (high frequency region). It is due to the small responses of vessel because of the high frequency excitation of the mooring lines [71], which again is not considered in the simulation following the assumption that linearised wave is used.

4.4 Validation of Coupled Time Domain Analysis

The coupled time domain simulation performed using SESAM DeepC V5.0-06 and the procedures adopted were verified by doing a validation by comparing the published results from model tests performed at the OTRC wave basin and numerical simulations by Kim et al [42].

4.4.1 FPSO and Metocean Conditions

The coupled analysis program is validated by using the published results by Kim et al [42]. The prototype of turret moored FPSO was moored at 1828.8 m water depth using 12 chain-polyester-chain taut lines. The 12 mooring lines were divided into four groups normal to each other and each group consists of lines 5° apart. Four equivalent mooring lines were used in model testing with each mooring line having the combined effect of three mooring lines in prototype. Since the length of the mooring lines were not able to model as per the scale used, a truncated mooring system was used with equivalent static surge stiffness of the prototype mooring design in the model testing. The main dimensions of the FPSO are given in Table 4.2. The turret of the FPSO was located at 38.73 m (12.5 % LBP) behind the forward perpendicular of the FPSO. The mooring line pretension is 1424 kN and the length of the mooring line is 2652 m. The other mooring details are given in Table 4.3 & Table 4.4.

Table 4.2: Main Particulars of OTRC FPSO [42]

Description	**Unit**	**Quantity**
LBP	m	310
Beam	m	47.17
Depth	m	28.04
Draft (80%)	m	15.121
Displacement (80%)	MT	186051
k_{xx} at CG	m	14.036
k_{yy} at CG	m	77.47
k_{zz} at CG	m	79.3

Table 4.3: Mooring Line Particulars for OTRC FPSO [42]

Description	**Unit**	**Quantity**
Segment 1: Chain		
Length at anchor point	m	121.9
Diameter	cm	9.52
Dry Weight	N/m	1856
Weight in Water	N/m	1615
Stiffness AE	kN	820900
Mean Breaking Load	kN	7553
Segment 2: Polyester Rope		
Length	m	2438
Diameter	cm	16
Dry Weight	N/m	168.7
Weight in Water	N/m	44.1
Stiffness AE	kN	168120
Mean Breaking Load	kN	7429
Segment 3: Chain		
Length at anchor point	m	91.4
Diameter	cm	9.53
Dry Weight	N/m	1856
Weight in Water	N/m	1615
Stiffness AE	kN	820900
Mean Breaking Load	kN	7553

Table 4.4: Hydrodynamic coefficients of the chain and polyester rope [42]

Hydrodynamic Coefficients	**Chain**	**Polyester Rope**
Normal Drag	2.45	1.2
Normal Added Inertia	2	1.15

The experiments and simulations were conducted for the 100-year hurricane condition in the Gulf of Mexico. The wave condition was given by JONSWAP spectrum with a peak enhancement factor of 2.5 and to generate wind loading, NPD spectrum is used. The metocean conditions are given in Table 4.5. The wind spectrum generated is compared with the published spectrum and given in Figure 4.14. The JONSWAP spectrum is given in Figure 4.15.

Table 4.5: Metocean Data used by Kim et al [42]

Description	**Unit**	**Quantity**
Wave		
Significant Wave Height	m	12.19
Peak Period	s	14
Direction	deg	180
Wind		
Velocity at 10m above MWL	m/s	41.12
Direction	deg	150
Current		
Profile		
At free surface 0m	m/s	0.9144
At 60.96m	m/s	0.9144
At 91.44m	m/s	0.0914
On the sea bottom	m/s	0.0914
Direction	deg	210

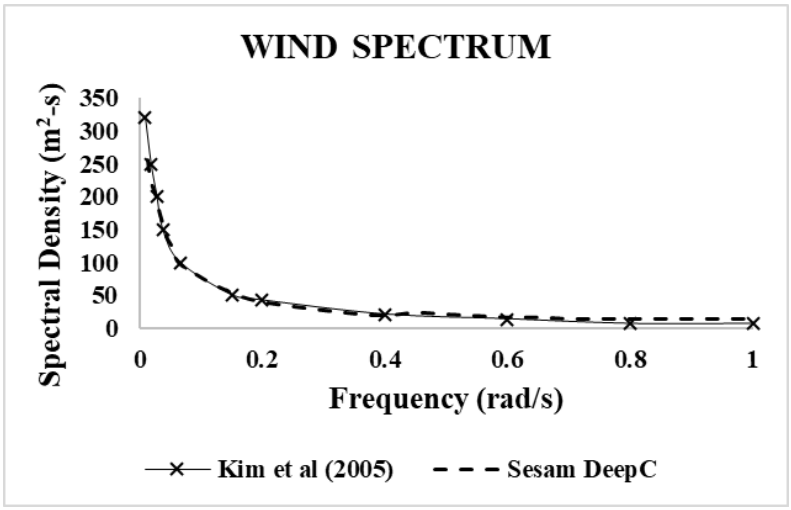

Figure 4.14: Wind Spectrum Comparison

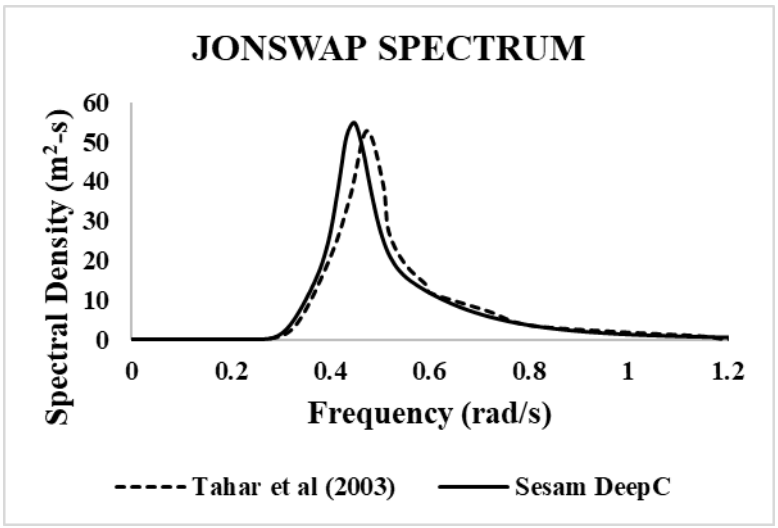

Figure 4.15: Wave Spectrum Comparison

4.4.2 Natural Periods & Damping Ratios

As explained in section 3.5.3, free decay analysis was performed using SESAM DeepC V5.0-06 to verify if the simulation model and the prototype has the same mass distribution and hydrodynamic performance. A specified force of 50000 kN was given in the respective directions for 20 s where the free decaying must be studied. The simulation model was calibrated to achieve the natural periods and damping ratios as given in Table 4.6. The free decay graphs are as shown in Figure 4.16 ~ 4.19 respectively. The comparison for natural periods and damping ratios shows that the

hydrodynamic behaviour of the simulated FPSO is matching well with the Kim et al [42] model. The results obtained from SESAM DeepC V5.0-06 varies less than 5 % from the experimental results and WINPOST simulations conducted by Kim et al [42]. The first peaks of the free decay curve were used in calculating natural period and damping ratios.

Table 4.6: Comparison of Natural Periods & Damping Ratios

DOF	**SESAM DeepC V5.0-06**		**OTRC Experiment (Published Results, Kim et al** [42]**)**		**WINPOST (4 mooring lines) (Published Results, Kim et al** [42]**)**	
	Natural Period (s)	**Damping Ratio (%)**	**Natural Period (s)**	**Damping Ratio (%)**	**Natural Period (s)**	**Damping Ratio (%)**
Surge	204.2	2.1	206.8	3	204.7	4.4
Heave	11.2	6.6	10.7	6.7	10.8	11.8
Roll	12.4	2.3	12.7	3.4	12.7	0.7
Pitch	10.6	10.45	10.5	8	10.8	10.5

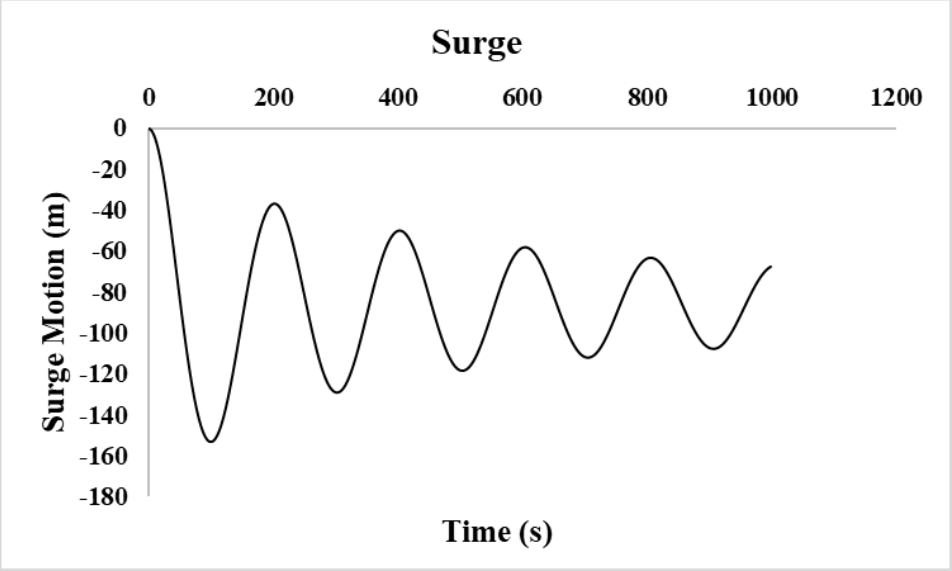

Figure 4.16: Free Decay Time Series – Surge (SESAM DeepC)

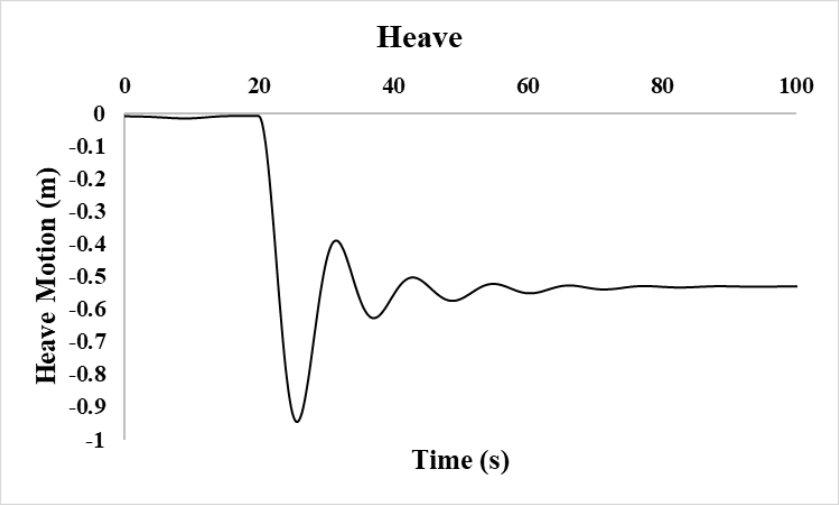

Figure 4.17: Free Decay Time Series – Heave (SESAM DeepC)

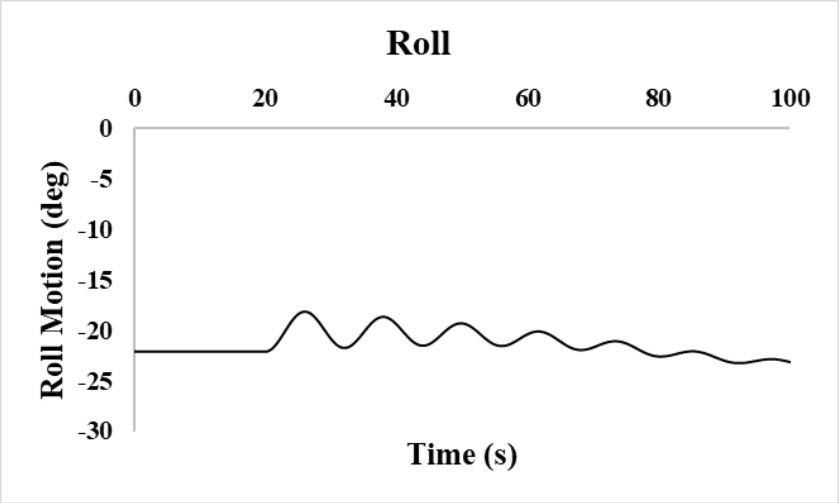

Figure 4.18: Free Decay Time Series – Roll (SESAM DeepC)

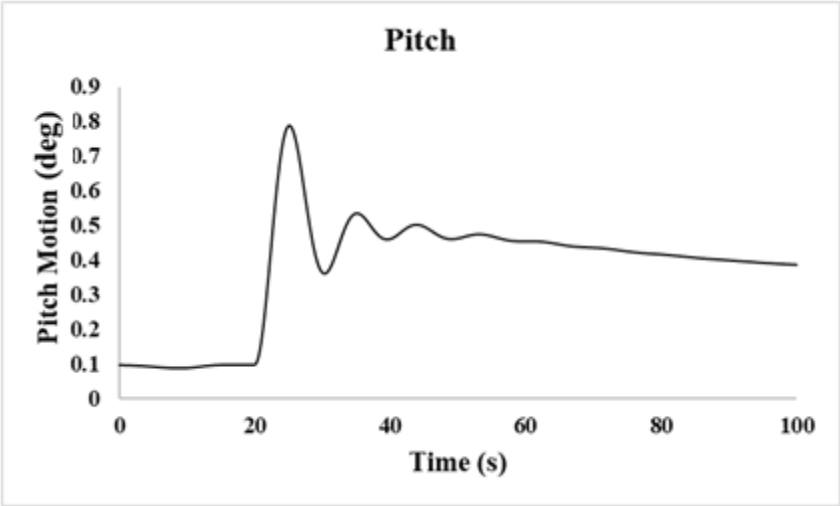

Figure 4.19: Free Decay Time Series – Pitch (SESAM DeepC)

4.4.3 Response Spectra

The motion spectrums generated using SESAM DeepC V5.0-06 after time domain analysis were compared with motion spectrums developed by Kim et al [42] from the model testing studies and the WINPOST- FPSO simulations in time domain. The horizontal motions of the FPSO, surge, sway and yaw are dominant in the low frequency whereas the vertical motions of the FPSO, heave, roll and pitch are pronounced in wave frequency ranges. The spectral density curves for the six degrees of freedom response of the OTRC FPSO is given in Figure 4.20 ~ Figure 4.25.

Figure 4.20 illustrates the surge response of OTRC FPSO subjected to long crested waves by experimental and numerical study conducted by Kim et al [42] and SESAM DeepC V5.0-06 in the present study.

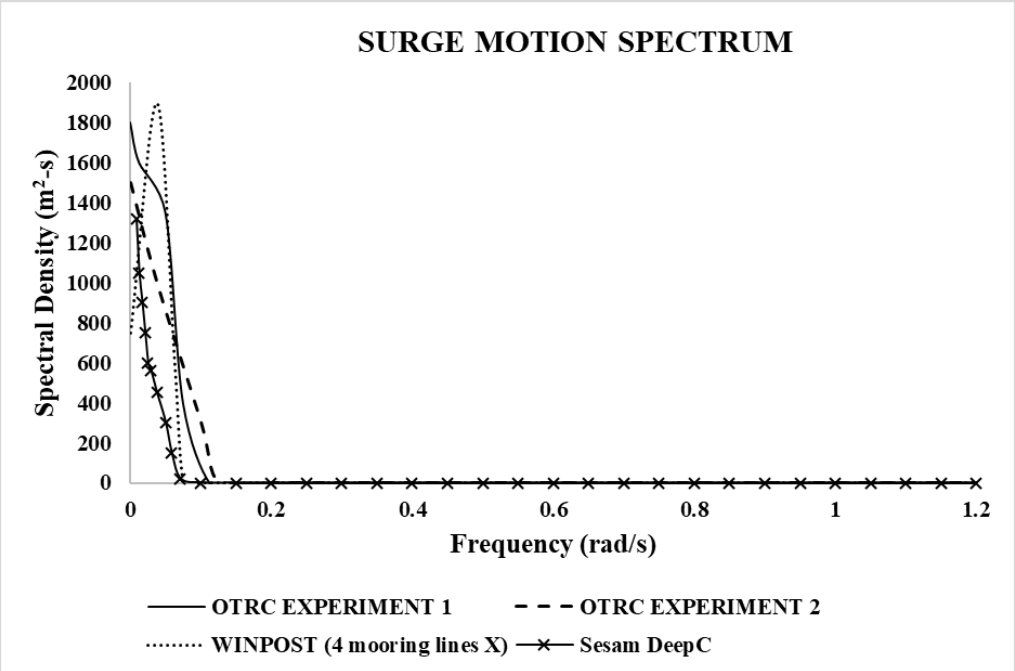

Figure 4.20: Surge Motion Spectrum Comparison (SESAM DeepC and Kim et al results [42])

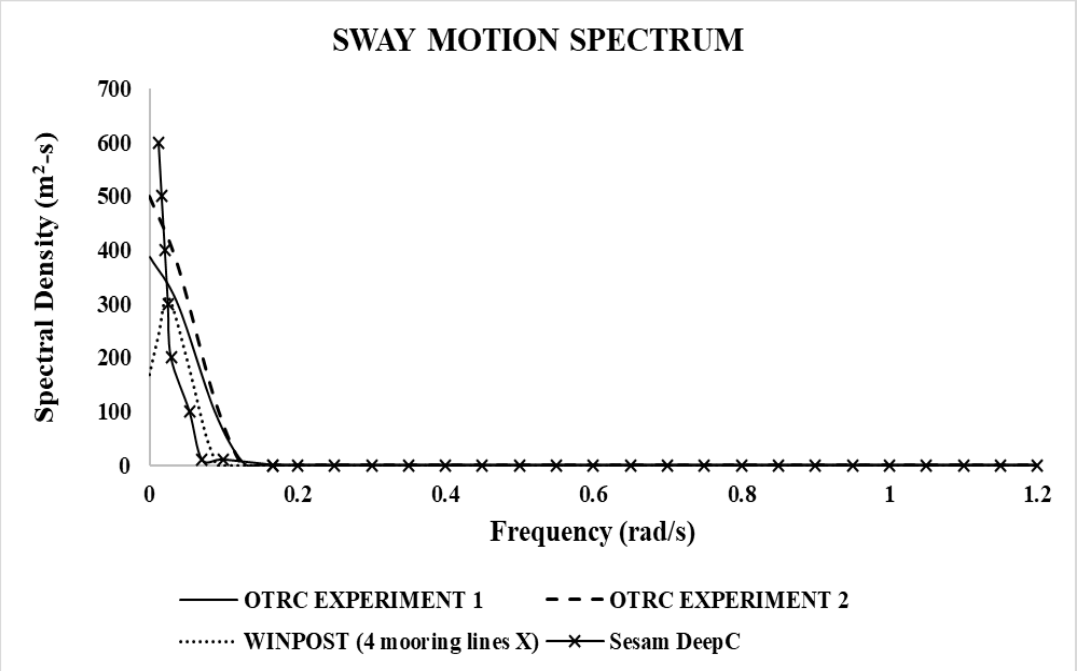

Figure 4.21: Sway Motion Spectrum Comparison (SESAM DeepC and Kim et al results [42])

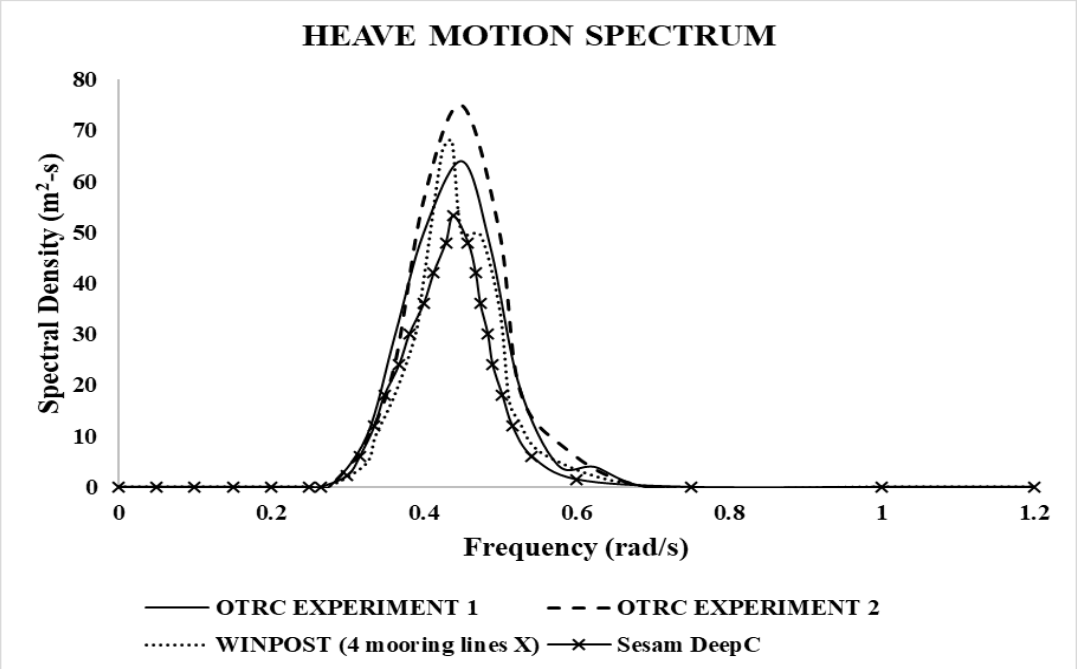

Figure 4.22: Heave Motion Spectrum Comparison (SESAM DeepC and Kim et al results [42])

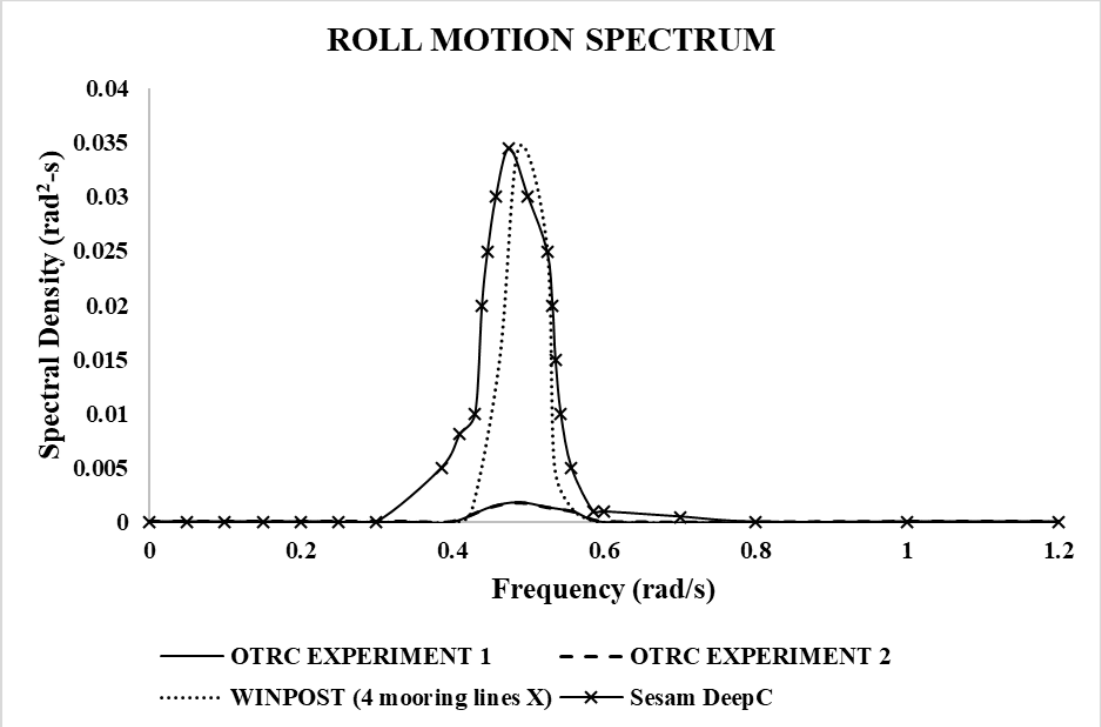

Figure 4.23: Roll Motion Spectrum Comparison (SESAM DeepC and Kim et al results [42])

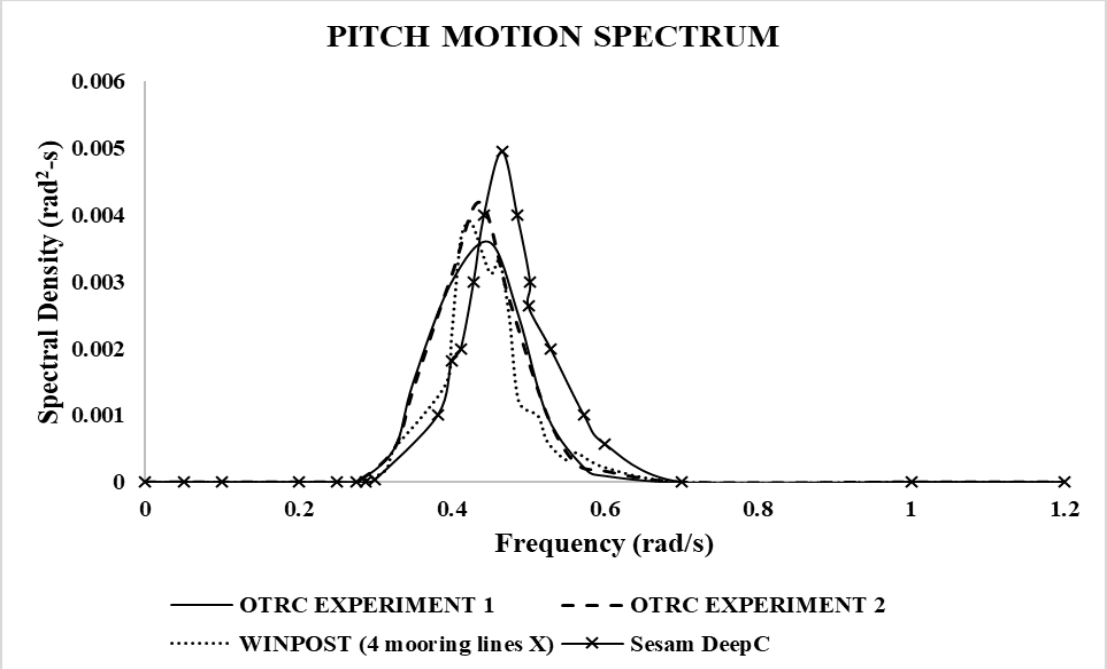

Figure 4.24: Pitch Motion Spectrum Comparison (SESAM DeepC and Kim et al results [42])

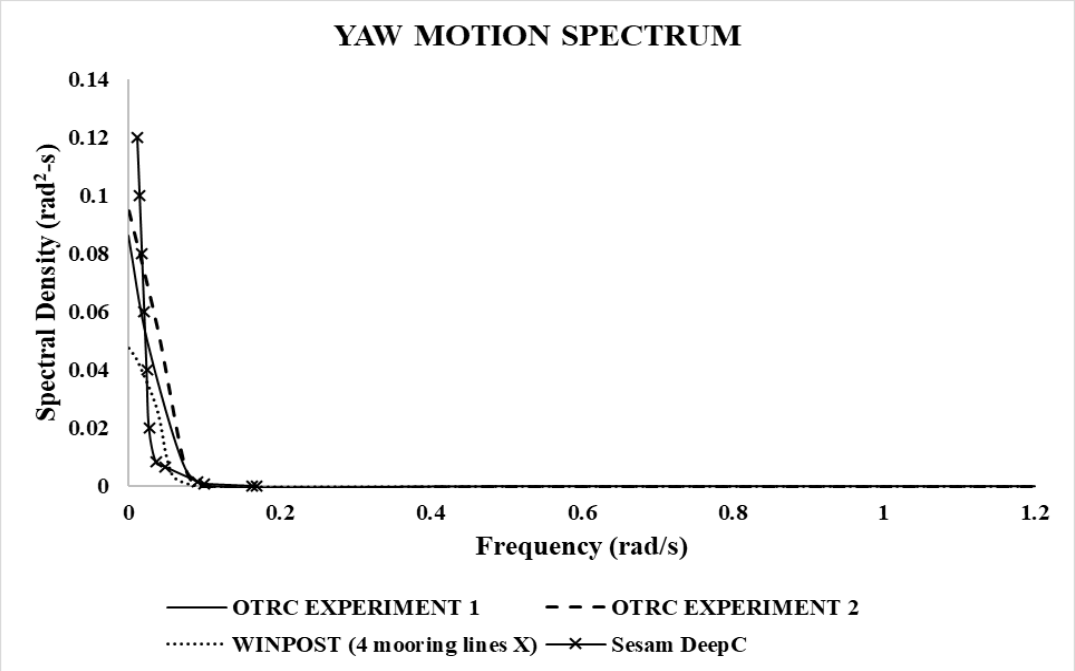

Figure 4.25: Yaw Motion Spectrum Comparison (SESAM DeepC and Kim et al results [42])

The comparison of sway responses is shown in Figure 4.21 with average difference in peak values of 25%. The heave motion RAO shown in Figure 4.22 shows an average difference of 7% with the OTRC 1 experimental and software simulation results. Pitch and yaw motion spectrum computed using software simulation shown in Figure 4.24 and Figure 4.25 respectively varies by an average of less than 25% with the published experimental results.

Except roll, other degrees of freedom response are matching well with the published experimental results by Kim et al [42]; though roll motions match well with the WINPOST simulations by Kim et al [42]. The differences between the experimental and numerical results can be attributed to the uncertainty related to wind and current generation or the mismatch in numerical and physical model of the FPSO mooring system, as truncated mooring system is used in the model testing at OTRC wave basin. The difference in the roll motion can be corrected by giving additional roll damping during simulation [42]. Despite the differences, the results look reasonable. There by the calibrated model and the coupled analysis procedure can be repetitively used for further investigative study of different parameters.

4.5 Parametric Study

Influence of metocean data, hull details and mooring line parameters are studied using model testing, uncoupled frequency domain analysis in SESAM HydroD V4.5-08, where mooring lines are not significant to determine RAO and coupled time domain analysis in SESAM DeepC V5.0-06, where mooring line coupling effects are predominant in deep water conditions. The following sections details the findings from the extensive parametric study conducted on FPSOs and the configurations used.

4.5.1 Influence of Metocean Data on FPSO Motions

In this section, the influence of wave height and presence of current and wind on FPSO motions are studied using the calibrated OTRC FPSO model and Berantai FPSO model. These two FPSOs were given both turret moored and spread moored configuration to identify the influence of mooring system in this scenario. Since the influence of mooring lines are significant in this case, fully coupled time domain analysis in SESAM DeepC V5.0-06 has been performed to study the same. The OTRC FPSO with dimensions given earlier in Table 4.2 were moored using the mooring line details given in Table 4.3 and Table 4.4 at water depth of 1828.8 m. Fully loaded Berantai FPSO with DWT 57999 MT and draft 12.603 m, having mooring line details as shown in Table 4.7 at water depth 1350 m is also used for the study. Mooring line details for Berantai FPSO were chosen such that the natural periods of the FPSO are within the typical range after conducting a free decay analysis in SESAM DeepC V5.0-06.

To study the first harmonic motion response of turret moored and spread moored FPSO configurations in crossing sea condition under the influence of wind, unidirectional random waves and current, wave height was varied from 4 m to 8 m, while peak period ranged from 5 s to 25 s. Wave height was not increased beyond 8 m as wave breaks at height more than 8 m for low wave periods [65] [158]. The current velocity was 4.38 m/s acting at 210°, wind velocity was 36.91 m/s acting at 225° and the wave was directed at 225°.

Table 4.7: Mooring Line Details for Berantai FPSO Model

Description	**Unit**	**Quantity**
Segment 1: Chain		
Length at anchor point	m	120
Diameter	cm	23.5
Dry Weight	N/m	1748.32
Stiffness AE	kN	794848
Segment 2: Polyester Rope		
Length	m	2220
Diameter	cm	9.2
Dry Weight	N/m	371.42
Stiffness AE	kN	689858
Segment 3: Chain		
Length at anchor point	m	80
Diameter	cm	23.5
Dry Weight	N/m	1748.32
Stiffness AE	kN	794848

In total, the significant motion responses are studied under 8 cases. They are:

- Case1: Motion response of turret moored OTRC FPSO subjected to wind, wave and current as shown in Figure 4.26.
- Case2: Motion response of turret moored OTRC FPSO subjected to only wave as shown in Figure 4.27.
- Case3: Motion response of spread moored OTRC FPSO subjected to wind, wave and current as shown in Figure 4.28.
- Case4: Motion response of spread moored OTRC FPSO subjected to only wave as shown in Figure 4.29.
- Case5: Motion response of turret moored Berantai FPSO subjected to wind, wave and current as shown in Figure 4.30.
- Case 6: Motion response of turret moored Berantai FPSO subjected to only wave.

- Case 7: Motion response of spread moored Berantai FPSO subjected to wind, wave and current as shown in Figure 4.31.
- Case 8: Spread moored Berantai FPSO subjected to only wave as shown in Figure 4.32.

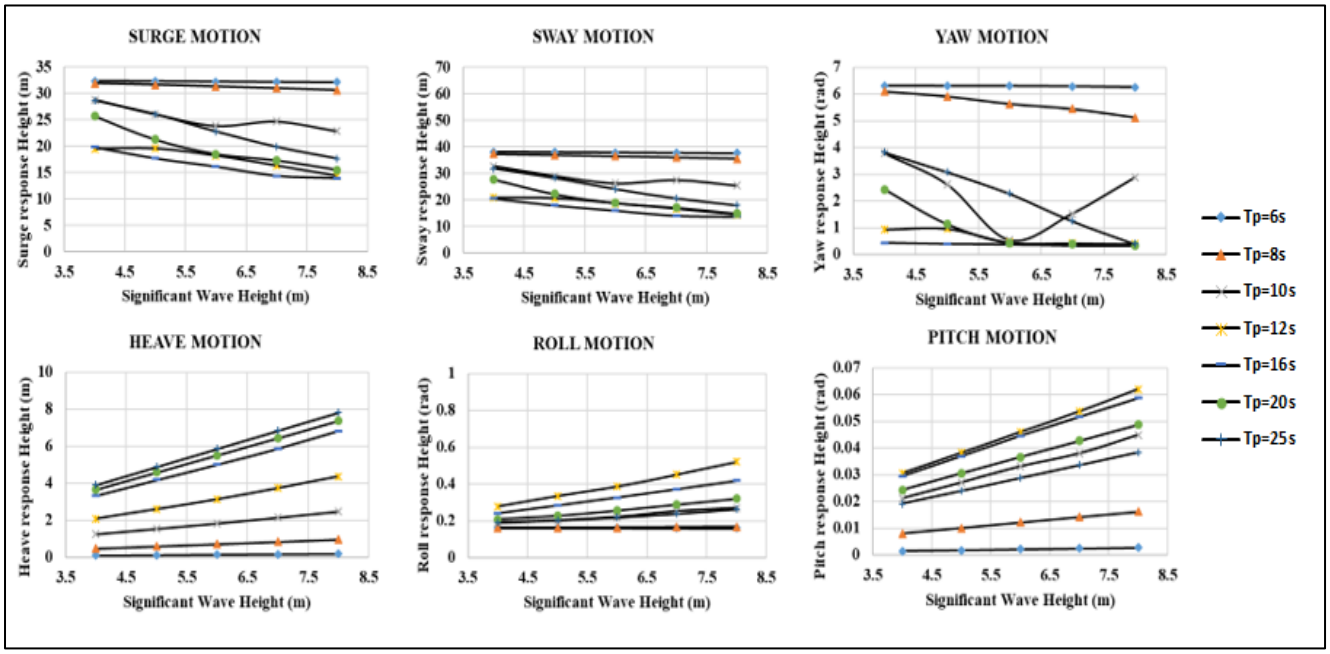

Figure 4.26: Motion response of turret moored OTRC FPSO subjected to wind, wave and current (SESAM DeepC results)

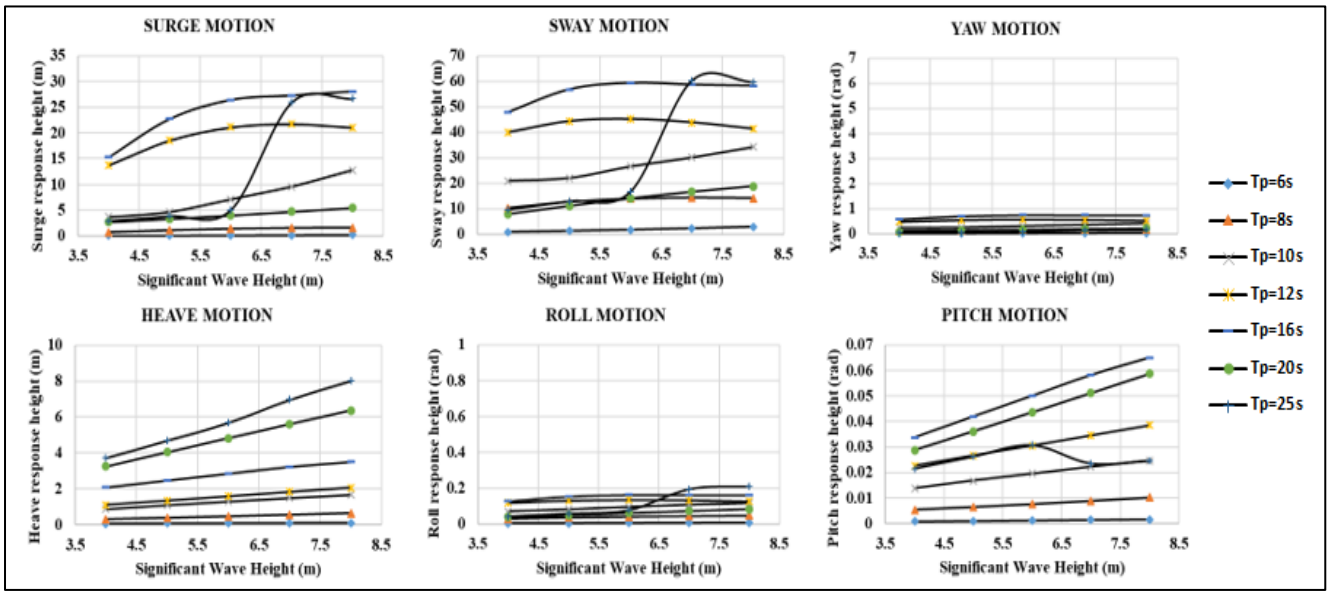

Figure 4.27: Motion response of turret moored OTRC FPSO subjected to only wave (SESAM DeepC results)

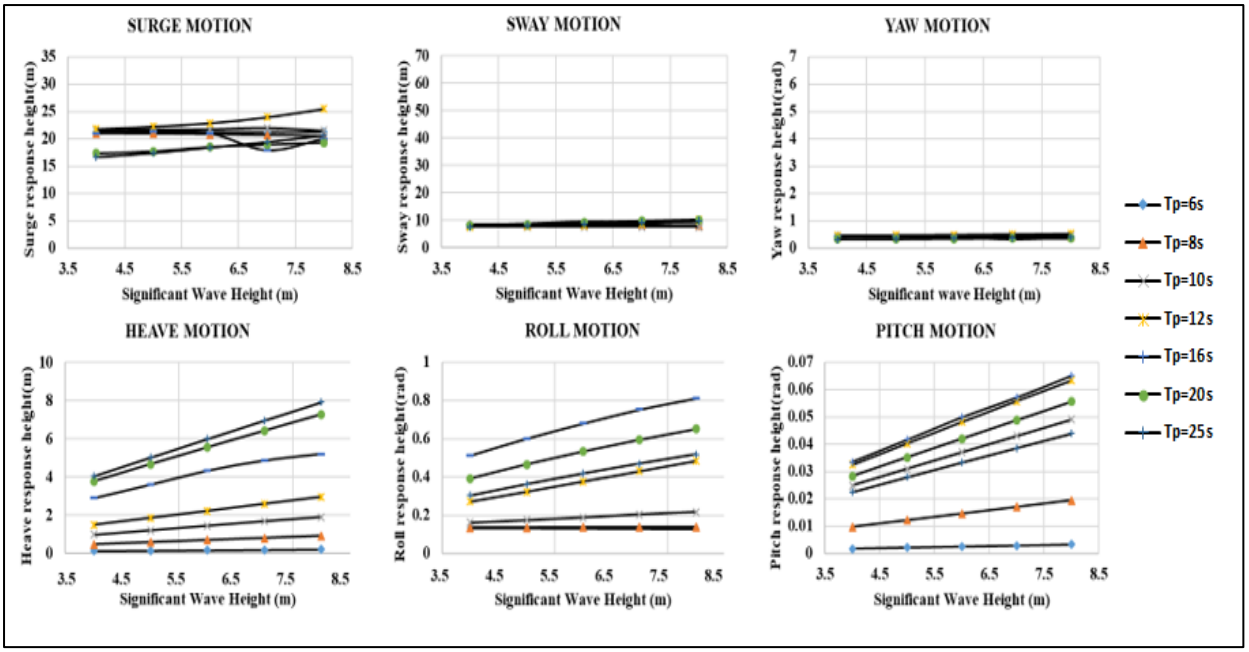

Figure 4.28: Motion response of spread moored OTRC FPSO subjected to wind, wave and current (SESAM DeepC results)

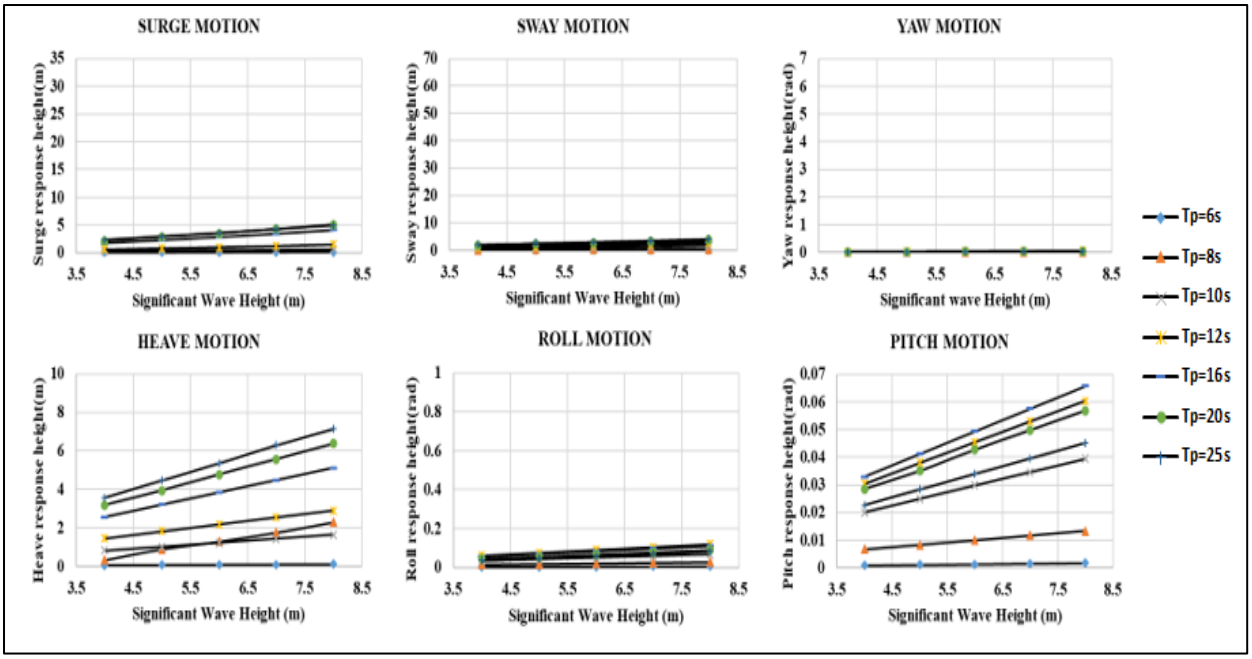

Figure 4.29: Motion response of spread moored OTRC FPSO subjected to only wave (SESAM DeepC results)

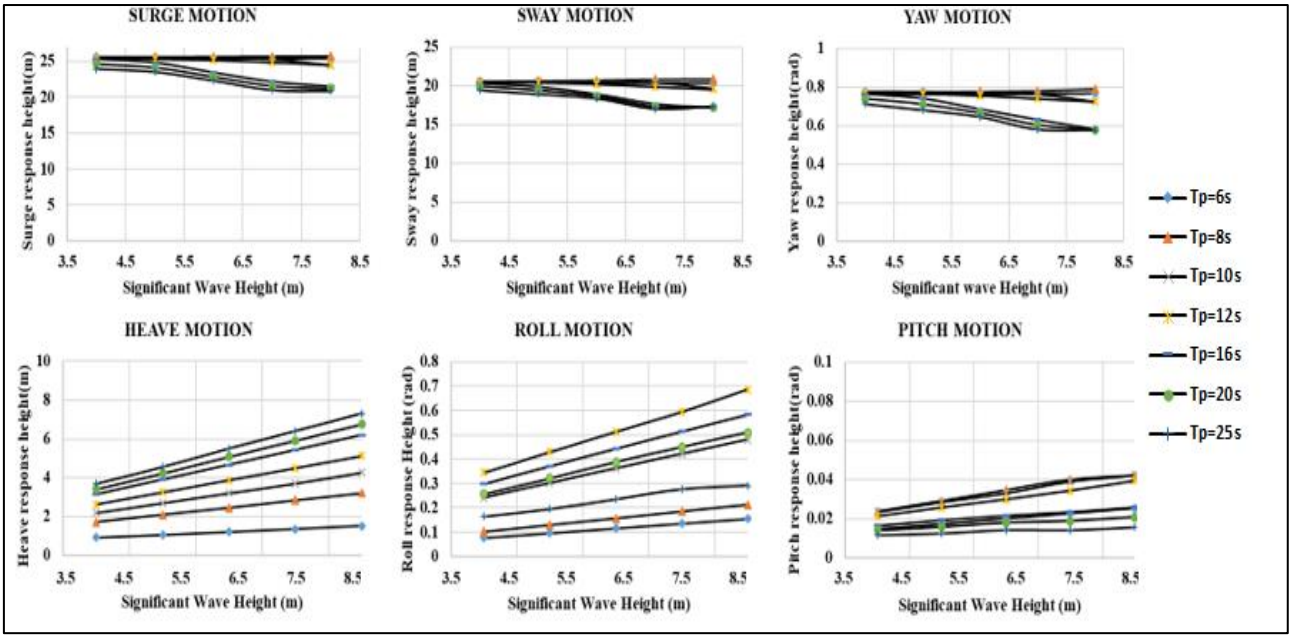

Figure 4.30: Motion response of turret moored Berantai FPSO subjected to wind, wave and current (SESAM DeepC results)

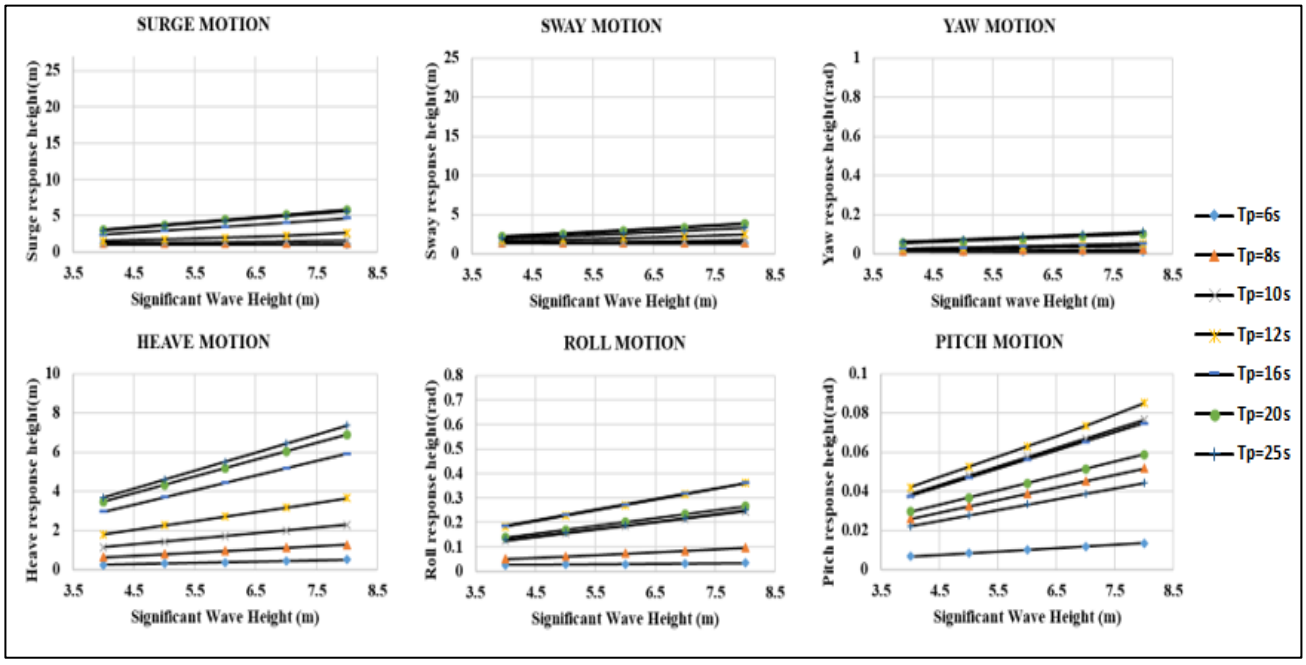

Figure 4.31: Motion response of spread moored Berantai FPSO subjected to wind, wave and current (SESAM DeepC results)

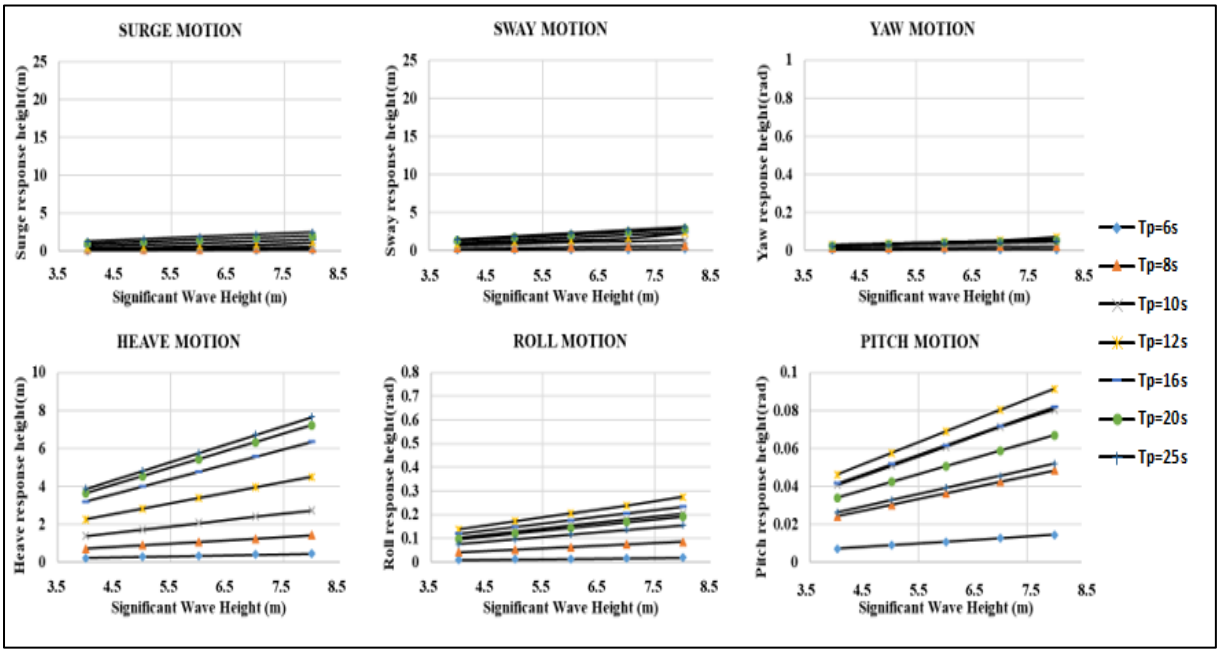

Figure 4.32: Spread moored Berantai FPSO subjected to only wave (SESAM DeepC results)

For cases 1 and 5, in the presence of wind, wave and current for turret moored FPSOs, it is seen from Figure 4.26 and Figure 4.30 that, as the wave height increases, the FPSO motions in the horizontal plane decrease while those in the vertical plane increase. For per meter increase in wave height, surge motion decreases by 0.05 m to 2.81 m for turret moored OTRC FPSO and 0.01 m to 1 m for turret moored Berantai FPSO. Sway motion decreases by 0.09 m to 3.6 m and yaw motion decreases by 0.02 rad to 0.9 rad for turret moored OTRC FPSO, per 1 m increase in wave height. Sway motion decreases by 0.01 m to 0.8 m and yaw motion decreases by 0.01 rad to 0.05 rad for turret moored Berantai FPSO, per 1 m increase in wave height. The reason is that, the hydrodynamic damping in the wave are amplified due to the presence of wind and current [62], [159], [84]. Also, larger wave heights cause a higher velocity of the floater which in turn results in increased hydrodynamic damping [62], [160], [161]. This limits the FPSO motions to small amplitudes in turret moored FPSOs at higher wave heights.

The fluctuations seen for the surge, sway and yaw motions of the turret moored OTRC FPSO subjected to wind, wave and current for wave period 10 s occur when the wave length is odd or even multiple of FPSO length. This results in the fluctuation of the FPSO motions. In the presence of wave only, it can be seen from Figure 4.27 that,

for the wave period 25 s, all the FPSO motions other than heave, show unexpected behaviour as functions of significant wave height and wave period. It is worthwhile to note that T_p = 25 s or more is an exceptionally rare case. At the wave period of 25 s, the wave length is relatively high when compared to the FPSO length and, since a turret moored configuration is used, the FPSO being smaller compared to the wave, offers nominal resistance to the first order wave excitations and, the motions fluctuate rapidly in all the degrees of freedom [162]. This can also be attributed to the mooring line stiffness. When compared to the Berantai FPSO motions, the OTRC FPSO motion amplitudes in surge, sway and yaw are relatively higher. The lesser the mooring stiffness, the higher will be the motion amplitudes. This lesser mooring stiffness along with the higher wave period cause the unexpected motion behaviour in case 2.

However, in cases 3 and 7, where a spread moored configuration is used, it can be seen in Figure 4.28 and Figure 4.31 that, above certain wave period, the FPSO motions in horizontal plane increase even in the presence of wind and current. For surge, sway and yaw, the FPSO motions increase for wave periods above 12 s for OTRC FPSO and above 8 s for Berantai FPSO. When the wave period increases, the wave length increases. If the wind velocity is not high, due to the large wave area, the effect of wind on wave damping is very small. Also, since the FPSO is restrained in all directions, it is more sensitive to first order wave excitations [57]. Hence, due to the drop in damping and increased sensitivity to wave motion, the amplitudes of motion in a horizontal plane increase for a spread moored configuration. For spread moored OTRC FPSO, the surge, sway and yaw motions increases to a maximum of 1 m, 0.6 m, 0.02 rad respectively per 1 m increase in wave height. For spread moored Berantai FPSO, the surge, sway and yaw motions increases to a maximum of 0.7 m, 0.4 m, 0.01 rad respectively per 1 m increase in wave height. The fluctuations in motion at certain wave periods occur when the wave length becomes an odd or even multiple of FPSO length. When wave length is half of FPSO length, cancellation of wave occurs, and hence the FPSO motions decrease. It can be seen from Figure 4.26 and Figure 4.28 for OTRC FPSO and Figure 4.30 and Figure 4.31 for Berantai FPSO that the sway and yaw motions decrease significantly when spread moored configuration is used.

The surge and sway offsets are significantly reduced in the absence of wind and current for spread moored OTRC FPSO. The same is applicable to Berantai FPSO in the absence of wind and current. Also, when comparing the mooring system used, the maximum significant surge response is 32.5 m in the case of turret moored FPSO as shown in Figure 4.26 while the maximum significant surge response for spread moored FPSO is 26.2 m as shown in Figure 4.28 for wave frequency ranges, 5 s - 25 s. This is almost a 20% decrease when a spread mooring system is used. Similarly, for Berantai FPSO, the surge response is higher when turret mooring is used as shown in Figure 4.30 and Figure 4.31.

In turret moored FPSOs, in the presence of wind, wave and current as seen in Figure 4.26 and Figure 4.30, the horizontal offsets are maximum for high frequency wave (at low wave periods) even though the FPSO motion decreases with increase in wave heights due to the drift force from the influence of wind and current. The mooring system allows the FPSO to weathervane when turret moored and hence resist the combined effects of wind, wave and current for reducing motions. This is the main reason why turret moored FPSOs are chosen over spread moored FPSOs for adverse climates. The horizontal plane motions of turret moored FPSO are relatively higher when compared to that of spread moored FPSO in the presence of wind, wave and current due to the drift force. But the interesting fact is that, the horizontal FPSO motions for turret moored FPSO decreases as wave height increases and becomes comparable to those of spread moored FPSO; however, if we use a spread moored configuration in adverse climates, the motions escalate resulting in mooring line damage. This very nature of turret moored FPSOs makes them the preferred choice for locations with hostile weather.

Irrespective of the mooring configuration, heave motion increases from 0.02 m to 1 m, roll motion increases by 0.01 rad to 0.08 rad and pitch motion increases by 0.001 rad to 0.01 rad, per 1 m increase in wave height in wave period ranges 5 s – 25 s. Heave, Roll and pitch motions remain relatively similar for both mooring configurations increases maximum by 1 m, 0.08 rad and 0.01 rad respectively per meter increase in wave height, whether current and/or wind are present or not. It is also observed that the rate of increase in heave motion is directly proportional to wave period ranging 5 s

– 25 s. Higher the wave period, higher will be the heave motion in the wave frequency ranges.

4.5.2 Influence of Water Depth and Wave Periods on FPSO Motions

Influence of water depth on FPSO motions were investigated using model tests conducted as described in section 3.3.4.7. The horizontally moored Berantai FPSO in head sea was subjected to calibrated regular waves shown in Table 3.3. Tests were conducted at 62 m, 70 m, 75 m, 85 m and 100 m (prototype scale). Surge, heave and pitch motions were studied as they are the predominant motions for a spread moored FPSO in head sea. The variations in surge, heave and pitch RAO are plotted for different water depths and shown in Figure 4.33.

The plot shows that the mean values of surge and heave RAOs increase as the water depth increases. At a wave period of 9.09 s, the surge RAO is minimum and then it is increasing until a wave period of 12.5 s and then declining at the same wave period a bit, again to increase until the wave period of 16 s. This pattern of deviation in surge RAO is seen as the same for all the water depths. The heave RAO shows a general trend in increase of its value from the wave period of 8 s and a slight decline in the value for the RAO at the wave period of 11.11 s. The general trend in the variation of heave RAO for all the wave periods for different water depths is the same. The pattern of change in pitch RAO for different wave periods in the range 9.09 s to 12.5 s is seen to be same as the surge RAO. The pitch RAO is minimum at the wave period of 9.09 s and then increasing until 12.5 s and then takes a sudden dip. The variation in pitch RAO for different wave periods is also same for different water depths.

Most of the wave momentum is directed in the horizontal direction, which results in an increase of FPSO motion in the horizontal direction as the wave period (or wave length) increases. As the wave length gets very large when compared to the tanker length, the tanker in effect becomes a particle floating on the surface of the wave and as such offers no resistance resulting in large amplitude of motion [162].

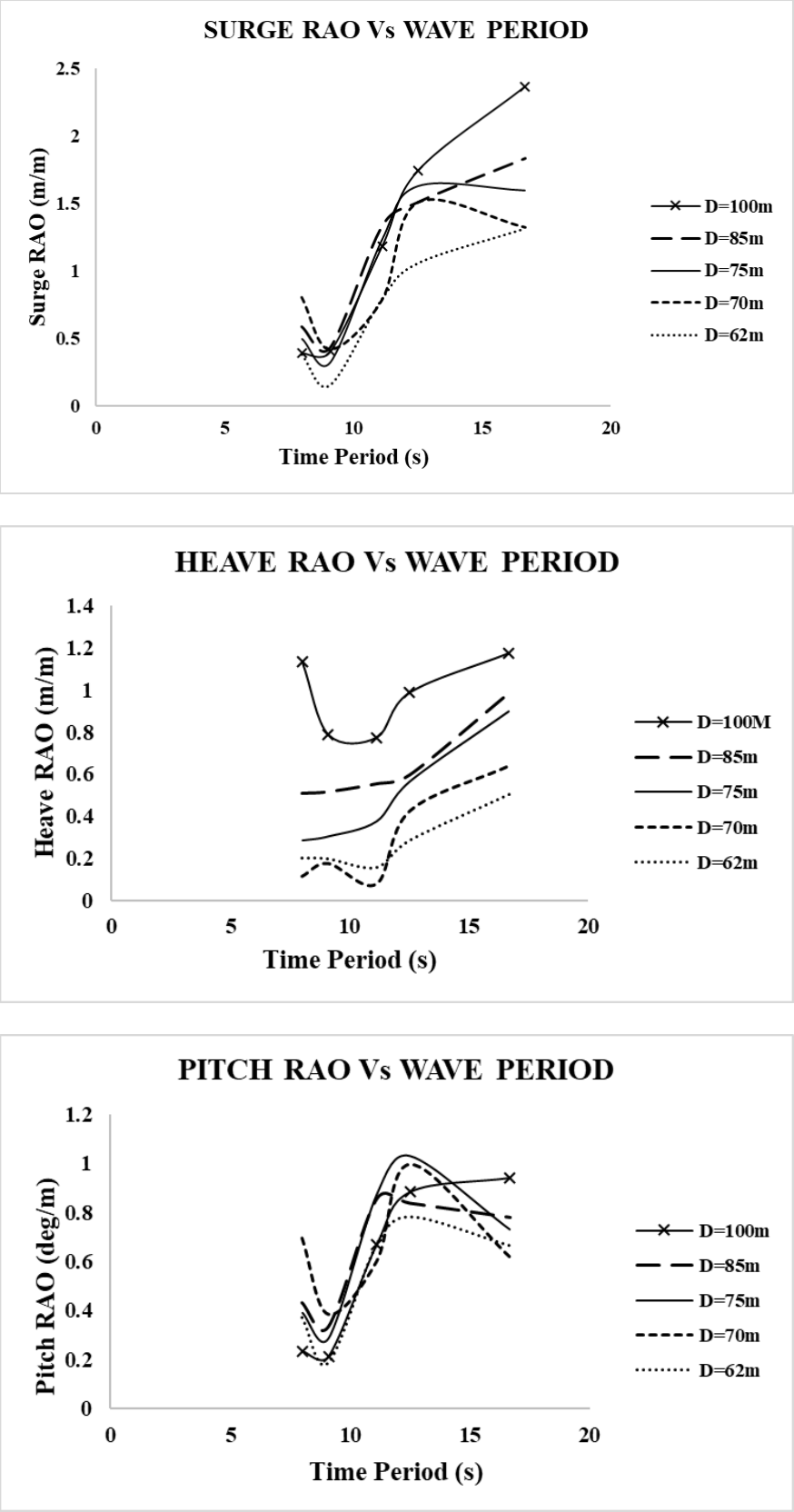

Figure 4.33: Variation of Surge, Heave and Pitch Motion with Water Depth (Experimental results in prototype scale)

The decrease in response during the wave period of 8 s to 9 s is because, at 8 s to 9 s, the ship length is approximately twice the wave length and the effect of waves on FPSO will be reduced as the resulting wave will be very small due to cancellation. This is mainly because at low wave periods, shorter waves are present which gets cancelled due to large vessel. As the wave period increases, waves get longer and will have significant effects on vessel motion and contribute to amplifying the vessel motion.

If the length of a ship is half the waves generated, the resulting wave will be very small due to cancellation, and if the length is the same as the wavelength, the wave will be large due to enhancement. At 8.5 s, the wave length is half of the ship length which results in decrease in wave momentum and hence results in decrease in response.

The study covers water depths of domestic oil zones in Malaysia (62 m – Erb West, 70 m – PMO, 75 m – Baram Delta) [163] and in Australia (80 m- Montara) [2]. The study also helps in understanding variation in heave motion in shallow waters which can contribute to green water as seen later in section 4.7.1.

4.5.3 Influence of Mooring Line Azimuth Angle on FPSO Motions

Influence of mooring line azimuth angle on FPSO motions were investigated using model tests conducted as described in section 3.3.4.7. The horizontally moored Berantai FPSO in head sea was subjected to calibrated long crested and short crested random waves shown in Table 3.4 and Table 3.5 respectively at 1 m water depth (model scale). Surge, heave and pitch motions were studied as they are the predominant motions for a spread moored FPSO in head sea. The variations in surge, heave and pitch motions are plotted for different mooring line azimuth angles under the action of long crested random waves as shown in Figure 4.34.

Figure 4.34 illustrates the variation of FPSO motion with mooring line azimuth angle when subjected to long crested random waves. The surge motion was found to be declining when the mooring line azimuth angle was increased to 30º from 15º and then gradually increasing when the mooring line azimuth angle was increased again to

45º and 55º. The surge motion declines by 8%-25% when the mooring line azimuth angle is changed to 30º from 15º as seen in Figure 4.34.

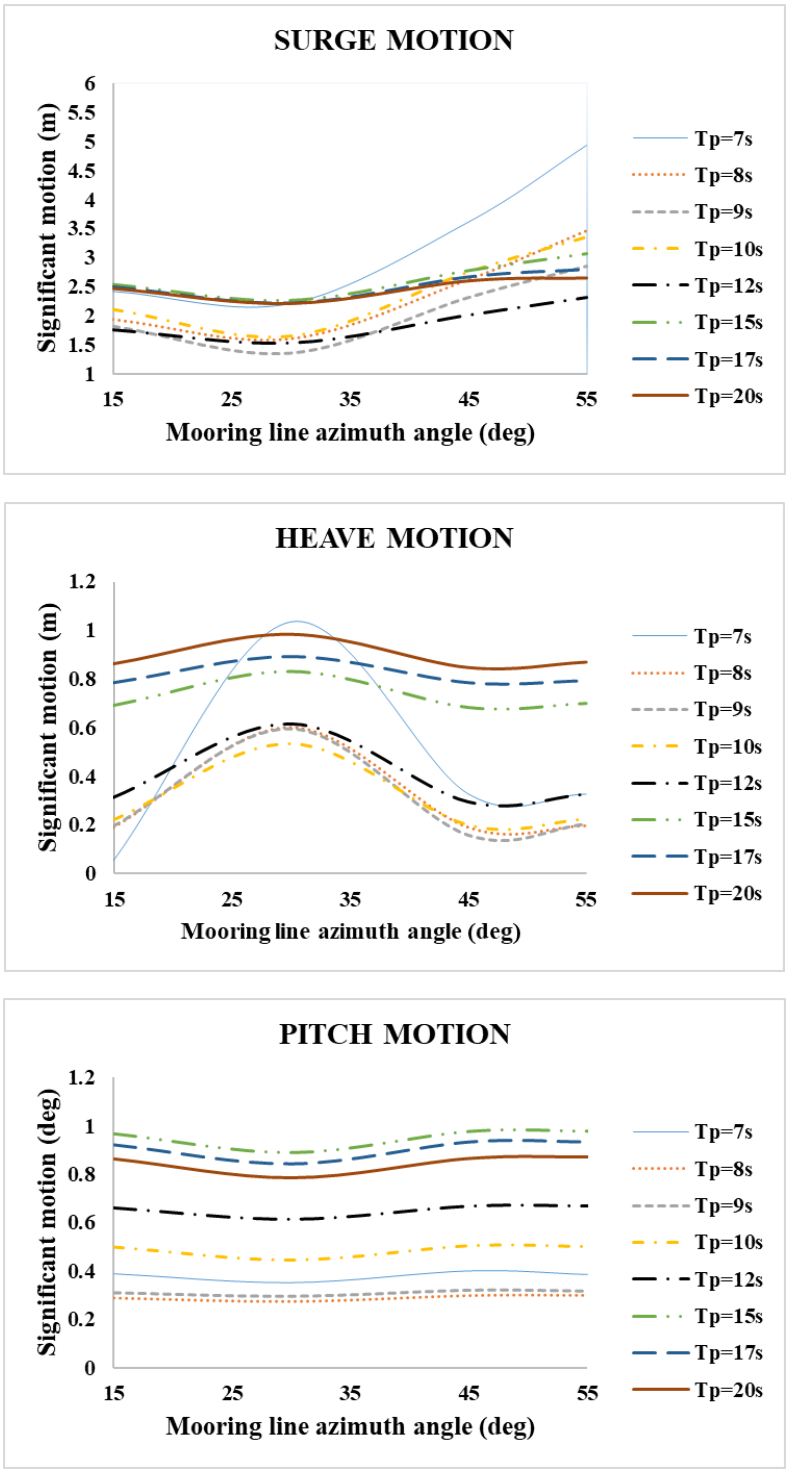

Figure 4.34: Variation of Surge, Heave and Pitch Motion with Mooring Line Azimuth Angle under Long Crested Waves (Experimental results in prototype scale)

The surge motion increases by 5%-50% when the mooring line azimuth angle is changed to 45º from 15º; increasing as wave period decreases. In the case of heave motion, the motion is at its least when 15º mooring line azimuth angle is used, while it is at its maximum when the mooring line azimuth angle is kept as 30º. Then again, the heave motion reduces when the mooring line angle is increased from 30º to 45º and slightly increases when the angle is increased to 55º. The pitch motion is the least sensitive to the mooring line azimuth angle variation. Out of the three responses, surge motion is highly sensitive towards mooring line azimuth angle and found to be minimum at a mooring line azimuth angle of 30º.

Figure 4.35 illustrates the variation of FPSO motion with mooring line azimuth angle when subjected to short crested random waves. At 8 s, the surge motion declines by 22% when the mooring line azimuth angle was increased to 30º from 15º. For other wave periods, the surge motion is minimum with negligible variation at mooring line azimuth angles 15º and 30º. The surge motion increases by 1%-20% when the mooring line azimuth angle is changed to 45º from 15º; increasing as wave period decreases. Like the action of long crested waves, heave motion increases when the mooring line azimuth angle is varied from 15º to 30º and then decreases when the mooring line azimuth angle is 45º.

Hence it is visible that at high wave periods (low frequency waves), the surge and heave motions are minimum at mooring line azimuth angle 15º and 45º. Pitch motions are least sensitive to mooring line azimuth angle variation. Motions are always low when the mooring line azimuth angle is 15º and to prevent high amplitude heave motion, it is best to avoid mooring line azimuth angle 30º for FPSOs with similar configuration.

The difference in amplitude of FPSO motion when subjected to short crested waves and long crested waves are clearly visible from Figure 4.34 and Figure 4.35. The motion amplitude in surge declines by 6% to 34% when short crested waves are used. Except from wave periods 15 s – 20 s, heave and pitch motion increases in the presence of short crested waves. Directional spreading sometimes increases the motions, loads and accelerations, which might be due to the sensitivity of the motions to wave heading angle [164].

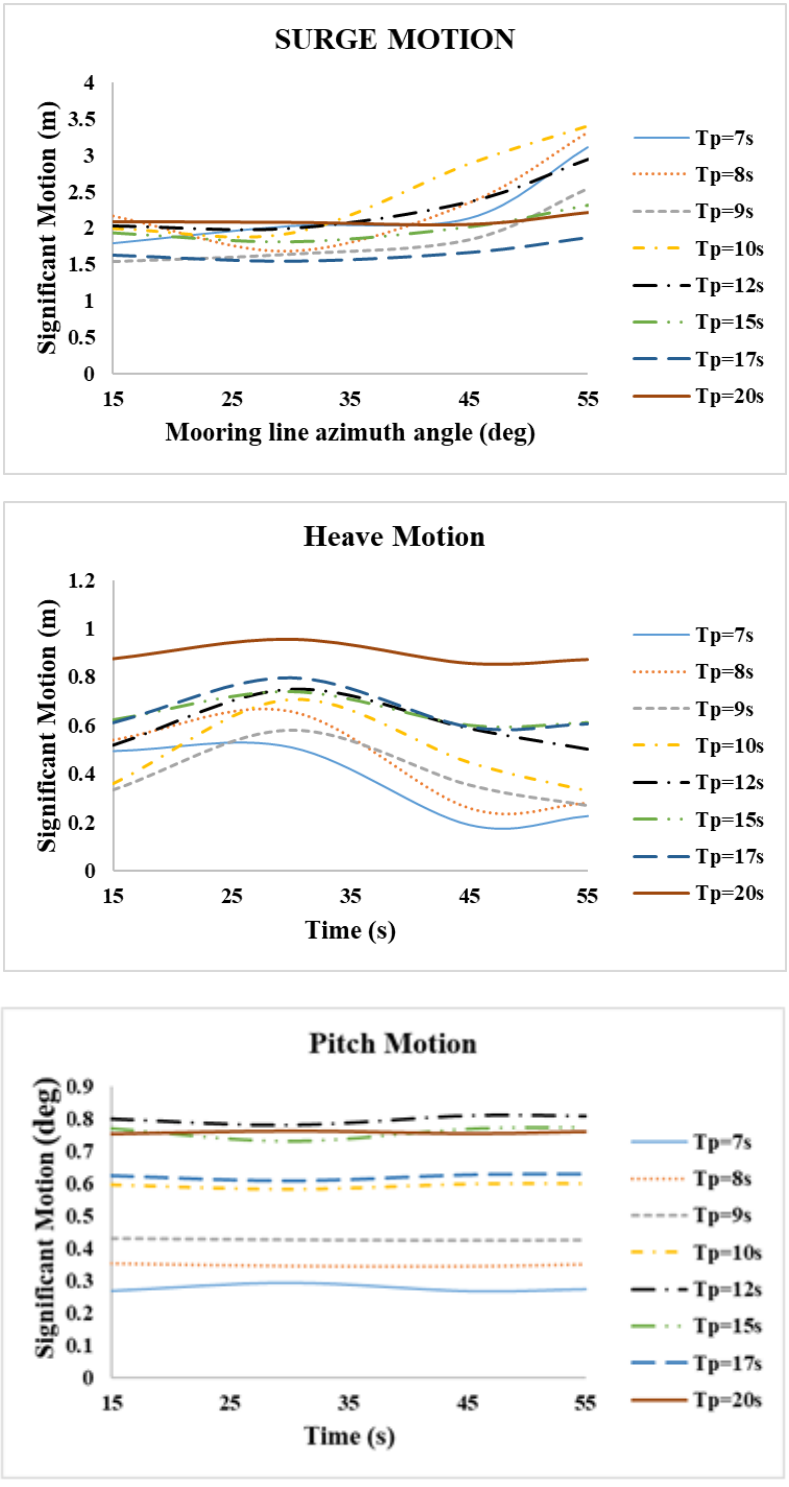

Figure 4.35: Variation of Surge, Heave and Pitch Motion with Mooring Line Azimuth Angle under Short Crested Waves (Experimental results in prototype scale)

4.5.4 Influence of Mooring Line Length on FPSO Motions

The mooring line length parametric study has been conducted using fully coupled analysis in SESAM DeepC V5.0-06. The spread moored coupled Berantai Model with mooring line details shown earlier in Table 4.7 at fully loaded DWT with draft 12.6 m at a water depth of 1350 m was exposed to waves with significant wave height 6.3 m and peak period 16 s acting at 225º, current with velocity 3.66 m/s acting at 210º and wind of velocity 30.3 m/s acting at 225º. The mooring line length was varied from 2200 m to 2700 m. The six FPSO motions were studied and plotted against the ratio of ship length to mooring line length. The ratio of ship length (S_L) to mooring line length (M_L) varies from 0.074 to 0.086. If the mooring line length is below 2200 m, the analysis fails as the mooring line breaks as it becomes too taut and when the mooring line length was increased above 2700 m, the mooring line slackness increases and doesn't offer much resistance.

All the six FPSO motions were found to be increasing as the mooring length was increased from 2200 m to 2700 m or as the ratio of ship length to mooring line length decreases. The surge motion declines by 14% to 60% as the mooring line length was reduced to 2200 m from 2700 m as seen in Figure 4.36. Also, the rate of reduction in surge motion with mooring line length reduction is found to be inversely proportional to the wave period.

The sway motion declines by 10% to 40%, the roll motion declines by 50% to 70% and the yaw motion declines up to 75% when the mooring line length was reduced to 2200 m from 2700 m.

The pitch motion is least sensitive to the mooring line length variation with the difference in FPSO motion falling under 6.4% when the mooring length was reduced to 2200 m and the second least varying FPSO motion is the heave degree of freedom, falling under 18% difference in FPSO motion as seen in Figure 4.36 ~ 4.37. Hence it is best to keep the mooring line length minimum to minimise the FPSO motions with appropriate pretension for similarly configured FPSOs.

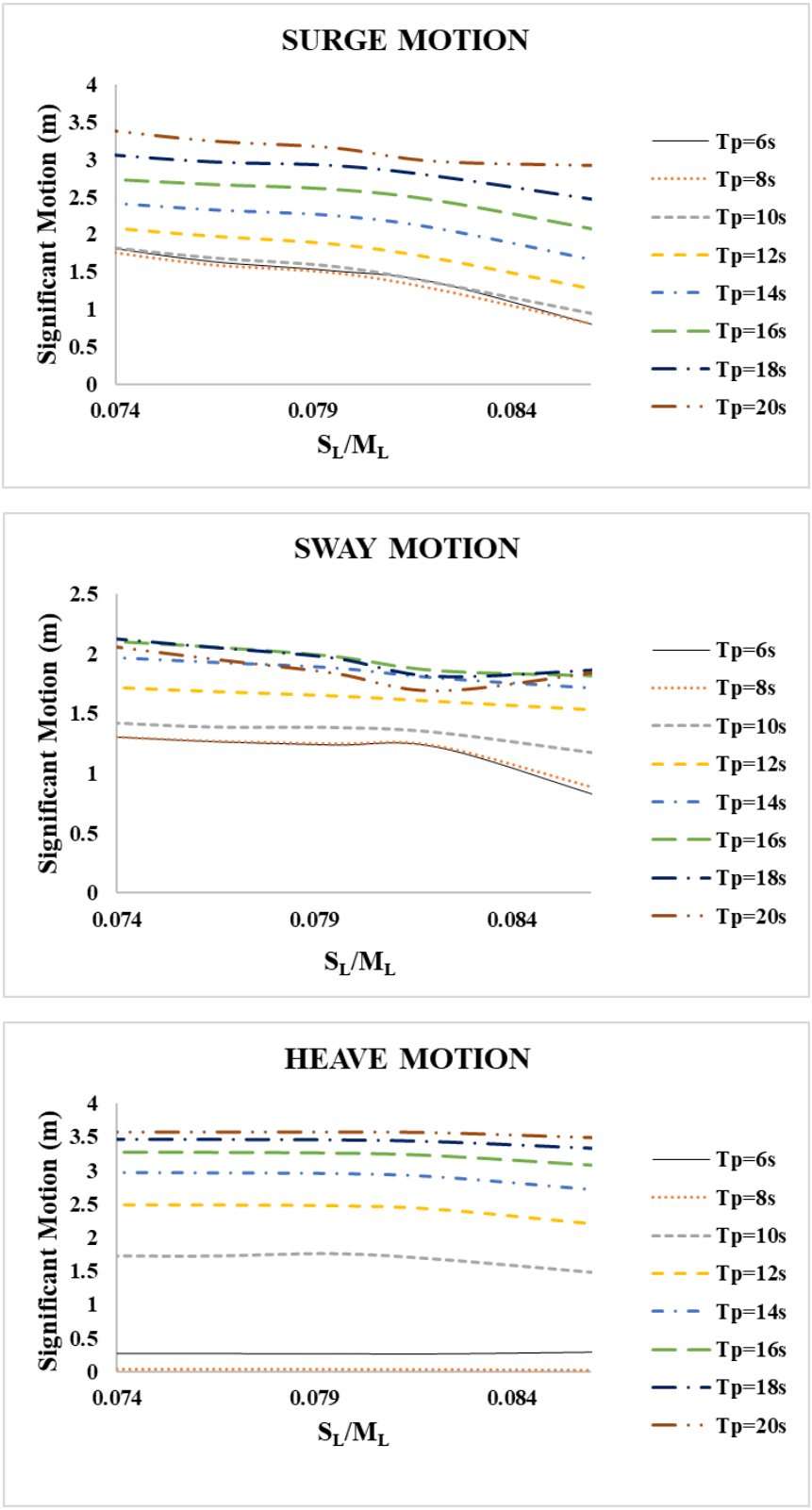

Figure 4.36: Variation of FPSO Translational Motions with Mooring Line Length (SESAM DeepC results)

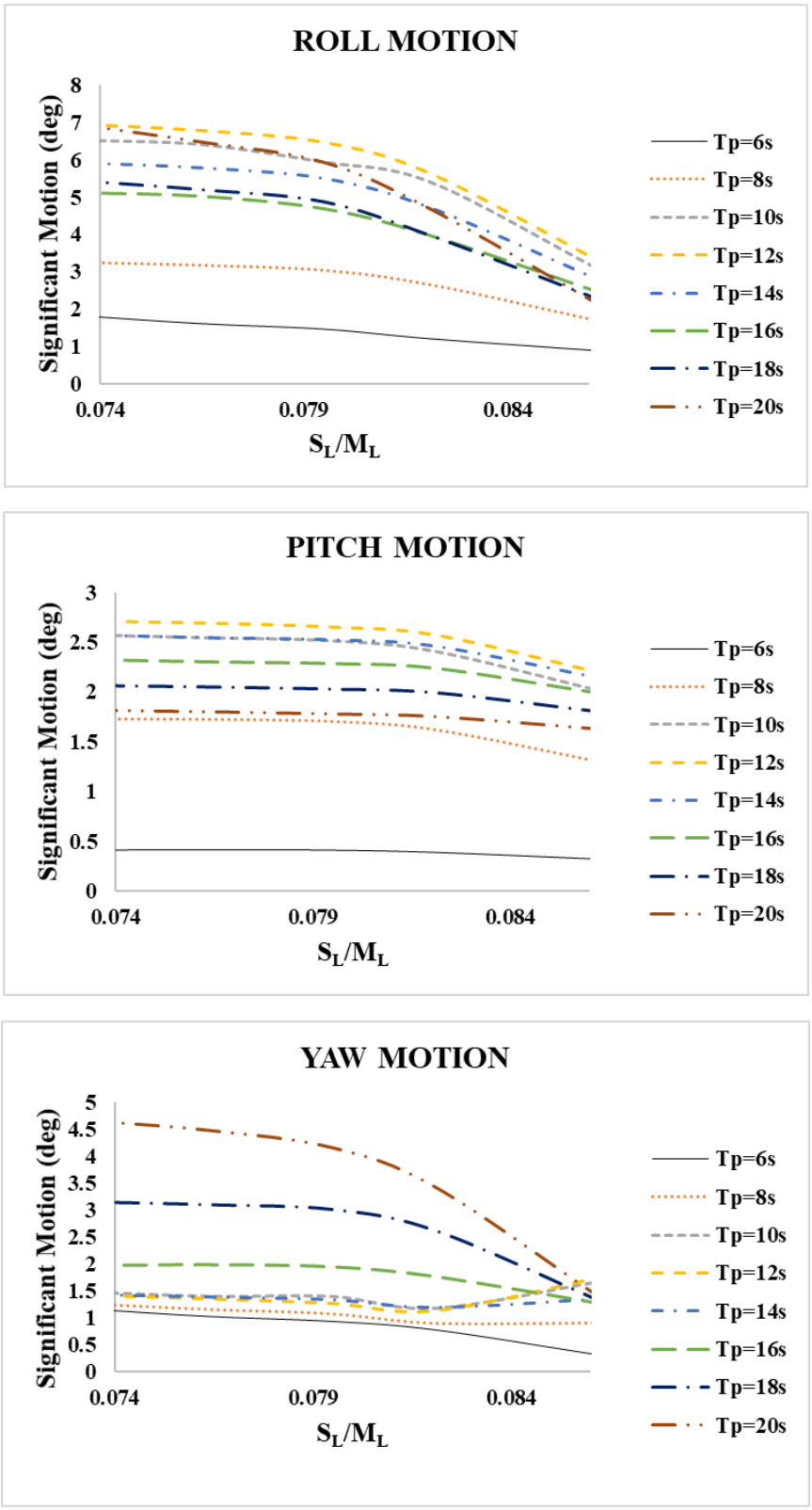

Figure 4.37: Variation of FPSO Rotational Motions with Mooring Line Length (SESAM DeepC results)

4.5.5 Influence of Spread Mooring Fairlead Location on Hull on FPSO Motions

The location of spread mooring fairleads on hull was changed to study the variation in six degrees of freedom FPSO motions using SESAM DeepC V5.0-06. The metocean data and mooring line parameters are the same as used in the mooring line length parametric study in section 4.5.4 for water depth of 1350 m. The location of spread mooring fairleads is varied from 12% to 26% of LOA of FPSO from aft and fore.

Surge motions are the minimum when the spread mooring fairleads are kept at 21% of LOA from aft and fore and increases highly when the mooring fairleads are kept at 25% of LOA from aft and fore, i.e. when the mooring lines are connected near to the mid ship as seen in Figure 4.38. Per percent increase in spread mooring position as percentage of LOA from aft and fore causes a maximum of 0.16 m increase in surge and sway motion.

Roll motion increases maximum by 1.1º and yaw motion by 1º per percent increase in spread mooring position as percentage of LOA from aft and fore as seen in Figure 4.39.

The sway, roll and yaw motions are minimum when the fairleads are at 12% of LOA from aft and fore and varies to a maximum increase of 20%, 28% and 25% respectively when the fairleads are at 21% of LOA from aft and fore.

Heave motion remains nearly the same when the mooring fairleads are varied from 12% to 21% of LOA from aft and fore and increases only maximum 0.01 m per percent increase in spread mooring position as percentage of LOA from aft and fore. Pitch motion is the least sensitive towards spread mooring fairlead location. But under the action of wave with peak period 6 s, the pitch motion of FPSO seems to suddenly increase when the spread mooring fairleads are at 18% of LOA from aft and fore. This might be because of the unexpected motion from the high frequency excitation of mooring lines. Hence the location of mooring lines needs to be between 12% and 21% of LOA from aft and fore to minimise the FPSO motions for similar configured FPSOs in the wave frequency ranges.

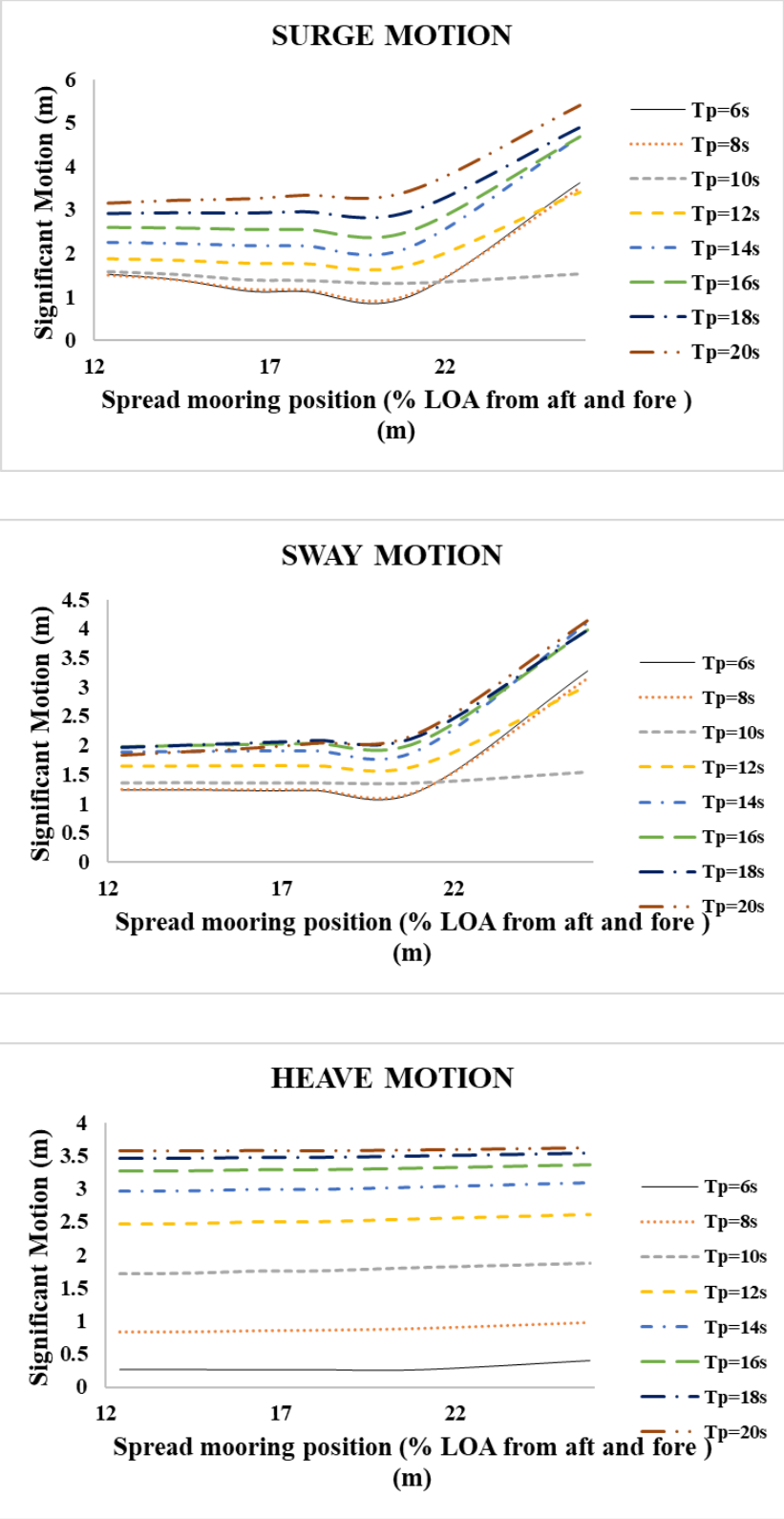

Figure 4.38: Variation in Translational FPSO Motions with Location of Spread Mooring Fairleads on Hull (SESAM DeepC results)

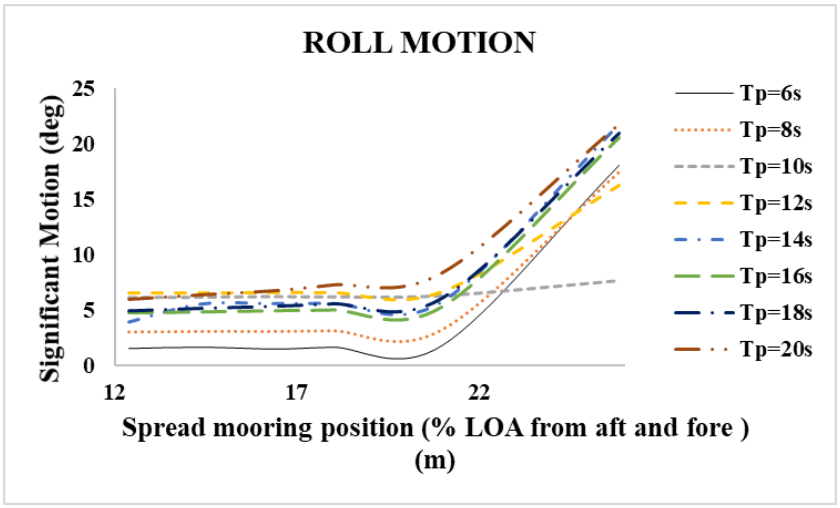

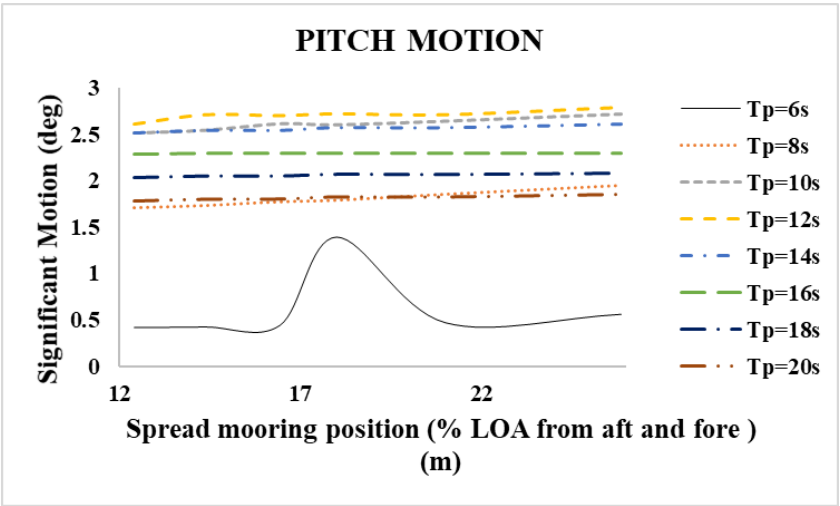

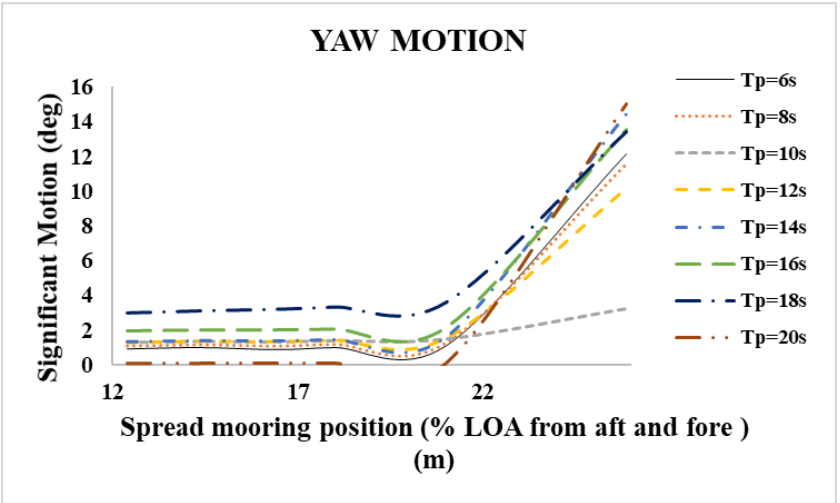

Figure 4.39: Variation in Rotational FPSO Motions with Location of Spread Mooring Fairleads on Hull (SESAM DeepC results)

4.5.6 Influence of Hull Length to Beam Ratio on FPSO Motions

Based on the existing FPSOs in Malaysia and Australia, Length to Beam ratio of hull ranges from 5.4 to 6.5. Uncoupled analysis using SESAM HydroD V4.5-08 has been performed to study the influence of hull length to beam ratio in this range on 6 DOF FPSO motions and the motion responses are shown in Figure 4.40 and Figure 4.41. The modelling of vessels with length and beam shown in Table 4.8 has been done using procedure mentioned in section 3.4.1. The hull depth 24 m and loading condition DWT 137852 MT were kept as same for all the FPSO models at water depth 1350 m with heading 45º subjected to unidirectional random waves with significant wave height 6 m in the wave frequency ranges.

Table 4.8: Vessel dimensions for hull length to beam ratio parametric study

FPSO Model Name	Hull Length (m)	Beam (m)	Length to Beam ratio (L/B)
FPSO1	233	43	5.419
FPSO2	243	44	5.523
FPSO3	253	45	5.622
FPSO4	263	46	5.717
FPSO5	283	49	5.776
FPSO6	303	51	5.941
FPSO7	313	52	6.019
FPSO8	323	53	6.094

Figure 4.40 illustrates the variation in surge, sway and heave motion when the length to beam ratio of the hull is varied. Surge motion is found to be increasing with the increase in length to beam ratio up to 2 m when length to beam ratio equals unity and the rate of increase in surge motion is found to be proportional to the wave period with rate of surge motion varying with the increase in length to beam ratio from 0.3% to 32 % when the peak period is varied from 7 s to 20 s. At all the wave periods, surge motion is found to be minimum when the length to beam ratio is 5.4 and the variation in motion is negligible until the peak period is varied up to 12 s. Sway motion is found to be declining with the increase in length to beam ratio when the peak period was varied from 5 s to 12 s and then increasing proportional to the wave period up to 0.8 m when length to beam ratio equals unity with rate of sway motion varying with the

increase in length to beam ratio from 6% to 15 % when the peak period is varied from 14 s to 20 s. Heave motion is declining with the increase in length to beam ratio, reducing from 1% to 80% as the length to beam ratio is varied from 5.419 to 6.094.

Figure 4.41 shows the variation of roll, pitch and yaw motions with the length to beam ratio of vessel hull. Roll motion increases with increase in length to beam ratio up to wave period of 10 s and then declines with the increase in length to beam ratio up to 60% for peak period of 20 s proportional to the wave period. Pitch motion is found to be declining as the length to beam ratio is increased. Pitch motion is highly reduced up to 161% as the length to beam ration is varied from 5.419 to 6.094. Yaw motion is declining with increase in length to beam ratio up to 121 % for wave periods 5 s to 15 s. After 15 s, the yaw motion increases with increase in length to beam ratio for wave periods up to 20 s a maximum of 8%.

It can be concluded that, for wave heights of 5 m and peak period ranging from 5 s to 12 s, the surge, sway, heave, pitch and yaw motions are minimum for length to beam ratio of 6.094 and for peak period ranging from 14 s to 20 s, the heave, roll and pitch motions are minimum again at a length to beam ratio of 6.094. The horizontal motions, surge, sway and yaw are found to be increasing with length to beam ratio after 12 s and this is probably because mooring lines were not given to find the vessel RAOs and could be reduced by giving proper mooring which can be verified by doing a coupled analysis as a future scope of work.

For Malaysian seas, the most probable peak period is usually in the range of 6 s to 7 s [132]. It can be seen from Figure 4.40 ~Figure 4.41, for FPSOs having beam to length ratio in the same range as the Malaysian and Australian FPSOs, the heave, roll and pitch motion remains almost the same for peak period less than 7 s. This means that for the Malaysian FPSOs, the combined vertical motion will be less for the Malaysian metocean conditions and thus risk from green water is less when compared to Australian FPSOs where the peak period of wave is higher as seen later in section 4.7.1. As in higher wave periods, these FPSOs have higher motion in heave, roll and pitch as seen in Figure 4.40 ~Figure 4.41. The Australian sea is prone to extreme cyclones with longer wave periods [4].

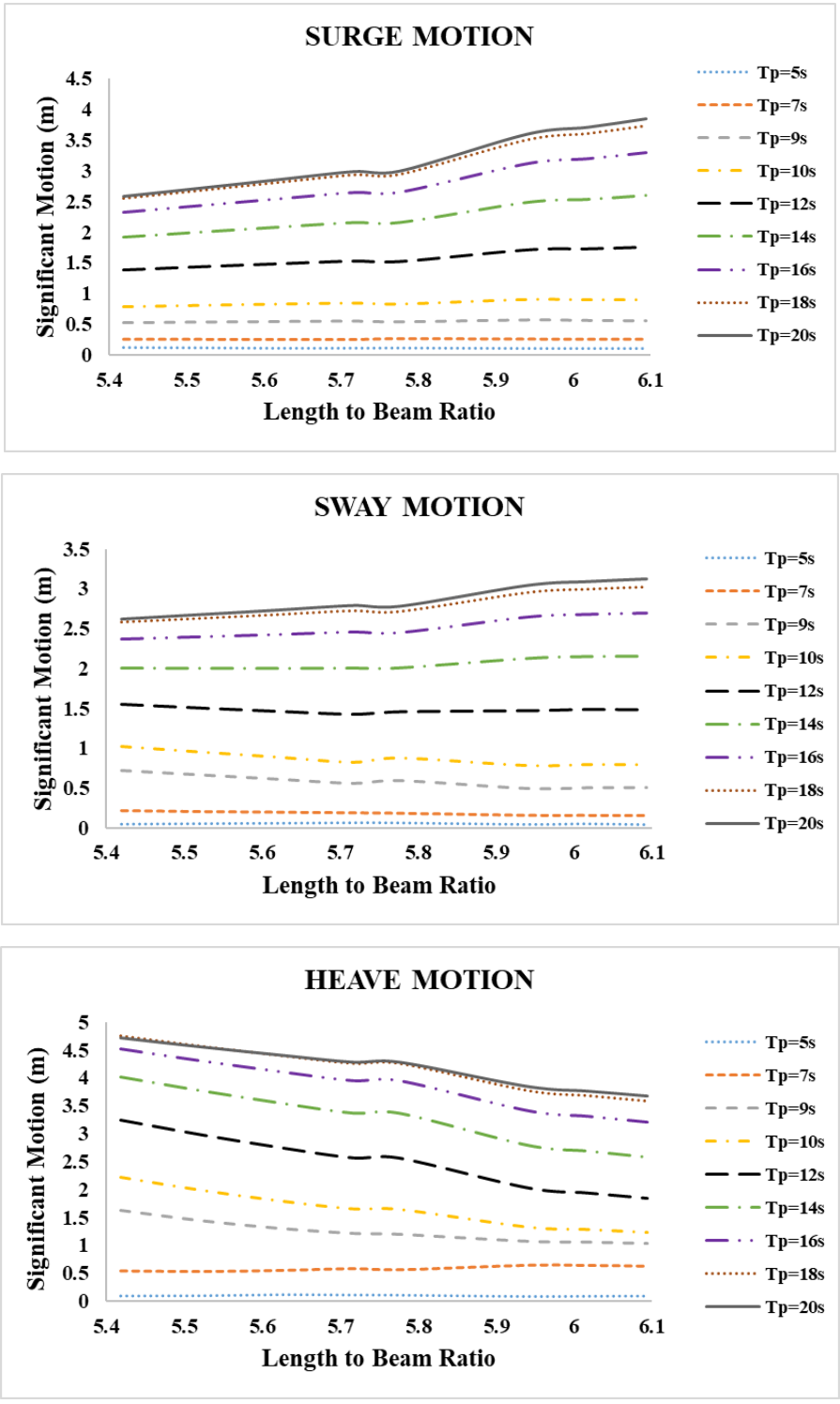

Figure 4.40: Variation in Translational FPSO Motions with Length to Beam Ratio of Hull (SESAM HydroD results)

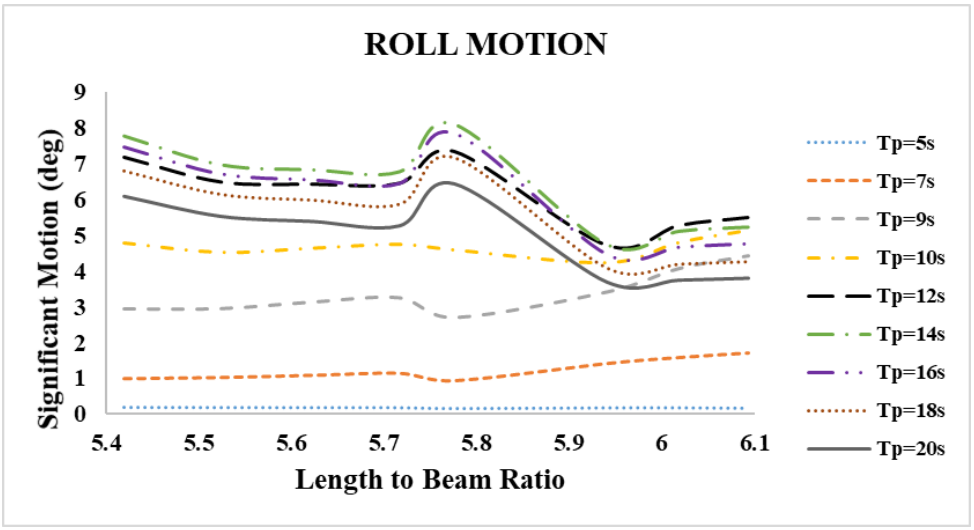

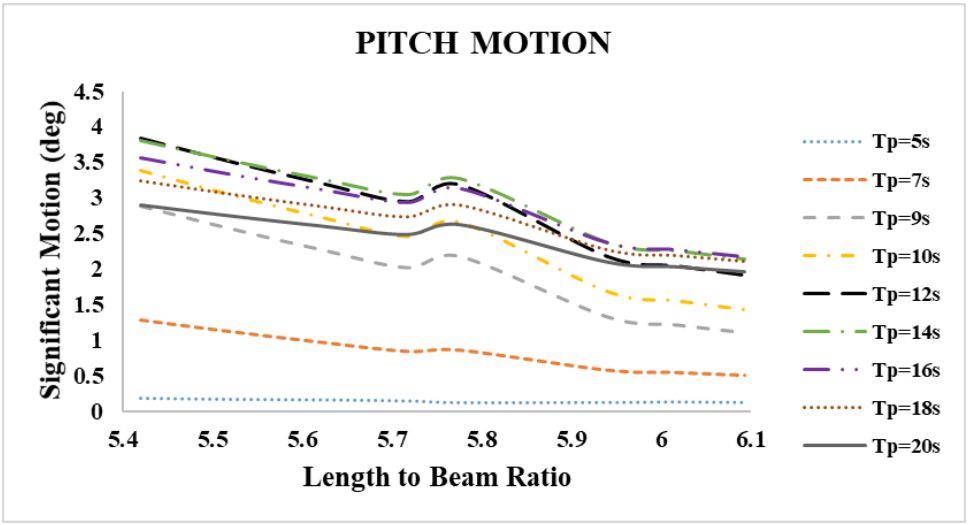

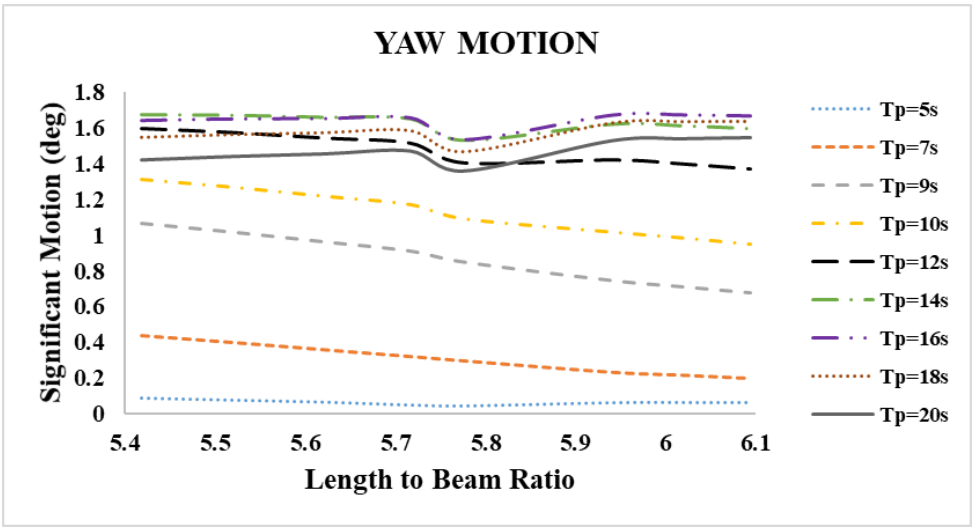

Figure 4.41: Variation in Rotational FPSO Motions with Length to Beam Ratio of Hull (SESAM HydroD results)

4.5.7 Influence of Hull Loading Condition on FPSO Motions

Influence of hull loading condition on FPSO motion is studied using the models developed with dimension as shown earlier in Table 4.8 using SESAM HydroD V4.5-08. The fully loaded FPSOs are having DWT 137852 MT. Parametric study was conducted for 100%, 75%, 50% and 25% hull loading condition with respective drafts. FPSO models with hull depth 24 m at water depth 1350 m with heading 45º were subjected to unidirectional random waves with significant wave height 6.3 m and peak period 16 s. The variation of FPSO motions with loading condition is shown in Figure 4.42 and Figure 4.43.

Surge motion declines up to 20%, sway motion declines up to 33%, heave motion declines up to 11% and pitch motion declines up to 15% at full loading condition when compared to 25% loading condition. Roll rotation increases up to 51% and yaw rotation increases up to 38% at full loading condition when compared to 25% loading condition.

Surge, sway and heave motion declines by maximum 0.0074 m, 0.015 m and 0.007 m respectively per percent increase in loading condition. While pitch rotation declines by maximum 0.005º per percent increase in loading condition. Roll motion increases by maximum 0.02º and yaw motion increases by maximum 0.006º per percent increase in loading condition.

Surge, sway, heave and pitch motion decreases as vessel loading increases and roll and yaw motion increases with vessel loading for the given metocean data and vessel dimensions (covering vessel dimensions operating in Australia and Malaysia). Roll and yaw rotation are found to be increasing with loading condition could be reduced by giving proper mooring and roll damping which can be verified by doing a coupled analysis as a future scope of work.

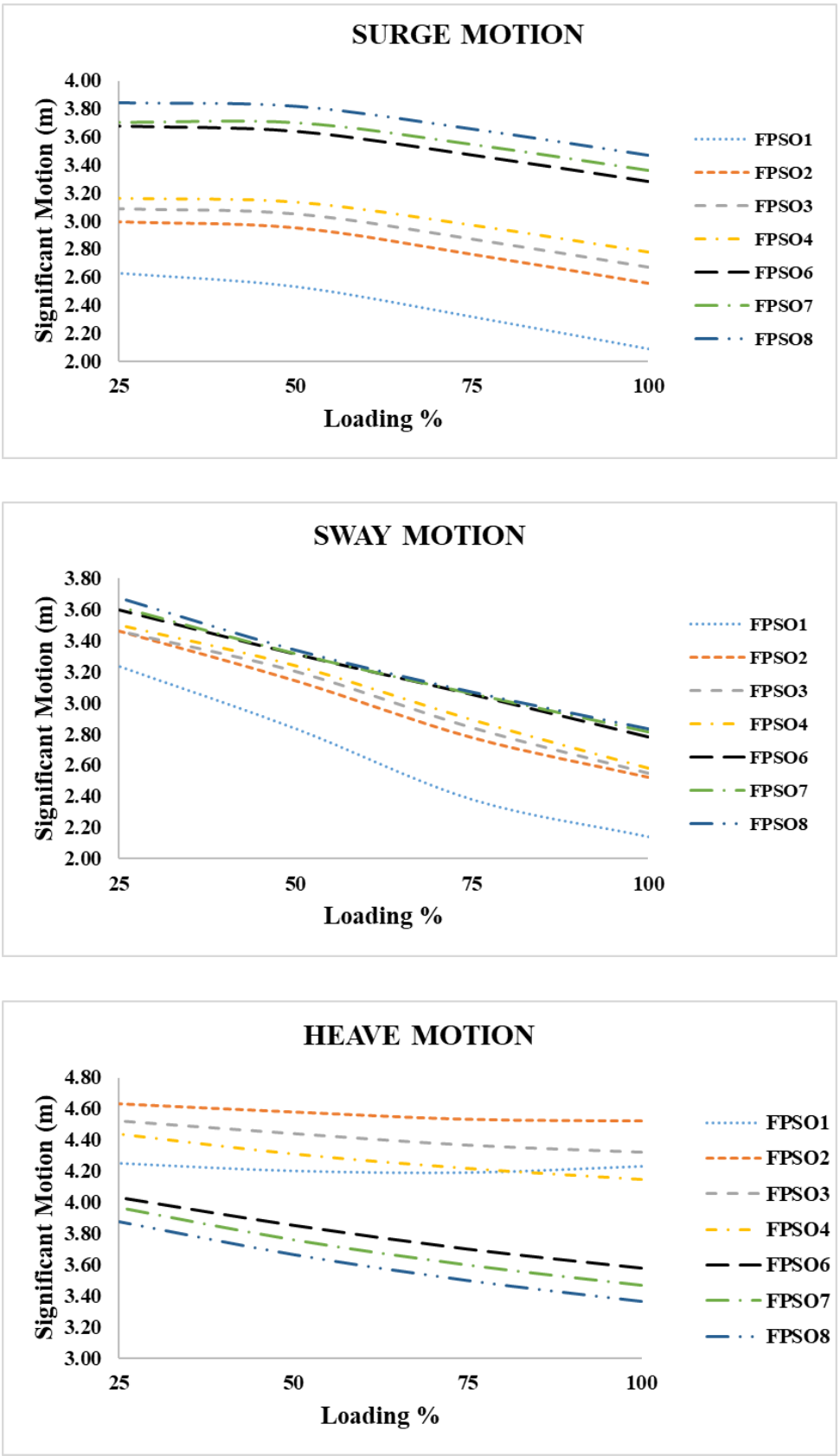

Figure 4.42: Variation in Translational FPSO Motions with Hull Loading Condition (SESAM HydroD results)

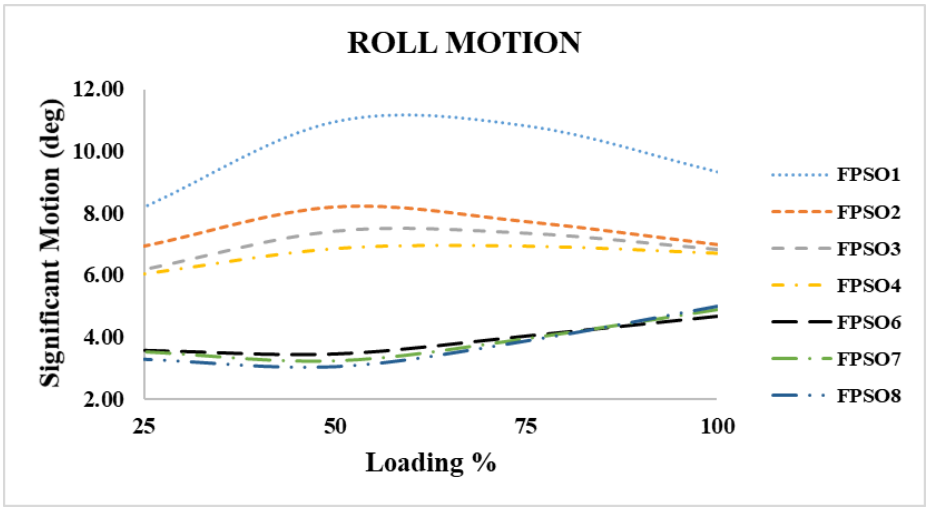

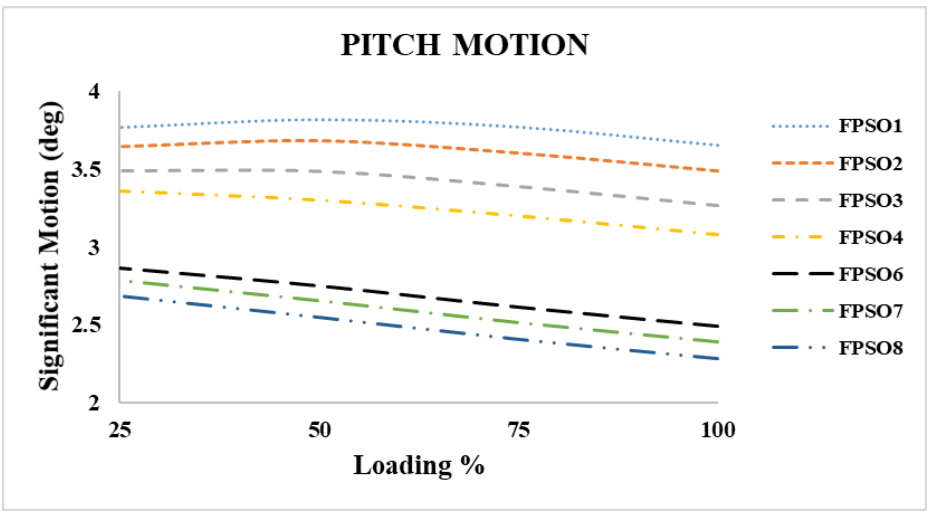

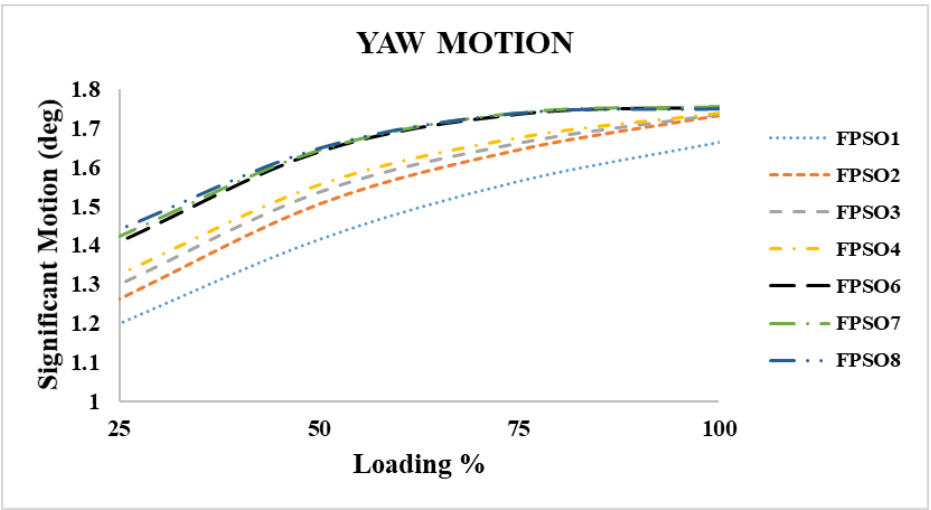

Figure 4.43: Variation in Rotational FPSO Motions with Hull Loading Condition (SESAM HydroD results)

4.6 Motion Response of FPSOs with Similar Dimensions as Operating FPSOs in Malaysia and Australia

The vessel RAOs of FPSOs with dimensions similar as the operating FPSOs in Malaysia (shown in Table 4.9) and Australia (shown in Table 4.11) in 2016 are computed using SESAM HydroD V4.5-08. For the respective FPSO dimensions, the operating water depth, loading condition and operating draft is used for its operating locations and the sea state was represented using JONSWAP spectrum. The extreme metocean condition, 100 year wind, wave and current at the deepest oil field in Malaysia, i.e. Kikeh oil field, has been used for the analysis of Malaysian FPSOs and for Australian FPSOs, the extreme metocean conditions, 100 year cyclonic condition of North West Australia has been used [61], so that the results are conservative to be used in association with deep water analysis. The metocean data used for the analysis of Malaysian FPSOs and Australian FPSOs at collinear condition, 315º are tabulated as shown in Table 4.10.

Table 4.9: Operating FPSOs in Malaysia 2016 [2]

FPSO Name	**Dimension similar as FPSO**	**LOA (m)**	**B (m)**	**Hull Depth (m)**	**Operating Draft (m)**	**DWT (MT)**	**Water Depth (m)**
FPSO A	Berantai	207	32	17	12.6	55337	55
FPSO B	Bunga Kertas	233	43	19	12	87768	60
FPSO C	Cendor II	245	41	21.6	14	100020	63
FPSO D	Kikeh	337	55	27	21	273000	1350
FPSO E	Perisai Kamelia	264	41	22	13	127540	60

Table 4.10: Extreme Metocean Conditions used for the Analysis

Metocean Details	**Malaysia**	**Australia**[61]
Significant Wave Height (m)	6.3	14 m
Peak Period (s)	16	14.5
JONSWAP, γ	1.5 [68]	1.6
wind velocity (m/s)	15.58	44
Current Velocity (m/s)	3.66	1.9

Table 4.11: Operating FPSOs in Australia 2016 [2]

FPSO Name	Dimension similar as FPSO	LOA (m)	B (m)	Hull Depth (m)	Operating Draft (m)	DWT(MT)	Water Depth (m)
FPSO F	Armada Claire	241	42	23	14.09	102123	135
FPSO G	Glas Dowr	242	42	21	15	105000	344
FPSO H	Maersk Nguima - Yin	261	58	31	23	308490	340
FPSO I	Modec Venture II	258	46	24	16.86	149686	492
FPSO J	Montara Venture	274	43	24	16.7	146251	80
FPSO K	Nganhurra	260	46	26	14	150000	400
FPSO L	Ningaloo Vision	238	42	24	15	101832	350
FPSO M	Northern Endeavour	273	50	28	19	177529	380
FPSO N	Okha	274	48	23	16.89	158000	78
FPSO O	Pyrenees Venture	274	48	23	15.8	143690	200

The RAOs generated for the FPSOs with similar dimensions as operating FPSOs in Malaysia and Australia are given in Figure 4.44 and Figure 4.45 respectively. It can be observed from Figure 4.44 that the FPSO D with dimensions similar as Kikeh FPSO has minimum motion response when compared to other FPSOs, having same dimensions as Malaysian FPSOs for the Kikeh metocean condition, which shows the suitability in choosing the particular hull dimensions for the location. Kikeh FPSO is a converted FPSO and its motion performance is suitable for the Kikeh metocean conditions. Specific roll damping was not provided in the analysis and it shows, except FPSO C with dimensions of Cendor II, all other FPSOs in Malaysia are having similar roll performance. The maximum surge and sway RAO falls below 1.1 m/m for the Malaysian FPSOs. Maximum heave, roll, pitch and yaw are 0.9 m/m, 4.791 deg/m, 0.9 deg/m and 0.5 deg/m respectively.

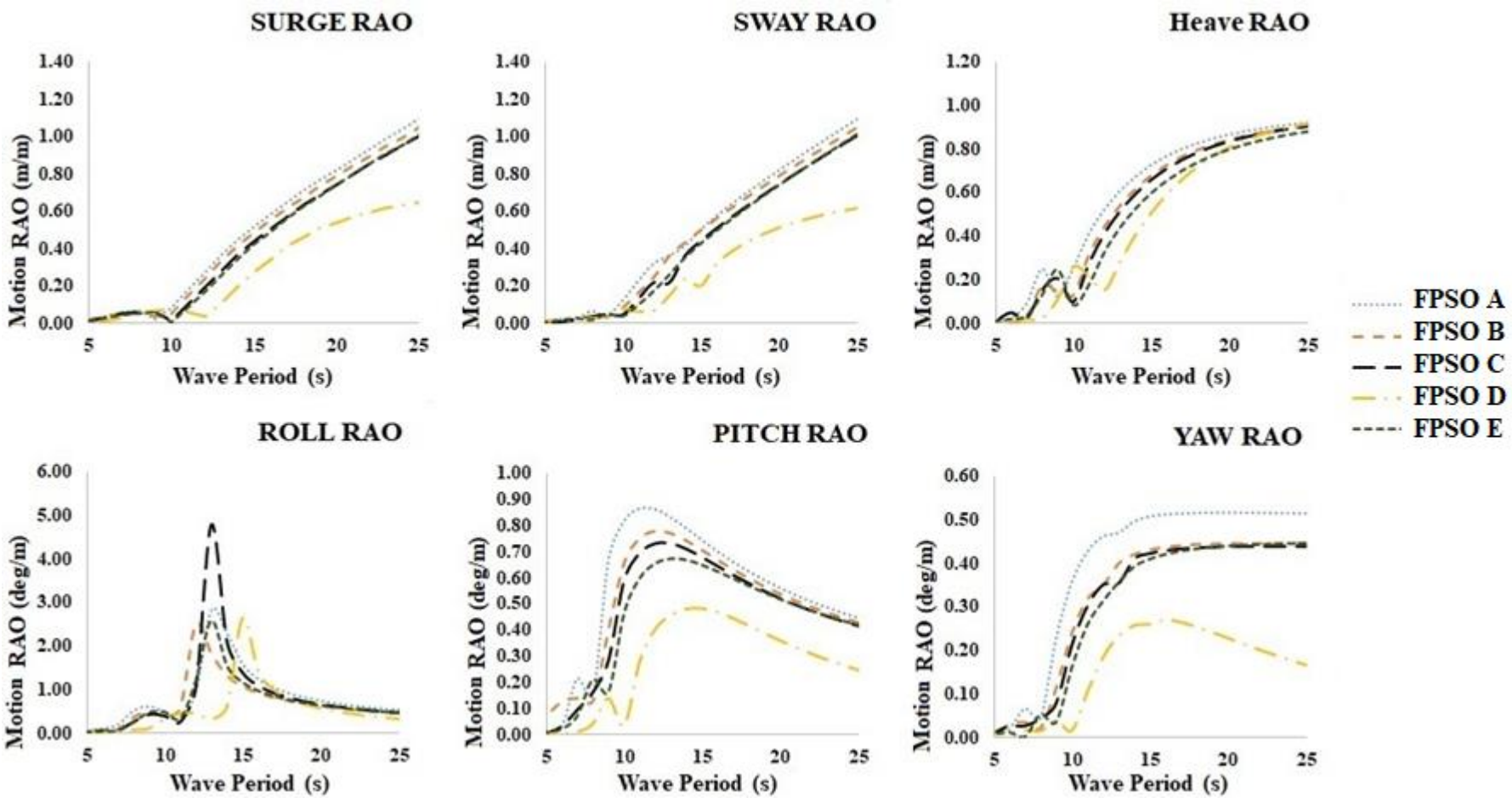

Figure 4.44: RAOs of Operating Malaysian FPSOs (SESAM HydroD results)

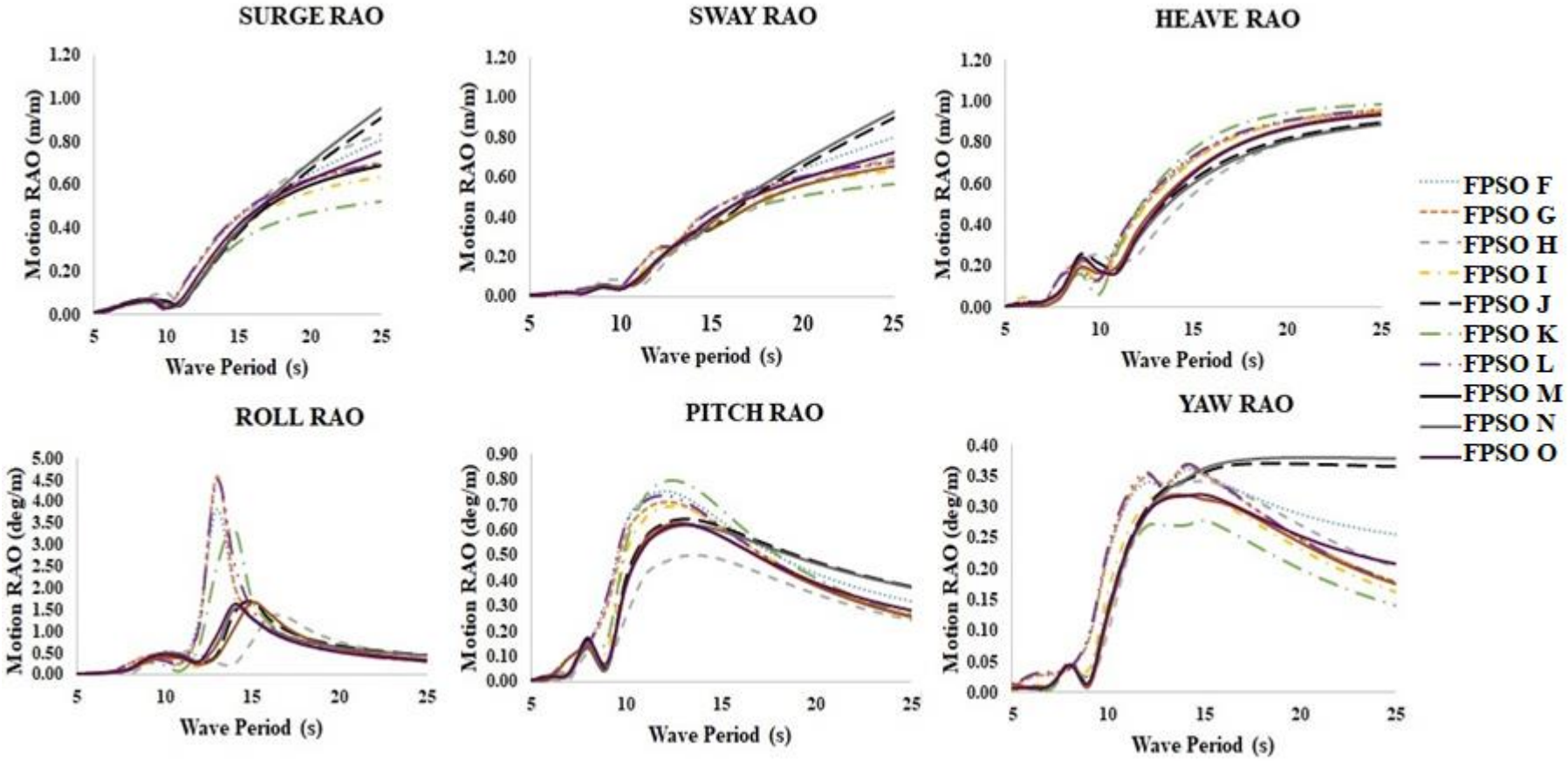

Figure 4.45: RAOs of Operating Australian FPSOs (SESAM HydroD results)

Similarly, for FPSOs with same dimensions as Australian FPSOs shown in Figure 4.45, the maximum surge and sway RAO falls below 0.95 m/m. Maximum heave, roll, pitch and yaw are 0.93 m/m, 4.5 deg/m, 0.8 deg/m and 0.4 deg/m respectively. The RAOs generated for wave frequency ranges can be used for initial design of FPSOs in these regions and in choosing roll damping methods and mooring system.

4.7 Green Water on FPSOs

Freeboard exceedance for chosen FPSOs as given in Table 3.6 to be used in LCCA are calculated using the method detailed in section 3.5.1 to identify green water events, that is if any exists for specific metocean conditions and the freeboard exceedance calculated are approximate since ship lines were drawn using the corresponding FPSO dimensions and scaled to proper DWT as original ship lines are unavailable for the analysis and confidential data for the FPSO operators. However, the results indicate whether the FPSO dimensions will result in low, medium or high susceptibility to green water on FPSO deck. Also, no specific roll damping was given so that the result will be on conservative side and the design engineers can choose appropriate roll damping measures based on the results generated as in section 4.6.

4.7.1 Relative motion and freeboard exceedance for Malaysian and Australian FPSOs

Approximate most probable maximum relative motion has been calculated for FPSOs by using vessel models with dimensions similar to Malaysian FPSOs by subjecting them to site specific metocean conditions obtained from Omar et al [132] for locations shown in Figure 3.22. The maximum annual MPM relative motion for each FPSO considering all the motions at specific points is shown in table format corresponding to each joint annual probability of H_s and T_p. H_s and T_p are taken to be the threshold value of each range during operability analysis. Table 4.12 shows the approximate annual MPM relative motion for Perisai Kamelia FPSO in m corresponding to the wave scatter

Table 3.7. Table 4.13 ~Table 4.15 show the approximate annual MPM relative motion for Berantai, Bunga Kertas and Cendor II FPSO respectively in m corresponding to the wave scatter Table 3.8. Table 4.16 shows the approximate annual MPM relative motion for Kikeh FPSO in m corresponding to the wave scatter Table 3.9.

Table 4.12**:** Annual MPM relative motion for Perisai Kamelia FPSO in m

H_s(m)											
>3.0											
3.0											
2.5								0.79	0.86		
2.0					0.31		0.53	0.64	0.69		
1.5				0.07	0.23	0.33	0.40	0.48	0.52	0.56	0.60
1.0				0.05	0.16	0.22	0.27	0.32	0.34		
0.5				0.02	0.08	0.11					
T_p(s)	1	2	3	4	5	6	7	8	9	10	>10

Table 4.13: Annual MPM relative motion for Berantai FPSO in m

H_s(m)											
>3.0											
3.0									1.14		
2.5								0.87	0.95		
2.0							0.60	0.69	0.76		
1.5				0.08		0.37	0.45	0.52	0.57		
1.0				0.05	0.17	0.25	0.30	0.35	0.38		
0.5			0.00	0.03	0.08						
T_p(s)	1	2	3	4	5	6	7	8	9	10	>10

Table 4.14: Annual MPM relative motion for Bunga Kertas FPSO in m

H_s(m)											
>3.0											
3.0									1.10		
2.5								0.83	0.92		
2.0							0.56	0.66	0.74		
1.5				0.08		0.36	0.42	0.50	0.55		
1.0				0.06	0.18	0.24	0.28	0.33	0.37		
0.5			0.00	0.03	0.09						
T_p(s)	1	2	3	4	5	6	7	8	9	10	>10

Table 4.15: Annual MPM relative motion for Cendor II FPSO in m

H_s(m)											
>3.0											
3.0									1.07		
2.5								0.81	0.89		
2.0							0.54	0.65	0.71		
1.5				0.07		0.34	0.40	0.49	0.53		
1.0				0.05	0.16	0.22	0.27	0.32	0.36		
0.5			0.00	0.02	0.08						
T_p(s)	1	2	3	4	5	6	7	8	9	10	>10

Table 4.16: Annual MPM relative motion for Kikeh FPSO in m

H_s(m)											
>3.0											
3.0											
2.5								0.71	0.81		
2.0							0.49	0.56	0.64	0.69	
1.5						0.32	0.37	0.42	0.48	0.51	
1.0				0.05	0.15	0.21	0.24	0.28			
0.5				0.02	0.08						
T_p(s)	1	2	3	4	5	6	7	8	9	10	>10

Approximate most probable maximum relative motion has been calculated for FPSOs by using vessel models with dimensions similar to Australian FPSOs by subjecting them to site specific metocean conditions obtained from Metocean View [133] for locations shown in Figure 3.23. The maximum annual MPM relative motion for each FPSO considering all the motions at specific points is shown in table format corresponding to each joint annual probability of H_s and T_p. Table 4.17 ~ Table 4.19 shows the approximate annual MPM relative motion for Nganhurra, Pyrenees Venture and Ningaloo Vision FPSO respectively in m corresponding to the wave scatter Table 3.10. Table 4.20 ~Table 4.21 show the approximate annual MPM relative motion for Okha and Modec Venture FPSO respectively in m corresponding to the wave scatter Table 3.11. Table 4.22 shows the approximate annual MPM relative motion for Glas Dowr FPSO in m corresponding to the wave scatter Table 3.12.

It can be seen from Table 4.12~ 4.22 that the maximum annual MPM relative motion for these FPSOs are far below their freeboard given in Table 3.6 and will not

result in green water incidents when subjected to wind generated sea state given in Table 3.7 ~Table 3.12.

Table 4.17: Annual MPM relative motion for Nganhurra FPSO in m

H_s(m)															
1						0.46	0.47	0.46	0.44						
1.5					0.62	0.69	0.71	0.68	0.65	0.61	0.56	0.52		0.44	
2	0.44	0.51	0.61	0.71	0.83	0.92	0.94	0.91	0.87	0.82	0.75	0.69	0.64	0.59	0.55
2.5		0.64	0.76	0.89	1.04	1.15	1.18	1.14	1.09	1.02	0.94	0.87	0.80	0.74	0.68
3		0.77	0.91	1.07	1.25	1.38	1.42	1.37	1.31	1.22	1.13	1.04	0.96	0.88	0.82
3.5			1.06	1.25				1.60	1.53	1.43	1.32	1.21	1.12		
4									1.74	1.63	1.51	1.39	1.28		
4.5										1.83	1.56	1.44	1.35		
5												1.73			
T_p(s)	6	7	8	9	10	11	12	13	14	15	16	17	18	19	20

Table 4.18: Annual MPM relative motion for Pyrenees venture FPSO in m

H_s(m)															
1						0.28	0.30	0.31	0.31						
1.5					0.40	0.42	0.45	0.46	0.45	0.44	0.42	0.40		0.36	
2	0.48	0.51	0.52	0.52	0.53	0.57	0.60	0.61	0.60	0.58	0.56	0.53	0.50	0.47	0.45
2.5		0.64	0.65	0.65	0.66	0.71	0.75	0.77	0.76	0.73	0.70	0.66	0.63	0.59	0.56
3		0.77	0.79	0.78	0.79	0.85	0.90	0.92	0.91	0.88	0.84	0.61	0.75	0.71	0.67
3.5			0.86	0.86				1.03	1.01	0.97	0.93	0.88	0.83		
4									1.16	1.11	1.06	1.00	0.95		
4.5										1.25	1.19	1.13	1.07		
5												1.25			
T_p(s)	6	7	8	9	10	11	12	13	14	15	16	17	18	19	20

Table 4.19: Annual MPM relative motion for Ningaloo Vision FPSO in m

H_s(m)															
1						0.41	0.40	0.39	0.36						
1.5					0.59	0.61	0.60	0.58	0.55	0.50	0.46	0.43		0.36	
2	0.45	0.54	0.68	0.72	0.79	0.82	0.80	0.77	0.73	0.67	0.62	0.57	0.52	0.48	0.44
2.5		0.68	0.82	0.90	0.98	1.02	1.00	0.97	0.91	0.84	0.77	0.71	0.65	0.60	0.55
3		0.81	0.99	1.08	1.18	1.22	1.20	1.16	1.09	1.01	0.93	0.85	0.78	0.72	0.66
3.5			1.16	1.26				1.35	1.27	1.18	1.08	0.99	0.91		
4									1.45	1.34	1.23	1.13	0.95		
4.5										1.51	1.38	1.27	1.17		
5												1.42			
T_p(s)	6	7	8	9	10	11	12	13	14	15	16	17	18	19	20

Table 4.20: Annual MPM relative motion for Okha FPSO in m

H_s(m)	T_p(s) 5	6	7	8	9	10	11	12	13	14	15	16	17	18	19	20
0.5																
1						0.36	0.39	0.4	0.39	0.39	0.38	0.36	0.34		0.31	
1.5	0.24	0.34	0.4	0.46	0.51	0.55	0.58	0.59	0.59	0.56	0.56	0.54	0.51	0.49	0.46	0.43
2		0.45	0.53	0.62	0.69	0.73	0.77	0.79	0.78	0.77	0.75	0.72	0.68	0.65	0.61	0.58
2.5		0.56	0.6	0.77	0.86	0.91	0.96	0.99	0.98	0.97	0.94	0.9	0.85	0.81	0.76	0.72
3			0.8	0.92	1.03				1.18	1.13	1.13	1.08	1.03	0.97		
3.5				1.08	1.2						1.31	1.26	1.2	1.13		
4				1.23	1.37											

Table 4.21: Annual MPM relative motion for Modec Venture II FPSO in m

H_s(m)	T_p(s) 5	6	7	8	9	10	11	12	13	14	15	16	17	18	19	20
0.5																
1						0.39	0.41	0.41	0.4	0.38	0.36	0.33	0.3		0.26	
1.5	0.23	0.33	0.4	0.47	0.53	0.58	0.62	0.62	0.6	0.57	0.53	0.49	0.46	0.42	0.39	0.36
2		0.44	0.53	0.63	0.71	0.78	0.82	0.82	0.79	0.76	0.71	0.66	0.61	0.56	0.52	0.48
2.5		0.55	0.66	0.79	0.89	0.97	1.03	1.03	0.99	0.95	0.89	0.82	0.76	0.7	0.65	0.6
3			0.79	0.95	1.06				1.19	1.14	1.07	0.99	0.91	0.84		
3.5				1.04	1.24						1.25	1.15	1.06	0.98		
4				1.26	1.42											

Table 4.22: Annual MPM relative motion for Glas Dowr FPSO in m

H_s(m)	T_p(s) 4	5	6	7	8	9	10	11	12	13	14	15	16	17	18	19	20
0.5		0.08	0.11	0.14			0.19	0.2	0.19	0.19	0.18	0.16	0.15	0.14			
1	0.11	0.16	0.23	0.27	0.33	0.35	0.38	0.39	0.38	0.37	0.35	0.33	0.3	0.28	0.25	0.23	0.23
1.5		0.24	0.34	0.41	0.49	0.53	0.57	0.59	0.58	0.56	0.53	0.49	0.45	0.41	0.38	0.35	0.33
2			0.45	0.55	0.66	0.7	0.76	0.78	0.77	0.75	0.71	0.65	0.6	0.55	0.51	0.47	
2.5				0.68	0.82	0.88	0.94					0.82	0.75	0.69			
3					0.99												

Also, it is seen from Table 4.12 ~ Table 4.22 relative motion of FPSO holds a linear relation with wave height. This is because heave, roll and pitch motion increases with wave height irrespective of the mooring used as seen in Figure 4.26 ~Figure 4.32. This is also the reason why linear analysis produce good results and why only vessel model can be used to simulate green water on FPSOs without mooring lines.

For FPSOs to be used in shallow waters, care should be taken while designing them, as in shallow waters up to 100 m, heave and pitch motion increases as seen in Figure 4.33 which can make the FPSO susceptible to green water. For Malaysian seas, the most probable peak period is usually in the range of 6 s to 7 s. It can be seen from Figure 4.40 ~Figure 4.41, for FPSOs having beam to length ratio in the same range as the Malaysian and Australian FPSOs, the heave, roll and pitch motion remains almost the same for peak period less than 7 s. This means that for the Malaysian FPSOs, the risk from green water is less when compared to Australian FPSOs where the peak period of wave is higher. As in higher wave periods, these FPSOs have higher motion in heave, roll and pitch as seen in Figure 4.40 ~Figure 4.41. Hence utmost care should be taken while designing FPSOs to be installed in Australian seas as 100-year extreme cyclones shown in Table 3.13 can make them highly susceptible to green water as shown in Table 4.23 while extreme metocean conditions for the deepest oil field, that is Kikeh field as shown in Table 4.10 will only leave the FPSO with a low susceptibility to green water as seen in Table 4.24. The 100-year extreme cyclonic condition given in Table 3.13 is representative of all of North Western Australia and not specific to the operating location of chosen FPSOs for operability analysis.

Table 4.23: Annual maximum freeboard exceedance of FPSOs for extreme cyclonic condition in NWA

FPSO Name	**Dimension similar as FPSO**	**Max Freeboard Exceedance (m)**	**Susceptibility to green water**
FPSO F	Armada Claire	10.07	High Susceptibility
FPSO G	Glas Dowr	13.54	High Susceptibility
FPSO H	Maersk Nguima - Yin	8.80	High Susceptibility
FPSO I	Modec Venture II	11.49	High Susceptibility
FPSO J	Montara Venture	11.42	High Susceptibility
FPSO K	Nganhurra	9.20	High Susceptibility
FPSO L	Ningaloo Vision	10.46	High Susceptibility

FPSO Name	Dimension similar as FPSO	Max Freeboard Exceedance (m)	Susceptibility to green water
FPSO M	Northern Endeavour	9.36	High Susceptibility
FPSO N	Okha	12.98	High Susceptibility
FPSO O	Pyrenees Venture	6.46	High Susceptibility

Table 4.24: Annual maximum freeboard exceedance of FPSOs for extreme metocean condition in Kikeh field

FPSO Name	Dimension similar as FPSO	Max Freeboard Exceedance (m)	Susceptibility to green water
FPSO A	Berantai	2.53	LOW Susceptibility
FPSO B	Bunga Kertas	0.22	LOW Susceptibility
FPSO C	Cendor II	1.24	LOW Susceptibility
FPSO D	Kikeh	2.87	LOW Susceptibility
FPSO E	Perisai Kamelia	-1.49	LOW Susceptibility

4.7.2 Downtime cost due to green water

As seen from Table 4.12- 4.22 and discussed in section 4.7.1, there is no freeboard exceedance for chosen FPSOs for LCCA study in Table 3.6 as freeboard for these FPSOs are higher than the annual MPM relative motion. Therefore, there is no downtime cost due to green water when annual wind generated wave scatter data is considered. Even though the original ship lines were not used, from Table 4.12 ~ Figure 4.22 it can be seen that the MPM relative motion is not varying much for the different FPSO dimensions and is expected to be in the same range even when original ship lines are used to create vessel model. Also, for Malaysian FPSOs, it seen from Table 4.24 that even in extreme metocean conditions, FPSO is only susceptible to low level of green water incidents. When considering Australian FPSOs, extreme cyclonic

conditions with 1-year return period as shown in Table 3.13 will not cause green water incidents as the relative motion will be in the range as shown in Table 4.17 ~Figure 4.22, but, 100-year return period is causing high level of green water incidents. Also, the 100-year extreme cyclonic conditions are representative for the whole of NWA and not specific to the operating location for these FPSOs. However, this event occurring in a 10-year life-cycle of FPSO (life-cycle period used in LCCA) is very low and the downtime cost due to such event will be negligible as discussed later in this thesis regarding the main cost driving components for FPSO life-cycle cost as capital, operation and maintenance cost in section 4.9. Hence the downtime cost is approximated to be zero due to green water incidents under wind generated sea conditions.

4.8 Life-Cycle Cost of FPSOs in Malaysia and Australia

Table 4.25 gives the cost data of selected FPSOs given earlier in Table 3.6. The FPSOs under study involve: spread mooring, internal turret mooring, external turret mooring, submerged turret mooring and finally riser turret mooring. The cost data given in Table. 4.25 is obtained as per the procedure mentioned in section 3.6.4. As given in section 4.7.2, downtime cost due to green water incidents, when FPSOs are subjected to wind generated sea is zero. Oil price for calculating revenue from oil production is taken as 71.5 USD per barrel as annual average of past 5 years [165]. The capital cost for the chosen FPSOs are given in Figure 4.46. In these FPSOs, Kikeh FPSO with external turret mooring has the maximum capital cost of 7195 million USD. Also, FPSOs with riser turret mooring have comparatively high capital costs when compared to other moored FPSOs with Nganhurra FPSO costing 5234 million USD. Out of the spread moored FPSOs under study, Ningaloo Vision has the highest capital cost of around 1391 million USD, while Cendor II and Berantai have capital costs under 800 million USD. Out of the internal turret moored FPSOs, Pyrenees venture has the highest capital cost of 3359 million USD; the others having capital cost under 1125 million USD. Okha and Nganhurra, two of the riser turret moored FPSOs have capital cost 4214 million USD and 5234 million USD respectively.

Table 4.25: Cost Data of selected FPSOs [2] [141]–[153]

FPSO/ FSO NAME	CAPITAL COST (US DOLLARS)	ANNUAL OPERATION & MAINTENANCE COST (US DOLLARS)	ANNUAL BARE BOAT CHARTER RATE (US DOLLARS)	MAXIMUM OIL PRODUCTION CAPACITY OF FPSO (MBOPD)	ANNUAL REVENUE FROM MAXIMUM OIL PRODUCTION (US DOLLARS)
PERISAI KAMELIA	272100000	6750000	45000000	100	600233333
KIKEH	7195000000	7837500	59418700	120	720280000
CENDOR II	660000000	14726250	98175000	35	210081667
BERANTAI	800000000	7700000	49500000	30	180070000
NINGALOO VISION	1391000000	63454545	423030300	63	378147000
BUNGA KERTAS	150000000	3507595	7737400	30	180070000
GLAS DOWR	175100000	3000000	20000000	60	360140000
MODEC VENTURE II	624000000	52700000	351333333	100	600233333
STYBARROW	1125000000	61071429	407142857	80	480186667
PYRENEES VENTURE	3359000000	63333333	422222222	96	576224000
OKHA	4214000000	55600000	NA	30	180070000
NGANHURRA	5234000000	2806000000	NA	100	600233333

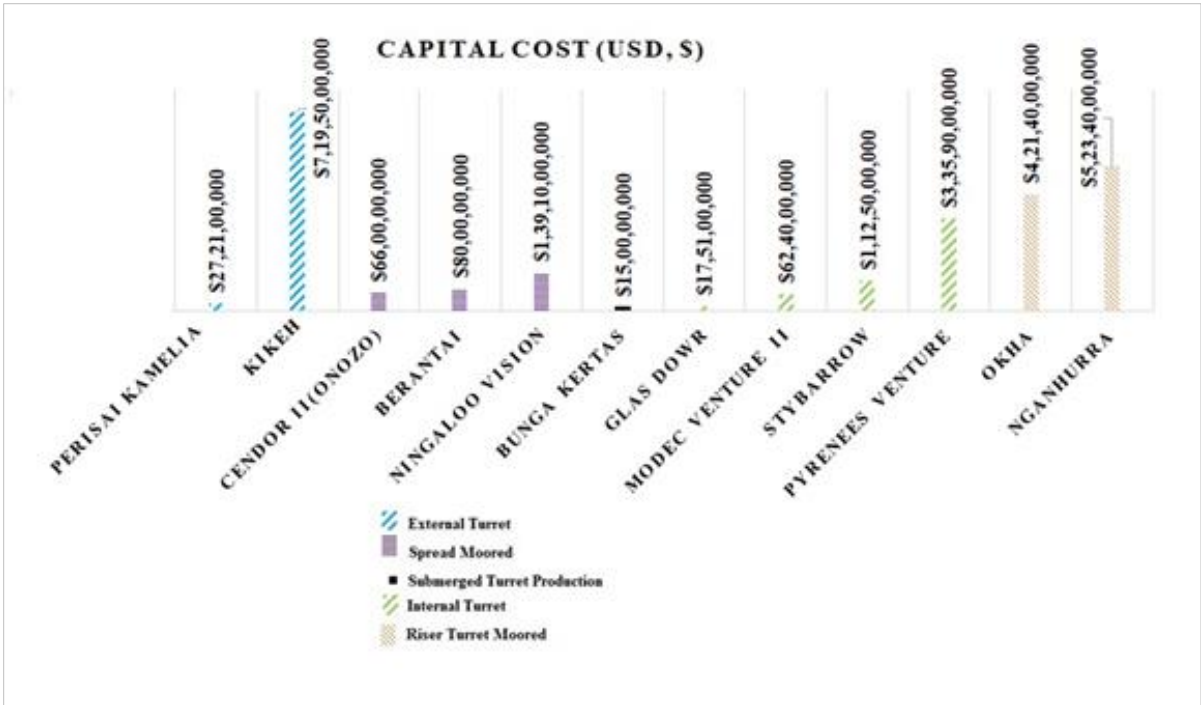

Figure 4.46: Capital Cost of FPSOs in Malaysia and Australia under study

The total life-cycle cost of FPSOs accounting only for capital, operation and maintenance which are the expenses, are given in Figure 4.47 and the total life cycle cost is maximum for Nganhurra FPSO with 75348 million USD for 25-year life-cycle period, noted as a riser turret moored. Even though the capital cost was higher for Kikeh FPSO, the life-cycle cost of Ningaloo Vision FPSO (SM), Modec venture II (IT), Stybarrow FPSO (IT), Pyrenees venture (IT) and Nganhurra FPSO (RTM) is higher when compared to the life-cycle costs of Kikeh FPSO (ET) with an average difference in life-cycle costs of 16721 million USD for 25-year life-cycle period. Notably Stybarrow and Nganhurra FPSO have newly built hulls. The riser turret moored FPSOs have an average life-cycle cost of 40494 million USD for 25-year life-cycle period and 19032 million USD for the 10-year life-cycle period. Compared to the average life-cycle cost of riser turret moored FPSOs, the average life-cycle cost of external turret moored FPSOs are 13%, spread moored FPSOs are 16% and internal turret moored FPSOs are 25% for 25 years life-cycle period. Whereas for 10-year life-cycle period, the average life-cycle cost of spread moored FPSOs are 16%, external turret moored FPSOs are 22% and internal turret moored FPSOs are 25% of that of riser turret moored FPSOs. The rise in average life-cycle cost of external turret moored FPSOs in 25 years

are contributed by the initial high capital cost of Kikeh FPSO. Hence ranking the costliest FPSO and associated mooring system in terms of its life-cycle cost: the riser turret moored FPSOs are the costliest, followed by internal turret moored FPSOs for both 10-year and 25-year life-cycle periods, based on the available FPSO cost data from different reliable sources. The least expensive option for 10-year life-cycle period is spread moored FPSO, while for 25-years, it is external turret moored FPSO.

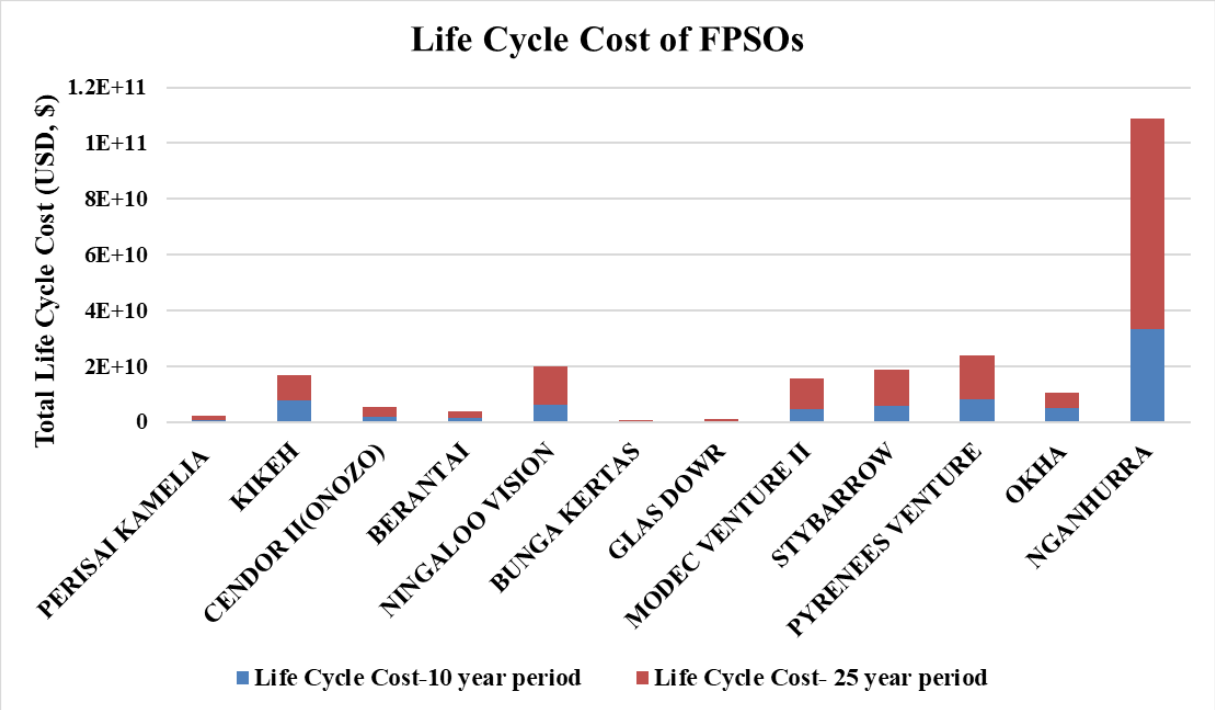

Figure 4.47: Total Life-Cycle cost of FPSOs in Malaysia and Australia for 10-year and 25-year life-cycle period

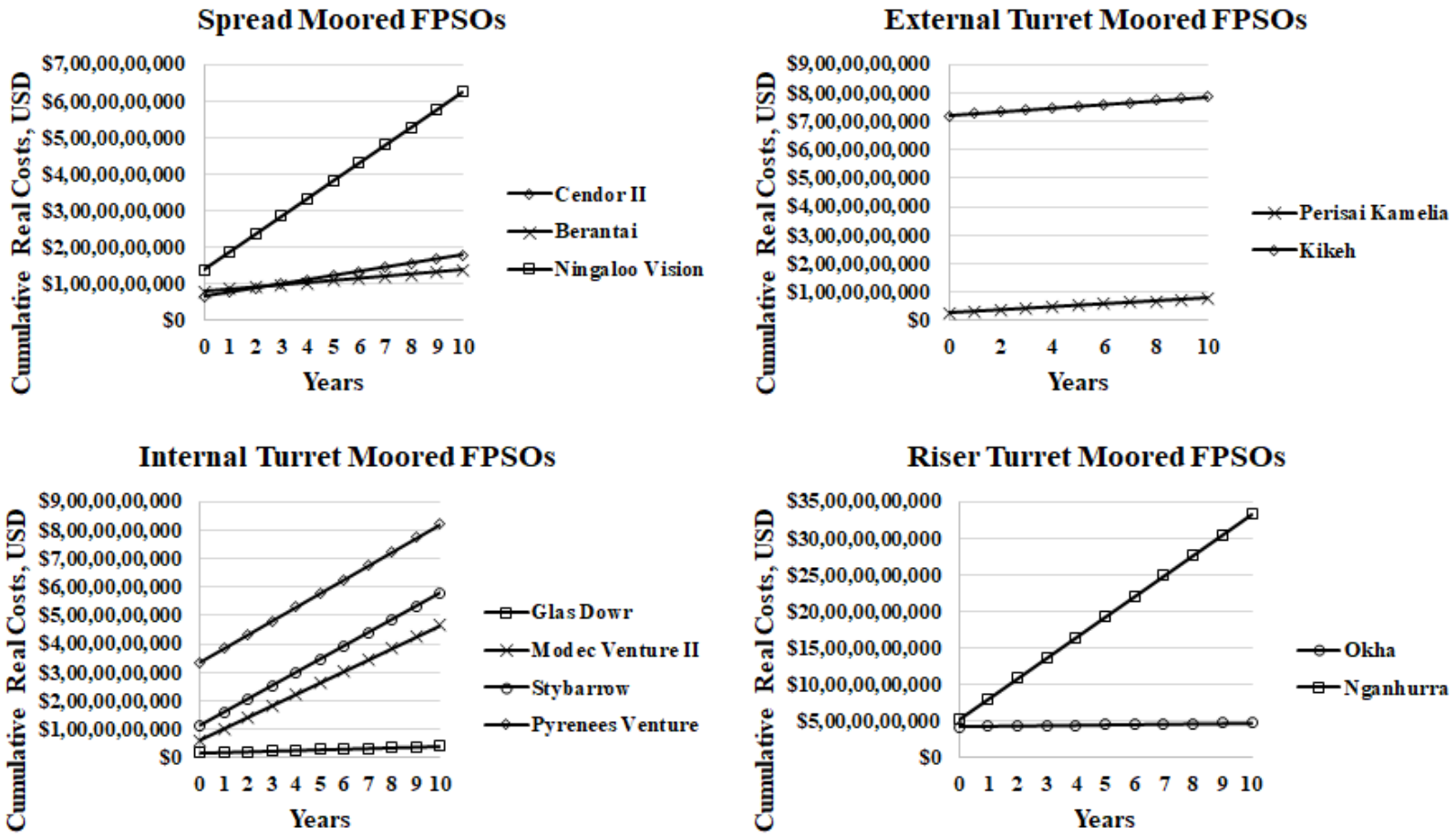

Figure 4.48: Cumulative Real Cost of FPSOs in Malaysia and Australia for 10-year Life-cycle Period

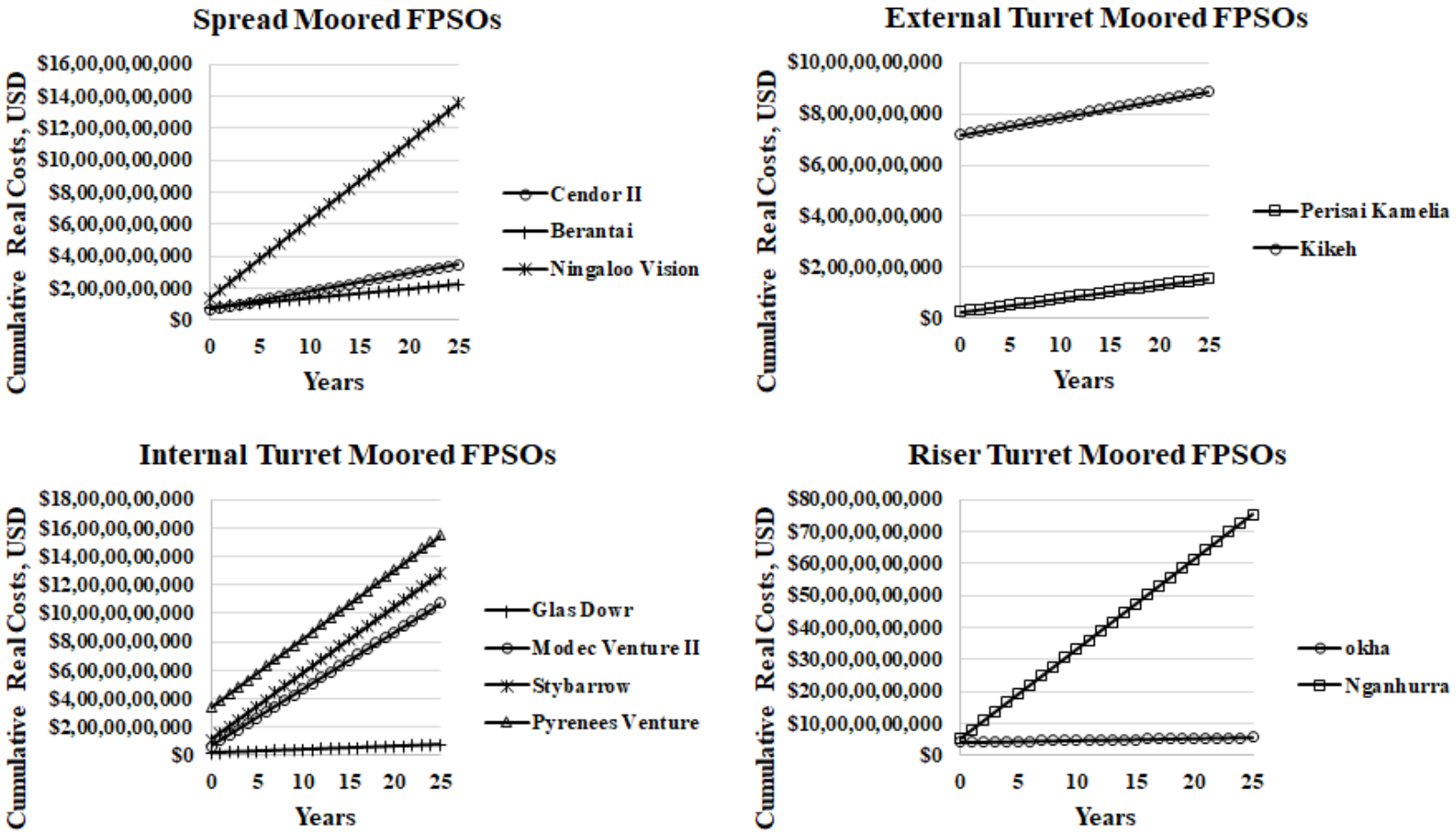

Figure 4.49: Cumulative Real Cost of FPSOs in Malaysia and Australia for 25-year Life-cycle Period

The cumulative real cost of FPSOs including capital, operation and maintenance cost for 10-year life-cycle period is given in Figure 4.48 and for 25-year life-cycle period is given in Figure 4.49. The rate of increase of cumulative costs per annum ranges from 60 million USD to 500 million USD for spread moored FPSOs. The average increase in cumulative costs per year for external turret moored FPSOs range from 50 million USD to 70 million USD, whereas for internal turret moored FPSOs, the annual rise in cumulative costs are from 20 million USD to 500 million USD.

The highest annual cost increase is for the riser turret moored FPSOs, ranging from 60 million USD to 3000 million USD. Market fluctuation in cost is not considered and is assumed to be constant while calculating life-cycle cost. Hence to include market fluctuations in the cost components a sensitivity analysis has been carried out in section 4.11.

4.9 Net Present Value of FPSOs in Malaysia and Australia

Net present value for FPSOs are calculated as per section 3.6.6 for different mooring configurations at a discount rate of 2% for the capital cost and NPV comparison and are shown in Figure 4.50. NPV calculated with only expenses, capital, operation and maintenance are given in Figure 4.50. NPV calculated with expenses and revenue from oil are shown in Figure 4.51.

The NPVs of FPSOs calculated with only expenses are all negative as the main source of income from oil production is not included as in Figure 4.51. It can be seen from the scatter diagram shown in Figure 4.50 that, maximum number of FPSO configurations are having capital costs less than 2000 million USD and NPV greater than -20,000 million USD. For these FPSOs, the capital costs are minimum and NPVs are closer to zero. The other FPSOs which do not fall in this area are Pyrenees venture with IT, Okha and Nganhurra with RTM and Kikeh with ET. Even though the capital costs of these FPSOs are higher, the NPV of all the FPSOs except Nganhurra, is greater than -10,000 million USD. Bunga Kertas, Glas Dowr and Perisai Kamelia FPSOs have the highest NPV with values greater than -1000 million USD and capital costs less than

300 million USD. Also, it is to be noted that, these are turret moored FPSOs. For spread moored FPSOs, the NPV falls between -1674 million USD to -5760 million USD with capital cost less than 1391 million USD. The profitability of these FPSOs can be accurately presented where the revenue obtained by the oil production is known, and is shown in Figure 4.51.

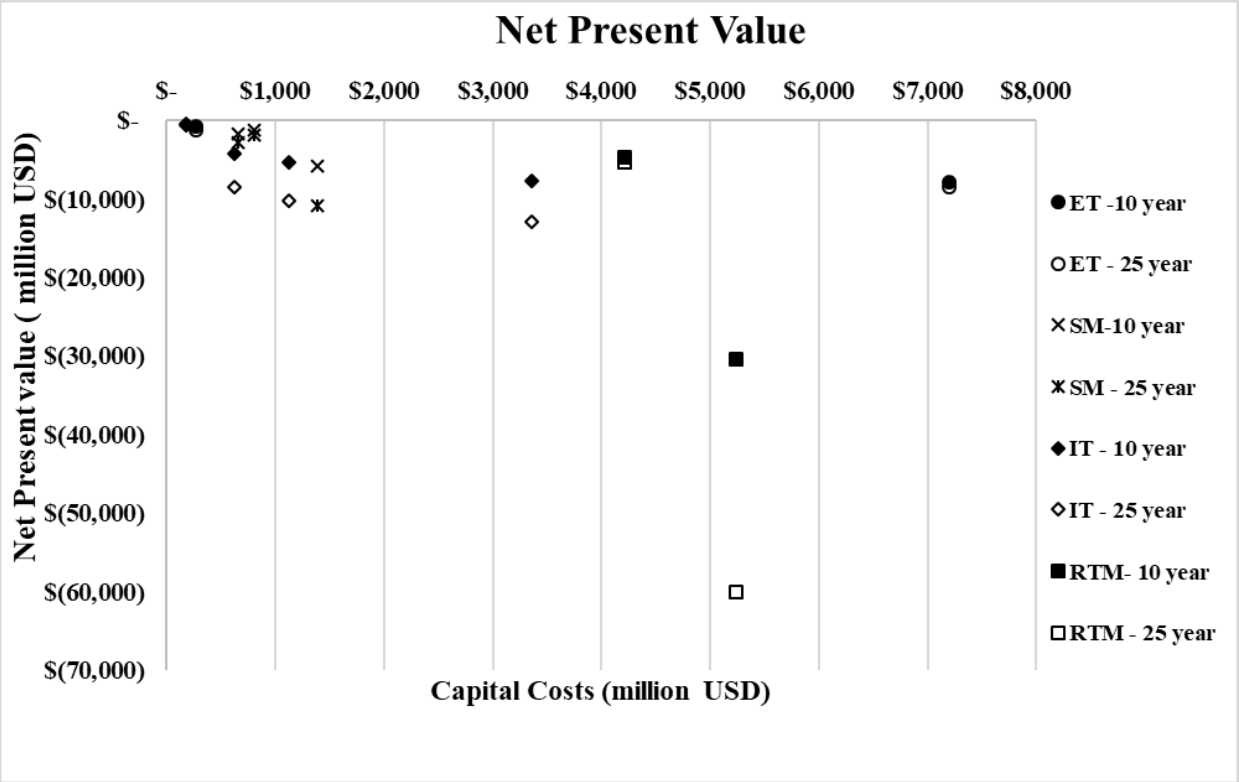

Figure 4.50: NPV of FPSOs plotted against their capital cost (NPV calculated with only expenses)

Again, when the revenue from oil is included, the highest NPV is for Perisai Kamelia, Glas Dowr, Modec Venture II and Bunga Kertas, starting from the FPSO with highest NPV onwards and all of them being turret moored FPSOs. Hence it cannot be generalised that all the turret moored FPSOs are costlier than the spread moored versions when their life-cycle worth is considered. Also, it is seen from Figure 4.50 and Figure 4.51 that as the life-cycle period increases, the NPV decreases.

FPSOs with negative NPV even after the inclusion of income from oil production are Okha and Nganhurra, which are riser turret moored FPSOs with lowest NPV from the chosen FPSOs for study, followed by Pyrenees Venture, Ningaloo Vision, Kikeh

and Stybarrow FPSOs. This is mainly due to their high capital cost as seen in Figure 4.46. Downtime cost are negligible for all the FPSOs chosen for the study as seen in section 4.7.2. Also, the trend in NPV variation over the years seems to be similar with and without income from oil prices from Figure 4.50 ~Figure 4.51. Hence the main cost driving factor for NPV is capital, operation and maintenance cost.

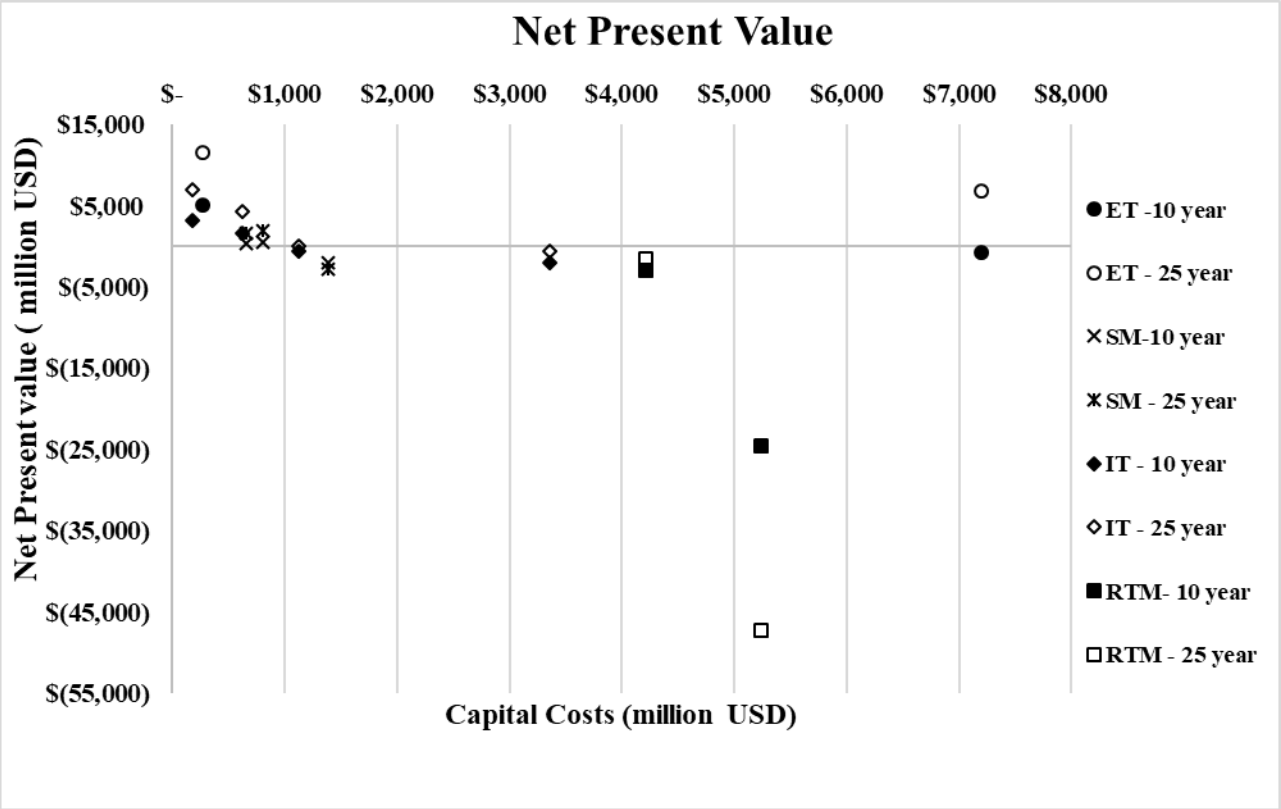

Figure 4.51: NPV of FPSOs plotted against their capital cost (NPV calculated with expenses and revenue from oil production)

4.10 Present Value of FPSOs in Malaysia and Australia

The present value of Australian FPSOs for a (calculated built-up) discount rate of 2.96% and Malaysian FPSOs for a (calculated built-up) discount rate of 1.87% for 10-year life-cycle period and 25-year life-cycle period is given in Figure 4.52 ~Figure 4.55. Present value of FPSOs are calculated for all expenses and income. The variation in the present worth of these FPSOs for the future cash flows are depicted over the number of years of respective life-cycles. The present worth increases as the life decreases except

for Nganhurra and Ningaloo Vision, as in the long term, the higher capital investment is retrieved through income from oil. Whereas for other FPSOs, the operation and maintenance cost is proving to be high in the long term, resulting in lower present values.

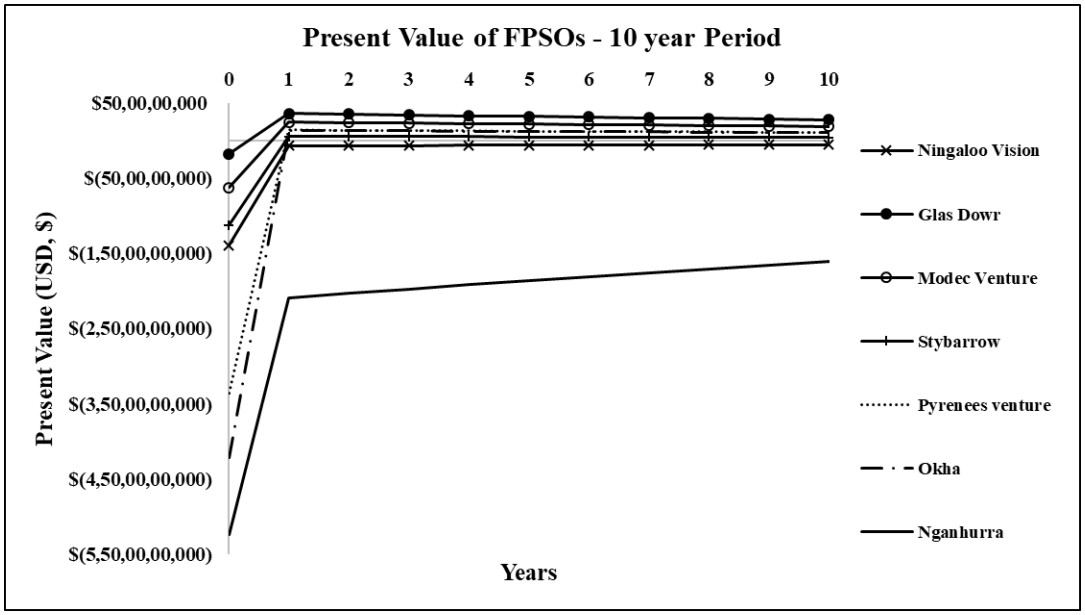

Figure 4.52: Present Value of Australian FPSOs chosen for study for 10-year life-cycle period

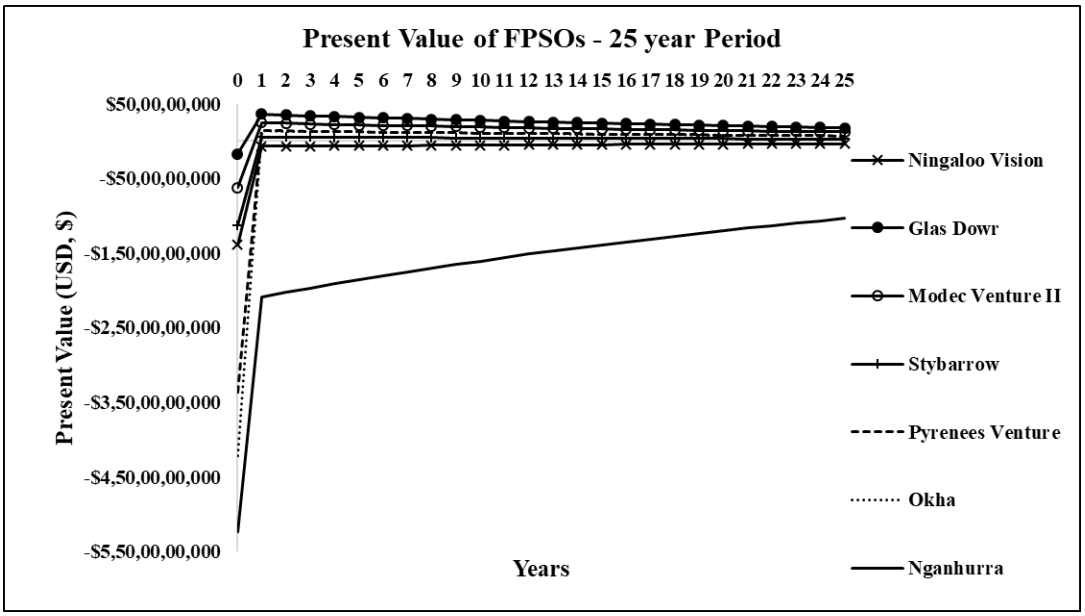

Figure 4.53: Present Value of Australian FPSOs chosen for study for 25-year life-cycle period

It can be seen from Figure 4.52 ~ Figure 4.55 that the present value takes a sudden rise in the year 1 and then slightly decreases towards the end of life of the asset from first year of operations except for Nganhurra and Ningaloo Vision for the reasons mentioned above. After the initial year, the present value decreases from 10 million to 1 million USD per year for the various FPSOs over the life period.

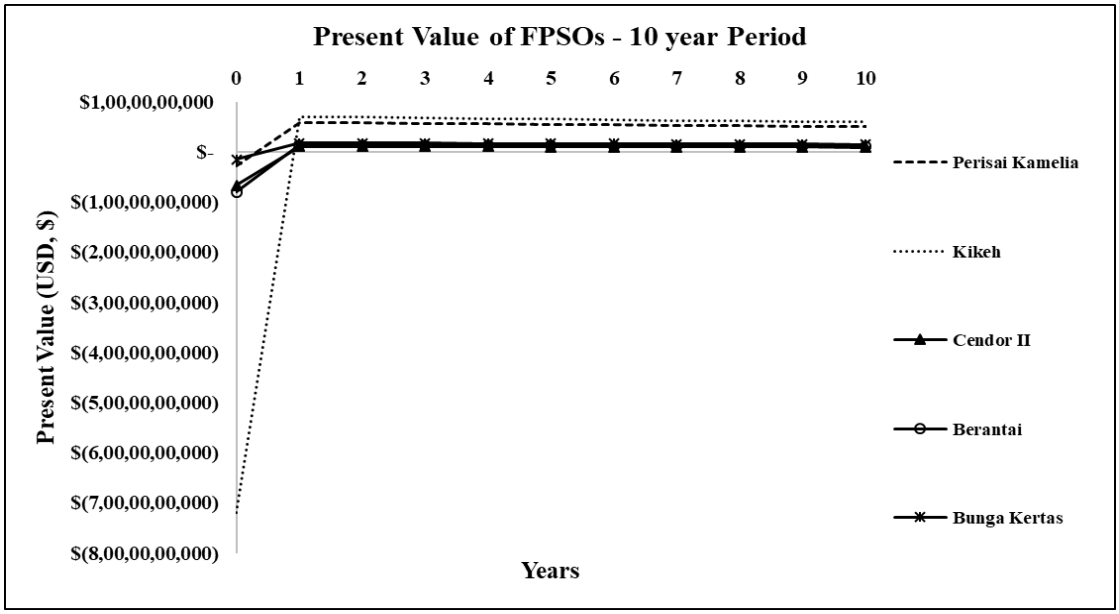

Figure 4.54: Present Value of Malaysian FPSOs chosen for study for 10-year life-cycle period

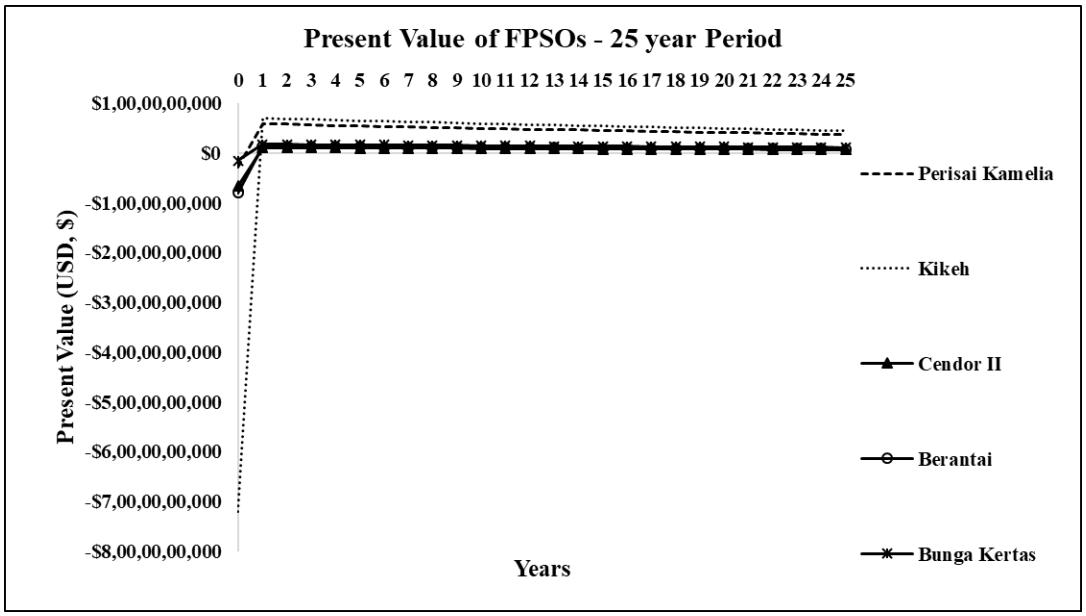

Figure 4.55: Present Value of Malaysian FPSOs chosen for study for 25-year life-cycle period

The present value graph can be used to identify the sum of the future cash inflows discounted for inflation and interest for a period of 10 years and 25 years to represent the value of this money in present day dollars. As per the study, for Australian FPSOs, except Nganhurra and Ningaloo Vision, the present value of all other FPSOs are greater than 41 million USD for a period of 10 years and 27 million USD for a period of 25 years. Similarly, for Malaysian FPSOs, the minimum present value is 96 million USD for 10 years and 73 million USD for a life period of 25 years.

4.11 Sensitivity Analysis

Sensitivity analysis is performed to identify which FPSO configuration should be adopted for any given interest rate without additional calculations as per the procedure mentioned in section 3.6.7. The calculated discount rate for the present Australian and Malaysian economy is 2.96% and 1.87% respectively. For sensitivity analysis (including risk factor in analysis), the discount rate is varied from 2% to 10% which presents the best and worst scenarios in the market rates. The NPV of FPSOs in Malaysia and Australia for 10-year life-cycle period is plotted along with the respective discount rates as shown in Figure 4.56 ~ Figure 4.59. Also, NPV of FPSOs for discount rate of 2% is plotted against their capital cost to show the relation between capital cost and their respective NPVs. The expenses and revenue from oil is included in the life-cycle cost and NPV calculation.

Figure 4.56 shows the NPV profile for spread moored FPSOs. As the discount rate is increased from 2% to 10%, the net present value decreases up to a rate of 50 million USD per percent discount rate. For external turret moored FPSOs, the NPV decreases up to 30 million USD per percent discount rate as seen in Figure 4.57. Figure 4.58 shows the decrease of NPV as 50 million USD to 100 million USD per percent increase in discount rate for internal turret moored FPSOs. Nganhurra, which is a riser turret moored FPSO shows an increase in NPV, as in the long term, the higher capital investment is retrieved through income from oil as seen in Figure 4.59.

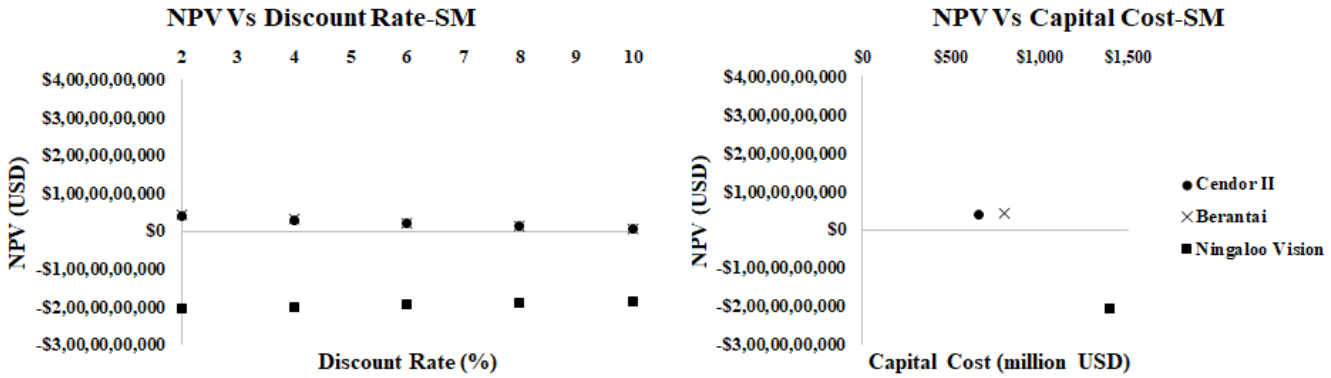

Figure 4.56: NPV Profile for Spread Moored FPSOs

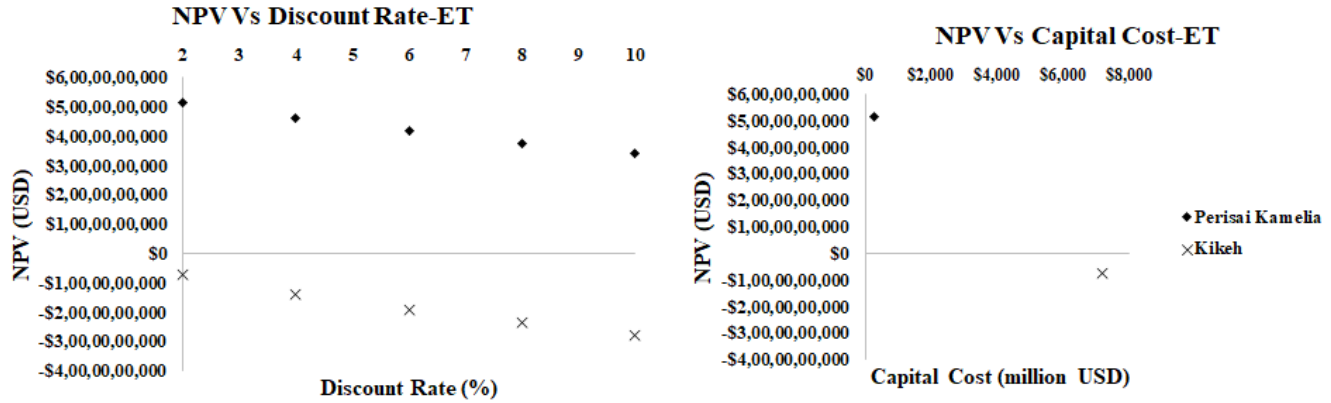

Figure 4.57: NPV Profile for External Turret Moored FPSOs

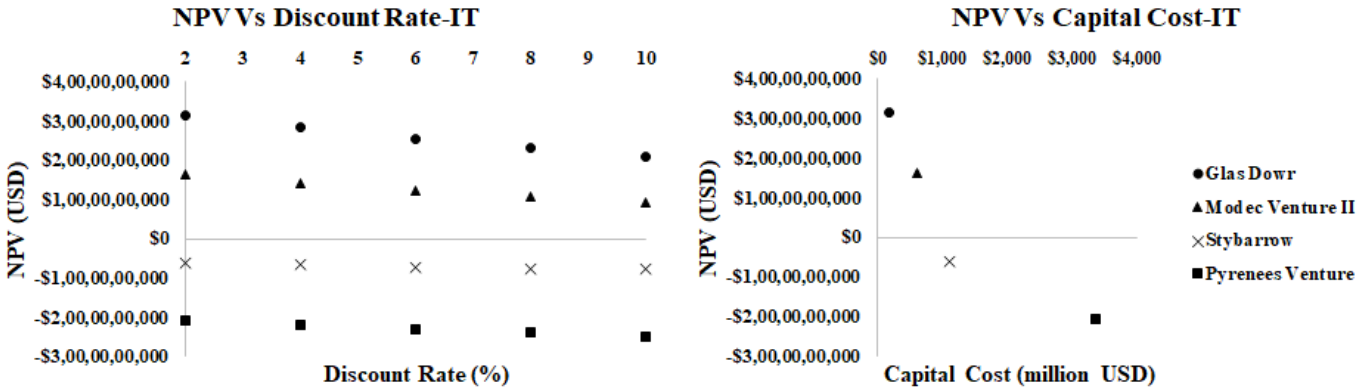

Figure 4.58: NPV Profile for Internal Turret Moored FPSOs

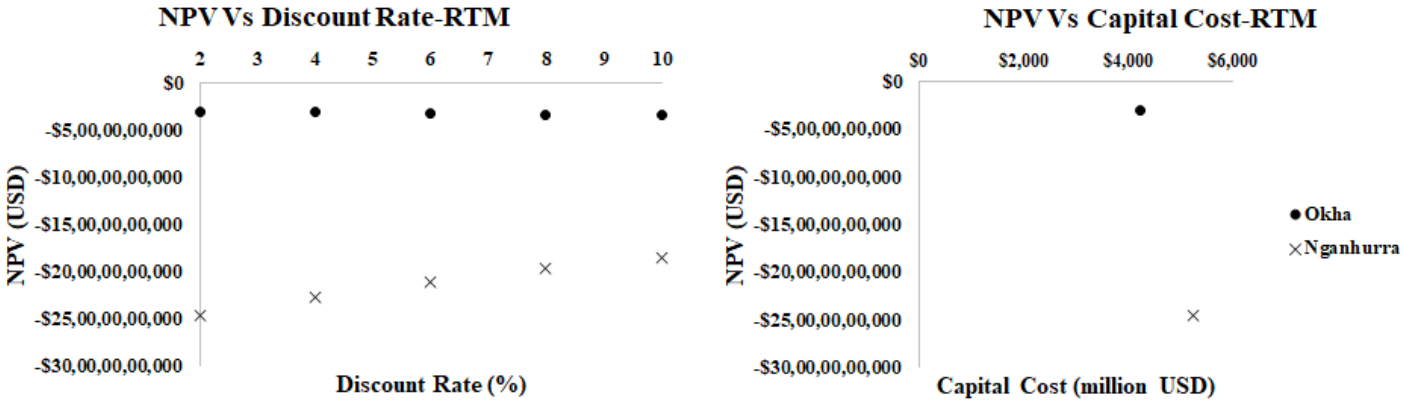

Figure 4.59: NPV Profile for Riser Turret Moored FPSOs

In general, as the discount rate increases, the net present value of the asset decreases as the risk associated with the investment increases. Also, it can be seen from Figure 4.56 ~ Figure 4.59 that, NPV decreases as capital cost increases. The NPV profile reflects the net present worth of these FPSOs, at a varying market situation and can be used as a reference in the initial estimate of similar configured FPSOs.

4.12 Cost Proportions

FPSOs with similar dimensions and dead weight tonnages are compared to find the difference in cost proportion for FPSOs with different mooring configurations and hull conditions. A discount rate of 2% is used for the comparison purpose and NPV is calculated for all expenses (Capital, operation and maintenance) and income from oil production.

4.12.1 Cendor II and Glas Dowr FPSO

Figure 4.60 compares Cendor II FPSO with spread mooring and converted hull to Glas Dowr FPSO with internal turret mooring and newly built hull for 10-year analysis period. Table 4.26 gives the cost and dimensions of these FPSOs. Even though converted hull is used for Cendor II, the initial cost of Cendor II FPSO is higher than Glas Dowr FPSO. Again, the operation and maintenance cost of FPSO with a converted hull and spread mooring, i.e. Cendor II FPSO is higher than Glas Dowr FPSO.

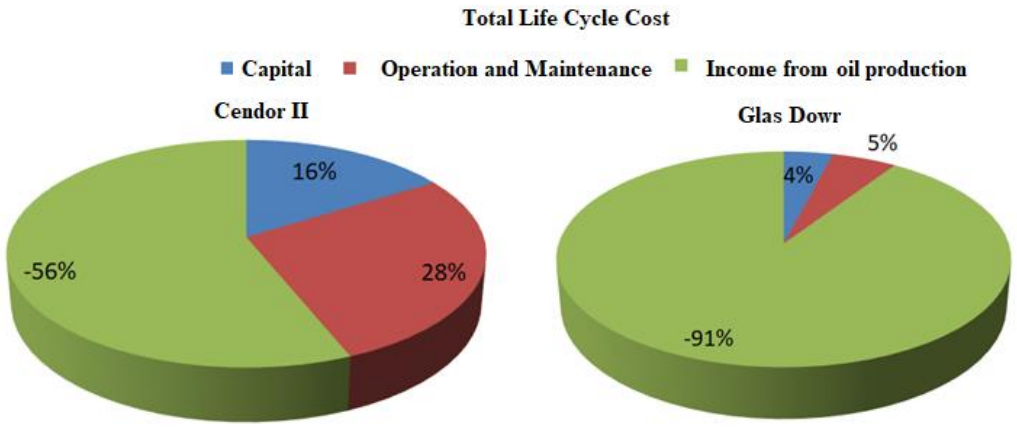

Figure 4.60: Cost Proportions of Cendor II and Glas Dowr

It is to be noted that, the NPV of Glas Dowr is more with value -3151 million USD for 10-year life period. NPV of Cendor II is 386 million USD. So, even though Glas Dowr FPSO has internal turret and newly built hull, over the whole life period, it proves to be the better option when compared to the spread moored Cendor II FPSO.

Table 4.26: Cost, Dimensions and DWT of Cendor II and Glas Dowr

FPSO	Cendor II	Glas Dowr
Cost		
Capital Cost (Million USD)	-660	-175
Operation and Maintenance Cost (Million USD)	-1129	-230
Revenue from Oil Production (Million USD)	2294	3933
NPV (Million USD)	386	3151
Dimensions		
DWT	100020	105000
Hull Length (m)	245	242
Hull Width (m)	41	42
Hull depth (m)	21.6	21

4.12.2 Nganhurra and Stybarrow FPSO

Figure 4.61 compares Nganhurra with riser turret mooring to Stybarrow FPSO with internal turret with cost and dimensions as shown in Table 4.27. Both are having newly built hulls, while Stybarrow FPSO is leased, Nganhurra FPSO is owned. Nganhurra having riser turret mooring, costs more than Stybarrow with internal turret.

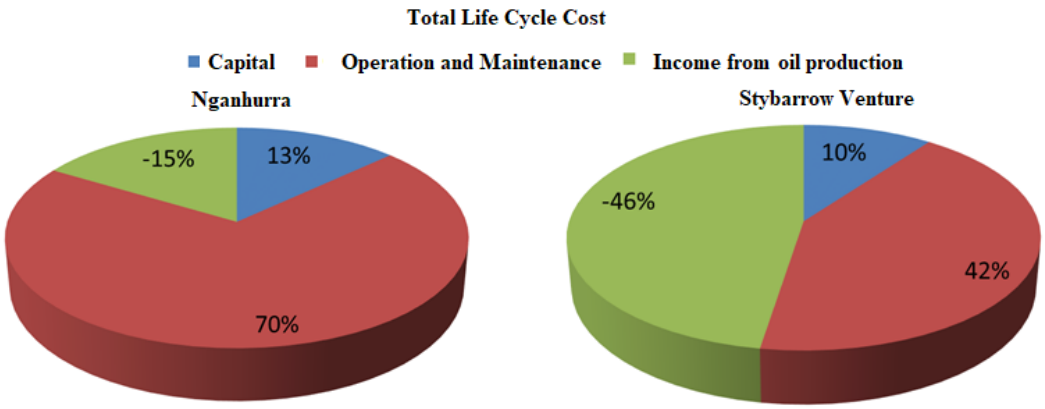

Figure 4.61: Cost Proportions of Nganhurra and Stybarrow Venture

The operation and maintenance cost of Nganhurra FPSO is also higher when compared to Stybarrow Venture. The NPV of Stybarrow FPSO is -621 million USD which is higher than Nganhurra FPSO with NPV -24552 million USD for 10-year life period.

Table 4.27: Cost, Dimensions and DWT of Nganhurra and Stybarrow Venture

FPSO	Nganhurra	Stybarrow
Cost		
Capital Cost (Million USD)	-5234	-1125
Operation and Maintenance Cost (Million USD)	-28060	-4682
Revenue from Oil Production (Million USD)	6554	5243
NPV (Million USD)	-24552	-621
Dimensions		
DWT	150000	140000
Hull Length (m)	260	265
Hull Width (m)	46	48
Hull depth (m)	26	24

4.12.3 Okha and Pyrenees Venture FPSO

Figure 4.62 compares Okha FPSO with riser turret mooring to Pyrenees Venture with internal turret with cost and dimensions as shown in Table 4.28. Both are having converted hulls but Pyrenees Venture is on lease while Okha is owned. Even though both these FPSOs are having same dimensions and nearly same DWT, the initial cost varies by 25%, Okha costing more than Pyrenees venture as Okha is owned and having riser turret mooring.

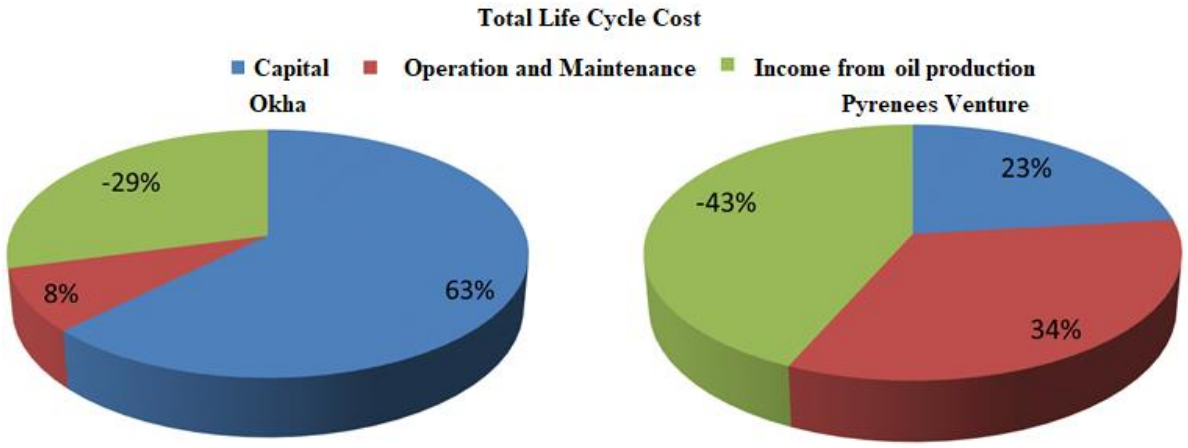

Figure 4.62: Cost Proportions of Okha and Pyrenees Venture

The maintenance cost is higher for Pyrenees venture with internal turret mooring when compared to Okha. NPV of Okha FPSO is -2947 million USD, while that of Pyrenees Venture is -2069 million USD. The NPV of Pyrenees Venture is more than that of Okha even though it is leased, having internal turret mooring and higher maintenance and operation cost.

Table 4.28: Cost, Dimensions and DWT of Okha and Pyrenees Venture

FPSO	**Okha**	**Pyrenees Venture**
Cost		
Capital Cost (Million USD)	-4214	-3359
Operation and Maintenance Cost (Million USD)	-556	-4856
Revenue from Oil Production (Million USD)	1966	6292
NPV (Million USD)	-2947	-2069
Dimensions		
DWT	158000	143690
Hull Length (m)	274	274
Hull Width (m)	48	48
Hull depth (m)	23	23

4.12.4 Perisai Kamelia and Glas Dowr FPSO

Figure 4.63 compares Perisai Kamelia with external turret mooring and converted hull to Glas Dowr FPSO with internal turret mooring and newly built hull with details shown in Table 4.29. The initial cost and operation and maintenance cost of Perisai Kamelia FPSO is higher when compared to Glas Dowr FPSO. Even after having newly built hull, Glas Dowr FPSO have NPV more than that of Perisai Kamelia proving to be the better option.

Hence among the FPSOs compared, internal turret moored FPSOs are found to be having higher NPV. Internal turret moored FPSOs are found to be profitable in the long run even after having newly built hull in some cases and in some cases, being leased.

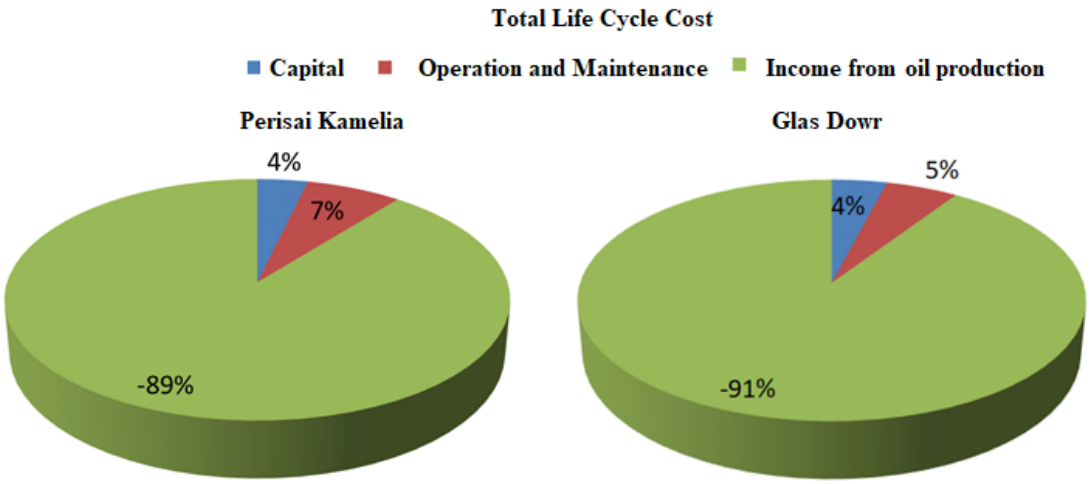

Figure 4.63: Cost Proportions of Perisai Kamelia and Glas Dowr

Table 4.29: Cost, Dimensions and DWT of Perisai Kamelia and Glas Dowr

FPSO	**Perisai Kamelia**	**Glas Dowr**
Cost		
Capital Cost (Million USD)	-272	-175
Operation and Maintenance Cost (Million USD)	-518	-230
Revenue from Oil Production (Million USD)	6554	3933
NPV (Million USD)	5150	3151
Dimensions		
DWT	127540	105000
Hull Length (m)	264	242
Hull Width (m)	41	42
Hull depth (m)	22	21

4.13 Cost and Motion Performance of FPSOs

Excessive motion of FPSOs can lead to production down time and thus result in loss of profit from the project. Hence motion and cost of the FPSOs are interlinked to such an extent that, a basic dynamic response study is required while choosing the cost effective FPSO options suitable to the oil field. Most of the cost related decisions are taken without considering the performance of the FPSO. As seen from section 4.12, even though the initial investments are higher for FPSOs with newly built hull and turret mooring system, their net present values are higher than their counter parts with converted hull and other type of turret/spread moorings.

Turret moored FPSOs are preferred mostly in environment with extreme weather conditions due to their weathervaning capabilities and spread moored FPSOs are preferred in calm weather condition due to their comparatively lower CAPEX. The main reason behind the same is established through the present study. It was shown in section 4.5.1 that the horizontal motions are decreasing for higher wave heights in the presence of wind and current when turret moored FPSOs are used and the same is increasing when spread moored FPSOs are used. Also, from the life-cycle cost analysis, it was seen that the average life-cycle cost is minimum for spread moored FPSOs. Whereas, the NPV of these spread moored FPSOs are lower than some of the external turret moored and internal turret moored FPSOs as seen in Figure 4.50 and Figure 4.51. Even though, the capital cost is minimum, when comparing FPSOs with similar dimensions and DWT, spread moored FPSOs with converted hull are shown to have higher OPEX as seen in Figure 4.50 and Figure 4.51 resulting in much lower NPV than the turret moored FPSO with newly built hull. This may be due to the use of converted hulls which are not specifically designed for the metocean conditions. This emphasizes the need for a site specific dynamic motion response study of the converted hull to be used to minimise the future operational down time and cost. As mentioned before, most of the oil companies use converted tankers for small projects, even then, the use of appropriate tanker can lead to huge profit in terms of its life-cycle cash flows.

Also, during the motion response study, 100- year return period should be used because, when the structure is not designed for 100-year condition, they may induce much greater vessel motion than the 1 year return extreme storm condition, causing operation shut downs and structural integrity problems. The RAOs generated and shown in Figure 4.44 and Figure 4.45 can be used as reference while choosing similar configured FPSOs for Malaysian and Australian oil fields as they are generated by subjecting FPSOs to extreme weather condition for 100 years. For FPSOs with same dimension as operating FPSOs in Malaysia and Australia, downtime cost due to green water events in the presence of wind generated sea is approximately zero. Since NWA is prone to extreme cyclonic conditions, a future study can include site specific swells as well.

From LCCA, the riser turret moored FPSOs are the costliest, followed by internal turret moored FPSOs for both 10-year and 25-year life-cycle periods, based on the available FPSO cost data from different reliable sources. The least expensive option for 10-year life-cycle period is spread moored FPSO, while for 25-years, it is external turret moored FPSO. Among the FPSOs compared in section 4.12, internal turret moored FPSOs are found to be having higher NPV. Internal turret moored FPSOs are found to be profitable in the long run even after having newly built hull in some cases and in some cases being leased.

The range of other significant parameters to be adopted to minimise the vessel motions are mentioned from section 4.5.2 ~ section 4.5.7. The parametric charts developed for motion response variation of FPSOs and NPV profiles for FPSOs can be used as benchmarks for future FPSO projects, with similar configuration and dimension, in changing market condition and oil price.

4.14 Chapter Summary

In this chapter, the motion RAOs in 6 DOF obtained using software simulation based on 3D potential theory were compared with experimental results to verify the modelling and analysis procedure adopted and to calibrate the simulation model for parametric study. Verification was done for both coupled and uncoupled analysis procedures. The parametric study results were presented identifying the range of mooring line length, mooring line azimuth angle, spread mooring fairlead location, hull length to beam ratio and hull loading condition at which the FPSO motion is minimum. Influence of metocean conditions and water depth on FPSO motions were also presented. Motion RAOs for operating FPSOs in Malaysia and Australia subjected to 100-year extreme weather conditions were also presented. Downtime due to green water and subsequent downtime cost is evaluated. Subsequently, the life cycle costs and NPVs of the FPSOs in Australian and Malaysian waters with different mooring systems and hull conditions were discussed along with the cost proportions due to each life cycle phase. Finally, a discussion has been made on the factors affecting the selection of FPSO in terms of its cost and motion performance.

CHAPTER 5

CONCLUSIONS AND RECOMMENDATIONS

5.1 Conclusions

The simulation procedure adopted is capable to predict the wave frequency motion responses with reasonable accuracy as shown in section 5.1.1 and the relative motions found by the dynamic analysis of FPSOs leads to the calculation of subsequent downtime cost due to green water events in the presence of wind generated sea as given in section 5.1.4. These downtime cost are used as an input to the life-cycle cost analysis of FPSOs along with other cost data, capital cost, operation and maintenance and income generated from oil production collected from industry personnel, asset reports, offshore magazine and industry news. Section 4.13 discusses the cost and motion results obtained through this research. This is a unique attempt to bring the cost and motion response of FPSO under one umbrella enabling the design engineers to make logical decisions supported by research data while choosing initial configuration of FPSO for a particular oil field under specific metocean conditions.

This is enabled by conducting extensive parametric studies covering metocean conditions, hull parameters and mooring line parameters for spread moored and turret moored FPSOs. The parametric charts help in understanding the trend and variation in motion amplitude in 6 DOF with the chosen parameters. Parametric study was conducted using experimental test, uncoupled and coupled dynamic analysis using SESAM suit of programs. The gaps in previous FPSO parametric studies are identified in Table 2.2, critical literature review and the present study fills the gap in FPSO motion parametric studies as shown below in section 5.1.2 and 5.1.3.

The life-cycle cost and NPV of FPSOs for 10-year and 25-year life period are calculated and the cost comparison for FPSOs with similar capacities fills the gap in

knowledge by revealing the best economical FPSO option and associated mooring system for the chosen life cycle periods in section 5.1.5. Comparison was made between FPSOs with newly built/converted hull and spread/ET/IT/RTM mooring system.

Thus section 5.1.1 – 5.1.5 concludes the research in alignment with the five research objectives given earlier in section 1.7. The problems discussed earlier in section 1.6 pointed towards reducing the 6 FPSO motions and life-cycle costs to achieve increased operational time and maximum productivity. In the iterative FPSO design procedure, the initial step is the sizing of an FPSO vessel to define a hull geometry and mooring system and the initial configuration is chosen such that the motion criteria are under limit when it comes to vessel displacement and air gap to avoid green water phenomenon. The research contributes heavily to the selection of FPSO configuration with the motion performance studied for similar configured FPSOs operating in Malaysia and Australia, parametric charts developed and life-cycle cost calculated. The results of the research could help in the selection of appropriate initial hull geometry and mooring system so that the burden of iteration and modelling procedure could be reduced. The life-cycle cost aspects of FPSO will help take logical cost decisions in the early phase of FPSO project, bringing managerial aspect to the engineering work and reduce monetary wastage later in the life-cycle of FPSO ensuring maximum productivity and performance.

5.1.1 Adequacy of simulation model and simulation procedure adopted to predict wave frequency motion responses

Software simulation model is developed for uncoupled analysis and from the comparisons discussed in Chapter 4, it can be concluded that the software simulation procedure for the uncoupled frequency domain analysis has produced response results agreeing closely with the trend of experimental results. Also, the magnitudes of the results have been found to be having very low RMSD value, maximum being 0.16 in

surge compared with experimental results. Hence, this simulation procedure can be very well adopted for the parametric study where mooring line details are not key.

Also, software simulation model is developed for coupled analysis, when mooring lines are significant to study the variation in motion response of FPSO. Coupled software simulation procedure has been validated against the experimental tests conducted by Kim et al [42] at the OTRC wave basin. The developed simulation model could predict the natural frequencies of the FPSO with less than 5% error. The motion responses were found to have acceptable accuracy with less than 25% difference with the experimental results produced by Kim et al [42].

5.1.2 Suitability of spread moored and turret moored FPSOs in extreme weather conditions

To assess the suitability of turret moored and spread moored FPSO in extreme weather, wave height parametric study was conducted with and without the presence of wind and current. Heave, Roll and pitch motions remain relatively similar for both spread mooring and turret mooring configurations with or without wind and current. It was also observed that the rate of increase in heave motion is directly proportional to wave period. The higher the wave period, the higher will be the heave motion. This can contribute to higher vertical combined motion and subsequent relative motion as seen in section 4.7.1, Table 4.12 ~Figure 4.22. So, at higher wave heights, FPSOs are prone to risk from green water and thus downtime.

In the absence of wind and current, all the six motions for turret moored and spread moored FPSOs increase. In reality, wind and current exists and the amplitude of horizontal plane motions of turret moored FPSO are relatively higher when compared to that of spread moored FPSO in the presence of wind, wave and current due to the drifting force. Sway and yaw motions are significantly reduced when spread moored

system is used. But, the horizontal FPSO motions for turret moored FPSO decreases as wave height increases and becomes comparable to those of spread moored FPSO; however, if we use a spread moored configuration in adverse climates, the motions escalate resulting in mooring line damage. This is the main reason for preferring turret moored FPSO over spread moored FPSO in adverse climates and this very behaviour shows the weathervaning nature of the turret moored FPSOs in extreme weather conditions. The metocean parametric charts developed could be used to obtain motion response amplitudes of similar configured FPSOs in varying wave heights and make decision while choosing mooring system based on metocean conditions.

5.1.3 Effect of water depth, mooring line and hull parameters on FPSO motions

The water depth parametric study covers water depths of domestic oil zones in Malaysia (62 m – Erb West, 70 m – PMO, 75 m – Baram Delta) [163] and in Australia (80 m-Montara) [2]. In surge, heave and pitch the mean RAO increases as the water depth increases from 62 m to 100m (as per model tests). For FPSOs to be used in shallow waters, care should be taken while designing them, as in shallow waters up to 100 m, heave and pitch motion increases resulting in high combined vertical motion of FPSO which can make the FPSO susceptible to green water and subsequent downtime.

At high wave periods (low frequency waves), the surge and heave motions are minimum at mooring line azimuth angle 15º and 45º. Motions are always low when the mooring line azimuth angle is 15º. To prevent high amplitude heave motion, it is best to avoid mooring line azimuth angle 30º for FPSOs with similar configuration. The six degrees of freedom FPSO motions decline with an increase in the ratio of hull length to mooring line length. It is best to keep the mooring line length minimum to minimise the FPSO motions with appropriate pretension for similarly configured FPSOs. The FPSO motions are minimum when the mooring line fairleads are located at 12% to 21% of LOA from aft and fore. The FPSO motions increase heavily when the spread mooring

fairleads are kept closer to mid ship. Pitch motions are least sensitive to mooring line parameters.

For Malaysian seas, the most probable peak period is usually in the range of 6 s to 7 s [132]. It can be seen from Figure 4.40 ~Figure 4.41, for FPSOs having beam to length ratio in the same range as the Malaysian and Australian FPSOs, surge, sway and yaw motion remains almost the same for peak period less than 7 s and heave and pitch reduces as hull length to beam ratio increases. This means that for the Malaysian FPSOs, for hull length to beam ratio of 6.094, the combined vertical motion will be less for the Malaysian metocean conditions and thus risk from green water is less. The peak period of wave is higher in Australian seas and the Australian sea is prone to extreme cyclones with longer wave periods [4] as seen in section 4.7.1. Again, at higher wave periods, the heave, pitch and roll motion decreases with increase in hull length to beam ratio. Thus, risk from green water will be less when hull length to beam ratio of 6.094 is used. However, surge and sway motion increases in higher wave periods with increase in hull length to beam ratio, which again could be handled using weathervaning FPSOs. Surge, sway, heave and pitch motion decreases as vessel loading increases and roll and yaw motion increases with vessel loading for the given metocean data and vessel dimensions. Increase in roll could be controlled by providing additional roll damping. Even though, the vertical motions will be minimum at full loaded condition, care should be taken while designing to avoid green water effects and operational downtime at higher wave heights as the FPSO will have the least freeboard and maximum draft in fully loaded condition.

5.1.4 Downtime cost due to green water effects for site specific conditions of Malaysia and Australia

Downtime cost due to green water effects under location specific wind generated sea condition is evaluated to be zero for FPSOs with dimensions shown in Table 3.6 using

location specific annual wave scatter diagram approach. Relative motions are found for FPSOs with similar dimensions as operating FPSOs in Malaysia and Australia as given in Table 3.6 and it was found that freeboard for those FPSOs in maximum draft is higher than the relative motions in section 4.7. However, for 100-year extreme operating conditions, FPSOs are highly susceptible to green water in Australian sea, while FPSOs in Malaysian seas have only low susceptibility. The downtime cost is calculated to be included for the 10-year and 25-year life-cycle cost study of FPSOs in Table 3.6 and the 100-year extreme conditions might not occur during those periods or probability of those events are very low. Hence a future work is recommended to study downtime due to green water under location specific swells due to cyclones for annual conditions in Australian seas.

5.1.5 Cost effective FPSO configurations for 10-year and 25-year use in Malaysia and Australia

Comparing the total life-cycle cost, riser turret moored FPSOs are the costliest, followed by internal turret moored FPSOs for both 10-year and 25-year life-cycle periods, based on the available FPSO cost data from different reliable sources. The least expensive option for 10-year life-cycle period is spread moored FPSO, while for 25-years, it is external turret moored FPSO. Turret moored FPSOs are shown to have higher NPV including and excluding revenue from oil price among the FPSOs used for LCCA and the main cost driving factor for NPV is identified to be capital, operation and maintenance cost.

Among the FPSOs compared in section 4.12, internal turret moored FPSOs are found to be having higher NPV. Internal turret moored FPSOs are found to be profitable in the long run even after having newly built hull in some cases and in some cases, being leased.

Also, as the discount rate increases, the net present value of the asset decreases as the risk associated with the investment increases. And, it can be seen from Figure 4.56 ~ Figure 4.59 that, NPV decreases as capital cost increases. The NPV profile reflects the net present worth of these FPSOs, at a varying market situation and can be used as a reference in the initial estimate of similar configured FPSOs.

Hence considering both motion performance and cost of FPSO configurations, spread moored FPSOs are preferred option for short term use in benign ocean environment due to less life cycle cost as seen in section 5.1.5 and reduced motion amplitude as mentioned in section 5.1.2, whereas turret moored options are effective in the long run in extreme metocean conditions for higher NPV, less total life-cycle cost for 25 years as mentioned in section 5.1.5 and weathervaning nature as seen in section 5.1.2.

5.2 Recommendation for Future Work

This research was aimed to study the motion responses and cost of FPSO to enable better selection of FPSO configuration to have increased productivity and better performance. The results of this study are region specific to Malaysia and Australian sea for chosen FPSO dimensions. The following studies should help in the ultimate endeavor for a better understanding of this topic:

- Sea keeping performance for FPSOs under multi directional waves and higher order waves could be studied varying the structural and metocean parameters including both mooring and risers in the analysis.
- Downtime cost for FPSOs in Australia could be calculated due to green water incidents when FPSO is subjected to site specific swells due to extreme cyclonic conditions.

- Obtaining original ship lines from FPSO operators are difficult due to company policies. However, the simulation procedure adopted could be used to conduct dynamic analysis, downtime calculation and LCCA of any FPSOs and original ship lines can be used for the same upon availability in future.
- The need for LCCA while choosing mooring system is recommended to be included in the standards for design of floating platforms while choosing hull and mooring system.

REFERENCES

[1] J. K. Paik and K. T Anil., *Ship Shaped offshore Installations Design , Building and Operation,* Cambridge University Press, 2007.

[2] C. Barton, H. Hambling, E. K. Albaugh, B. Mahlstedt and D. Davis. (2017, August). *2017 Worldwide Survey of Floating Production, Storage and Offloading (FPSO) Units*. Offshore Magazine [Online]. Available: www.offshore-mag.com/maps-posters.html

[3] T. Moan, J. Amdahl, X. Wang and J. Spencer, "Risk Assessment of FPSOs, with Emphasis on Collision, " *ABS Tech. Paper,* pp. 200 – 229, 2002.

[4] J. Xia (2013, July). *Proper FPSO hull and mooring designs can improve production uptime*. Offshore Magazine [Online]. Available: https://www.offshore-mag.com/articles/print/volume-73/issue-6/engineering-construction-installation/proper-fpso-hull-and-mooring-designs.

[5] L. T. England, A. S. Duggal and L. A. Queen, "A Comparison Between Turret and Spread Moored FPSO for Deep Water Field Developments," *Deep Offshore Technology* , pp. 1-23, 2001.

[6] D. M. Mattos and C. F. G. Mastrangelo , "PORTRAIT OF FPSO USE OFFSHORE BRAZIL, " *FPSO Workshop Proc.,* Houston, TX, pp. 54-63, 2000.

[7] "Rationalisation of FPSO design issues, " Noble Denton Europe Ltd., London, Offshore Technology Report 2000/097, 2001.

[8] B. Buchner, "Green Water From the Side of an Weathervaning FPSO," *Proc. of OMAE99,* Newfoundland, Canada pp. 1–11, 1999.

[9] *SESAM USER MANUAL, DeepC Theory*, Marintek and DNV, 2005.

[10] J. A. Pinkster and G. F. M. Remery, "The Role of Model Tests in the Design of Single Point Mooring Terminals ," *Offshore Technology Conference*, Texas, OTC 2212, pp 679 - 703, 1975.

[11] J. E. W. Wichers, "A Simulation Model for a Single Point Moored Tanker," Ph.D. dissertation, Tech. Univ. Delft, 1988.

[12] D. L. Garrett, “Coupled analysis of floating production systems,” *Ocean Eng.*, vol. 32, no. 7, pp. 802–816, 2005.

[13] G. A. Gratsos, H. N. Psaraftis, and P. Zachariadis, “Life cycle cost of maintaining the effectiveness of a ship’s structure and environmental impact of ship design parameters: An update,” *Int. Conf. Des. Oper. Bulk Carriers*, pp. 169–182, 2009.

[14] E. P. D. Mansard and B. D. Pratte, "Moored Ship Response in Irregular Waves," *Coastal engineering*, pp. 2621–2640, 1982.

[15] S. K. Chakrabarti, “Physical model testing of floating offshore structures,” *Proc. MTS Dyn. Position. Conf.*, 1998.

[16] C. Fournier and D. Anglin, “The Use of Moored Ship Response Modelling Coupled With Pianc Vessel Motion Criteria for the Estimate of Port Downtime the Case of Complejo Portuario De Mejillones , Chile,” *Canadian Coastal Conf.*, pp. 1–14, 2003.

[17] B. V. Korvin-Kroukovsky, "Investigation of ship motions in regular waves," *Transactions of the society of Naval Architects and Marine Engineers*, vol. 63, pp. 386-435, 1955.

[18] N. Salvesen, E. Tuck, and O. Faltinsen, “Ship motions and sea loads,” *Trans. SNAME*, vol. 78, pp. 250–287, 1970.

[19] J. N. Newman, "The theory of ship motions," *Advances in Applied Mechanics*, vol. 18, pp. 221- 283, p. 1978.

[20] P. D. Sclavounos, "The diffraction of free-surface waves by a slender ship," *Journal of Ship Research*, vol. 1, no. 28, pp. 29-47, 1984.

[21] Chang, M.S, "Computations of three-dimensional ship-motions with forward speed", *Proc. 2nd Int. Conf. on Numerical Ship Hydrodynamics*, Berkeley, USA, pp. 124-135, 1977.

[22] R. B. Inglis and W. G. Price, "A three dimensional ship motion theory- comparison between theoretical predictions and experiment data of the hydrodynamic coefficients with forward speed," *Transactions of the Royal Institution of Naval Architects*, vol. 124, 1982.

[23] R. B. Inglis and W. G. Price, "A three dimensional ship motion theory: Calculation of wave loading and responses with forward speed," *Transactions of the Royal Institution of Naval Architects*, vol. 124, pp. 183-192, 1982.

[24] G. X. Wu and R. E. Taylor, R.E, "The numerical solution of the motions of a ship advancing in waves," *Proc. 5th Int. Conf. on Numerical Ship Hydrodynamics*, Hiroshima, Japan, pp. 529-538, 1989.

[25] X. B. Chen, L. Diebold and Y. Doutreleau, "New green-function method to predict wave-induced ship motions and loads," *Proc. 23rd Symp. on Naval Hydrodynamcis*, Val de Reuil, France, pp. 66-81, 2000.

[26] C. W. Dawson, "A practical computer method for solving ship-wave problems," *Proc. 2nd Int. Conf. on Numerical Ship Hydrodynamics*, Berkeley, USA, pp. 124-135, 1977.

[27] Y. T. Fan and P. A. Wilson, "Time-domain non-linear strip theory for ship motions," *Int. Journal of Maritime Eng.*, pp. 33-47, 2004.

[28] J. H. Vugts, "The hydrodynamic coefficients for swaying, heaving and rolling cylinders in a free surface," *Int. Shipbuild. Prog.*, vol. 15, pp. 251–276, 1968.

[29] J. N. Newman, "The Exciting Forces on Fixed Bodies in Waves," *J. Sh. Res. Soc. Nav. Archit. Mar. Eng.*, vol. 6, pp. 1–10, 1962.

[30] J. Journée, "Quick strip theory calculations in ship design," *PRADS'92 Conf. Pract. Des. Ships*, vol. I, pp. 5–12, 1992.

[31] S. N. Das and S. K. Das, "Determination of coupled sway, roll, and yaw motions of a floating body in regular waves," *Int. J. Math. Math. Sci.*, no. 41, pp. 2181–2197, 2004.

[32] K. P. W. Hem Lata and Thiagarajan, "Comparison of added mass coefficients for a floating tanker evaluated by conformal mapping and boundary element methods," *Mech. Eng.*, vol. 1, pp. 1388–1391, 2007.

[33] T. Momoki, T. Kneko and T. Fukasawa, "On the Calculation Method of Surface Pressure Distribution of a Container Ship in Wave," *Proc. Twenty-second ISOPE Conference*, Greece, pp 961 - 967, 2012.

[34] T. Jiang and G. Lloyd, "Motion Prediction of a Single- Point Moored Tanker Subjected

to Current, Wind and Waves," *Journal of Offshore Mechanics and Arctic Engineering*, vol. 112, pp. 83-90, 1990.

[35] G. Feng, X. Jiang, H. Ren, and Q. Zhang, "Motion Response Analysis of Multi-point Moored FPSO," *Proc. 25th ISOPE*, Hawaii, USA, pp. 1666–1674, 2015.

[36] J. M. Heurtier, P. Buhan, E. Fontane, C. Cunff, F. Biolley and C. Berhault, "Coupled Dynamic Response of Moored FPSO with Risers," *Proc. of the Eleventh ISOPE Conference*, Norway, Vol I, pp. 319 – 326, 2001.

[37] J. E. W. Wichers, H. J. Voogt, H. W. Roelofs and P. C. M Driessen,. DeepStar-CTR 4401-Benchmark Model Test, Technical Report No. 16417-1-OB, MARIN, Netherlands, 2001.

[38] J. E. W. Wichers and P. Devlin, "Effect of Coupling of Mooring Lines and Risers on the Design Values for a Turret Moored FPSO in Deep Water of the Gulf of Mexico," *Proc. 11th Int. Offshore Polar Eng. Conf.*, Stavanger, Norway, pp. 480–487, 2001.

[39] Y. Lou and S. Baudic, "Predicting FPSO responses using model tests and numerical analysis," *Proc. of the Thirteenth ISOPE*, USA, pp. 167-174, 2003.

[40] Y. M. Low and R. S. Langley, "Time and frequency domain coupled analysis of deepwater floating production systems," *Appl. Ocean Res.*, vol. 28, no. 6, pp. 371–385, 2006.

[41] A. Tahar and M. H. Kim, "Hull/mooring/riser coupled dynamic analysis and sensitivity study of a tanker-based FPSO," *Appl. Ocean Res.*, vol. 25, no. 6, pp. 367–382, 2003.

[42] M. H. Kim, B. J. Koo, R. M. Mercier and E. G. Ward, "Vessel/mooring/riser coupled dynamic analysis of a turret-moored FPSO compared with OTRC experiment," *Ocean Eng.*, vol. 32, no. 14–15, pp. 1780–1802, 2005.

[43] A. Priyanto, Erwandi and Samudro, "Surge Forces of a FPSO at Lee Side of Submerged Plate in Regular Waves," *2nd Reg. Conf. on Vehicle Eng. and Tech.*, Kuala Lumpur, pp. 1 - 6, 2008.

[44] C. L. Siow, J. Koto, H. Yasukawa, A. Matsuda, D. Terada, C. G. Soares and M. Z. M Samad, "Experiment Study on Hydrodynamics Characteristic of Rounded- Shape FPSO," *The 1st Conf.on Ocean, Mechanical and Aerospace -Science and Eng.*, pp. 1–

6, 2014.

[45] C. L. Siow, J. Koto, H. Yasukawa, A. Matsudad, D. Teradad, C. G.Soarese, A. Incecikf, M. A. G. Pauzi, "Full paper Mooring Effect on Wave Frequency Response of Round Shape FPSO," Jurnal Teknologi, vol. 5, no. 74, pp. 59–68, 2015.

[46] A. O. Vázquez-hernández, G. B. Ellwanger, and L. V. S. Sagrilo, "Long-term response analysis of FPSO mooring systems," *Appl. Ocean Res.*, vol. 33, pp. 375–383, 2011.

[47] Y. Rho, K. Kim, C. Jo, and D. Kim, "Static and dynamic mooring analysis - Stability of floating production storage and offloading (FPSO) risers for extreme environmental conditions," *Inter J Nav Arch. Oc Engng*, vol. 5, pp. 179–187, 2013.

[48] E. Fontaine, P. Orsero, A. Ledoux, R. Nerzic, M. Prevosto, and V. Quiniou, "Reliability analysis and Response Based Design of a moored FPSO in West Africa," *Struct. Saf.*, vol. 41, pp. 82–96, 2013.

[49] Q. W. Ma, S. Yan, D. Greaves, T. Mai, and A. Raby, "Numerical and experimental studies of Interaction between FPSO and focusing waves," *Proc. of the 25th ISOPE*, Hawaii, USA, 2015.

[50] J. Chen, Y. Sun, and P. Zhang, "Dynamic Response Analysis of FPSO Based on SESAM," *Adv. Mater. Res.*, vol. 694–697, pp. 267–270, 2013.

[51] C. Ji, Y. Cheng, Q. Yan, and G. Wang, "Fully coupled dynamic analysis of a FPSO and its MWA system with mooring lines and risers," *Appl. Ocean Res.*, vol. 58, pp. 71–82, 2016.

[52] C. Kang, C. Lee, S. Jun, and Y. Oh, "Fatigue Analysis of Spread Mooring Line," *International Journal of Geological and Environmental Eng.*, vol. 10, no. 5, pp. 504–510, 2016.

[53] J. T. Lopez, L. Tao, L. Xiao, and Z. Hu, "Experimental study on the hydrodynamic behaviour of an FPSO in a deepwater region of the Gulf of Mexico," *Ocean Eng.*, vol. 129, pp. 549–566, 2017.

[54] S. Hong, J. Lew, D. Jung, H. Kim, D. Lee, and J. Seo, "A study on the impact load acting on an FPSO bow by steep waves," *Int. J. Nav. Archit. Ocean Eng.*, vol. 9, pp. 1–10, 2017.

[55] DNV, “DeepC Coupled Analysis Tool. A white Paper. Rev 3,” 2004.

[56] *Global Performance Analysis of Deepwater Floating Structures*, Recommended Practice DNV-RP-F205, October, 2010.

[57] M. Caire, C. E. S. de Souza, and J. P. R. Cortina, “The influence of wind-wave energy spreading on the riser system response of a spread-moored FPSO,” *Mar. Syst. Ocean Technol.*, no.10, pp. 26-37, 2015.

[58] Y. M. Low and R. S. Langley, “A hybrid time/frequency domain approach for efficient coupled analysis of vessel/mooring/riser dynamics,” *Ocean Eng.*, vol. 35, no. 5–6, pp. 433–446, 2008.

[59] *Dynamic Loading Approach for Floating Production , Storage and Offloading (FPSO) Installations*, ABS, May 2010.

[60] O. M. Faltinsen, *Sea loads on ships and offshore structures*, Cambridge University press, vol. 1. pp. 223–228, 1990.

[61] J. Xia, “FPSO Design to Minimise Operational Downtime due to Adverse Metocean Conditions off North West Australia,” *Deep Offshore Technol.*, pp. 1–15, 2012.

[62] S. K. Chakrabarti , *Offshore Structure Modeling*, Advanced Series on Ocean Engineering Vol.9, World Scientific Publishing Co. Ptc. Ltd, Singapore, 1994.

[63] R. Mercier, “FPSO Responses in Gulf of Mexico Environments,” OTRC Report, 2007.

[64] A. S. Duggal, C. N. Heyl, and P. F. Poranski, “Terra Nova FPSO: Integration of model tests and global analysis,” JMR03, pp. 1-6, 2000.

[65] S. K. Chakrabarti, *Hydrodynamics of Offshore Structures* , Computational Mechanics Publications, Heidelberg, 1987.

[66] R. L. Wiegel and J. W. Johnson, “Elements of Wave Theory,” *Coast. Eng.*, no. 1893, pp. 5–21, 1950.

[67] Y.M. E. Abbas, “Studies on the non-linear interactions associated with moored semi-submersible offshore platforms,” Ph.D Thesis, Universiti Teknologi PETRONAS, 2011.

[68] R. S. Sharizal Amurol, Kevin Ewans, “Measured Wave Spectra Offshore Sabah &

Sarawak, Malaysia," in *Offshore Technology Conference Asia held in Kuala Lumpur, Malaysia*, 2014, no. March, pp. 1–13.

[69] J. Morison, "The force exerted by surface waves on piles," University of California, Dept. of Engineering, Fluid Mechanics Laboratory, 1949.

[70] *SESAM USER MANUAL, Wadam*, DNV, 2010.

[71] "Review of model testing requirements for FPSO's, " BMT Fluid Mechanics Ltd., United Kingdom, Offshore Technology Report 2000/123, 2001.

[72] R.V. Whitman, "Evaluating Risk in Geotechnical Engineering", *ASCE Convention and Exposition*, 1981

[73] T. Cepowski, "The modeling of seakeeping qualities of Floating Production , Storage and Offloading (FPSO) sea-going ships in preliminary design stage," *Polish Maritime Research*, vol. 17, no. 4, pp. 3–12, 2010.

[74] X. Li, J. Yang, and L. Xiao, "Motion Analysis on a Large FPSO in Shallow Water," *Proc. of the 13th ISOPE*, Hawaii, USA, pp. 235–239, 2003.

[75] S.Q. Wang, S. Y. Li and X. H. Chen, "Dynamical Analysis of a Soft Yoke Moored FPSO in Shallow Waters," *Proc. of the sixth Int. conf. on Asian and Pacific Coasts*, Hong Kong, China. pp. 956 - 963, 2011.

[76] C. G. Soares, N. Fonseca and R. Pascoal, "Experimental and Numerical Study of the Motions of a Turret Moored FPSO in Waves, *Journal of Offshore Mechanics and Arctic Engineering*, Vol. 127,pp. 197 - 204, 2005.

[77] J. Munipalli and K. Thiagarajan, "Effect of Wave Steepness on Yaw Motions of a Weathervaning Floating Platform," *16th Australasian Fluid Mechanics Conference*, Gold Coast, Australia, pp. 1007–1011, 2007.

[78] T. R. Kannah and R. Natarajan, "Experimental Study on the Hydrodynamics of a Floating, Production, Storage, and Offloading System," *Journal of waterway, port, coastal and ocean engineering*, no.132, pp. 66-70, 2006.

[79] T. R. Kannah and R. Natarajan, "Effect of Turret Location on the Dynamic Behaviour of an Internal Turret Moored FPSO System," *Journal of Naval Architecture and Marine*

Engineering, pp. 23 - 27, 2006.

[80] A. Yadav, S. Varghese and K. P. Thiagarajan, "Parametric Study of Yaw Instability of a Weathervaning Platform," *16th Australasian Fluid Mechanics Conference*, Gold Coast, Australia, pp. 1012 - 1015, 2007.

[81] N. Baghernezhad, P. Edalat, and M. Etemaddar, "Hull Performance Assessment and Comparison of Ship-Shaped and Cylindrical FPSOs With Regards To : Stability , Sea-Keeping , Mooring and Riser Loads In Shallow Water," Int. Journal of Maritime Technology, Vol. 8, pp. 1 - 13, 2017.

[82] M. O. Ahmed and A. Musaad, "Effects of mooring lines and water depth parameters on the dynamic motion of a turret moored FPSO, " *Engineering Challenges for Sustainable Future*, 2016.

[83] K. C. Ewans, L. Vanderschuren, P. S. Tromans, "FPSO Conference-Estimating Wind-Sea and Swell for FPSO Operability," *Journal of Offshore Mechanics and Arctic Eng.*, no. 128,pp. 314-321, 2006.

[84] A. Hassan, M. Downie, and A. Incecik, "Wave drift forces and responces in deep water and extreme environmental conditions," *Proc. HYDRALAB III Jt. User Meet.*, pp. 3–6, February 2010.

[85] C. T. Stansberg, E. M. Hermundstad, J. R. Hoff, R. Baarholm, "Wave Drift Forces in Current," *Proc. OMAE*, France, 2013.

[86] M. J. Teles, M. Benoit, A. A. P. Silva, "Modelling Combined Wave-Current Flows Using a RANS CFD Solver with Emphasis on the Effect of the Turbulent Closure Model," *Advances in Hydroinformatics* , Springer Hydrogeology, Singapore, pp. 473-485, 2014.

[87] "Analysis of green water susceptibility of FPSO/FSU's on the UKCS, " BOMEL Ltd., United Kingdom, Offshore Technology Report 2001/005, 2001.

[88] B. Buchner, "The Impact of Green Water on FPSO Design," *Offshore Technology Conference*, Texas, USA, pp. 45–57, 1995.

[89] B. Buchner, *Green Water on Ship-type Offshore Structures*, Grafisch Bedrijf Ponsen & Looijen by, Wageningen, The Netherlands, 2002.

[90] K. B. Nielsen, “Numerical Prediction of Green Water Loads on Ships, ” Ph.D Thesis, Technical University of Denmark , Lyngby, Denmark, 2003.

[91] E. Ballard, N. Barltrop, E. Falkenberg, S. Fyfe, C. G. Soares, B. Iwanowski, T. Kleefsman, “ Summary Report on Desing Guidance and Assessment Methodologies for Wave Slam and Green Water Impact,” Safe Flow, Rep. no. 15874-1-OE, February, 2004.

[92] K. M. T. Kleefsman, G. E. Loots, A. E. P. Veldman, B. Buchner, T. Bunnik and E. Falkenberg, “ The Numerical Simulation of Green Water Loading Including Vessel Motions and the Incoming Wave Field, ” *Proc. of 24th Int.Conf. on Offshore Mechanics and Arctic Engineering,* Halkidiki, Greece, pp. 1 - 12, 2005.

[93] H. Lu, C. Yang, and L. Rainald, “Numerical Studies of Green Water Effect on a Moored FPSO,” *Proc. of the Eighteenth Int.Offshore and Polar Engineering Conf*., Vancouver, Canada, 2008.

[94] N. Tao, W. Yun, L. Bingnan, T. Shentao and Z. Yongkang, “State-of-the-art of green water on FPSO in harsh environment,” *Key Engineering Materials*, 2011.

[95] E. Akandu, A. Incecik, and N. Barltrop, “The Susceptibility of FPSO Vessel to Green Water in Extreme Wave Environment,” *The 1st Conf. on Ocean, Mechanical and Aerospace*, pp. 82–87, 2014.

[96] R. V. Veer and A. Boorsma, “Towards an improved understanding of Green water exceedance at the Bow of an FPSO, ” *35th Int. Conf. on Ocean, Offshore and Arctic Engineering*, Busan, South Korea, Vol 1, 2016.

[97] R. Werter, “Green water along the side of an FPSO,” MSc Thesis, Delft University of Technology, 2016.

[98] X. Zhang, H. Wolgamot, S. Draper, W.Zhao and L. Cheng, “The role of overtopping duration in greenwater loading Xiantao,” *33rd IWWWFB workshop*, Guidel-Plages, France, pp. 1–4, 2018.

[99] B. Buchner and J. L. Garcia, “Design aspects of Green Water Loading on FPSOs ,” *The 22nd Int. Conf. on Offshore Mechanics & Arctic Engineering*, Cancun, Mexico, pp. 1–11, 2003.

[100] R. J. Van Der Wal and G. De Boer, “Downtime Analysis Techniques for Complex Offshore and Dredging Operations,” *Proc. 23rd Int. Conf. on Offshore Mechanics and Arctic Engineering*, Vancouver, Canada, pp. 1–9, 2004.

[101] E. B. Djatmiko, Murdjito and I. Prasetyawan, “Operability analysis of an FPSO on the basis of its slamming and green water,” *The 5th Biennale Conf. on Marine Technology*, Makassar, Indonesia, pp. 1 -16, 2006.

[102] D. C. Corea, A. C. de Oliveira, E. A. Tannuri and S. H. Sphaier, “Comprehensive Downtime Analysis of DP- Assisted Offloading Operation of Spread Moored Platforms in Brazilian Waters,” *Proc. of the 32nd Int. Conf. on Ocean, Offshore and Arctic Eng*., Nantes, France, pp. 1 -8, 2013.

[103] A. Whyte, Life –cycle cost analysis for built assets: LCCA framework, VDM Verlag Dr. Muller, Germany, 2011.

[104] K. V. Oeveran K. V. and M. Wilks, "Life cycle costing qualification document," Rev 3 , pp 1 – 7, 2009.

[105] I. Thalji, J. P. Liyanage and M. Hjollo, "Scalable and Customer – Oriented Life Cycle Costing Model: A Case Study of an Innovative Vertical Axis Wind Turbine Concept (Case – VAWT)," *Proc. Twenty – second ISOPE Conference*, Rhodes, Greece, pp 423-425, 2012.

[106] J. Emblemsvag, Life-cycle costing, John Wiley a sons, USA, ISBN 978-0-4713-5885-5, 2003.

[107] J. Roubal, ‘Product life cycle cost management--necessary tool for industrial companies," The Free Library 01, January 2009.

[108] K. Nam, D. Chang, K. Chang, T. Rhee and I. B. Lee, "Methodology of Lifecycle Cost with Risk Expenditure for Offshore Process at Conceptual Design Stage," *Energy*, No. 36, pp 1554 – 1563, 2011.

[109] L. C. Santos, G. P. Gareia and V. D. Casas, “Methodology to study the life cycle cost of floating offshore wind farms,” *Energy Procedia*, pp 1- 8, 2013.

[110] G. B. Howell, A. S. Duggal, C. Heyl, and O. Ihonde, “Spread Moored or Turret Moored FPSO’s for Deepwater Field Developments,” *Procedings Offshore West Africa*, pp. 1–

21, 2006.

[111] D. Kayrbekova, “Activity-Based Life-Cycle Cost Analysis, ” PhD Thesis, University of Stavanger, Norway, 2011.

[112] H. A. Kurniawati, W. D. Aryawan, A, “Long-term fso/fpso charter rate estimation 1), *KAPAL*, Vol. 13, No.1, pp. 7–12, 2016.

[113] J. M. Cabrera-miranda, P. M. Sakugawa, R. Corona-Tapia, J. K. Paik, “On design criteria for a disconnectable FPSO mooring system associated with expected life- cycle cost,” *Ships Offshore Struct.*, vol. 13, no.4, pp. 432 - 442, 2018.

[114] L. Greene and B. Shaw, “The steps for successful life cycle cost analysis," *Proc. IEEE*, Ch 2881, pp.1209-1216, 1990.

[115] D.J.O. Ferry and R. Flanagan (1991). Life cycle costing – a radical approach, CIRIA report no.122, London, UK.

[116] S. Kirk and A. Dell’Isola, Life cycle costing for design professionals, 2nd ed., McGraw-Hill, 1995.

[117] A. Al Hajj, "Simple cost-significant models for total life-cycle costing in buildings," Ph.D. dissertation, University of Dundee, UK, 1991.

[118] A. Ashworth, "Life Cycle Costing:predicting the unknown," *Building Engineer*, vol. 71, no. 3, pp. 18-20, 1996.

[119] H. Barringer and D. Weber, "Life Cycle Cost Tutorial," *Fifth Int. Conf.on Process Plant Reliability*, Houston, TX, no.3, 1996.

[120] J.K. Hwang, M. I. Roh, and K. Y. Lee, “Detailed design and construction of the hull of a floating, production, storage and off-loading (FPSO) unit,” *Ships Offshore Struct.*, vol. 5, no. 2, pp. 93–104, 2010.

[121] *HR Multi-element wave generation system with AC derives and dynamic wave absorption for Universiti Teknologi PETRONAS user manual* , Wallingford - UK CQR 4187, 2008.

[122] *QTM User Manual*, 2011.

[123] M. O. A. Ali, “Numerical and Experimental Studies on the slow drift motions and the mooring line responses of truss spar platforms, ” Ph.D Thesis, Universiti Teknologi PETRONAS, 2012.

[124] *Laboratory instrumentation and software Wave generation software manual*, HR Wallingford.

[125] H. R. Wallingford Ltd., “FPSO Response in Long and Short Crested Seas,” OTC Report, no.18, 2002.

[126] A. Ruina and R. Pratap, “Center of mass and gravity,” *Introd. to Statics Dyn.*, vol. 1, pp. 78–91, 2010.

[127] MARINET, *Best Practice Manual for Wave Simulation*, 2015.

[128] *Instrumentation and software for physical models*, HR Wallingford.

[129] DNV GL, “SE-23 FPSO Global Strength and Spectral Fatigue Analysis - Workshops,” Kuala Lumpur, 2014.

[130] *SESAM User Manual DeepC*, Marintek and DNV, 2010.

[131] *Structural Design of Offshore Ships*, DNV-OS-C102, 2012.

[132] O. Yaakob, F. E. Hashim, K. M. Omar, A. H. M. Din, and K. K. Kong, “Satellite-based wave data and wave energy resource assessment for South China Sea,” *Renew. Energy*, vol. 88, pp. 359–371, 2016.

[133] Metocean Solutions. (2018). *Hindcast*. [Online]. Available:www.metoceanview.com.

[134] Offshore Magazine. (2013, 22 July). *Offshore Map Atlas E-book*. [Online]. Available:www.offshore-mag.com.

[135] Reserve Bank of Australia. (2018, 24 April). *Measures of Consumer Price Inflation*. [Online]. Available: https://www.rba.gov.au/inflation/measures-cpi.html.

[136] Fusion Media Limited. (2018, May). *10 year Bond Yield*. [Online]. Available: https://au.investing.com/rates-bonds.

[137] Fenebris. (2018, March 31). *Application of Valuation Parameters in Practice*. [Online].

Available: http://www.market-risk-premia.com.

[138] State of Victoria, Australia. (2018, May 2). *Wage Inflationa and Discount Rates*. [Online]. Available: https://www.dtf.vic.gov.au/financial-reporting-policy/wage-inflation-and-discount-rates." .

[139] Bank Negara Malaysia. (2018, May). *Malaysia Inflation Rate*. [Online]. Available: http://www.bnm.gov.my.

[140] *Petroleum and natural gas industries – Life cycle costing – Part 1: Methodology*, DS/EN ISO 15663-1, 2007.

[141] S. Thomas, private communication, March 2017.

[142] H. B. Taib, private communication, March 2017.

[143] Bluewater Holding B.V. (2014, june 30). *Half-year report*. [Online]. Available: http://stamdata.no/documents/NO0010697485_IB_20140829.pdf.

[144] Rigzone. (2016, August 22). *Malaysia's Perisai Gets 6 Months Charter Extension for FPSO Perisai Kamelia*. [Online]. Available: http://www.rigzone.com/news/oil_gas/a/146264/malaysias_perisai_gets_6_months_charter_extension_for_fpso_perisai_kamelia.

[145] Wood Mackenzie, (2016, June). *Enfield Area Key facts*. [Online]. Available: https://www.woodmac.com/store/

[146] Wood Mackenzie, (2015, July). *Cossack-Wanaea-Lambert-Hermes Key facts*. [Online]. Available: https://www.woodmac.com/store/

[147] Wood Mackenzie, (2017, February). *Mutineer Exeter Area Key facts*. [Online]. Available: https://www.woodmac.com/store/

[148] Aurelia Energy N. V. (2012). *Annual report pursuant to Section 13 or 15(d) of the securities Exchange Act of 1934*. [Online]. Available: https://www.sec.gov/Archives/edgar/data/1172374/000110465906021216/a06-8054_120f.html.

[149] Petrofac. (2011, January 31). *Petrofac to Lead Development of Berantai Field For Petronas*. [Online]. Available: https://www.petrofac.com/en-gb/media/news/petrofac-

to-lead-development-of-berantai-field-for-petronas/

[150] PETROLIAM NASIONAL BERHAD (PETRONAS). (2012). *Reimagining Energy PE 2011 Annual Report.* [Online]. Available: http://www.petronas.com.my/investor-relations/Documents/annual-report/AnnualReport_FinancialStatement_PE2011.pdf.

[151] Wood Mackenzie, (2016, October). *Kikeh Key facts*. [Online]. Available: https://www.woodmac.com/store/

[152] L. S. Wah and M. M. Chandrashegaran. (2012, June 25). *FORGINGAHEAD Annual Report 2012*. Perisai Petroleum Teknologi Bhd. [Online]. Available: http://ir.chartnexus.com/perisai/docs/AR/2012.pdf.

[153] C. Barton, H. Hambling, E. K. Albaugh, B. Mahlstedt and D. Davis. (2016, August). *2016 Worldwide Survey of Floating Production, Storage and Offloading (FPSO) Units*. Offshore Magazine. [Online]. Available: www.offshore-mag.com/maps-posters.html.

[154] P. C. Tulsian, *Cost Accounting*, Tata Mc-Graw Hill Publishing company Ltd, New Delhi, 2011.

[155] M. Terrill and H. Batrouney. (2018, February 27).*Why the discount rate for major projects needs to be lowered.* [Online]. Available: https://www.macrobusiness.com.au/2018/02/discount-rate-major-projects-needs-lowered/

[156] H. Ormberg, H. Lie, and C. T. Stansberg, "Coupled analysis of offshore floating systems," *Numerical Models in Fluid-Structure Interaction*, Chapter 10, vol. 18, WIT Press, pp. 389-429, 2005.

[157] Z. T. Xie, J. M. Yang, Z. Q. Hu, W. H. Zhao and J. R. Zhao, The horizontal stability of an FLNG with different turret locations, *Int. Journal of Naval Architecture and Ocean Eng*., No. 7, pp 244--258, 2015.

[158] A. Muzathik, W. Wan Nik, M. Ibrahim, and K. Samo, “Wave Energy Potential of Peninsular Malaysia,” *J. Eng. Appl. Sci.*, vol. 5, no. 7, pp. 11–23, 2010.

[159] H. M. Morishita and J. R. Souza Junior, "Dynamic Behaviour of a DICAS FPSO and Shuttle Vessel under the Action of Wind, Current and Wave," *Proc. Of the Twelth ISOPE*, Kitakyushu, Japan, pp. 142-150, 2002.

[160] D. Faulkner, M. J. Cowling and A. Incecik, A, *Integrity of Offshore Structures- 4*, Elsevier Appl. Science, Elsevier Science Publishers Ltd., England, 1990.

[161] T. Ishihara, P. V. Phuc, H. Sukegawa, K. Shimada and T. Ohyama, "A study on the dynamic response of a semi submersible floating offshore wind turbine system part 1: A water tank test," *ICEW 12*, Cairns, Queensland, Australia, pp. 2511-2518, 2012.

[162] B. J. Gernon, J. Y. K. Lou, "Dynamic Response of a Tanker Moored to an Articulated Loading Platform," *Ocean Engineering*, vol.14, no.6, pp.489 – 512, 1987.

[163] *Design of Fixed Offshore Structures*, PTS 34.19.10.30, 2010.

[164] R.G. Standing, S.J. Rowe, and W.J. Brendling, "Jacket Transportation Analysis in Multidirectional Waves," *18th Annual Offshore Technology Conf.*, Houston, Texas, May, 1986.

[165] Statista. (2018). *Average annual Brent crude oil price from 1976 to 2018*. [Online]. Available: https://www.statista.com/statistics/262860/uk-brent-crude-oil-price-changes-since-1976/

PUBLICATIONS LIST

Published Papers

1. Rini N., Kurian V.J. & Whyte A., (2018), 'Floating Production Storage and Offloading Systems cost and motion performance: a system thinking application', Frontiers of Engineering Management.

2. Rini N., Kurian V.J. & Whyte A., (2016), 'Dynamic Behaviour of FPSOs in the Kikeh-Field under Different Loading Conditions', ARPN Journal of Engineering and Applied Sciences, vol-11, no-4, pp.2302-2307, ISSN 1819-6608.

Conference Proceedings

1. Rini N, Whyte A, & Kurian J, (2015), 'Floater Responses: Life-Cycle Considerations Off West Australia', Proc of the 1st International Conference on Decommissioning & Offshore & Subsea Structures, UK, pp.96-101, ISBN: 978-0-9930121-1-2.
2. Kurian J, Rini N & Whyte A, (2015), 'Mooring-Line Serviceability for Floating Production Storage & Offloading (FPSO) Facilities', Proc of the 1st Int. Conference on Decommissioning & Offshore & Subsea Structures, UK, pp.34-39, ISBN: 978-0-9930121-1-2.
3. Gadja P, Whyte A, Rini N & Kurian J, (2015), 'Offshore Substructure Design-Specification Options Comparison using Life-Cycle Cost Analysis', pp.56-59, ISBN: 978-0-9930121-1-2.
4. N. Rini, V.J. Kurian, M.S. Liew & A. Whyte., (2016), 'Coupled Analysis for the Effect of Wave Height on FPSO Motions', Engineering Challenges for Sustainable Future, pp 69-73, ISBN 978-1-138-02978-1.
5. V.J. Kurian, N. Rini, M.S. Liew & A. Whyte., (2016), 'FPSO response and water depth: A study using model tests', Engineering Challenges for Sustainable Future, pp 51-54, ISBN 978-1-138-02978-1.
6. Rini Nishanth, Velluruzhathil John Kurian & Andrew Whyte, 'Coupled motion responses of turret moored and spread moored FPSO under the Influence of wave, wind and current,' pp 217, Proceedings of the International Conference on Ships and Offshore Structures (ICSOS), Hamburg, Germany, 2016.